NYO - 10211
MITNE - 33

ANALYTICAL AND EXPERIMENTAL INVESTIGATIONS OF THE BEHAVIOR OF THERMAL NEUTRONS IN LATTICES OF URANIUM METAL RODS IN HEAVY WATER.

by

R. Simms, I. Kaplan, T.J. Thompson, D.D. Lanning

Contract AT (30-1) 2344
U.S. Atomic Energy Commission

October 11, 1963

Department of Nuclear Engineering
Massachusetts Institute of Technology
Cambridge, Massachusetts.

MASSACHUSETTS INSTITUTE OF TECHNOLOGY

DEPARTMENT OF NUCLEAR ENGINEERING

Cambridge 39, Massachusetts

ANALYTICAL AND EXPERIMENTAL INVESTIGATIONS OF THE BEHAVIOR OF THERMAL NEUTRONS IN LATTICES OF URANIUM METAL RODS IN HEAVY WATER

by

R. Simms, I. Kaplan, T. J. Thompson, D. D. Lanning

October 11, 1963

MITNE - 33

NYO - 10211

AEC Research and Development Report

UC - 34 Physics

(TID - 4500, 20th Edition)

Contract AT(30-1)2344

U.S. Atomic Energy Commission

DISTRIBUTION

NYO-10211 MITNE-33

AEC Research and Development Report

UC-34 Physics

(TID-4500, 20th Edition)

1. USAEC, New York Operations Office (Max Plisner)
2. USAEC, Division of Reactor Development (P. Hemmig)
3. USAEC, New York Patents Office (H. Potter)
4. USAEC, New York Operations Office (S. Strauch)
5. USAEC, Division of Reactor Development, Reports and Statistics Branch
6. USAEC, Maritime Reactors Branch
7. USAEC, Civilian Reactors Branch
8. USAEC, Army Reactors Branch
9. USAEC, Naval Reactors Branch
10. Advisory Committee on Reactor Physics (E. R. Cohen)
11. ACRP (G. Dessauer)
12. ACRP (D. de Bloisblanc)
13. ACRP (M. Edlund)
14. ACRP (R. Ehrlich)
15. ACRP (I. Kaplan)
16. ACRP (H. Kouts)
17. ACRP (F. C. Maienschein)
18. ACRP (J. W. Morfitt)
19. ACRP (B. I. Spinrad)
20. ACRP (P. F. Zweifel)
21. ACRP (P. Gast)
22. ACRP (G. Hansen)
23. ACRP (S. Krasik)
24. ACRP (T. Merkle)
25. ACRP (T. M Snyder)
26. ACRP (J. J. Taylor)
27. - 29. O.T.I.E., Oak Ridge, for Standard Distribution, UC-34, TID-4500 (20th Edition)
30. - 49. R. Simms
50. - 100. Internal Distribution

ACKNOWLEDGMENTS

The success of the M.I T. Lattice Project has been due to the contributions of a number of individuals. The results of this particular report are primarily due to the work of its principal author, Richard Simms, who has submitted substantially this same report in partial fulfillment for the Ph.D. degree at M.I.T. He has been assisted by other graduate students as well as those mentioned specifically below.

Over-all direction of the project and its research is shared by Professors I. Kaplan, T. J. Thompson and D. D. Lanning. Messrs. Joseph Barch and Albert Supple have been of invaluable assistance in the setup of experiments and in the operation and maintenance of the facility. Miss Barbara Kelley has helped in the preparation of foils and in the reduction of the data.

Staffs of the M.I.T. Reactor, Machine Shop, Electronics Shop and Radiation Protection Office have provided much assistance and advice during the experimental portion of this work. Miss Rae Visminas and Mrs. Mary Bosco have given valuable aid in the typing of this report.

Dr. Henry Honeck, of the Brookhaven National Laboratory, has given much assistance in the calculational aspects of this work, a portion of which were made on the B.N.L. computer. The majority of the calculations were performed at the M.I.T. Computation Center. Dr. C. N. Kelber, of the Argonne National Laboratory, was kind enough to provide a copy of a computer program. Dr. Paul Brown, Dr. John Suich, Messrs. Walter D'Ardenne, Phillip Kier, Sang Kyong and David McGoff have contributed to various portions of the research program.

All of these individuals and groups were essential to the completion of this work.

ABSTRACT

Measurements of the intracellular distribution of the activation of foils by neutrons were made in lattices of 1/4-inch diameter, 1.03% U-235, uranium rods moderated by heavy water, with bare and cadmium-covered foils of gold, depleted uranium, lutetium, europium and copper. The measurements were made in the M.I.T. Heavy Water Lattice Facility with source neutrons from the M.I.T. Reactor. Two lattices were studied in detail in this work. The more closely packed lattice had a triangular spacing of 1.25 inches, and the less closely packed lattice had a triangular spacing of 2.5 inches. The results of the experiments were compared to one-dimensional, 30-energy group, THERMØS calculations based on the available energy exchange kernels. The comparison indicated that the approximation that the hexagonal cell may be replaced by an equivalent circular cell (the Wigner-Seitz approximation) can lead to serious discrepancies in closely packed lattices moderated by heavy water. A modified one-dimensional, and a two-dimensional, calculation were shown to predict the intracellular activation distribution in the closely packed lattice.

An analytical treatment of the problem of the flux perturbation in a foil was developed and compared to the experimental results obtained by using gold foils of four different thicknesses in the lattice cell; the method was shown to be adequate. An analytical method to treat the effect of leakage from an exponential assembly was formulated; the results indicated that only in small exponential assemblies would leakage be a significant problem in intracellular flux measurements. A method was developed to predict the cadmium ratio of the foils used in the lattice cell; comparison with available measurements with gold foils indicated good agreement between theory and experiment, except for a lattice having very large ratios of moderator volume, to fuel volume, e.g., 100:1. Calculations of the fuel disadvantage factor by the method of successive generations for gold, lutetium and europium detector foils were compared to the results of THERMØS calculations, because THERMØS was shown to predict the experimental distributions. The comparison indicated that the method of successive generations is a good alternative to the THERMØS calculation, if all that is required is η and the thermal utilization.

TABLE OF CONTENTS

TABLE OF CONTENTS (Concluded)

LIST OF TABLES

LIST OF TABLES (Continued)

LIST OF TABLES (Concluded)

LIST OF FIGURES

LIST OF FIGURES (Continued)

LIST OF FIGURES (Continued)

LIST OF FIGURES (Concluded)

CHAPTER I
INTRODUCTION

1.1 THE M.I.T. HEAVY WATER LATTICE PROJECT

The Department of Nuclear Engineering of M.I.T. with the support of the United States Atomic Energy Commission, has undertaken a program of experimental and theoretical studies of the physics of D_2O-moderated lattices of slightly enriched uranium rods. The emphasis so far has been on the development of techniques that may lead to a better understanding of reactor lattices. The work of the M.I.T. Heavy Water Lattice Project has been summarized in several reports (T3, K1, K9, M2, P1, W3, W5, P5, B14).

1.2 THE IMPORTANCE OF THE NEUTRON ECONOMY

One of the major problems in the design of a nuclear reactor is that of the neutron economy. Neutrons can react with fertile and fissionable materials in a reactor core at all energies, and a quantitative understanding of these reactions is required to specify the design of the reactor. For a large class of reactors, the majority of fissions occur at energies in the neighborhood of the energy corresponding to the moderator temperature, so that these reactors are called "thermal." The lattices investigated by M.I.T. fall into this category. To achieve economic power, it is necessary to predict reactor criticality, core power distribution, core lifetime and the production of fissionable material (conversion or breeding). These quantities depend on the reaction rates of neutrons with the materials of the core, and a knowledge of the neutron economy is required to predict them.

It has become necessary in the past few years, because of increased design requirements, to re-evaluate the methods, both analytical and experimental, that pertain to the study of the neutron economy. The availability of improved electronic equipment and of digital computers has made possible more precise evaluations of the methodology of reactor

physics measurements and calculations. The demands imposed on both the experimental and theoretical methods have become more stringent as reactor design becomes more nearly competitive with conventional power sources. There is, therefore, an incentive to improve the methods in order to reduce the experimental uncertainty and to uncover systematic errors in these methods. Recent reviews by Kaplan (K9) and Crandall (C10, C11) discuss the present status of the methods used to measure and calculate the reactor parameters related to the study of the neutron economy. They each conclude that there still remain areas for improvement in both the experimental and theoretical methods.

As examples of this type of research, we may cite recent work at the Brookhaven National Laboratory, the Savannah River Laboratory and the Chalk River Laboratory. Measurements involved in our understanding of the capture of resonance neutrons in uranium are receiving much attention. Thus, Arcipiani, Ricabarra and Ricabarra (A1) have studied the methods used to measure the U^{238} cadmium ratio, which is related to the plutonium production in a reactor. They obtained a systematic difference in the cadmium ratio of about 3%, depending on whether or not the foils they used were homogenized (by dissolving them) before they were counted. Tassan(T5) has considered the measurement of the cadmium ratio of U^{235} fission in lattices of slightly enriched uranium rods moderated by H_2O. He indicates that there is a discrepancy between conversion ratios deduced from U^{238} and gold cadmium ratio measurements and those deduced from U^{238} and U^{235} cadmium ratio measurements. Tunnicliffe et al. (T6) have developed a method for the determination of the relative initial conversion ratio based on the coincidence method of neptunium, which has a precision of $\pm$ 1/2%. The measurement of the material buckling has also been critically examined. Hellens and Andersen (H4) have studied in great detail the methods used to measure the material buckling in H_2O-moderated lattices, and have reported that a difference exists between the "variable loading" method and the "flux shape" method used to obtain the material buckling of exponential assemblies. Graves (G4) has considered the problem of inferring the material buckling by the "substitution technique" and concludes that the analytical methods presently used "gave satisfactory results in all cases."

The M.I.T. Heavy Water Lattice Project has analagous studies under

way to investigate the methods for possible systematic errors as they may apply to D_2O-moderated lattices. This report deals with the results of one such study of the experimental and theoretical methods of analyzing the behavior of thermal neutrons in the lattice cell.

1.3 THE CONTENTS OF THIS REPORT

From the standpoint of reactor design, the quantities of interest in the thermal energy range are the thermal utilization, f (the ratio of captures in the uranium to the captures in the cell in the thermal energy range), and the number of fast neutrons produced per thermal neutron captured in uranium, η. It is not possible to measure these quantities directly, but experiments can be made that yield enough information so that η and f can be inferred from them with some confidence. This report deals with the kind of experiment made to infer the thermal utilization; it involves the measurement of the intracellular distribution of the activation of bare and cadmium-covered foils in a lattice cell. In a lattice cell, the neutron flux is a function of position and energy. The variation with position is observed by using foils that are small enough to obtain the fine structure of the activation distribution. The variation with energy is observed by performing several separate experiments, each experiment with a set of foils having an activation cross section different, as a function of energy, from the cross sections of the other sets of foils. This technique yields only an integral index of the energy spectrum. The objective of the analytical methods is to predict these activation distributions. Since the experiments give, at best, only integral properties of the neutron flux, they are not absolute tests of the theoretical methods. However, a valid prediction by a theoretical method gives added confidence in its future use.

Brown (B14) has reviewed several of the methods used to "measure" the thermal utilization of a lattice cell. The more precise analytical methods used to predict the activation distribution are discussed in Chapter III; these methods have been programmed for use with digital computers. Neutrons in a lattice cell can diffuse through, and be scattered by, the moderator. A description of the scattering process forms the basis of the study usually called "Neutron Thermalization." Several reviews of this subject are available; among them are those of Cohen (C8), Hurwitz and Nelkin (H16), Nelkin and Cohen (N2), Amaldi (A3) and Nelkin (N5).

Because of the chemical binding between the atoms of the moderator, the scattering centers may not accurately be treated as free, monotomic gases. When the scattering process has been defined analytically, it is necessary to calculate the spatial dependence (transport) of the neutrons in the cell. Honeck (H14) has provided a good summary of the methods that are presently available for both the calculation of the scattering kernel and the calculation of the spatial dependence.

Chapter II of this report discusses the methods used to measure the intracellular activation distributions in lattices of 1/4-inch diameter, 1.03% U^{235}, uranium rods moderated by heavy water. Chapter III deals with the analytical methods used to calculate the activation distributions. The results of the experiments and the calculations are discussed in Chapters IV and V. The appendices are intended to implement the discussions of the text. Included in the report are discussions of energy exchange kernels, transport methods, leakage effects, flux perturbation effects, and the cell cylindricalization problem. The experiments were made to investigate various aspects of the problems discussed in Chapter III.

CHAPTER II
EXPERIMENTAL METHODS

2.1 INTRODUCTION

In this chapter, the experimental techniques used to measure the intracellular activation distributions in reactor lattices are discussed. The lattices studied were made up of 1/4-inch diameter, 1.03% U^{235}, uranium metal rods on 1.25- or 2.5-inch triangular spacing in a 3- or 4-foot diameter, exponential tank and moderated by 99.8 atom % D_2O. The height of the active fuel was 4 feet. Additional information on the details of the lattices is given in Appendix F. The experiments required the preparation of detector foils, the development of foil holders and cadmium covers, and the establishment of procedures for counting and data reduction.

2.2 THE M.I.T. LATTICE FACILITY

The intracellular activation distributions were measured in the M.I.T. Heavy Water Lattice Facility. Cross-sectional drawings of the facility are shown in Figs. 2.2.1 and 2.2.2. The facility consists of an exponential tank located above a graphite-lined cavity. Source neutrons for the exponential tank are reflected upward, by the cavity arrangement, from the MITR thermal column. The details of the cavity arrangement are discussed by Madell et al. (M2). The M.I.T. Heavy Water Lattice Facility has been described in previous reports (T3, K1).

2.3 DESCRIPTION OF THE FOILS USED IN THE EXPERIMENTS

Nine sets of 1/16-inch diameter foils were used in the experiments; the relevant properties of the foils are listed in Table 2.3.1. The foils, metal or alloy, were punched from a sheet of the appropriate material by means of a punch and dye. The dye was made to fit the punch closely, and was heat treated. The foils were examined and found to be almost free from burrs. They were weighed individually on a Fisher precision microbalance (Model 1-912); the scale was read

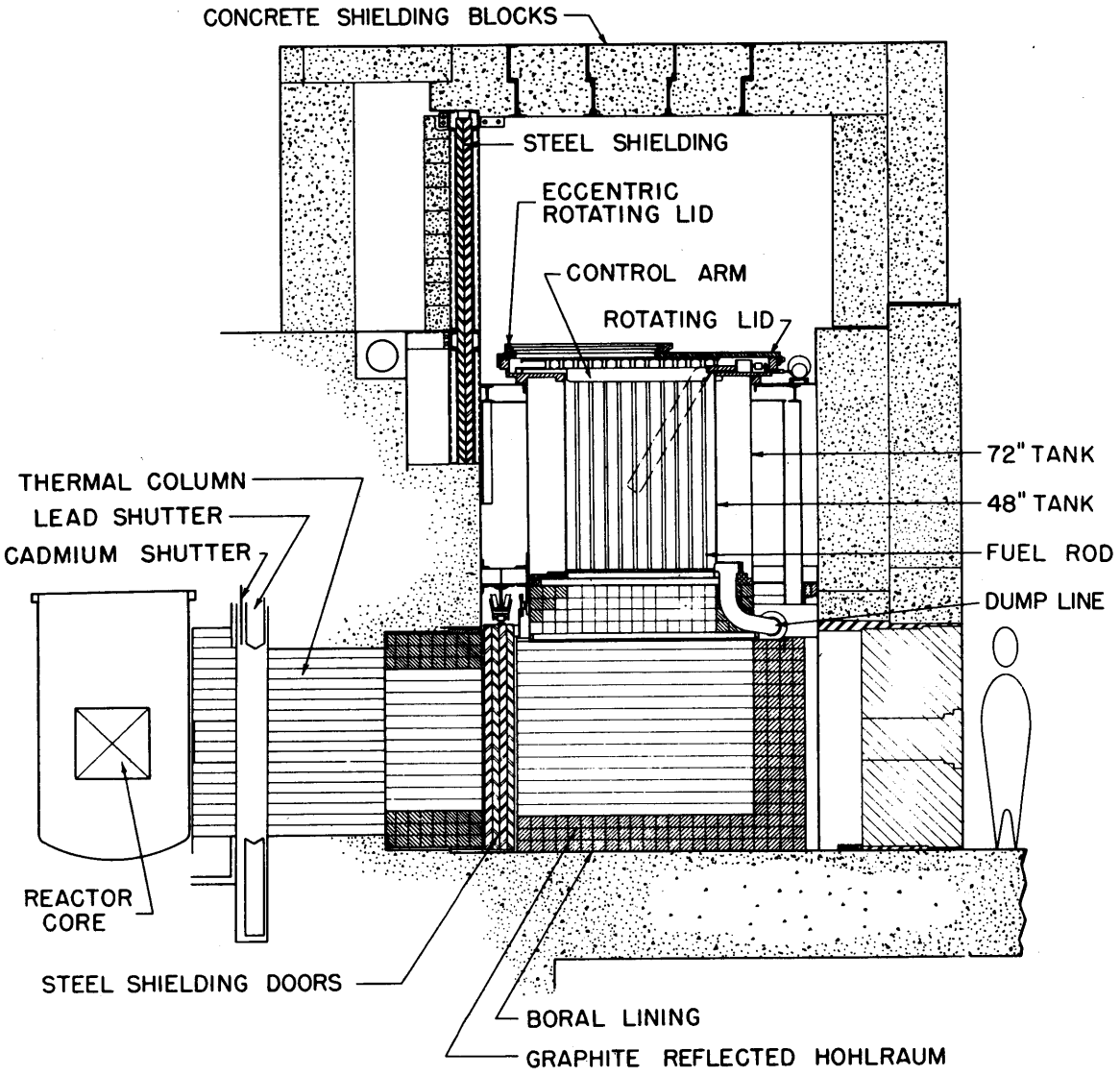

FIG. 2.2.1 VERTICAL SECTION OF THE SUBCRITICAL ASSEMBLY

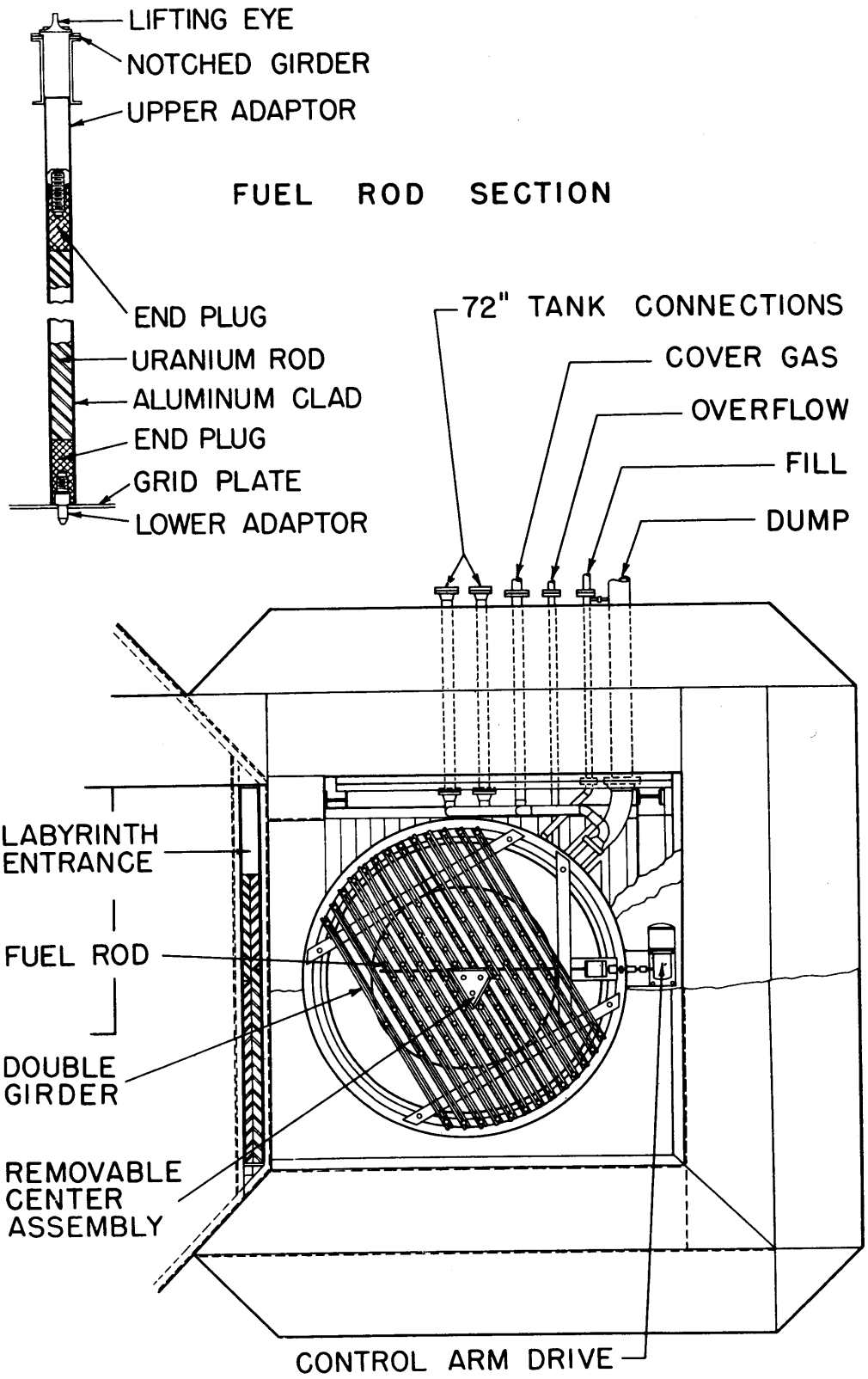

FIG. 2.2.2 PLAN VIEW OF THE SUBCRITICAL ASSEMBLY

TABLE 2.3.1

Properties of the Foils

Foil Set	No. of Foils	Average[(a)] Weight (mg)	Range[(b)] (mg)	Thickness (mils)
Dilute Gold (1% gold in 3 mil Al)	300	0.406 ± .07%	0.023	3.0 ± 0.1
2.5 mil Gold (metallic, 99.97% pure)	300	2.225 ± .11%	0.179	2.5 ± 0.1
4.3 mil Gold (metallic, 99.97% pure)	300	3.995 ± .05%	0.125	4.3 ± 0.1
10.2 mil Gold (metallic, 99.97% pure)	600	9.497 ± .02%	0.201	10.2 ± 0.1
5 mil Depleted Uranium (metallic, 18 ppm U-235)	300	3.851 ± .30%	0.868	5.0 ± 0.3
Lutetium Alloy (10 w/o Lu_2O_3 in 10 mil Al)	300	1.430 ± .06%	0.065	10.0 ± 0.2
5 mil Copper (metallic)	70	3.324 ± .10%	0.213	5.0 ± 0.2
Lutetium Powder (Lu_2O_3-glyptal on 5 mil Al)	200	–	–	–
Europium Powder (Eu_2O_3-glyptal on 5 mil Al)	200	–	–	–

(a) The standard deviation from the mean is given.

(b) The range is the maximum weight difference between any two foils in the set.

to the nearest microgram. The uncertainty for a single weighing was ±0.004 mg, as established by the repeated weighing of a single foil.

The foils, in sets of 300, were arranged in increasing order of weight and stored in a foil file. Each foil was assigned a number, and a record of the weights of the foils was punched in IBM cards. Since each experiment required no more than 70 foils, the weight corrections applied were always small. The distribution of weights for the set of 4.3 mil gold foils is given in Fig. 2.3.1. After an experiment, the foils were returned to the file, the numbering system being maintained, and were used again after at least 10 half-lives in time had elapsed. After 10 half-lives, the activity of a foil decreases to about 0.1% of its original value.

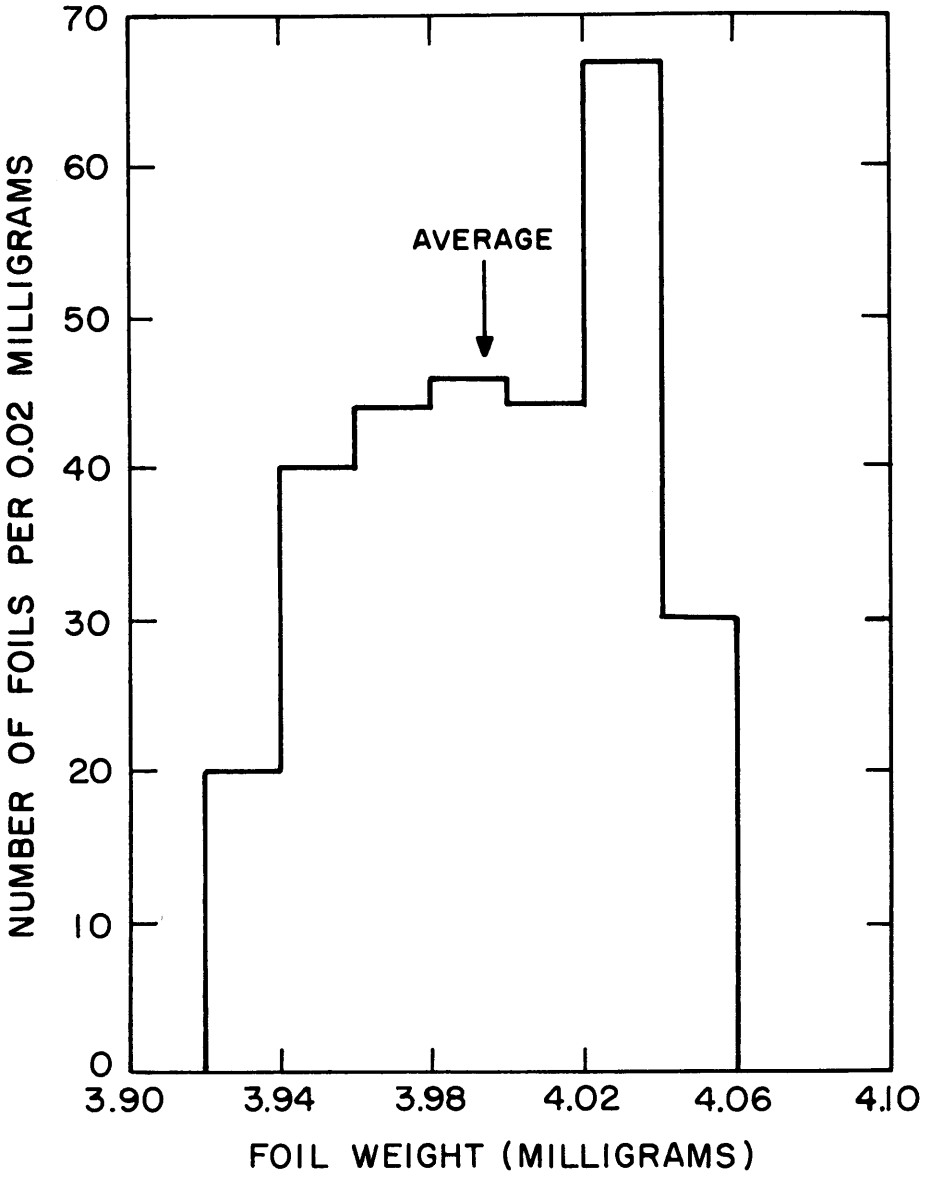

FIG. 2.3.1 THE DISTRIBUTION OF FOIL WEIGHTS IN THE 4.3 MIL GOLD FOIL FILE.

The thickness of a sheet from which foils were punched was measured with a micrometer at several positions; average values of the foil weights are listed in Table 2.3.1. The uncertainty in thickness was approximately ±0.1 mils for the gold foils. Each sheet was also weighed and the thickness calculated from the known density and dimensions; the result was found to agree with the measured thickness, within the uncertainty of the measurements.

Since the foils were all punched with the same punch and dye, there should be some correlation between the measured weight and thickness. Figure 2.3.2 indicates that the weight was proportional to the thickness. If it is assumed that there were no burrs on the foils, the line from the origin to the best known point, that for the 10 mil gold foils, provides a way of determining the thickness of the thinner foils from their weights. With the assumption that the 10 mil gold foils were perfect right circular cylinders, the diameter of the punch was calculated from the density of gold and the thickness of the sheet; the nominal punch diameter was 1/16 inch, while the calculation gave 0.060 inch, indicating that the punch was slightly undersized. A measurement of the diameter with a micrometer gave the diameter as 0.059 ± 0.001 inch, but this result should not affect the interpretation of the experiment.

The powder foils of lutetium and europium were fabricated and intercalibrated on a flux wheel by Brown (B14). In the calibration experiment the foils were irradiated in a tank filled with heavy water, and counted on the gamma-ray counter used in the experiments. The counting uncertainty was about one per cent.

2.4 THE FOIL HOLDERS

The small diameter of the rods and the small lattice spacings made the accurate positioning of the foils difficult. The foil holders used were improved with time, so that those used in the experiments in the lattice with the 2.5-inch triangular spacing differed from those used in the lattice with the 1.25-inch triangular spacing. The differences were minor so far as nuclear properties are concerned, but made the experiment easier to do.

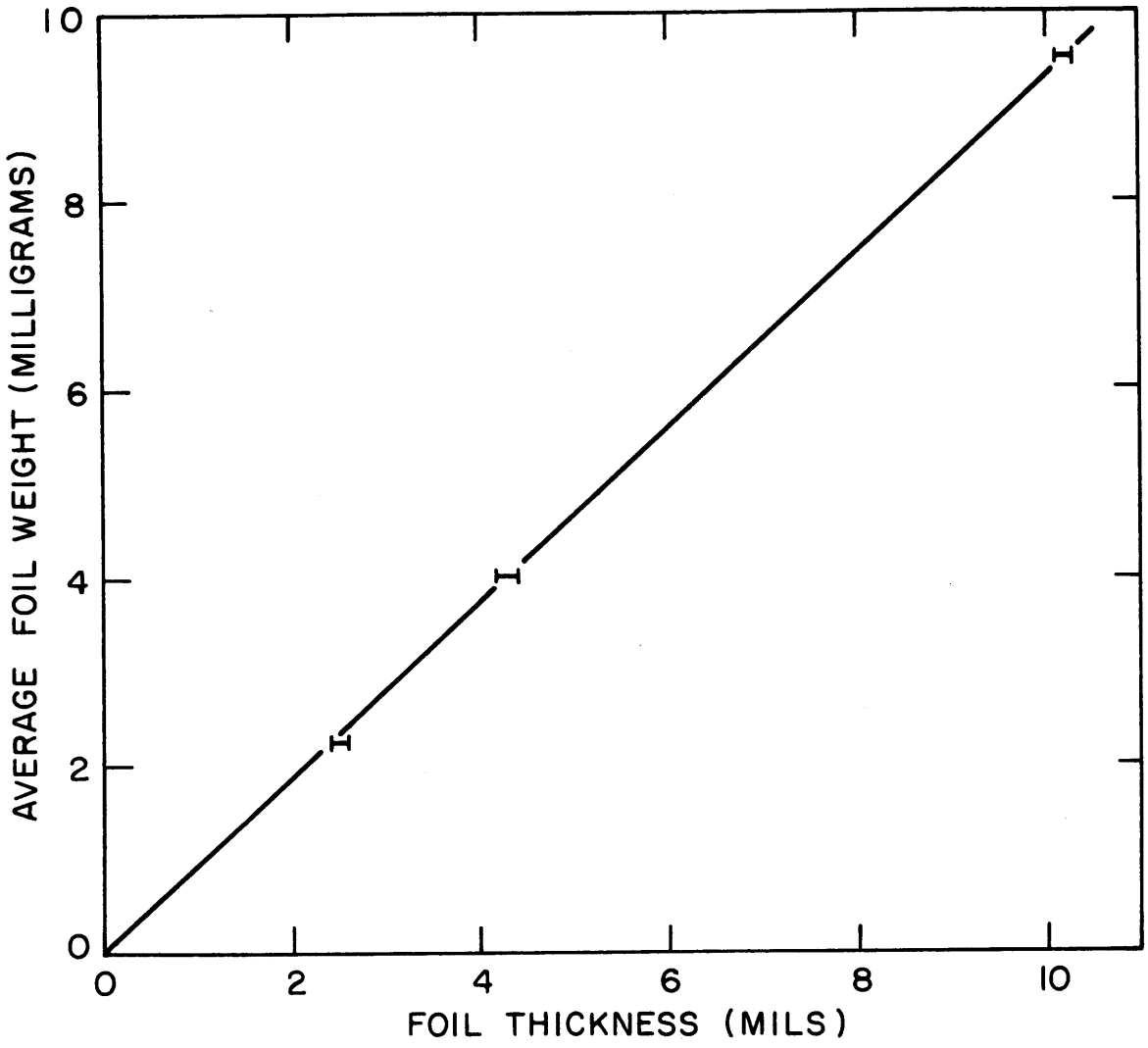

FIG. 2.3.2 AVERAGE WEIGHT OF GOLD FOILS AS A FUNCTION OF FOIL THICKNESS.

2.4.1 THE LATTICE WITH THE 2.5-INCH TRIANGULAR SPACING

The holder used for the bare and cadmium-covered foils irradiated in the fuel rod is shown in Fig. 2.4.1. The foils were placed in holes punched in a 1/4-inch diameter, 10 mil thick foil of 1.03% enriched uranium. To hold the foils in place, each side of the 1/4-inch foil was taped with mylar tape, 2 mils thick. The tape also served to prevent contamination of the foils by fission products. The effect of the mylar was found to be negligible (see Appendix B).

A schematic diagram of the foil holder used in the moderator is shown in Fig. 2.4.2. The bare foils irradiated in the moderator were placed in 1/16-inch holes milled in 12 mil thick aluminum holders, and were held in place by mylar tape. Brown (B14) has made experiments that indicate that this thickness of aluminum perturbs the flux by less than 0.3%. The foil holder was held fast to the rods of the three-rod cluster by wrapping the attached tabs around the rods and taping them in place with mylar tape. This procedure provided additional rigidity in the positioning of the three rods of the cluster.

Foils irradiated in the moderator were covered with cadmium (20 mils) by putting them in cadmium pill boxes, which were placed in 1/8-inch diameter holes milled in a 12 mil thick aluminum holder. The boxes were taped to the holder with mylar tape, and the foil holders were attached to the rods by means of the tabs.

2.4.2 THE LATTICE WITH THE 1.25-INCH TRIANGULAR SPACING

Because of the smaller spacing in this lattice, and the consequent greater importance of the positioning, the foil holders were improved. The foils irradiated, bare or cadmium-covered, in the rod were placed in 12 mil holes milled on both sides of 1.03% U^{235} uranium button, 60 mils thick and 1/4 inch in diameter, as shown in Fig. 2.4.3. An aluminum foil, one mil thick, was placed in the hole first to prevent contamination of the foils by fission products from the uranium button. The aluminum foils were counted and their activity was found to be negligible in comparison to the background. The foils were held in the uranium button with mylar tape, trimmed to the 1/4-inch diameter of the button. The mylar tape also served to prevent fission products from the uranium rod from contaminating the foils.

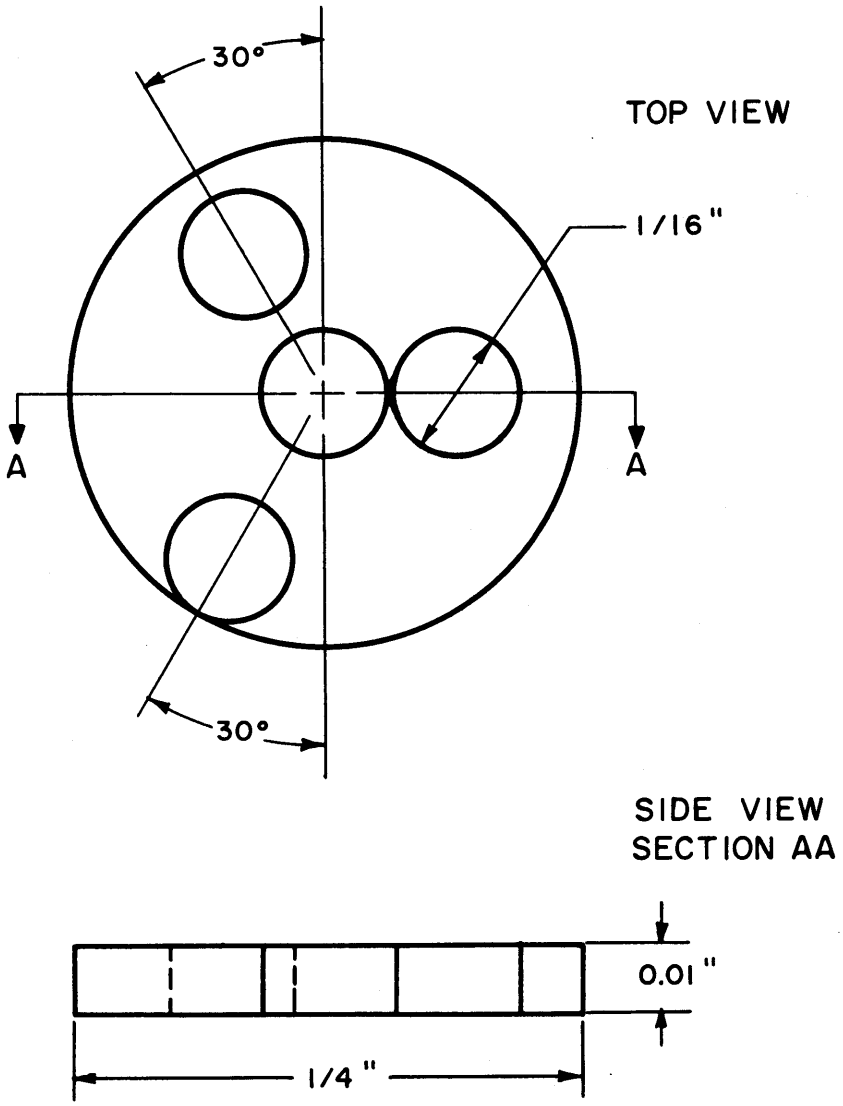

FIG. 2.4.1 THE HOLDER FOR THE FOILS IRRADIATED IN THE FUEL ROD USED IN THE LATTICE WITH THE 2.5-INCH TRIANGULAR SPACING.

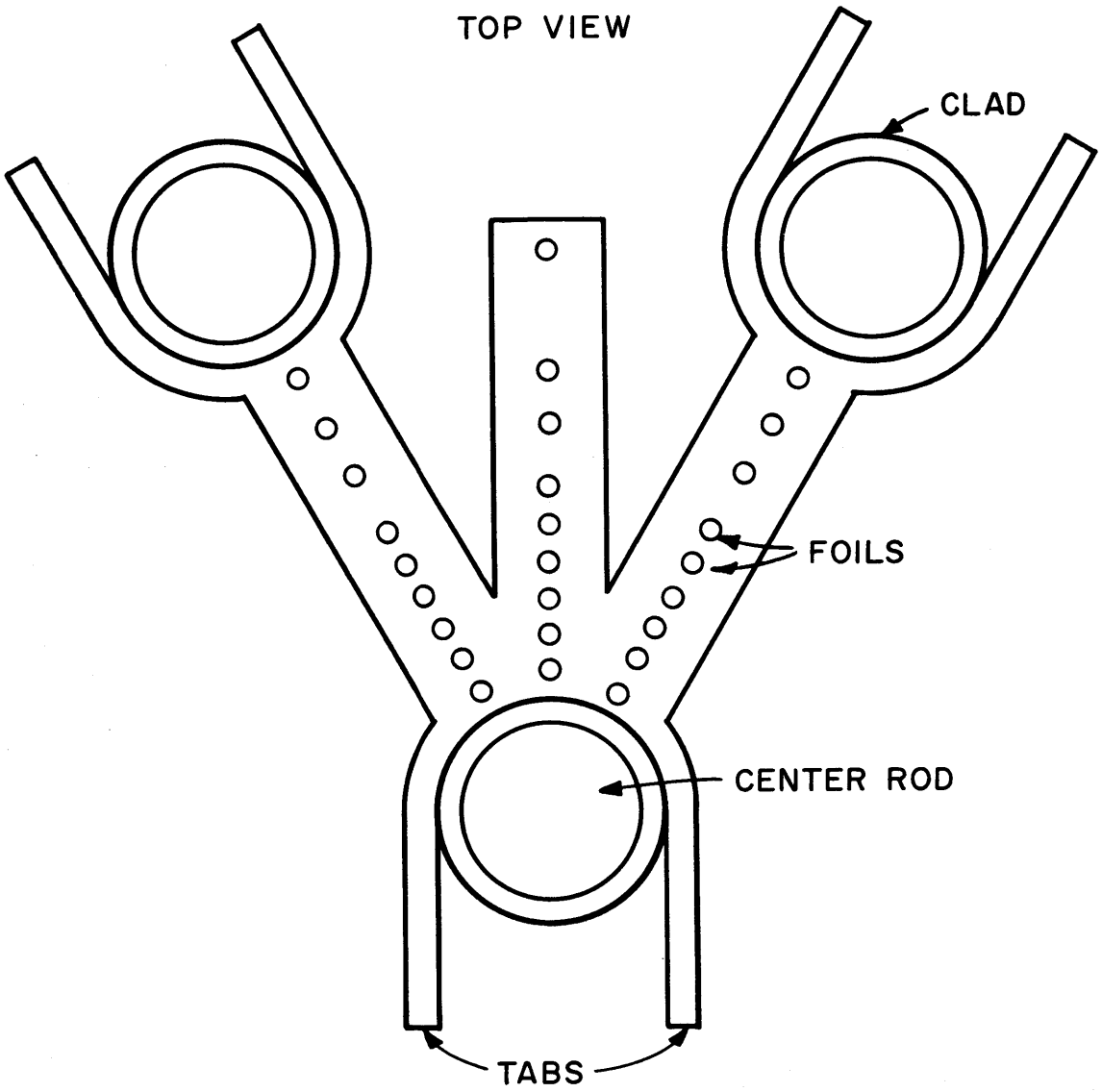

FIG. 2.4.2 THE HOLDER FOR THE BARE FOILS IRRADIATED IN THE MODERATOR USED IN THE LATTICE WITH THE 2.5-INCH TRIANGULAR SPACING.

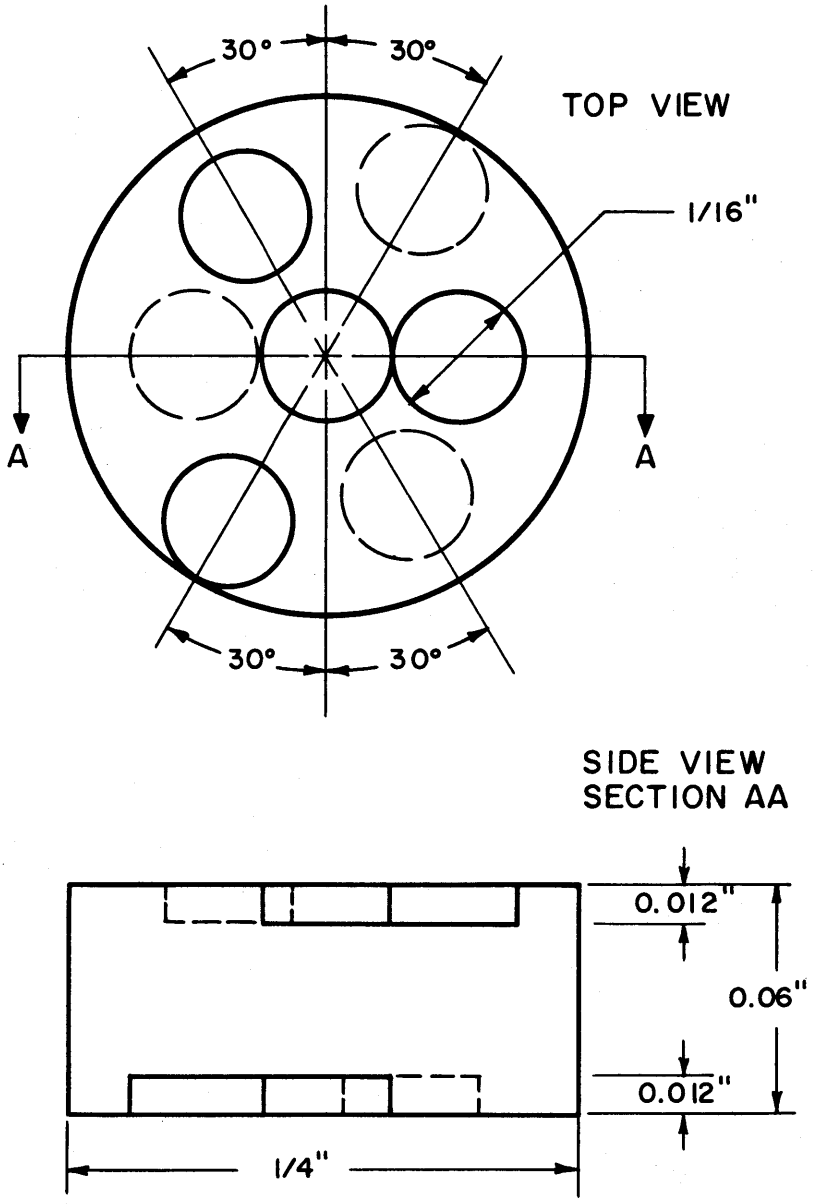

FIG. 2.4.3 THE HOLDER FOR THE FOILS IRRADIATED IN THE FUEL ROD USED IN THE LATTICE WITH THE 1.25-INCH TRIANGULAR SPACING.

The holders for the bare foils were fabricated from 12 mil thick aluminum machined with 1/16-inch holes as shown in Fig. 2.4.4. Mylar tape was used to hold the foils in position. The sides of the holder in a line tangential to the outer diameter were bent through 90° to provide the holder with additional rigidity along the rod-to-rod line. In an experiment, a holder was clipped onto the rods of the three-rod cluster and a strip of mylar tape was used to hold the foil holder to the cluster.

The holders for the cadmium-covered foils were made from 18 mil thick aluminum. Each cadmium pill box was placed in an 1/8-inch hole milled in the holder, recessed 10 mils deep in a 5/32-inch hole centered in the 1/8-inch hole as shown in Fig. 2.4.5. The boxes were permanently fixed in position with epoxy resin, and the foils could be loaded and unloaded without removing the boxes from the holder. Except for the sizes of the holes milled, the holders for the cadmium-covered foils were the same as those used for the bare foils.

2.4.3 THE CADMIUM BOXES

It was required that the cadmium boxes for the foils be leak-tight to water and to thermal neutrons, and that the foils could be removed easily, without damage to the foil or the box. After considering several designs, it was decided to use the rivet-like design shown in Fig. 2.4.5.

A sheet of cadmium, 60 mils thick, was taped to an aluminum backing block with two-sided tape. The aluminum block was clamped in a milling machine and a number of pill boxes machined at once. Depressions, 1/32 inch in diameter, were milled in the wall of the box to provide an easy way to pry off the cover. An 1/8-inch inside diameter trepan tool (a hollow mill) was used to mill the outer diameter of the cadmium pill, 50 mils deep. The final rivet-like cadmium pill box was obtained by punching the pill from the sheet with a special punch having a hollow center and an outer diameter of 5/32 inch.

Covers for the boxes were punched from a 20 mil sheet of cadmium with a 3/32-inch punch. No attempt was made to reuse the covers. The cadmium boxes epoxied to the holders were intact at the completion of all the experiments.

A box was filled with an indicator dye and dropped into a beaker of hydrochloric acid. No change of color was noted until the box had dissolved,

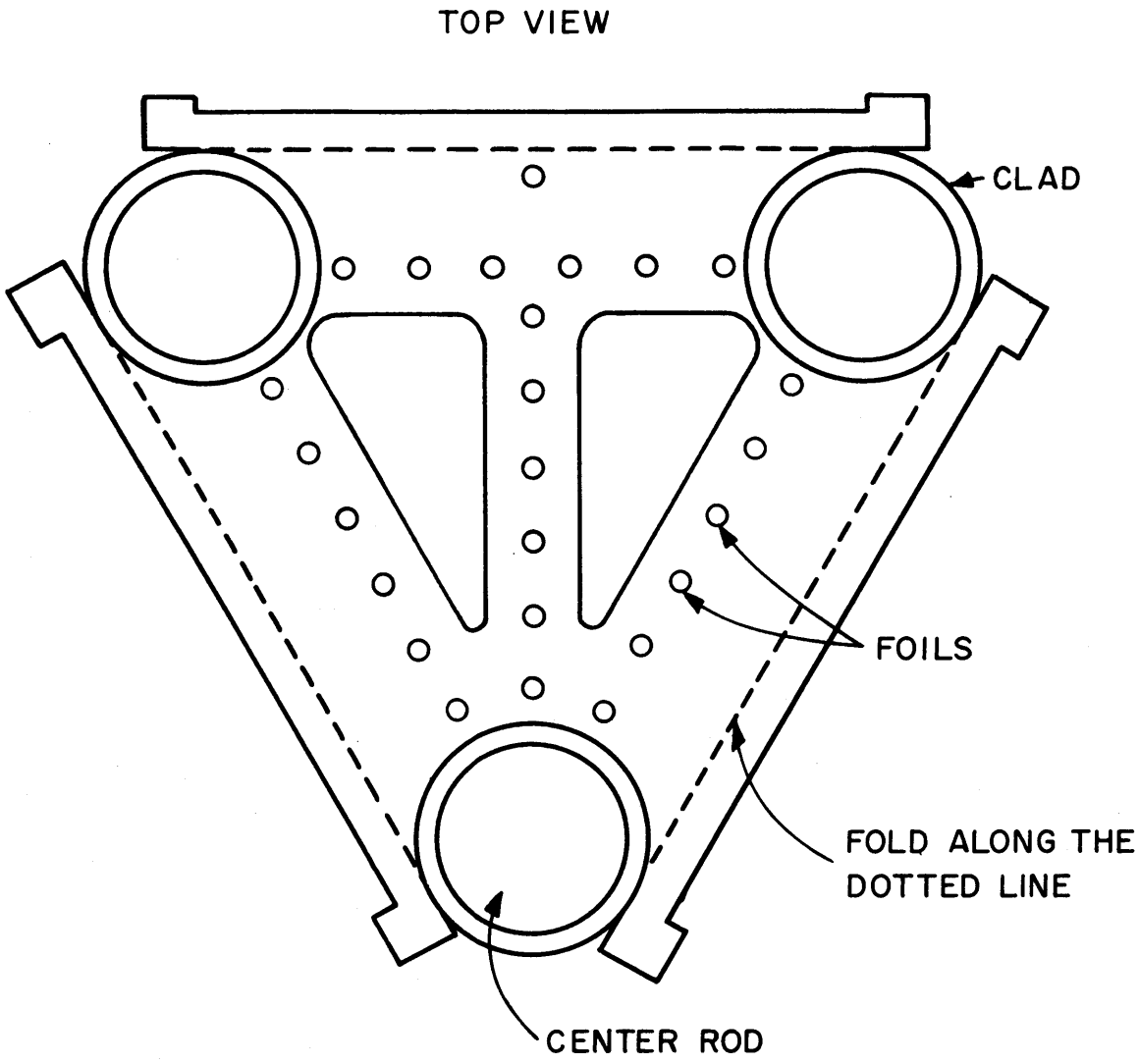

FIG. 2.4.4 THE HOLDER FOR THE BARE FOILS IRRADIATED IN THE MODERATOR USED IN THE LATTICE WITH THE 1.25-INCH TRIANGULAR SPACING.

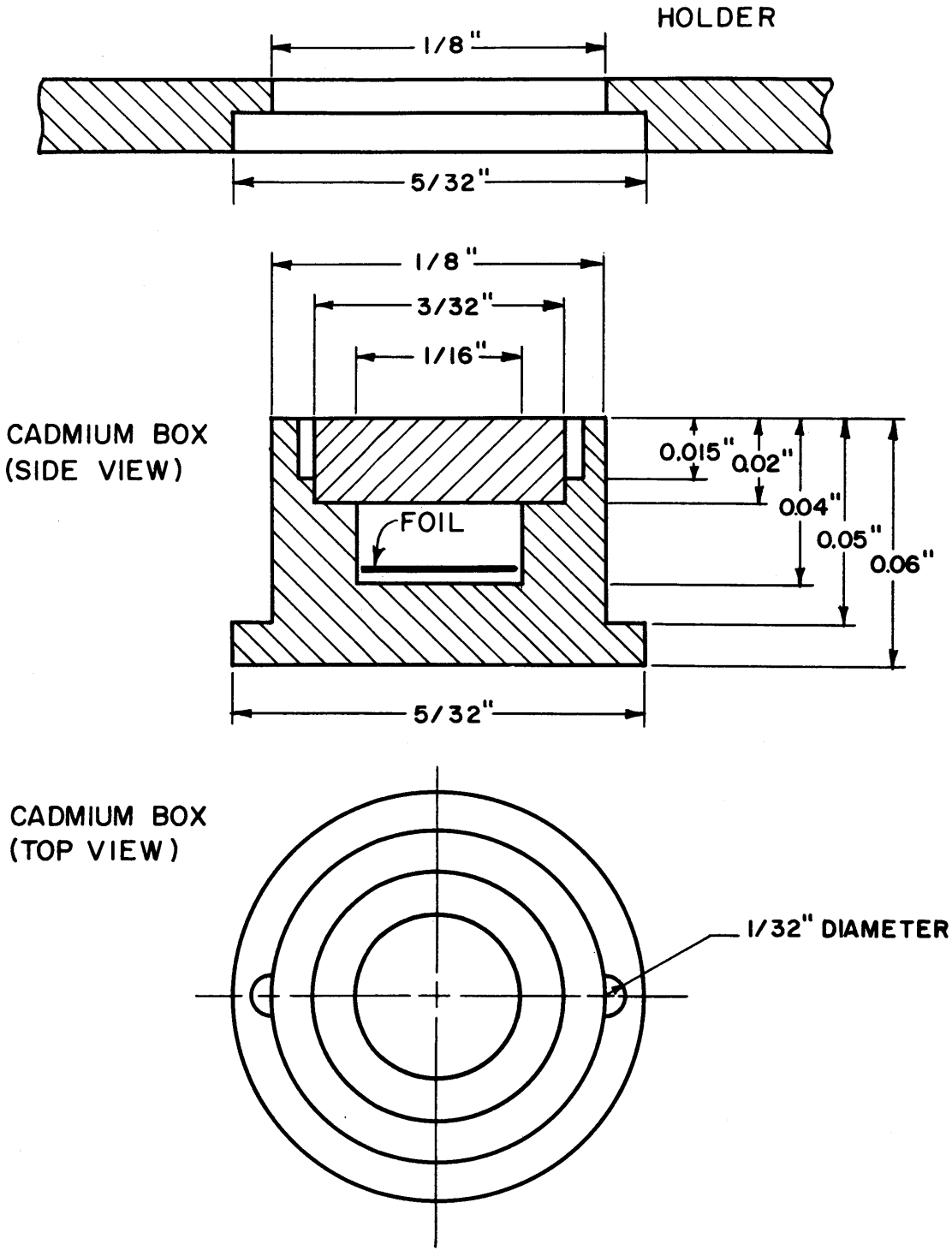

FIG. 2.4.5 THE CADMIUM BOX AND A SECTION OF THE HOLDER USED TO POSITION THE BOX IN THE MODERATOR.

so that the requirement that the box be leak-tight to water was met.

Cadmium ratio experiments were made in a thermal flux to determine if the cadmium boxes were leak-tight to thermal neutrons. Bare and cadmium-covered foils from the 4.3 mil gold foil file were irradiated in the cavity (see Fig. 2.2.1) and the cadmium ratio was found to be 600 ± 10%. Although the experiment does not yield absolute proof that the cadmium boxes do not leak, the value of the cadmium ratio agrees with values obtained in other experiments, with gold foils of different diameters and different cadmium boxes, made by D'Ardenne (D1).

2.5 THE THREE-ROD CLUSTER

The foil holders described in Section 2.4 were loaded in the exponential tank in the three-rod cluster shown in Fig. 2.5.1. The foils irradiated in the fuel were loaded into the central rod. With the exception of the measurement involving the dilute gold foils, the same positions in the rod were occupied by the foil holders relative to the active fuel height.

Figures 2.5.2 and 2.5.3 show the positions occupied by the foil holders. In the experiments in the lattice with the 2.5-inch spacing, only one type of foil was used per experimental run. As a result of the improvements in the experimental technique, the experiments in the lattice with the 1.25-inch spacing involved the use of two types of detectors per run. All experiments were repeated at least once. The experiments in each lattice were completed with the original sets of foil holders, thus attesting to the durability of the holders.

2.6 COUNTING OF THE ACTIVATED FOILS

In these experiments, γ-counting was used in preference to β-counting. For 1/16-inch foils, it is doubtful that a weight correction would be meaningful for β-counting. The count rate for β-counting is due to β-sources near the surface of the foil, because of the short range of β-particles in the metal foil. Any imperfections in the surface of the foil affect the count rate so that the foils would have to be calibrated on the β-counter. The γ-counting technique was free from these disadvantages and was used exclusively.

A Nuclear-Chicago automatic sample changer with a 1/2-inch sodium-iodide crystal was used to count the foils. A schematic diagram of the

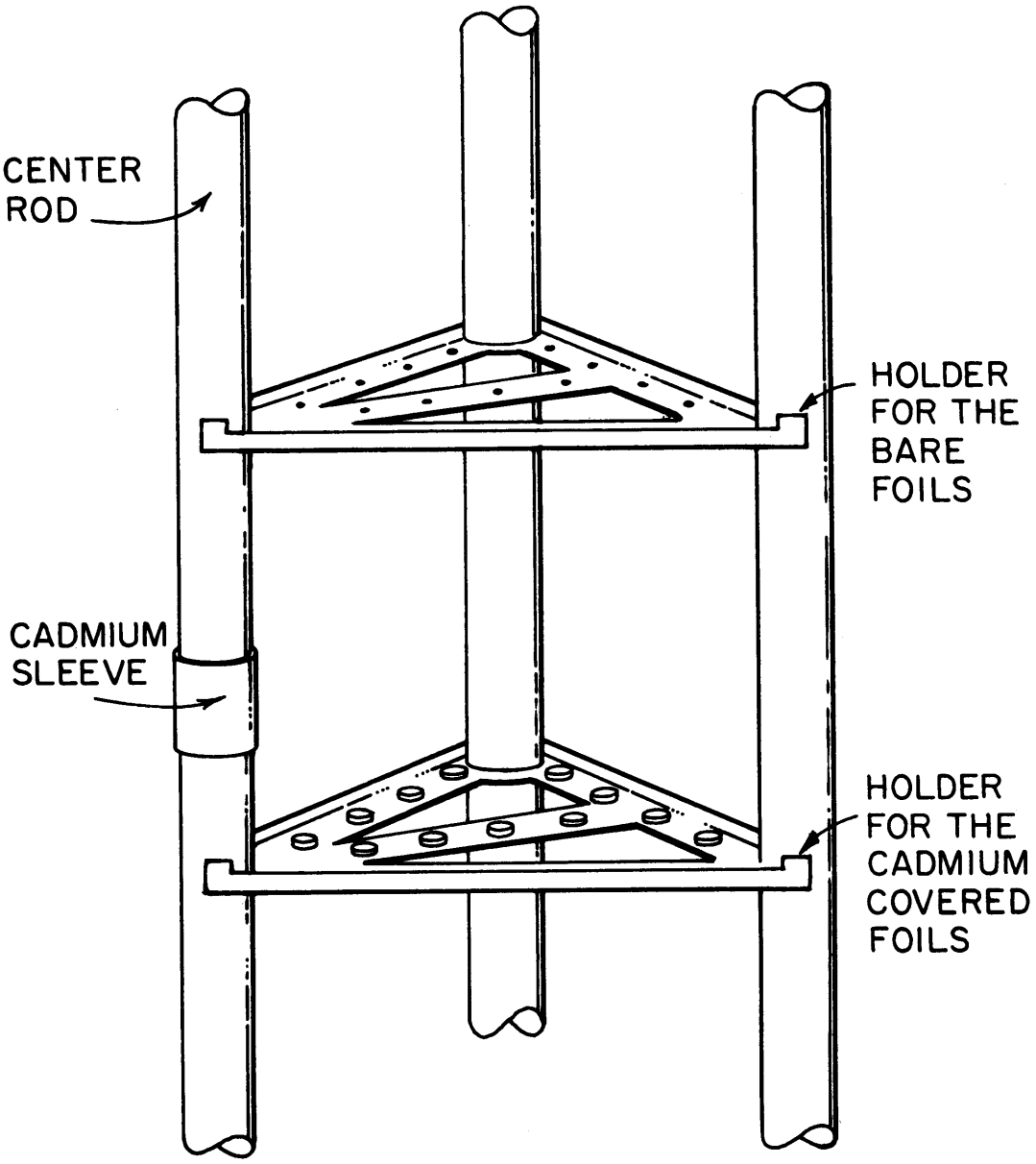

FIG. 2.5.1. THE THREE-ROD CLUSTER.

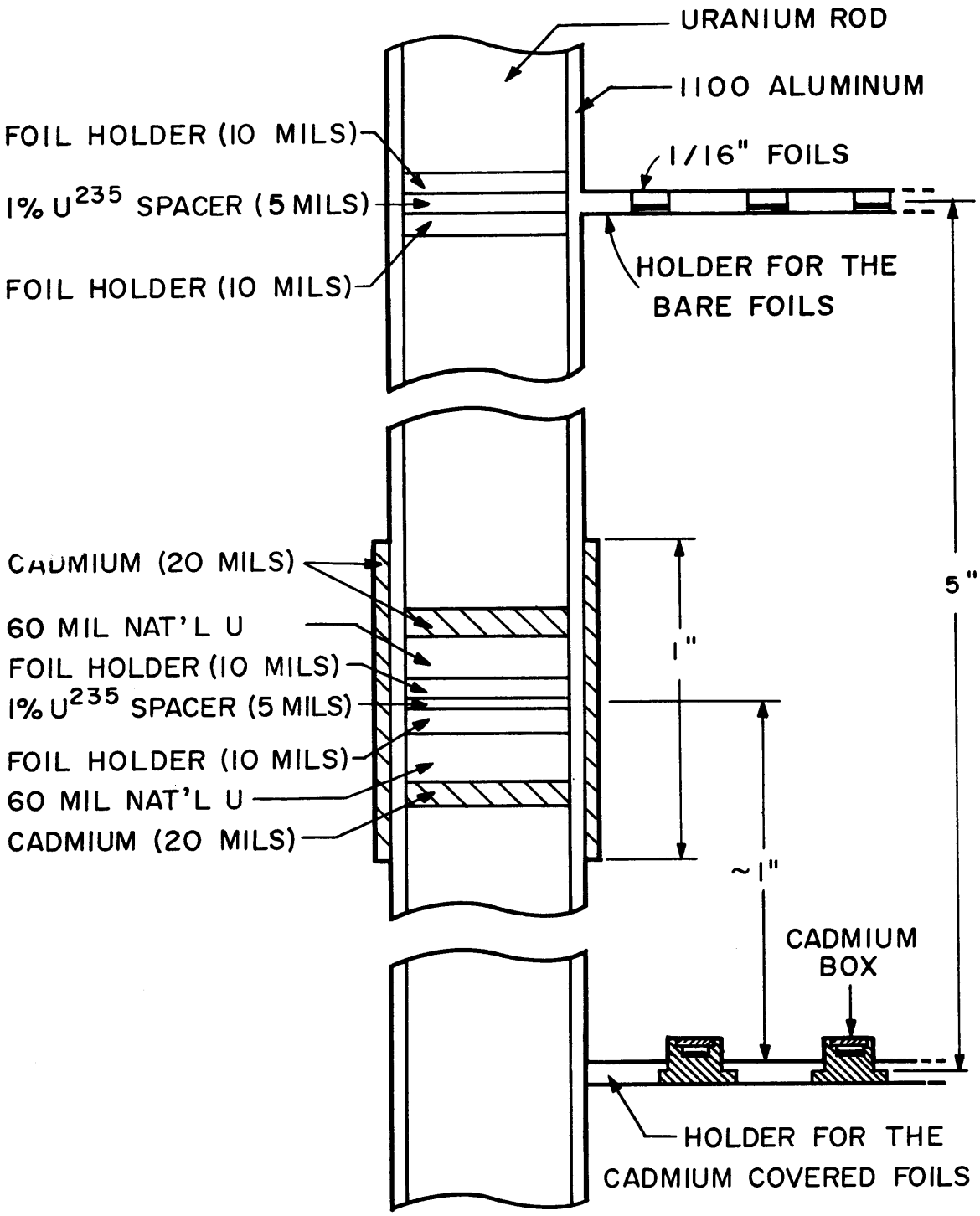

FIG. 2.5.2 POSITIONS OF THE FOIL HOLDERS IN THE EXPERIMENTS IN THE LATTICE WITH THE 2.5-INCH TRIANGULAR SPACING.

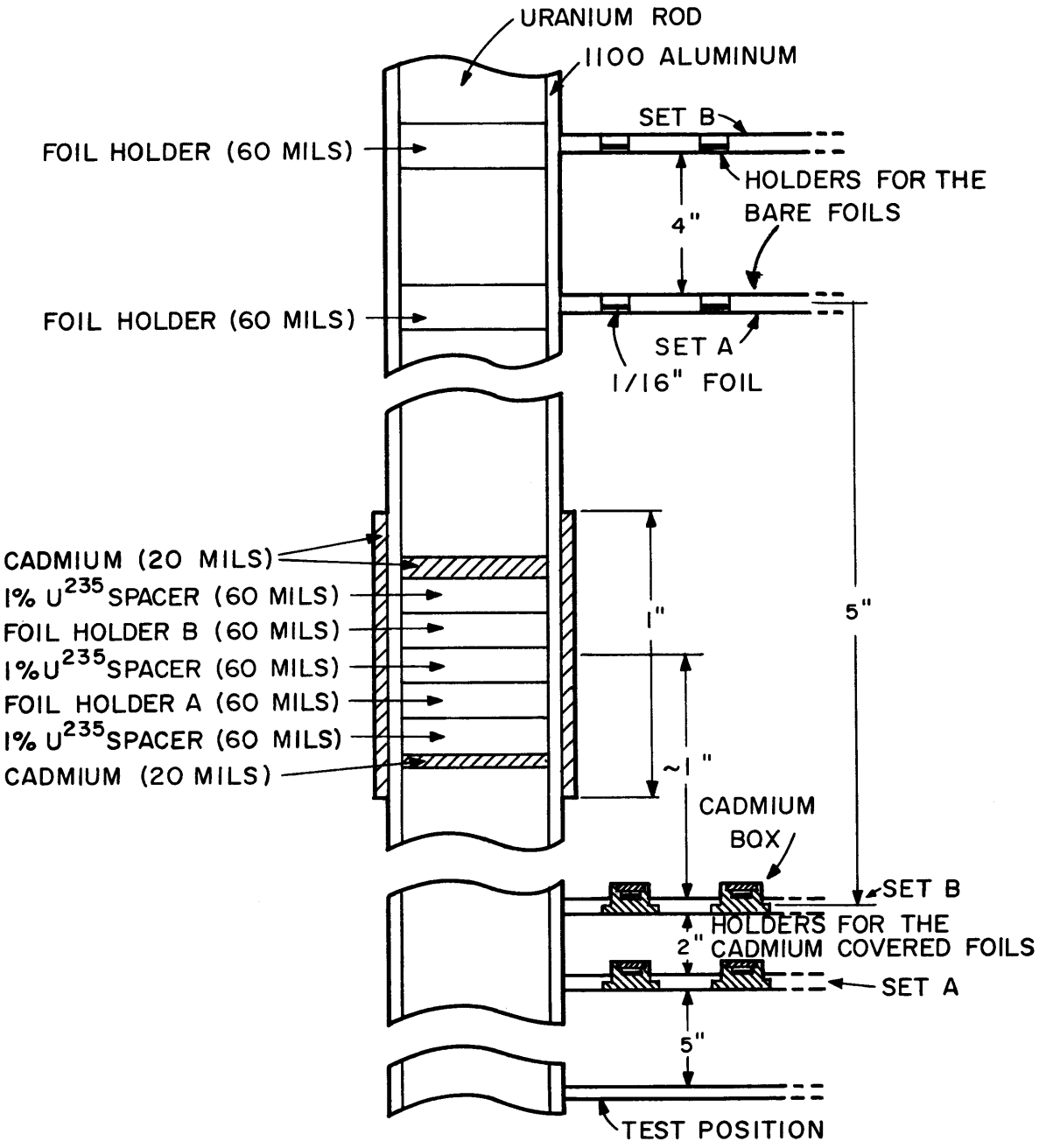

FIG. 2.5.3 POSITIONS OF THE FOIL HOLDERS IN THE EXPERIMENTS IN THE LATTICE WITH THE 1.25-INCH TRIANGULAR SPACING.

counting equipment is shown in Fig. 2.6.1. The single-channel analyzer was used for both differential and integral counting. The system was calibrated each time a run was counted.

The cadmium-covered foils were counted separately from the bare foils. Monitor foils were used to estimate the counter drift. The time correction for decay based on the monitor foils was within 0.5% of the correction calculated from the half-life and the elapsed time. By separating the two sets of foils when counting, it was possible to minimize the contribution to the count rate of the foils in the stack that were out of the counting chamber.

The preset count setting was adjusted so that a counting time of 5 to 10 minutes was obtained for most of the foils. The printer records the counting time to the nearest 0.01 minutes, so that a 5-minute counting time is needed to reduce the error below 0.2%. Since the timing is based on the 60 cycle per second line voltage, any variation in the voltage cycles could introduce errors in timing. The Cambridge Electric Light Company gives the variation of the voltage as $\pm 1/20$ cps, 95% of the time and $\pm 1/10$ cps, 5% of the time. Hence, the maximum error introduced by the variation in the voltage is $\pm 0.2\%$.

When possible, several passes were made for the foils in any given run to spread any counter drift over all the foils. For example, it seemed more desirable to count the foils for a total of 100,000 counts in five passes, at 20,000 per pass, rather than one pass at 100,000.

2.6.1 GOLD

Neutron activation of gold yields Au^{198}, with a half-life of 2.7 days. The principal gamma radiation is a 412 kev gamma ray. Both integral and differential counting methods were used; the results indicated no significant differences between the two methods. The differential method used was to straddle the 412 kev photopeak with a window width corresponding to 90 kev. The particular crystal used in the experiments had a full-width at half-maximum of 70 kev. The integral method used was to set the base line at 320 kev, the lowest point of the gamma spectrum just below the 412 kev photopeak. The window was opened so that all gamma rays above 320 kev could be counted.

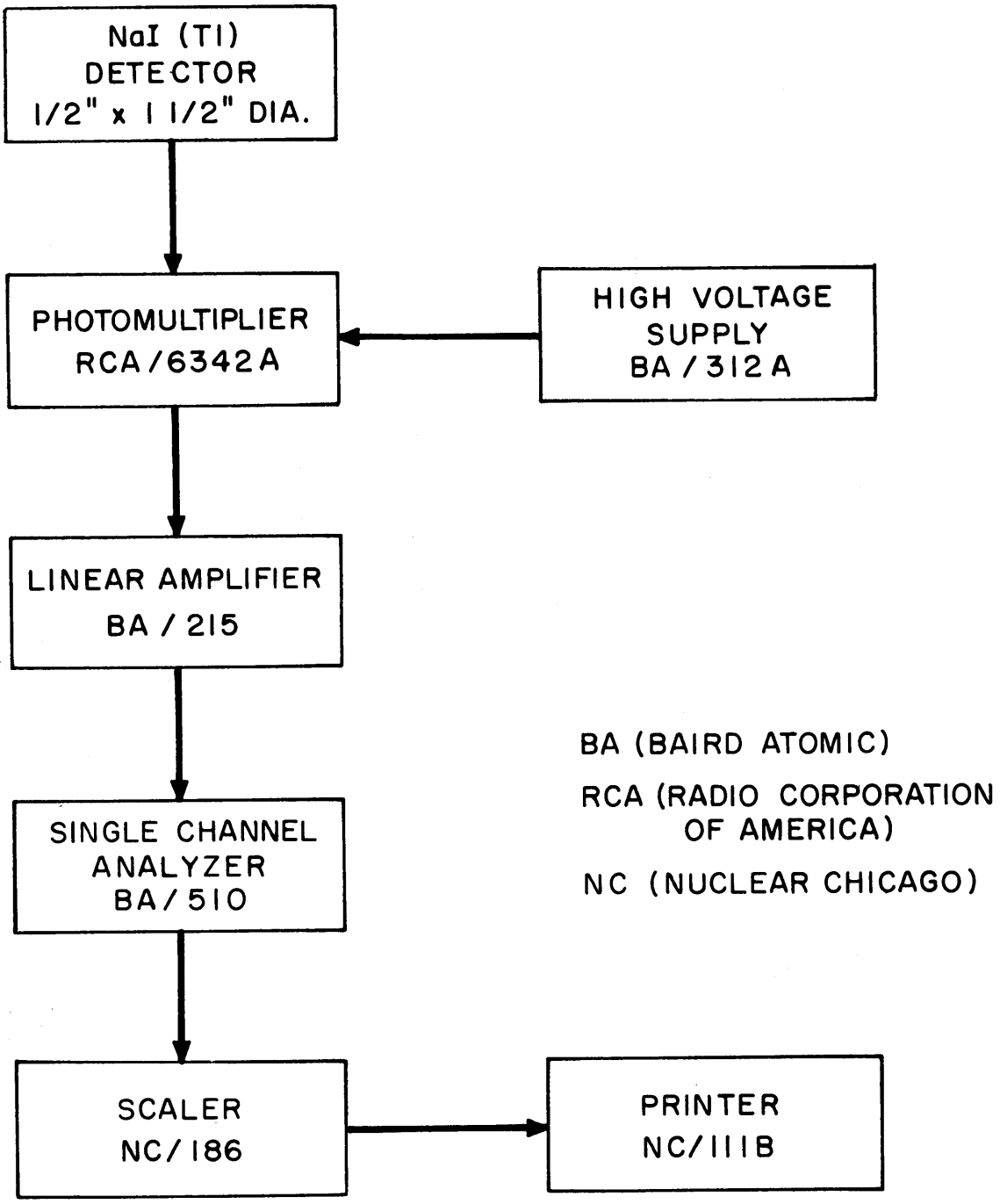

FIG. 2.6.1 BLOCK DIAGRAM OF GAMMA COUNTING SYSTEM.

2.6.2 LUTETIUM

After a cooling period of 48 hours, the 6.7-day Lu^{177} was counted with the integral method. The base line was set at 45 kev, just below the 57 kev Hf X-ray peak (B14). The window of the analyzer was opened so that all gamma rays above 45 kev could be counted.

2.6.3 EUROPIUM

The 9.2-hour half-life Eu^{152} was counted with the integral method. The base line was set at 80 kev, just below the 122 kev Sm^{152} peak (B14). The window of the analyzer was opened so that all gamma rays above 80 kev could be counted.

2.6.4 DEPLETED URANIUM

The 103 kev peak of the 2.3-day Np^{239} was straddled with a window width corresponding to 30 kev. This procedure was used by Weitzberg (W3). For the purpose of obtaining backgrounds, unirradiated depleted uranium foils were counted in various positions in the foil stack of the automatic sample changer.

2.7 DATA REDUCTION

The data reduction was accomplished with the aid of an IBM 7090 computer, with the ACTIVE code described in Appendix D. The use of the computer program insured that the calculations could be repeated and that storage could be provided for the raw experimental data. The ACTIVE code was designed for operation with the foil files discussed in Section 2.3 and with the automatic sample changer described in Section 2.6. Routine corrections were made by the code for background, counter dead time, decay during counting, decay from an arbitrary time and the weight of the foil.

For the intracellular activation experiments, a height correction factor was used to correct the activities of the cadmium-covered foils to activities corresponding to the height of the bare foils in the lattice. The corrections were based on the axial flux distributions measured by Kim (K4) and by Harrington (H3). The results of these axial buckling experiments indicated that the cadmium ratio for gold foils was constant in the region in which the intracellular measurements were made.

The experimental data were corrected for radial leakage by multiplying each experimental activity by a J_o-correction factor, based on the radial flux distribution measured in the buckling experiments by Kim (K4) and Harrington (H3). The number of cells along a radius of the exponential tank was large enough so that the greatest correction was less than 3%.

CHAPTER III
ANALYTICAL METHODS

3.1 METHODS OF SOLUTION OF THE SPACE-DEPENDENT TRANSPORT EQUATION

The analytical methods needed for the interpretation of the intracellular activation measurements are developed and discussed in this chapter. The comparison with experiment will be made in Chapter IV.

To predict the subcadmium, intracellular, activation distribution, it is necessary to be able to calculate the directional flux as a function of energy and position in the lattice cell. Several computer programs have been developed to treat the problem numerically, and the more useful ones will be reviewed.

The energy exchange kernel will be considered arbitrary; that is, only the spatial part of the calculation will be discussed in this section. The choice of a computer program depends on the amount of computer time that one is willing to spend; the more nearly exact the method, the longer the computer time required. Probably the most rapid method developed so far for computing space-dependent spectra for lattice cells is the variational method used as the basis for the SWAKRAUM code developed by Calame and Federighi (C1, C2). By using a non-self-adjoint variational method, the P_1 spherical harmonic multigroup equations (W2) are reduced to a few coupled Helmholz equations, the number depending on the number of trial spectra chosen. The space-dependent neutron spectrum is taken as a linear combination of the trial spectra. The coefficients of the linear combination are determined from the variational condition for a stationary absorption rate. The present version of SWAKRAUM includes an option for treating the spatial calculation in double spherical harmonic expansion (Y2, Z1) of order unity (double-P_1) or P_3 for slabs. Further work on the variational method has been done by Buslik (B15). The basic weakness with the variational method is that the final solution is sensitive to the choice of the trial spectra.

An alternative to the variational method involves the direct, iterative solution of the multigroup P_1 equations; ULCER (R1) and SLOP-1 (B9) are good examples of the use of multigroup diffusion theory. The SLOP-1 code has an option for the double-P_1 or P_3 approximations in slabs, but the treatment for cylinders is restricted to diffusion theory. Little incentive exists for extending the spherical harmonic treatment beyond the P_1-approximation for cylinders.

The TET code (D4) offers the desired degree of transport approximation for slabs. The code incorporates a form of the discrete ordinate method (G3) in that it uses six quadrature angles in the forward and in the backward directions. This order of approximation is considered to be equivalent to a double-P_5 approximation. Eventually, the code will incorporate terms up to the P_3-scattering term, with a P_3-source; but the method is not likely to be extended to cylinders in this form.

The S_n method developed by Carlson (C3, C4) has received much attention in recent years. This method can be considered to be a form of a discrete ordinate solution to the transport equation. It has been reported that a version of the SNG code, in the S_8-approximation for cylinders, has been used with good results (M1). Another version of the method has been extended to include the effects of anisotropic scattering up to the P_3-scattering component of the energy exchange kernel (A2).

The integral transport method has been programmed by Honeck as the basis of the THERMØS code (H8). The program treats slabs and cylinders with the assumption that the scattering is isotropic in the laboratory system. For slabs, Honeck has extended the method to include the effects of the P_1-scattering component of the energy exchange kernel (H9, H12).

The Monte Carlo method probably offers the most nearly exact method of solution. The accuracy depends on the number of case histories considered and, therefore, depends on the computer time used; TRAM (P6) is a good example of a computer program based on this method.

In most of the calculations discussed in this report, the THERMØS code has been used because of its proven usefulness (B12, B13) and the possibility of close cooperation with the Reactor Theory Group of the Brookhaven National Laboratory, where Honeck is developing the method further. Only the details of the method relevant to the work are considered;

for a more detailed discussion, the published literature should be consulted (H5, H6, H7).

The THERMØS calculation involves a direct, numerical solution of the integral Boltzmann equation for cylinders. It is assumed that the flux is independent of the axial position and that the boundary of the cylindrical cell is perfectly reflecting. The cell is divided into concentric regions, with a maximum of 20 permitted, because of computer storage requirements. Thirty thermal energy groups are considered. The source of thermal neutrons in the cell is usually taken to be that from a spatially flat, 1/E-distribution above 0.78 ev. The scattering is assumed to be isotropic, but the scattering kernel is arbitrary. The program reads the cross section information from a magnetic tape, thus eliminating the necessity for generating an energy exchange kernel each time a new problem is considered, and reducing the chance of errors due to the handling of punched cards. The final solution involves a direct iterative procedure until the scalar flux, $\phi(E,r)$, converges.

3.2 THE ENERGY EXCHANGE KERNELS FOR HEAVY WATER

The purpose of this section is to investigate the sensitivity of the spatially-dependent energy spectrum to the scattering model used. Information concerning this dependence should be helpful in the interpretation of the intracellular flux traverses. The energy exchange kernel involves the details of the scattering probability for neutron transfer from any initial energy to any final energy when the neutron interacts with a moderator molecule.

The development of the theory began with the work of Wigner and Wilkins (W4). Assuming that the atoms of the molecule can be treated as free, monotomic gas atoms, they derived an analytical expression for the scattering kernel, $\sigma_s(E_i \rightarrow E_f)$, for neutrons in a gas of atoms of arbitrary mass. They assumed that $\sigma_s(v_r)$, where v_r is the relative velocity between the neutron and target, is constant. This kernel, with a mass of two, is valid for a deuterium gas; it will be referred to as the Mass-Two kernel.

Brown and St. John (B11) recognized that they could obtain a solution for the scattering kernel for the case:

$$\sigma_s(v_r) = \sum_I A_i \exp(-\kappa_i v_r^2), \qquad (3.2.1)$$

where A_i and κ_i are constants that can be adjusted to fit the measured total scattering cross section for heavy water:

$$\sigma_s(v_r) = \int_0^\infty \sigma_s(E_i \rightarrow E_f)\, dE_f . \qquad (3.2.2)$$

They tried to account for the chemical binding of the deuterium atoms by considering the D_2O molecule to be a rigid rotator. With this assumption, the "effective" mass of D_2O to be used as the mass in the free gas model was 3.595. The scattering kernel used by Brown and St. John will be referred to as the BSJ kernel or as the Mass-3.595 kernel.

The theory of the scattering kernel was extended by Nelkin (N1,N2, N3,N4,N5,K7), who developed an incoherent scattering model for the H_2O molecule, which took into account the effects of chemical binding. He derived an expression for the differential scattering cross section, $\sigma_s(E_i \rightarrow E_f, \mu)$, where μ is the cosine of the angle between the directions of the incident neutron and the scattered neutron, which can be expanded in terms of Legendre polynomials in μ:

$$\sigma_s(E_i \rightarrow E_f, \mu) = \sigma_s(E_i \rightarrow E_f) + \frac{3}{2}\mu\sigma_{s_1}(E_i \rightarrow E_f) \ldots \qquad (3.2.3)$$

The model assumes that the H_2O molecule can be treated as a combination of a translator, a hindered rotator, and vibrational oscillators. Experimental data were used to evaluate the parameters describing the rotator and the oscillators.

Honeck (H10) has extended the Nelkin model to D_2O by replacing the experimental data for H_2O with those for D_2O. Table 3.2.1 gives a comparison of the parameters for H_2O and D_2O. Honeck notes that D_2O scatters more coherently than H_2O, but he concludes that the error introduced by the assumption of incoherent scattering should be small for $\sigma_s(E_i \rightarrow E_f)$. Figure 3.2.1 shows a comparison of the observed scattering cross section with the predictions of the Honeck-Nelkin model for D_2O. The failure to consider the coherent scattering is the cause of the disagreement in the low energy range.

The validity of the energy exchange kernel can be tested experimentally. The differential scattering kernel can be measured directly in the "Scattering Law" experiments reviewed by Eglestaff (E1, E2); Goldman

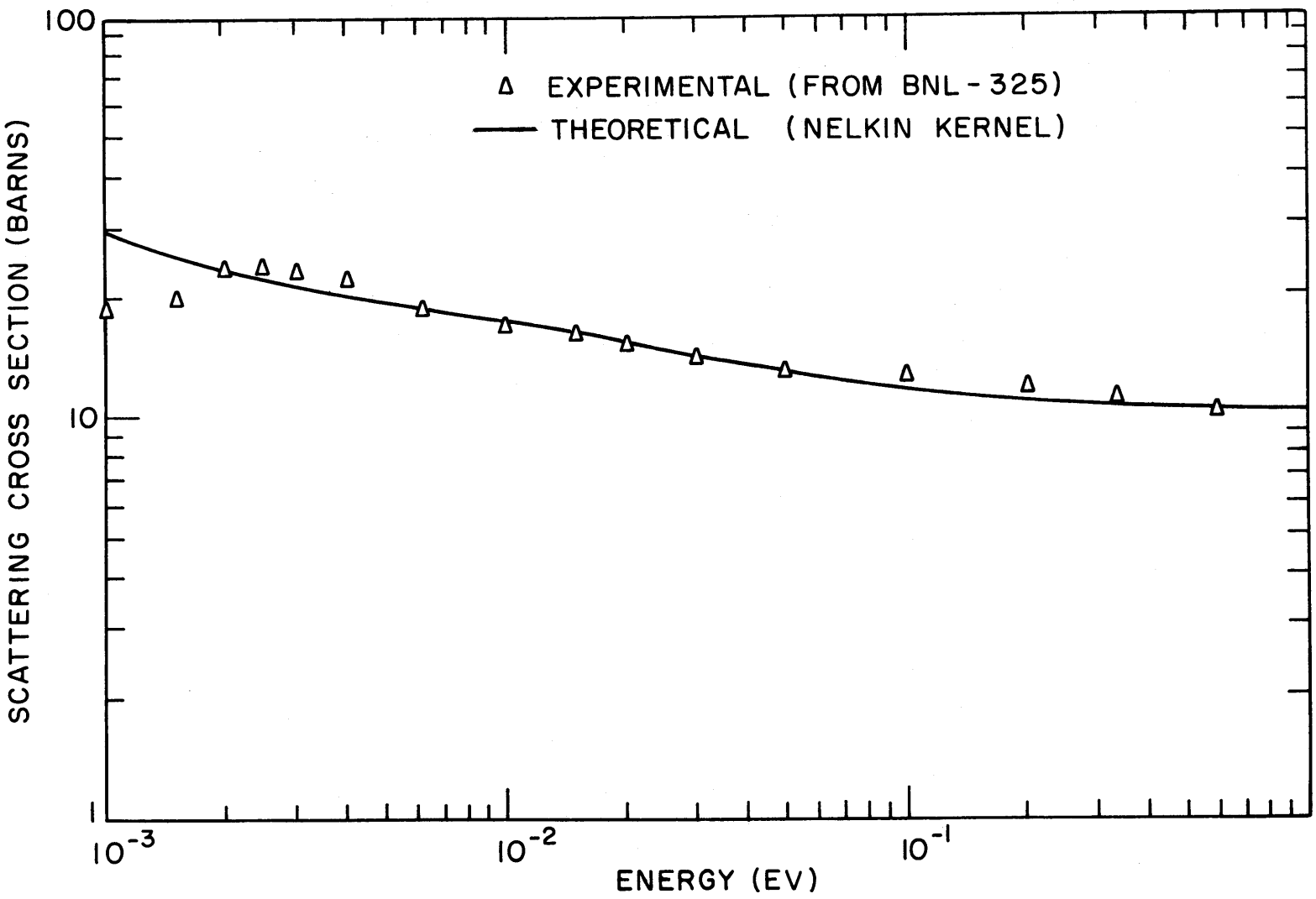

FIG. 3.2.1 THE MEASURED AND CALCULATED TOTAL SCATTERING CROSS SECTION OF HEAVY WATER.

TABLE 3.2.1
Constants for H_2O and D_2O

Constant	H in H_2O	D in D_2O
ω_r, energy of the rotator	0.06 ev	0.05 ev
ω_{v1}, energy of the 1st vibrator	0.205 ev	0.15 ev
$\omega_{v2} = \omega_{v3}$	0.480 ev	0.35 ev
M_t, mass of the translator	18.0	20.0
M_r, mass of the rotator	2.32	4.11
$M_{v1} = M_{v2} = M_{v3}$	5.84	4.52

and Federighi (G2) discuss one such comparison. An indirect measure can be made by comparing the calculated infinite-medium spectra with the spectra measured by Beyster (B4, B5, B6, B7, B8), Young (Y1) or Poole (P7, P8, P9). The latter experiments work best for poisoned moderators because, in a pure moderator, the spectrum is very close to a Maxwellian distribution regardless of the scattering model assumed. This comes about because the scattering kernel satisfies the condition of detailed balance, which places on the kernel the constraint that, in an infinite medium with no absorption, the spectrum is a Maxwellian distribution at the moderator temperature (W4). For H_2O systems, the Nelkin model leads to results which compare favorably with experiment.

Honeck has considered terms up to order P_3 for the differential scattering cross section of D_2O in calculations of the diffusion coefficient and the diffusion cooling coefficient measured in pulsed neutron experiments. The comparison of the calculations and the experiment are discussed by Malaviya and Profio (M3). It seems likely that the Nelkin model with the Honeck parameters is the best one available for D_2O.

The calculated kernels for D_2O are compared in Figs. 3.2.2 and 3.2.3. They are expressed as $P(E_i \rightarrow E_f)$, the probability per unit energy interval that a neutron of initial energy E_i will have energy E_f after a collision with a moderator atom; $P(E_i \rightarrow E_f)$ satisfies the normalization condition, $\int_0^\infty dE_f P(E_i \rightarrow E_f) = 1$. $P(E_i \rightarrow E_f)$ is related to $\sigma_s(E_i \rightarrow E_f)$ by:

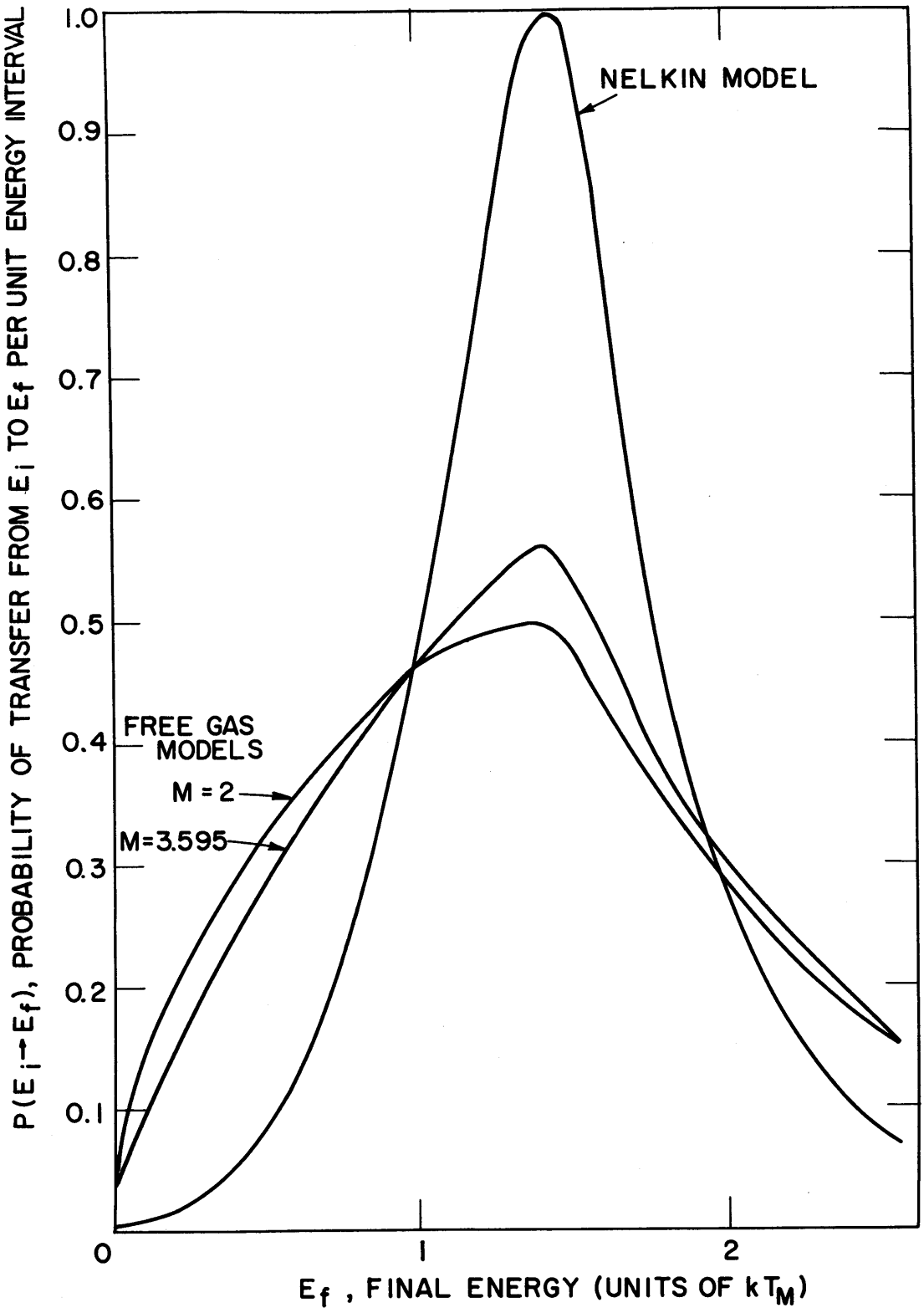

FIG.3.2.2 COMPARISON OF THE NELKIN AND FREE GAS ENERGY EXCHANGE KERNELS FOR HEAVY WATER FOR NEUTRONS HAVING AN INITIAL ENERGY, E_i, OF 1.44 kT_M.

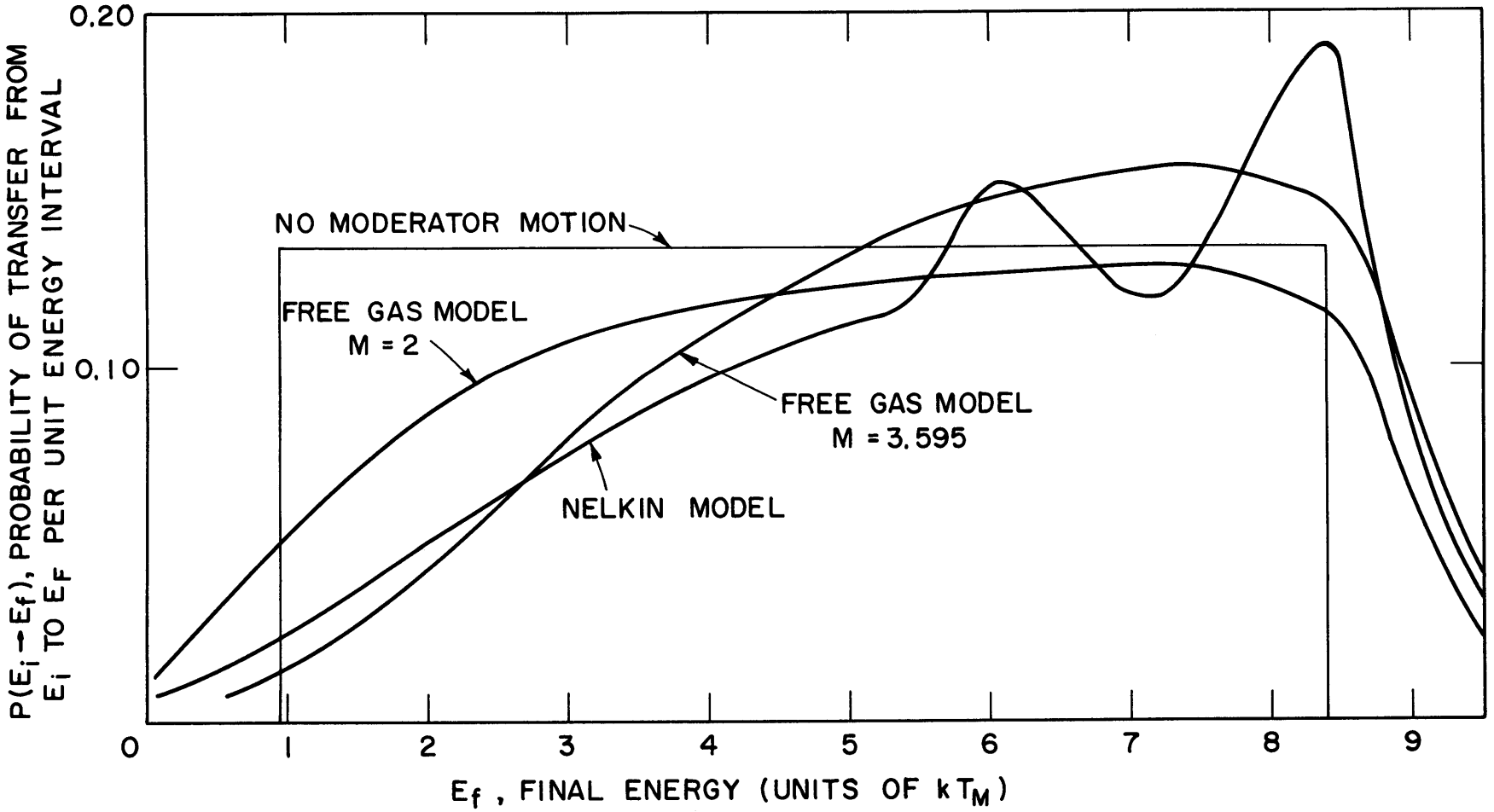

FIG. 3.2.3 COMPARISON OF THE NELKIN AND FREE GAS ENERGY EXCHANGE KERNELS FOR HEAVY WATER FOR NEUTRONS HAVING AN INTIAL ENERGY, E_i, OF 8.4 kT_M.

$$P(E_i \rightarrow E_f) = \frac{\sigma_s(E_i \rightarrow E_f)}{\sigma_s(E_i)} . \qquad (3.2.4)$$

The curves of Fig. 3.2.2 correspond to an initial energy, E_i, equal to 1.44 kT_M, where T_M is the moderator temperature. At this energy, the Nelkin kernel is more sharply peaked about E_i than either of the free gas kernels. The shapes of the curves are also different, a result which is not surprising since the Nelkin kernel should predict harder spectra because of the greater probability of small energy transfers.

At the higher initial energy considered in Fig. 3.2.3, the Nelkin model differs markedly from the two free gas models. The difference in the two peak energies of the Nelkin kernel corresponds to the energy transfer of neutrons that excite the rotational level of the D_2O molecule. These types of energy transfers are not considered in the free gas model; consequently, the gas model has only one peak, at the initial energy.

The THERMØS code is restricted to isotropic scattering. In an effort to estimate the effect of the neglect of the higher order terms of the scattering kernel, the following approximations were made:

(1) $\sigma_s(E_i \rightarrow E_f)$ was multiplied by $(1-\bar{\mu})$ where $\bar{\mu} = 2/3A_{eff}$ with A_{eff} as 3.595; this correction will be called the "$\bar{\mu}$ correction."

(2) The diagonal elements of $\sigma_s(E_i \rightarrow E_f)$ were adjusted so that the numerically integrated value of the kernel would correspond to the transport cross section, $\sigma_{tr}(E_i)$, as calculated from the Honeck-Nelkin model:

$$\sigma_s^*(E_i \rightarrow E_i) = \sigma_s(E_i \rightarrow E_i) - \int_0^\infty \sigma_{s_1}(E_i \rightarrow E_f)\, dE_f \Big/ \Delta E_i . \qquad (3.2.5)$$

The second procedure appears to be more realistic. (The oxygen of the D_2O molecule was treated as a free gas of mass 16.)

The THERMØS code, with the various energy exchange kernels discussed in this section, has been used in calculations made for the lattices investigated experimentally at M.I.T. The results indicate that the predicted values for the quantities that can be measured are not significantly affected by the details of the scattering model. Figure 3.2.4 shows the calculated spectra for the Nelkin and the Brown-St. John kernels at the center of a fuel rod in a lattice moderated by heavy water. The spectra

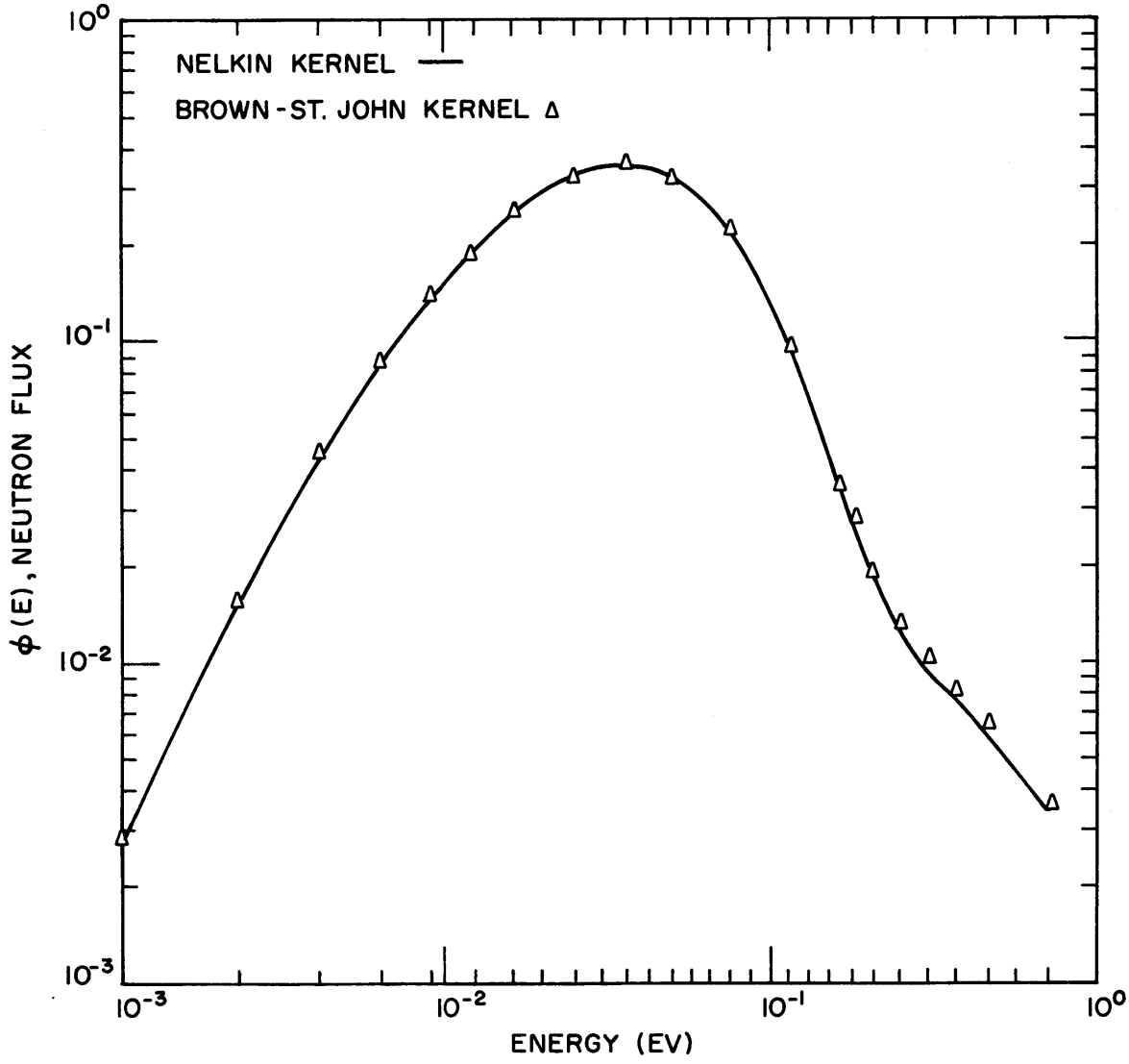

FIG. 3.2.4 THE CALCULATED THERMAL NEUTRON SPECTRA AT THE CENTER OF A 1.01-INCH DIAMETER, NATURAL URANIUM ROD IN A LATTICE ON A 4.5-INCH TRIANGULAR SPACING.

are nearly indistinguishable. The spectra are normalized so that one neutron is absorbed in the cell below 0.78 ev.

Tables 3.2.2 to 3.2.5 show the calculated results for the over-all disadvantage factors for a 1/v-activator, lutetium and europium:

$$\zeta = \frac{\int_{\text{mod}} dr \int_0^{E_c} dE\, \sigma_{ACT}(E)\, \phi(E,r)}{\int_{\text{fuel}} dr \int_0^{E_c} dE\, \sigma_{ACT}(E)\, \phi(E,r)} . \qquad (3.2.6)$$

The upper limit for the integration, E_c, is given in the tables as the cutoff energy. The values of η and f are also listed, although they cannot be measured directly for the lattice. The ratio of fissions in plutonium-239 to fissions in uranium-235 is included; it has been calculated on the assumption that the plutonium has no effect on the spectrum.

The most sensitive measurement in the lattice cell that can be made conveniently is the intracellular activation distribution. The results of the calculations are given in Tables 3.2.6 to 3.2.10. Apart from the Mass-Two kernel, the various kernels gave results that differ by no more than 3% for the activation distribution in the natural uranium lattices, and 2% in the lattices of uranium rods containing 1.03% U^{235}.

Nelkin (N6) has suggested that the results were insensitive to the kernel used because the lattices investigated at M.I.T. were well-moderated. Results of calculations in graphite-moderated lattices are discussed in Appendix E. Graphite is not as good a moderator as heavy water and the details of the energy exchange kernel should be more important. The results of Appendix E indicate that this is the case.

3.3 ANALYTICAL TREATMENT OF THE RADIAL AND AXIAL LEAKAGE IN AN EXPONENTIAL ASSEMBLY

In this section, a method is developed for calculating the intracellular flux distribution measured in an exponential assembly. The analysis should also be helpful in the determination of the size of an exponential assembly in which the intracellular flux distribution can be "corrected" to give the distribution in an infinite assembly. It is assumed that the radial and axial effects are separable. Although the method is specifically designed for use with the THERMØS code, generalization to other methods should be simple.

TABLE 3.2.2

Comparison of Calculated Nuclear Properties in a Lattice of 1.01-Inch Diameter, Natural Uranium Rods on a 4.5-Inch Triangular Spacing.

Quantity	Cutoff Energy (ev.)	Mass-Two Kernel	Brown-St. John Kernel	Honeck-Nelkin Kernel	Honeck-Nelkin Kernel, $\bar{\mu}$ Correction	Honeck-Nelkin Kernel, Diagonal Correction
$\zeta_{1/v}$ (a)	0.4	1.791	1.770	1.763	1.732	1.750
ζ_{Lu-176} (a)	0.4	1.565	1.543	1.540	1.519	1.528
ζ_{Eu-151} (a)	0.14	1.950	1.925	1.925	1.890	1.870
f	0.78	0.9846	0.9848	0.9848	0.9849	0.9848
η	0.78	1.334	1.333	1.333	1.332	1.333
$\bar{\sigma}^F_{Pu-239}/\bar{\sigma}^F_{U-235}$ (b)	0.78	1.56	1.64	1.62	1.68	1.62

(a) ζ is the over-all disadvantage factor.

(b) Fissions in plutonium per fission in U^{235}.

TABLE 3.2.3

Comparison of Calculated Nuclear Properties in a Lattice of 1.01-Inch Diameter, Natural Uranium Rods on a 5.0-Inch Triangular Spacing.

Quantity	Cutoff Energy (ev.)	Mass-Two Kernel	Brown-St. John Kernel	Honeck-Nelkin Kernel	Honeck-Nelkin Kernel, $\bar{\mu}$ Correction	Honeck-Nelkin Kernel, Diagonal Correction
$\zeta_{1/v}$ (a)	0.4	1.820	1.795	1.799	1.760	1.778
ζ_{Lu-176} (a)	0.4	1.590	1.568	1.562	1.535	1.550
ζ_{Eu-151} (a)	0.14	1.980	1.955	1.945	1.918	1.938
f	0.78	0.9824	0.9826	0.9826	0.9828	0.9827
η	0.78	1.335	1.334	1.334	1.334	1.335
$\bar{\sigma}^F_{Pu-239}/\bar{\sigma}^F_{U-235}$ (b)	0.78	1.52	1.59	1.57	1.62	1.58

(a) ζ is the over-all disadvantage factor.

(b) Fissions in plutonium per fission in U^{235}.

TABLE 3.2.4

Comparison of Calculated Nuclear Properties in a Lattice of 1.01-Inch Diameter, Natural Uranium Rods on a 5.75-Inch Triangular Spacing.

Quantity	Cutoff Energy (ev.)	Mass-Two Kernel	Brown-St. John Kernel	Honeck-Nelkin Kernel	Honeck-Nelkin Kernel, $\bar{\mu}$ Correction	Honeck-Nelkin Kernel, Diagonal Correction
$\zeta_{1/v}$ (a)	0.4	1.864	1.840	1.835	1.793	1.795
ζ_{Lu-176} (a)	0.4	1.625	1.600	1.595	1.565	1.560
ζ_{Eu-151} (a)	0.14	2.020	2.000	2.000	1.950	1.952
f	0.78	0.9787	0.9789	0.9789	0.9792	0.9792
η	0.78	1.338	1.335	1.335	1.338	1.336
$\bar{\sigma}^F_{Pu-239}/\bar{\sigma}^F_{U-235}$ (b)	0.78	1.48	1.53	1.52	1.57	1.56

(a) ζ is the over-all disadvantage factor.

(b) Fissions in plutonium per fission of U^{235}.

TABLE 3.2.5

Comparison of Calculated Nuclear Properties in a Lattice of 0.25-Inch Diameter, 1.03% U^{235}, Uranium Rods on a 1.25-Inch Triangular Spacing.

Quantity	Cutoff Energy (ev.)	Mass-Two Kernel	Brown-St. John Kernel	Honeck-Nelkin Kernel	Honeck-Nelkin Kernel, $\bar{\mu}$ Correction	Honeck-Nelkin Kernel, Diagonal Correction
$\zeta_{1/v}$ (a)	0.4	1.252	1.245	1.262	1.262	1.260
ζ_{Lu-176} (a)	0.4	1.183	1.178	1.213	1.192	1.194
ζ_{Eu-151} (a)	0.14	1.291	1.292	1.315	1.313	1.304
f	0.78	0.9774	0.9784	0.9784	0.9784	0.9773
η	0.78	1.491	1.500	1.505	1.505	1.504
$\bar{\sigma}^F_{Pu-239}/\bar{\sigma}^F_{U-235}$ (b)	0.78	1.57	1.67	1.66	1.72	1.65

(a) ζ is the over-all disadvantage factor.

(b) Fissions in plutonium per fission in U^{235}.

TABLE 3.2.6

Intracellular Activity Distribution Below 0.4 ev. for a 1/v-Activator in a Lattice of 1.01-Inch Diameter, Natural Uranium Rods on a 4.5-Inch Triangular Spacing.

Point	Radial Position (cm.)	Mass-Two Kernel	Brown-St. John Kernel	Honeck-Nelkin Kernel	Honeck-Nelkin Kernel, $\bar{\mu}$ Correction	Honeck-Nelkin Kernel, Diagonal Correction
1	0.000	1.000	1.000	1.000	1.000	1.000
2	0.284	1.018	1.018	1.018	1.018	1.018
3	0.568	1.067	1.066	1.065	1.065	1.066
4	0.853	1.161	1.157	1.156	1.156	1.158
5	1.137	1.332	1.325	1.323	1.322	1.326
6	1.324	1.520	1.508	1.504	1.504	1.509
7	1.658	1.726	1.705	1.699	1.691	1.701
8	2.236	1.920	1.890	1.885	1.864	1.881
9	2.815	2.030	1.996	1.991	1.961	1.983
10	3.394	2.104	2.065	2.062	2.024	2.049
11	3.972	2.164	2.123	2.121	2.078	2.105
12	4.551	2.208	2.166	2.164	2.119	2.147
13	5.130	2.240	2.198	2.196	2.149	2.178
14	5.708	2.265	2.222	2.220	2.175	2.203

TABLE 3.2.7

Intracellular Activity Distribution Below 0.4 ev. for a 1/v-Activator in a Lattice of 1.01-Inch Diameter, Natural Uranium Rods on a 5.0-Inch Triangular Spacing.

Point	Radial Position (cm.)	Mass-Two Kernel	Brown-St. John Kernel	Honeck-Nelkin Kernel	Honeck-Nelkin Kernel $\bar{\mu}$ Correction	Honeck-Nelkin Kernel, Diagonal Correction
1	0.000	1.000	1.000	1.000	1.000	1.000
2	0.284	1.018	1.018	1.018	1.018	1.018
3	0.568	1.067	1.066	1.066	1.066	1.066
4	0.853	1.162	1.159	1.157	1.157	1.159
5	1.137	1.334	1.328	1.325	1.325	1.328
6	1.324	1.523	1.513	1.508	1.508	1.512
7	1.699	1.743	1.724	1.718	1.708	1.718
8	2.361	1.939	1.911	1.906	1.881	1.899
9	3.024	2.076	2.043	2.039	2.003	2.026
10	3.686	2.137	2.101	2.099	2.056	2.081
11	4.348	2.199	2.161	2.159	2.111	2.138
12	5.010	2.244	2.204	2.203	2.152	2.180
13	5.672	2.276	2.236	2.235	2.182	2.211
14	6.334	2.299	2.258	2.258	2.206	2.234

TABLE 3.2.8

Intracellular Activity Distribution Below 0.4 ev. for a 1/v-Activator in a Lattice of 1.01-Inch Diameter, Natural Uranium Rods on a 5.75-Inch Triangular Spacing.

Point	Radial Position (cm.)	Mass-Two Kernel	Brown-St. John Kernel	Honeck-Nelkin Kernel	Honeck-Nelkin Kernel, $\bar{\mu}$ Correction	Honeck-Nelkin Kernel, Diagonal Correction
1	0.000	1.000	1.000	1.000	1.000	1.000
2	0.284	1.018	1.018	1.018	1.018	1.018
3	0.568	1.068	1.067	1.067	1.066	1.067
4	0.853	1.163	1.161	1.160	1.159	1.160
5	1.137	1.337	1.333	1.330	1.329	1.330
6	1.324	1.528	1.521	1.516	1.514	1.517
7	1.762	1.770	1.754	1.747	1.734	1.743
8	2.549	1.980	1.955	1.950	1.919	1.936
9	3.336	2.120	2.090	2.087	2.044	2.065
10	4.123	2.189	2.156	2.154	2.104	2.129
11	4.910	2.249	2.214	2.213	2.156	2.183
12	5.697	2.294	2.257	2.257	2.197	2.225
13	6.484	2.325	2.288	2.288	2.226	2.254
14	7.272	2.345	2.309	2.308	2.248	2.276

TABLE 3.2.9

Intracellular Activity Distribution Below 0.4 ev. for a 1/v-Activator in a Lattice of 1/4-Inch Diameter, 1.03% U^{235}, Uranium Rods on a 1.25-Inch Triangular Spacing

Point	Radial Position (cm.)	Mass-Two Kernel	Brown-St. John Kernel	Honeck-Nelkin Kernel	Honeck-Nelkin Kernel, $\overline{\mu}$ Correction	Honeck-Nelkin Kernel, Diagonal Correction
1	0.000	1.000	1.000	1.000	1.000	1.000
2	0.127	1.016	1.016	1.016	1.016	1.016
3	0.254	1.069	1.068	1.067	1.069	1.069
4	0.361	1.173	1.172	1.170	1.180	1.178
5	0.507	1.232	1.230	1.228	1.241	1.239
6	0.717	1.278	1.276	1.273	1.289	1.287
7	0.928	1.306	1.304	1.300	1.317	1.315
8	1.138	1.317	1.316	1.312	1.331	1.328
9	1.349	1.327	1.325	1.322	1.341	1.338
10	1.559	1.339	1.337	1.334	1.354	1.351

TABLE 3.2.10

Intracellular Activity Distribution Below 0.4 ev. for a 1/v-Activator in a Lattice of 1/4-Inch Diameter, 1.03% U^{235}, Uranium Rods on a 2.5-Inch Triangular Spacing.

Point	Radial Position (cm.)	Mass-Two Kernel	Brown-St. John Kernel	Honeck-Nelkin Kernel	Honeck-Nelkin Kernel, $\bar{\mu}$ Correction	Honeck-Nelkin Kernel, Diagonal Correction
1	0.000	1.000	1.000	1.000	1.000	1.000
2	0.127	1.015	1.015	1.015	1.015	1.015
3	0.254	1.061	1.061	1.061	1.061	1.061
4	0.361	1.146	1.146	1.146	1.148	1.148
5	0.647	1.217	1.216	1.215	1.218	1.217
6	1.135	1.260	1.258	1.257	1.260	1.260
7	1.622	1.272	1.270	1.270	1.272	1.272
8	1.970	1.279	1.278	1.277	1.281	1.281
9	2.179	1.290	1.288	1.288	1.290	1.290
10	2.388	1.291	1.289	1.289	1.291	1.291
11	2.597	1.292	1.290	1.290	1.292	1.292
12	2.806	1.294	1.292	1.292	1.294	1.294
13	3.015	1.296	1.294	1.294	1.296	1.296
14	3.224	1.297	1.295	1.295	1.296	1.297

3.3.1 THE RADIAL LEAKAGE

It is assumed that the problem of calculating the spatially dependent neutron spectrum in the radial direction is separable in space and energy on a macroscopic level. Brown (B14) has measured subcadmium and epicadmium intracellular flux distributions at different radial positions in a natural uranium lattice and has found that the variation with radial position was sufficiently small so that the assumption of separability should introduce no serious errors. Palmedo and Benoist (P2) have made similar experiments in Aquilon II lattices, but they indicate that the assumption of separability is not valid.

One problem is to calculate the intracellular flux distribution in an assembly that is finite in the radial direction only. To correct the measurements for the finite size of the assembly, the usual procedure is to divide the experimental activation at a point r by $J_o(\alpha r)$, where α is obtained from the measured radial macroscopic flux distribution. It seems more reasonable, physically, to calculate the intracellular flux distribution for the finite system, since this is what is actually measured. To do this, the present calculational schemes must be modified, since they treat an infinite array. The THERMØS calculation will now be extended to include the effect of radial leakage from the central cell of the lattice. It will be assumed that neutrons that leak out of the central cell are absorbed in a fictitious region bounding the cell as shown in Fig. 3.3.1. The absorption cross section of the outer region is so defined that the number of neutrons absorbed is equal to the net number of neutrons that leak out. The leakage is calculated at every energy by means of diffusion theory, which should be satisfactory for calculating the macroscopic flux distribution, except in a very small assembly. For these approximations,

$$\Sigma_a(E)\,\Delta R = \alpha D(E)\,\frac{J_1(\alpha R)}{J_o(\alpha R)}, \qquad (3.3.1)$$

where α is the radial buckling, R is the equivalent cell radius, ΔR is the thickness of the outer, fictitious region, Σ_a is the absorption cross section of the fictitious region, J_o and J_1 are the Bessel functions of order zero and unity, and D is the diffusion coefficient for the cell. It should be noted that $\Sigma_a \Delta R$ is a constant for any given lattice. The method can be tested by varying Σ_a and ΔR, while keeping the product of the two constant, to

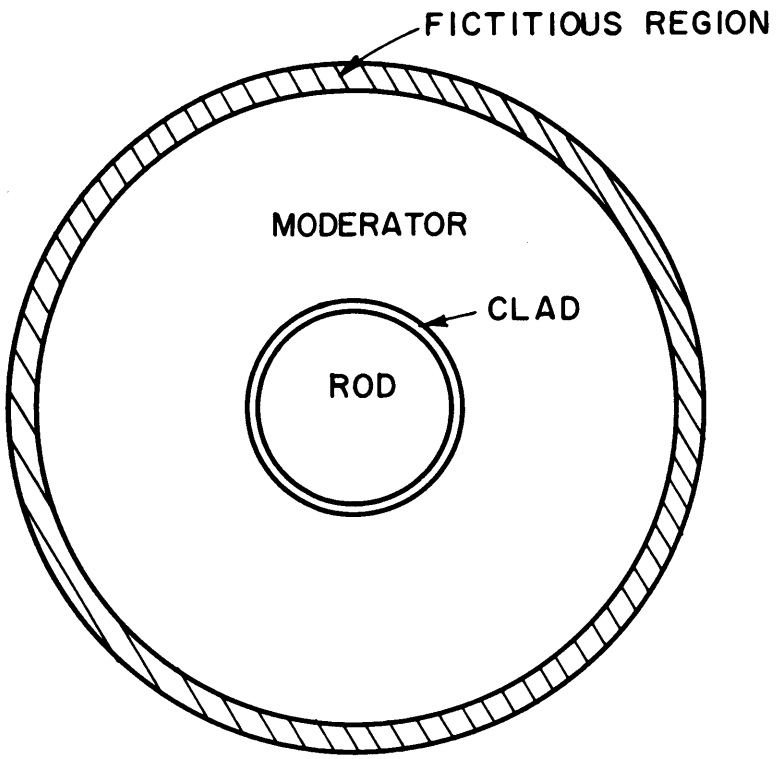

FIG. 3.3.1 THE FICTITIOUS ABSORBING REGION USED TO ACCOUNT FOR RADIAL LEAKAGE IN THE LATTICE CELL.

determine if the calculations give the same absorption rates. This has been done, and the results indicate that the procedure does not depend on the choice of ΔR, so long as $\Delta R \ll R$. For the cases studied, ΔR was fixed at 0.2 cm.

The radial buckling was taken from the measured values of Palmedo (P1) and was assumed to be the same at all energies. The diffusion coefficient for D_2O as a function of energy was calculated from the P_o and P_1 components of the Honeck-Nelkin model for the scattering of slow neutrons in D_2O:

$$D(E) = \frac{1}{3N\left[2\sigma^D_{s_o}(E) - 2\sigma^D_{s_1}(E) + \sigma^o_{tr}\right]}, \tag{3.3.2}$$

where σ^o_{tr}, the transport cross section of oxygen, is 3.58 barns, N is the atom density of oxygen,

$$\sigma^D_{s_o} = \int_{\text{all } E_f} dE_f \int_{-1}^{1} d\mu\, \sigma_s(E \rightarrow E_f, \mu), \tag{3.3.3}$$

and

$$\sigma^D_{s_1} = \int_{\text{all } E_f} dE_f \int_{-1}^{1} d\mu\, \mu\, \sigma_s(E \rightarrow E_f, \mu); \tag{3.3.4}$$

$\sigma_s(E \rightarrow E_f, \mu)$ is the differential scattering cross section for D_2O. Table 3.3.1 gives the values of $D_1(E)$ for D_2O and for H_2O, calculated from the Nelkin model and Eq. (3.3.2).

The values for $\overline{D}_1$ and $1/3\overline{\Sigma}_{tr}$ for mixtures of H_2O and D_2O averaged over a Maxwellian spectrum at the moderator temperature (0.0253 ev) are given in Fig. 3.3.2. Comparisons can be made with the results of integral experiments, such as pulsed neutron or poisoning experiments, to check the average value of $\overline{D}_1$. Bauman (B1) quotes a value of 0.84 ± 0.01 cm for $\overline{D}_1$. The calculated value of $\overline{D}_1$ was 0.849 and for $1/3\overline{\Sigma}_{tr}$ was 0.826. Although the agreement is for the average values, the calculations are not inconsistent with the experiment.

It is necessary to calculate D for the cylindrical cell for use in Eq. (3.3.1). For the one-velocity case, the problem has been treated by Selengut (S1), who used an electrical analogy to neutron diffusion and obtained the result:

TABLE 3.3.1

Values of the Diffusion Coefficient for H_2O and D_2O Calculated by the Nelkin Model for Slow Neutron Scattering

Group	Energy (ev)	Diffusion Coefficient (D:cm)	
		D_2O	H_2O
1	0.00025	0.2241	0.02231
2	0.00101	0.3729	0.03994
3	0.00228	0.4657	0.05274
4	0.00405	0.5270	0.06238
5	0.00632	0.5725	0.07043
6	0.00911	0.6111	0.07800
7	0.01240	0.6476	0.08581
8	0.01619	0.6847	0.09434
9	0.02049	0.7236	0.1039
10	0.02530	0.7651	0.1150
11	0.03061	0.8084	0.1276
12	0.03643	0.8506	0.1419
13	0.04276	0.8864	0.1568
14	0.04959	0.9114	0.1705
15	0.05692	0.9267	0.1804
16	0.06517	0.9386	0.1864
17	0.07485	0.9534	0.1906
18	0.08612	0.9739	0.1971
19	0.09919	0.9962	0.2082
20	0.11398	1.015	0.2213
21	0.13123	1.034	0.2326
22	0.15248	1.055	0.2436
23	0.17901	1.073	0.2595
24	0.21241	1.097	0.2750
25	0.25464	1.120	0.2925
26	0.30816	1.145	0.3112
27	0.37598	1.169	0.3358
28	0.46183	1.186	0.3591
29	0.57023	1.197	0.3841
30	0.70666	1.205	0.4080

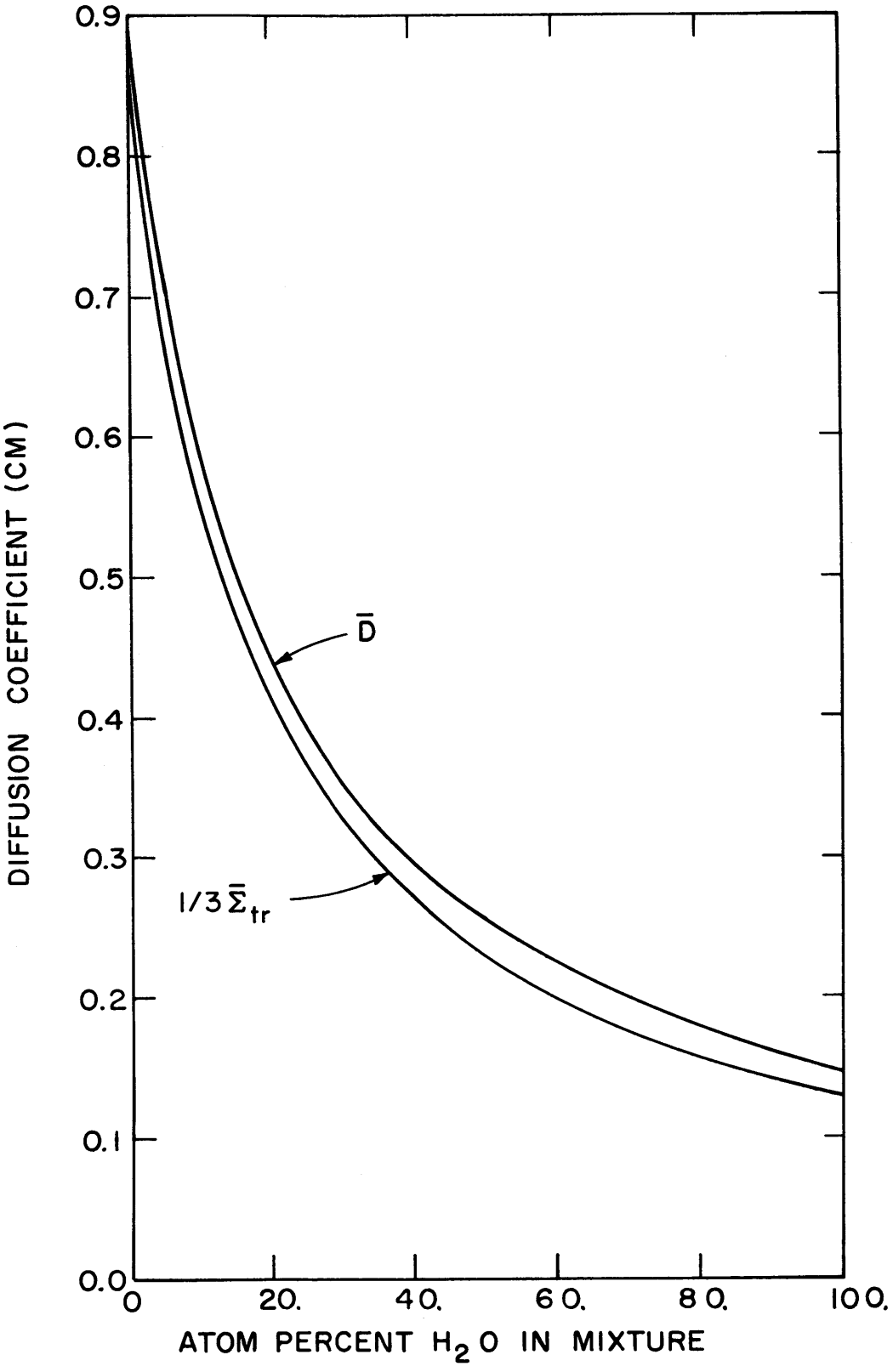

FIG. 3.3.2 MAXWELLIAN AVERAGE DIFFUSION COEFFICIENTS FOR MIXTURES OF LIGHT AND HEAVY WATER.

$$D = \frac{(1-n\beta\epsilon_n)}{(1-\beta\epsilon_n)} D_1 , \tag{3.3.5}$$

where

$$\epsilon_n = \frac{D_1 - D_o}{nD_1 + D_o} ; \tag{3.3.6}$$

β is the volume fraction of the region designated by 0 (the fuel rod here); n is an index which is 0, 1, or 2 for slabs, cylinders or spheres, respectively. For D_o much greater than D_1, D reduces to $\left(\frac{1+\beta}{1-\beta}\right) D_1$ for cylinders.

For the 1-inch natural uranium rods arranged on a 4.5-inch triangular spacing, the value of D is equal to 0.998 D_1, as calculated from Eq. (3.3.5). In view of the approximations in the method, it seems reasonable to take D equal to D_1, the moderator diffusion coefficient, thus assuming the rod to be as effective as the moderator. With R equal to 0.2 cm, Eq. (3.3.1) reduces to:

$$\Sigma_a(E) = 5\alpha D_1(E)\, J_1(\alpha R) \Big/ J_o(\alpha R) \text{ cm}^{-1} . \tag{3.3.7}$$

As a demonstration of the method, the intracellular flux traverse was calculated, in the single-velocity approximation, for the natural uranium lattice of 1.01-inch diameter rods on a 5.75-inch triangular spacing. The cross sections used were the 2200 m/sec values given in BNL-325. Figure 3.3.3 shows the results for three values of the radial buckling. When the radial buckling is equal to zero, the calculation corresponds to the infinite case. As the radial buckling increases, the flux in the moderator decreases. When the calculated flux is divided by $J_o(\alpha r)$, as in the procedure usually adopted, the "corrected" flux corresponds to the flux in the infinite case.

The revised method with thirty energy groups was next applied to several lattices studied by the M.I.T. Lattice Project. Experimental values of the radial buckling were used along with the Honeck-Nelkin kernel with the diagonal elements adjusted. The results were compared to the calculated results for the infinite radial lattices by dividing the finite calculated values by $J_o(\alpha r)$ for each point r. No noticeable difference was evident, indicating that the usual "experimental correction" to the infinite system is justified.

The method also allowed an estimate to be made of the diffusion

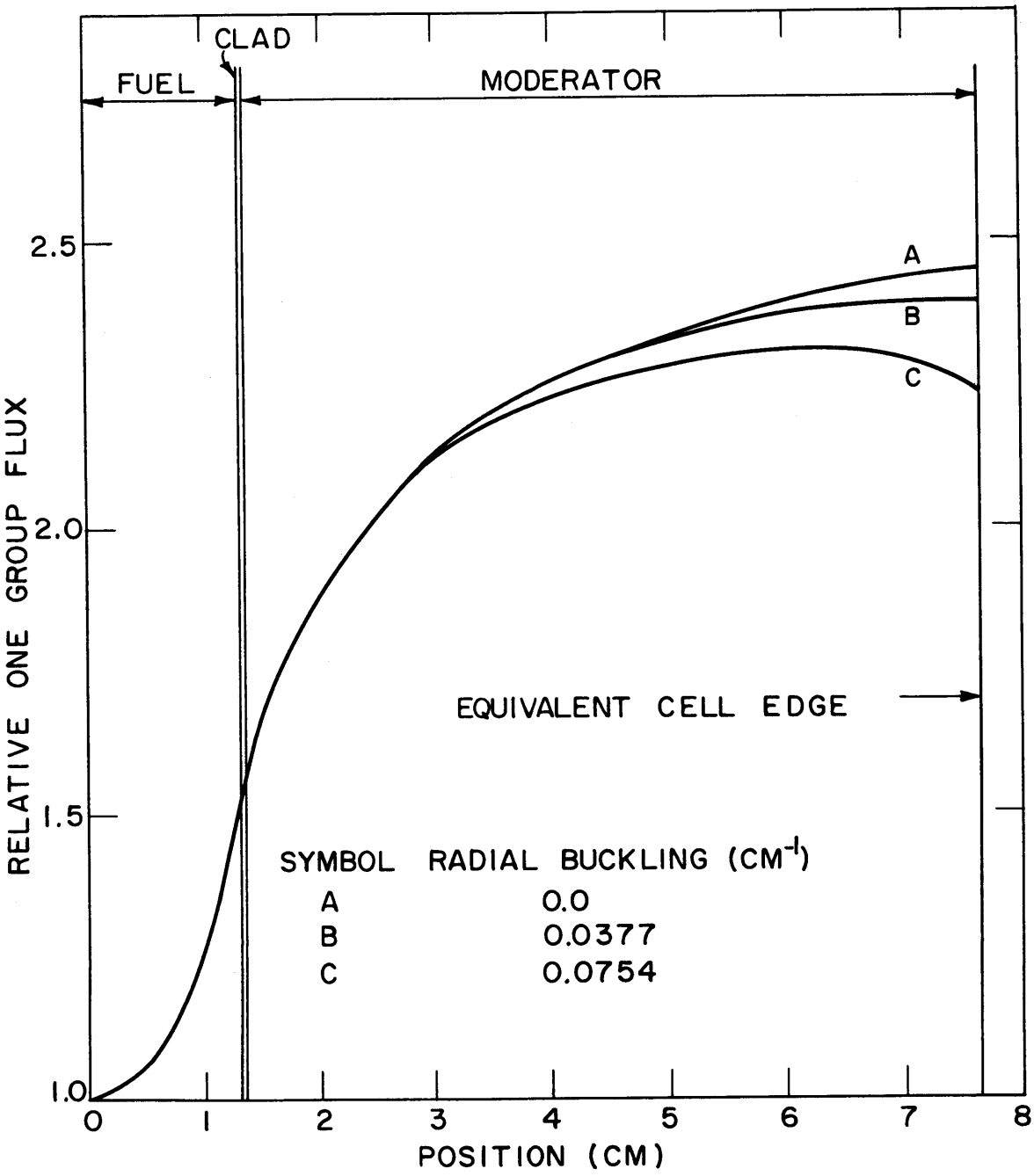

FIG. 3.3.3 COMPARISON OF THE ONE GROUP FLUX WITH THE VARIATION OF THE RADIAL BUCKLING.

length. If the calculation with the fictitious region gives the thermal utilization in the finite system, f_f, then the radial thermal diffusion length, L_r^2, is not needed to calculate k_{eff} for the lattice. However, L_r^2 may be defined by the relation:

$$f_f = \frac{f_\infty}{1 + L_r^2 a^2} . \tag{3.3.8}$$

To obtain a value for L_r^2, two THERMØS calculations must be made, one for the finite case and the other for the infinite case. Of course, the value of L_r^2 will be a function of the radial buckling. Table 3.3.2 gives the calculated results for the M.I.T. lattices. A common method for the calculation of L_r^2 is to find average values of the absorption and transport cross sections for the cell, and take L_r^2 equal to $1/3\overline{\Sigma}_a\overline{\Sigma}_{tr}$. The values obtained for $1/3\overline{\Sigma}_a\overline{\Sigma}_{tr}$ are included in Table 3.3.2. The values obtained for L_r^2 by both methods are within 10% for the natural uranium lattices, but are about 20% different for the lattice with rods with 1% U^{235}. Further work in this area is necessary before more definite conclusions can be reached.

TABLE 3.3.2

Calculated Values of the Thermal Diffusion Length for the M.I.T. Lattices

Lattice Spacing (in.)	U-235 Concentration (%)	a^2 (m^{-2})	L_r^2 (cm^2)	$\overline{\Sigma}_a$ (cm^{-1})	$\overline{\Sigma}_{tr}$ (cm^{-1})	$1/3\overline{\Sigma}_a\overline{\Sigma}_{tr}$ (cm^2)
4.50	Natural	14.10	99.4	0.00762	0.397	110.
5.00	Natural	14.12	127.	0.00617	0.400	135.
5.75	Natural	14.20	159.	0.00468	0.403	177.
1.25	1.03	13.83	67.5	0.0103	0.387	83.5
2.50	1.03	—	—	0.00302	0.405	273.

3.3.2 THE AXIAL LEAKAGE

In an exponential assembly, neutrons leak into the assembly at the bottom and out at the top and sides. In this sense, the leakage is a negative leakage, and the nature of the problem is different from that in a critical

assembly. Tralli and Agresta (T4) have calculated the flux distribution and thermal utilization in a critical system by using the P_3-approximation.

The method developed in this section involves a modification of the THERMØS code, whereas the radial correction could be treated with the existing version of the code. THERMØS calculates numerically the transport kernel describing the probability of transfer from a point in a cylinder to any other point. The method involves the assumption that the flux distribution in the axial direction is independent of the axial position. The probability, $F(\lambda)$, is then calculated that a neutron emitted from an infinite line source will reach a position d, λ mean free paths away:

$$F(\lambda) = \int_0^{\pi/2} e^{-\lambda \sec\theta} \cos\theta \, d\theta , \tag{3.3.9}$$

where $\lambda = \int_0^d \Sigma \, dr$, mean free paths. If the axial source distribution is assumed to be exponential from $-\infty$ to ∞, then the modified probability is:

$$F(\lambda,a) = \int_0^{\pi/2} \cosh(\lambda a \tan\theta) \; e^{-\lambda \sec\theta} \cos\theta \, d\theta , \tag{3.3.10}$$

where a is $\frac{\gamma d}{\lambda}$, and γ is the inverse of the axial relaxation length. Expansion of Eq. (3.3.10) in terms of the argument of the hyperbolic cosine indicates that the error introduced by neglecting the variation of the axial flux distribution introduces only quadratic errors:

$$F(\lambda,a) = \int_0^{\pi/2} d\theta \cos\theta \, e^{-\lambda \sec\theta}\left(1 + \frac{\lambda^2 a^2 \tan^2\theta}{2!} + \ldots\right) \tag{3.3.11}$$

The method will give reasonable results only when $\Sigma \gg \gamma$. If any region of the cell does not satisfy this criterion, the method will not be valid. An obvious example of such a region is a vacuum.

A table of 2000 values of $F(\lambda,a)$ was prepared by means of numerical integration by Simpson's rule with 40 intervals, for values of λ between 0 and 5 in steps of 0.05, and for a between 0 and 0.5 in steps of 0.025. The table, which is a 100 × 20 matrix, was stored on magnetic tape for use with THERMØS. The THERMØS code was modified to interpolate linearly the value of $F(\lambda,a)$ from this matrix instead of from the linear matrix for $F(\lambda)$.

To insure compatibility with other versions of THERMØS, the calculated values of $F(\lambda,a)$ were divided by $F(\lambda,0)$ calculated from the numerical integration of Eq. (3.3.10) and multiplied by the values used by Honeck for $F(\lambda)$. This procedure insured that when $\gamma = 0$, the two codes would give the same result; it was checked on a test problem and the result indicated that the two codes were compatible.

Table 3.3.3 compares the values of $F(\lambda,0)$ calculated by Simpson's rule and Honeck's expansion for $F(\lambda)$. In addition, values of $F(\lambda,a)$, for a between 0 and 0.5, are included for the direct integration.

TABLE 3.3.3

Calculated Values of $F(\lambda,a)$ for the Axial Correction.

λ \ a	0.0*	0.0	0.1	0.2	0.3	0.4	0.5
0	1.0000	1.0000	1.0000	1.0000	1.0000	1.0000	1.0000
1	0.2738	0.2736	0.2743	0.2766	0.2804	0.2859	0.2933
2	0.08575	0.08549	0.08606	0.08780	0.09083	0.09534	0.1016
3	0.02796	0.02793	0.02823	0.02918	0.03087	0.03346	0.03723
4	0.009362	0.009347	0.009493	0.009950	0.01077	0.01207	0.01405
5	0.003179	0.003178	0.003243	0.003447	0.003823	0.004436	0.005409

*Honeck's approximation for $F(\lambda)$ used in the THERMØS code.

It was found that values of $F(\lambda,a)$ are equal to or greater than values of $F(\lambda,0)$ for the same value of λ. Physically, this means that neutrons have a greater probability of traveling a given distance in the cell, which would result in a higher moderator flux, since the neutrons have a greater probability of escaping capture in the rod. Hence, the dip to the center of the rod from the outer boundary of the cell should be greater in an exponential assembly with $\gamma > 0$, than in an infinite assembly with $\gamma = 0$. Gamma (γ) was varied from 0.0 to 0.03 cm^{-1} in the single velocity test problem, shown in Fig. 3.3.3, with α's of 0, 0.0188, 0.0377, and 0.0754 cm^{-1}. In all cases, the one-group flux distribution was nearly independent of γ, but the trend of the dip was, as predicted, slightly greater with increasing γ. For $\gamma > 0.03$, the dip began to decrease, probably because of the breakdown of the approximations used.

3.3.3 THE COMBINED EFFECT

The extended and modified THERMØS code was applied to the lattices investigated by the M.I.T. Heavy Water Lattice Project. The 30-group Honeck-Nelkin kernel with the diagonal elements adjusted was used. The radial and axial corrections described above were included. The lattice of 1-inch diameter, natural uranium rods on a 5.75-inch triangular spacing should require the greatest corrections, since it was built up from the largest cell. Table 3.3.4 lists the results of the calculations for four combinations of α and γ. The values of α and γ were either equal to zero or to the experimental values of Palmedo (P1). When $\alpha = 0.0377\ cm^{-1}$, the calculation predicts a 2% difference from the case when $\alpha = 0$, the infinite case, in the activation rise to the cell edge. If the value at each radial position, r, is divided by $J_o(\alpha r)$, the difference is negligible (less than 0.3%). It appears reasonable to conclude that the exponential tank used in the M.I.T. experiments is large enough so that the measured intracellular activation distribution in the central cell is representative of an infinite assembly.

TABLE 3.3.4

Radial and Axial Corrected Intracellular 1/v-Activation Distribution in a Lattice of 1.01-Inch Diameter, Natural Uranium Rods Arranged on a 5.75-Inch Triangular Spacing.

Point	Position (cm)	α=0.0 γ=0.0	α=0.0 γ=0.0246 cm^{-1}	α=0.0377 cm^{-1} γ=0.0	α=0.0377 cm^{-1} γ=0.0246 cm^{-1}
1	0.0	1.0000	1.0000	1.0000	1.0000
2	0.284	1.0185	1.0184	1.0184	1.0183
3	0.568	1.0671	1.0669	1.0666	1.0665
4	0.853	1.1604	1.1598	1.1593	1.1588
5	1.137	1.3309	1.3296	1.3288	1.3276
6	1.324	1.5177	1.5174	1.5146	1.5143
7	1.762	1.7433	1.7457	1.7386	1.7412
8	2.549	1.9362	1.9383	1.9287	1.9310
9	3.336	2.0658	2.0679	2.0547	2.0571
10	4.123	2.1292	2.1314	2.1136	2.1162
11	4.910	2.1834	2.1856	2.1622	2.1650
12	5.697	2.2253	2.2275	2.1970	2.2001
13	6.484	2.2547	2.2570	2.2172	2.2205
14	7.272	2.2761	2.2784	2.2233	2.2271

3.4 THE PROBLEM OF FLUX PERTURBATIONS FOR FOILS IN A LATTICE

The activation per unit mass of a foil of finite thickness in a neutron flux is less than it would be for an infinitely thin foil. The extent to which the activations are different constitutes the flux perturbation problem for a foil. Analytical methods used to treat the problem are discussed in recent review articles by Osborn (O1) and Hanna (H2). A serious difficulty with the available methods is their failure to treat the energy-dependent effects adequately, since the emphasis thus far has been on the spatial effects. Hanna (H1) has noted this difficulty and has tried to modify one treatment.

In a lattice cell, the problem is complicated by the variation of the directional thermal neutron flux with position, energy and solid angle as well as the variation of the activation cross section of the foil with energy. To investigate the problem in a cell, an analytical procedure is described, similar to that discussed by Zweifel (Z3), which treats the energy dependence more accurately, but lacks the spatial rigor of the method of Dalton and Osborn (D2, D3). The procedure was used to obtain initial estimates of the effects of the foil perturbation in the interpretation of the measurements of the intracellular flux distributions.

In the intracellular thermal flux measurements, it is usually assumed (B14) that the neutron flux perturbation is the same for every foil and that this effect therefore cancels in any relative measurement. The activation cross section is simply multiplied by the scalar flux at the position of the foil and integrated over energy, up to the cadmium cutoff, E_c, to obtain the reaction rate:

$$R(r) = \int_0^{E_c} \sigma_{ACT}(E)\, \phi(E,r)\, dE\,, \tag{3.4.1}$$

where $\sigma_{ACT}(E)$ is the activation cross section of the foil and $\phi(E,r)$ is the scalar flux at position r. In the analytical procedure used in the present work, the effect of the flux perturbation is included in the activation cross section so that there is an explicit distinction, for example, between a 4 mil thick foil and that of a 10 mil thick foil:

$$R(r) = \int_0^{E_c} \sigma^*_{ACT}(E)\, \phi(E,r)\, dE\,, \tag{3.4.2}$$

where

$$\sigma^{*}_{ACT}(E) = f_{ss}(E)\,\sigma_{ACT}(E)\,, \tag{3.4.3}$$

and $f_{ss}(E)$ is the flux perturbation correction factor for the foil as a function of energy. It is assumed that the flux incident on the foil is not perturbed by the presence of the foil and that the directional flux is isotropic everywhere. If the presence of the foil perturbed the incident flux, this effect would have to be included explicitly in the THERMØS calculation; this type of calculation does not seem to be a possible one at this time. The assumption is discussed further in Appendix A. Of the two assumptions, the assumption that the flux is isotropic everywhere is probably subject to the greater error, since, in a lattice cell, the flux cannot be isotropic everywhere and currents exist.

If the flux of neutrons of a given energy at the surface of a foil is Φ, the directional flux, $\phi(\mu)$, where μ is the direction cosine, is $\Phi/4$. Let Γ_a be the probability that the neutrons entering the foil will be absorbed. Then the number of neutrons captured is:

$$\text{Number captured} = \Gamma_a \frac{\Phi}{4} S\,, \tag{3.4.4}$$

where S is the surface area of the foil. Γ_a may be expressed in terms of escape probabilities by means of the reciprocity theorem (T2):

$$\Gamma_a = \Sigma_a \overline{\ell}\,\overline{P}\,, \tag{3.4.5}$$

where

$\overline{\ell}$ is the mean chord length,

Σ_a is the absorption cross section,

and

$\overline{P}$ is the escape probability of neutrons from a flat, isotropic source in a non-reentrant volume. Hence the number of neutrons captured becomes:

$$\text{Number captured} = \Sigma_a \overline{\ell}\,\overline{P}\,\frac{\Phi}{4} S\,. \tag{3.4.6}$$

The number of neutrons that would have been captured, had the foil not perturbed the flux, is:

$$\text{Number captured when no perturbation occurs} = \Sigma_a \Phi V\,, \tag{3.4.7}$$

where V is the volume of the foil. The ratio of the number of neutrons captured by the foil to the number that would be captured by the foil if there were no flux perturbation, is the neutron flux perturbation factor, f_{ss}:

$$f_{ss} = \frac{\Sigma_a \bar{\ell} \overline{P} \Phi S}{4 \Sigma_a \Phi V} = \overline{P}, \tag{3.4.8}$$

where use has been made of the relation between $\bar{\ell}$ and the volume-to-surface ratio:

$$\bar{\ell} = 4V/S. \tag{3.4.9}$$

Since there is little energy transfer in scattering collisions in foils of high nuclear mass, and most commonly used foils are of this general type, the flux perturbation factor derived for monoenergetic neutrons can be generalized to all energies:

$$f_{ss}(E) = \overline{P}(E). \tag{3.4.10}$$

The escape probability for a flat, isotropic source in slabs has been tabulated by Shiff and Stein (S2), from the results of sensibly exact transport calculations, for various values of the optical thickness, $\Sigma_t t$, and the ratio of the scattering to total cross sections, Σ_s/Σ_t. An approximation for $\overline{P}$ is:

$$\overline{P} = \frac{P_o}{1 - \frac{\Sigma_s}{\Sigma_t}(1 - P_o)}, \tag{3.4.11}$$

where P_o is the first collision escape probability for the foil. For simple shapes, P_o has been tabulated by Case, de Hoffman and Placzek (C5). For slabs, P_o can be expressed in terms of the exponential integral of order 3, $E_3(\Sigma_t t)$:

$$P_o = \frac{1 - E_3(\Sigma_t t)}{2 \Sigma_t t}. \tag{3.4.12}$$

The validity of the approximation for $\overline{P}$ given by Eq. (3.4.11) is discussed by Francis (F1). He shows that the approximation can be derived either by means of a variational principle or by the method of successive

generations. The latter method is used in the calculation of the fast fission effect (W2). Francis shows that the approximation for $\overline{P}$ compares favorably with the results of Schiff and Stein until the optical thickness exceeds two mean free paths over the range of Σ_s/Σ_t.

To account for possible increased leakage from the sides of a finite foil, P_o is evaluated for a value of t having the same mean chord length as the finite foil. The equivalent foil thickness used in the calculation of P_o is designated as t^*; it is related to the actual foil thickness, t, and the radius of the foil, R, by:

$$t^* = \frac{t}{1 + t/R} . \qquad (3.4.13)$$

If R is much greater than t, then t^* reduces to t, as expected. Table 3.4.1 gives the values of t and t^* adopted in the calculations, for the gold foils used in the experiments.

TABLE 3.4.1

Values of Equivalent Foil Thickness for 1/16-Inch Diameter Foils

Actual Foil Thickness, t (mils)	Equivalent Foil Thickness, t^* (mils)
2.5	2.3
4.3	3.8
10.2	7.7

The effective activation cross sections, $\sigma^*_{ACT}(E)$, defined by Eq. (3.4.3), were calculated with the QUICK code, described in Appendix C, for the 30 energy groups corresponding to those of the THERMØS code, for the gold foils used in the experiments. Figure 3.4.1 shows the results of the calculations for the effective cross section as a function of energy; the results are also tabulated in Tables C.1 to C.10. The values of $f_{ss}(E)$ used to calculate $\sigma^*_{ACT}(E)$ were calculated for a foil of thickness t by evaluating P_o (defined by Eq. (3.4.12)) for a foil of equivalent thickness t^* (defined by Eq. (3.4.13)) and substituting P_o into Eq. (3.4.11) for $\overline{P}$; f_{ss} was shown to be equal to $\overline{P}$ by Eqs. (3.4.4) through (3.4.8). The Lu-Al alloy foils, the depleted uranium foils, and

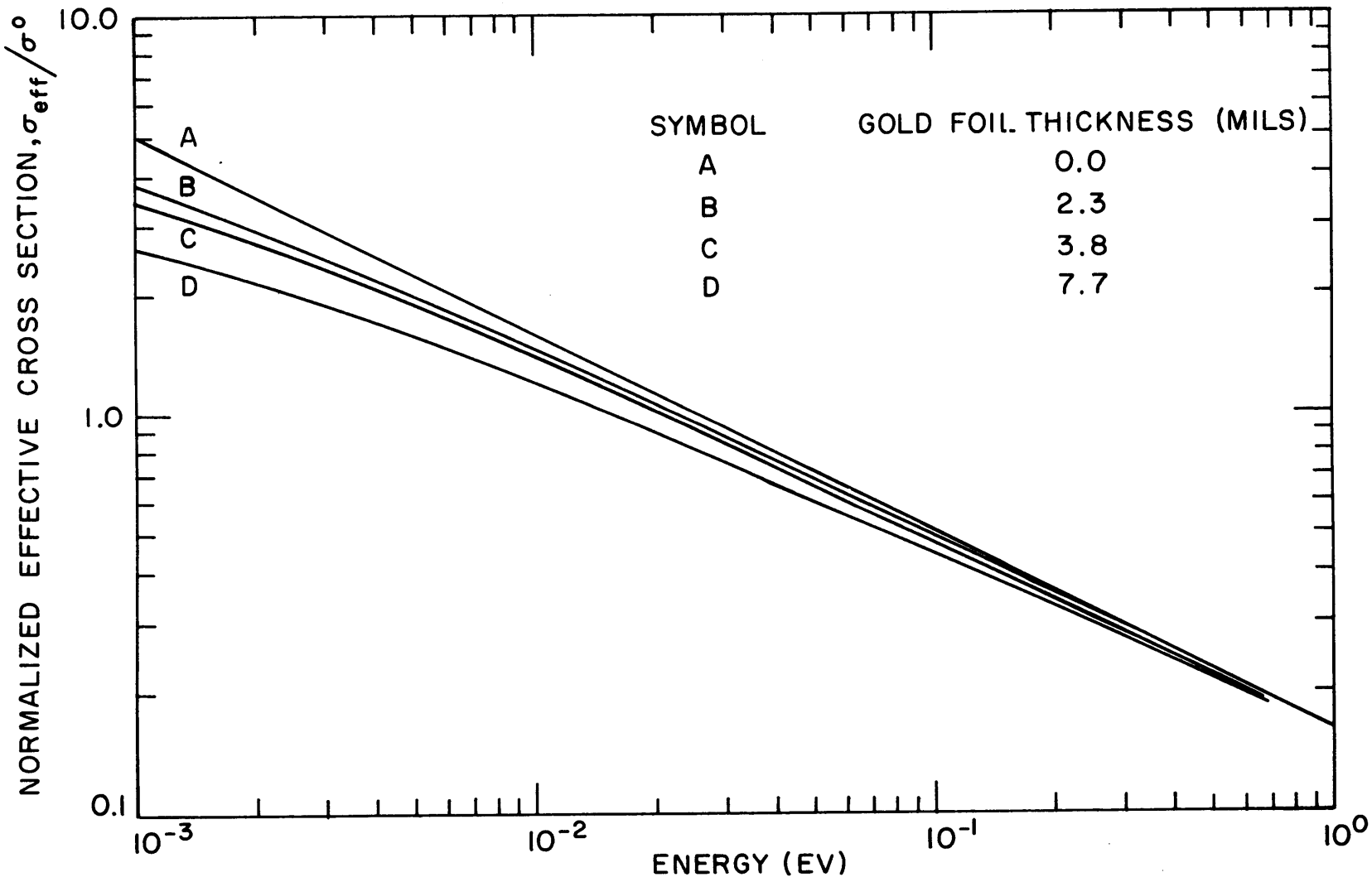

FIG. 3.4.1 EFFECTIVE ACTIVATION CROSS SECTIONS FOR METALLIC GOLD FOILS (NOTE: $\Sigma_s = 0.548\ CM^{-1}$, $\Sigma_A^o = 5.83\ CM^{-1}$).

the copper foils of the foil files discussed in Section 2.3 were found to be effectively infinitely thin in the thermal energy range. No estimate was made for the powder foils, because not enough information was available concerning their physical properties.

When the effective cross sections for the foils have been calculated, the THERMØS calculation can be used to evaluate the reaction rate for the foil from Eq. (3.4.2). The THERMØS code computes $\phi(E,r)$ and numerically integrates Eq. (3.4.2) for any desired cutoff energy, E_c. Calculations have been made for the lattices investigated by M.I.T. for the gold foils described in Section 2.3. A cutoff energy of 0.4 ev was used because the cadmium cutoff for gold corresponds to this energy for the thickness of cadmium covers used (B14). The results are given in Tables 3.4.2 and 3.4.3. The calculations indicate that the activation distribution in the cell is not very sensitive to the thickness of the foil used. Only about a 1% difference in the activation dip into the rod is predicted between the infinitely thin foil and the foil 7.7 mils thick (equivalent to the 10.2 mils thick foil). The comparison with the experimental results will be discussed in Chapter IV.

TABLE 3.4.2

Comparison of the Intracellular Activity Distributions for Gold Foils of Different Thickness in the Lattice of 1.03% Enriched, 1/4-Inch Diameter Rods on a 1-1/4-Inch Triangular Spacing.

Point	Radial Position (cm)	Infinitely Thin Foil	2.3 mil thick Foil	3.8 mil thick Foil	7.7 mil thick Foil
1	0.000	0.740	0.743	0.745	0.748
2	0.127	0.752	0.755	0.757	0.760
3	0.254	0.791	0.794	0.795	0.798
4	0.361	0.872	0.873	0.874	0.876
5	0.507	0.916	0.917	0.918	0.919
6	0.717	0.952	0.952	0.953	0.953
7	0.928	0.973	0.973	0.973	0.974
8	1.138	0.982	0.983	0.983	0.983
9	1.349	0.990	0.990	0.990	0.990
10	1.559	1.000	1.000	1.000	1.000

TABLE 3.4.3

Comparison of the Intracellular Activity Distributions for Gold Foils of Different Thickness in the Lattice of 1.03% Enriched, 1/4-Inch Diameter Rods on a 2-1/2-Inch Triangular Spacing.

Point	Radial Position (cm)	Infinitely Thin Foil	2.3 mil thick Foil	3.8 mil thick Foil	7.7 mil thick Foil
1	0.000	0.771	0.775	0.776	0.779
2	0.127	0.782	0.786	0.787	0.790
3	0.254	0.818	0.821	0.822	0.825
4	0.361	0.885	0.886	0.887	0.889
5	0.647	0.938	0.939	0.940	0.940
6	1.135	0.971	0.972	0.972	0.972
14	3.224	1.000	1.000	1.000	1.000

Since the calculations for the intracellular activation distributions are relative to one point in the cell, it is possible that, although the proper variation of f_{ss} with energy is predicted, the absolute magnitude of the factor, $\overline{f}_{ss}$, for the foil may be in error. The flux perturbation factor, $\overline{f}_{ss}$, was found to be predicted adequately by the procedures defined in this section; the subject is discussed further in Appendix A.

3.5 THE PREDICTION OF THE GOLD-CADMIUM RATIO IN A LATTICE CELL

The activity of cadmium-covered foils in a lattice is usually measured in the intracellular flux measurements simply to subtract it from the activity of the bare foils to obtain the thermal activity. In the experiments at B.N.L. (K5, K6), dysprosium was used to eliminate the necessity of measuring the epicadmium activity, since dysprosium has no strongly absorbing resonances. The epicadmium activity is, however, a useful piece of information because it is relevant to discussions involving assumptions of slowing-down density distributions. It may also suggest an alternative method for the normalization problem for theory and experiment to be discussed in Chapter IV.

Weitzberg (W3) and Peak (P5) discuss methods that are similar in nature to the prediction of cadmium ratios for detecting foils. Weitzberg's

method was to calibrate the lattice flux by making enough auxiliary experiments in known fluxes to eliminate most of the variables. He assumed the lattice flux to have a Maxwellian spectrum in the thermal energy range and to vary as 1/E in the epithermal region. Peak was concerned with the macroscopic flux in a small exponential facility. He found that to get agreement between experiment and theory, he had to change the value of the ratio of the effective resonance integral to the 2200 m/sec cross section, ERI'/σ_o, for a given foil from experiment to experiment. In the following discussion, the emphasis will be on the prediction of the gold-cadmium ratio in a lattice cell with a minimum number of adjustable parameters.

The thermal activation for a foil can be calculated, for one neutron absorbed in the cell, from the expression:

$$A_{th}(r) = \int_0^{E_c} f_{ss}(E)\, \sigma_{ACT}(E)\, \phi(E,r)\, dE\,, \tag{3.5.1}$$

where results obtained in Section 3.4 for the effect of flux perturbation have been used. Since the problem of the shape of the thermal flux is to be treated in Chapter IV, the cadmium ratio, although it varies across the lattice cell, will be calculated at the cell edge, at $r = R_{eq}$. Then, Eq. (3.5.1) becomes:

$$A_{th} = \int_0^{E_c} f_{ss}(E)\, \sigma_{ACT}(E)\, \phi(E)\, dE\,, \tag{3.5.2}$$

where the dependence of A_{th} on r has been suppressed and A_{th} is understood to be evaluated at the cell edge.

The epicadmium activity can be expressed by means of a similar integral extended from E_c to infinity, but it is more commonly written as

$$A_{epi} = C \cdot ERI', \tag{3.5.3}$$

where C is a constant and ERI' is the effective resonance integral for the foil; C relates the flux to the slowing-down density, q. An approximation (G1) for C is:

$$C = q/\xi\Sigma_s\,. \tag{3.5.4}$$

Since it has been required that one neutron be absorbed in the thermal range in the cell, the slowing-down density must satisfy this normalization.

If the slowing-down density is spatially flat in the moderator, then $q \cdot V_{mod} = 1$; V_{mod} is the volume of the moderator. It is assumed that leakage from the assembly between 4.9 ev and thermal energies is negligible, and that the resonance escape probability between these energies is unity. The first resonance for gold is at 4.9 ev. Then C is "known" and Eq. (3.5.3) becomes:

$$A_{epi} = ERI'/\xi \Sigma_s V_{mod} . \tag{3.5.5}$$

The cadmium ratio, R_{cd}, is, by definition, the ratio of the bare foil activity to the activity of the cadmium-covered foil:

$$R_{cd} = 1 + \frac{\int_0^{E_c} f_{ss}(E)\, \sigma_{ACT}(E)\, \phi(E)\, dE}{\frac{ERI'}{\xi \Sigma_s V_{mod}}} . \tag{3.5.6}$$

The calculation of the ERI for gold by the analytical method of Cohen and Goldstein (C9) has been made by Kelber (K2). Rather than interpolate between, and extrapolate from, the results of Kelber, it was decided to rerun his calculations with his computer code. Table 3.5.1 lists the resonance parameters for gold used in the calculations; Table 3.5.2 lists the results of the calculations for the effective resonance integrals for gold. The value of the resonance integral, RI, calculated from the resonance parameters given in Table 3.5.1, was 1555 barns; the value of the RI measured by Jirlow and Johansson (J2) was 1490 ± 40 barns.

Table 3.5.2 lists the contribution of the first resonance to the effective resonance integral. The contribution decreases from 95% for the infinitely thin foil to 88% for a foil 7.7 mils thick. The variation occurs because the first resonance becomes shielded while the higher resonances remain almost unshielded as the foil thickness increases. Even in the larger foils, however, most of the neutrons are captured at the first resonance. Consequently, it seems reasonable to consider leakage and resonance escape in the lattice just from the region around 4.9 ev, the energy of the first gold resonance, to thermal energies. Since the calculations do not include the 1/v-contribution to the total effective resonance integral, ERI', a total of 0.5 σ_o is added to the calculated

TABLE 3.5.1

Resonance Parameters for Gold

Number	Resonance Energy, E_o (ev)	Gamma Width, Γ_γ (ev)	Scattering Width, Γ_n (ev)	Peak Cross Section, σ_{pk} (barns)
1	4.906	0.125	0.0156	37030.
2	46.5	0.125	0.00013	36.5
3	58.1	0.125	0.013	2655.
4	61.5	0.170	0.11	10460.
5	80.2	0.170	0.15	1655.
6	110.0	0.170	0.009	748.
7	153.0	0.170	0.050	2432.
8	168.0	0.170	0.10	3610.
9	194.0	0.170	0.050	1918.

TABLE 3.5.2

Calculated Effective Resonance Integrals for Gold

Foil Thickness* (mils)	Effective Resonance Integral, ERI (barns)	Fractional Contribution of the First Resonance	Total ERI, (includes 1/v-contribution) (barns)	$\frac{ERI'}{RI'}$
12.4	152	0.876	201	0.125
7.7	192	0.881	241	0.150
6.66	205	0.882	254	0.158
3.8	268	0.887	317	0.197
3.33	286	0.888	335	0.208
2.3	340	0.893	389	0.242
2.22	345	0.894	394	0.245
1.66	394	0.898	443	0.275
1.11	473	0.904	522	0.325
0.833	536	0.908	585	0.364
0.555	635	0.915	684	0.426

*Density of gold; 19.3 gms/cm^3.

values of ERI and RI; this amount corresponds to a cadmium cutoff of 0.4 ev.

The measurement of the ERI' involves the irradiation of finite and infinitely thin foils, bare and cadmium-covered. The experimental ratio usually given is the ratio of $(R_{cd}-1)$ for the infinitely thin foil to that for the finite foil. It is usually called the "thickness correction" and will be designated by K_{exp}. The value of K_{exp} in terms of the theoretical values of the quantities involved is:

$$K_{exp} = \frac{(R_{cd}-1)^{\circ}}{(R_{cd}-1)^{t*}} = \frac{ERI'}{f'_{ss}(RI')} , \qquad (3.5.7)$$

where f'_{ss} is the value of the thermal flux perturbation factor for the experiment, and ERI' and RI' include the 1/v-contribution. Table 3.5.3 listed the theoretical values of $ERI'/(RI' \cdot f'_{ss})$ which are to be compared to the experimental values of K_{exp}. It is assumed that f'_{ss} is the same as that for a Maxwellian spectrum. In general, the values of the thermal flux perturbation factor used by experimentalists have been measured in thermal spectra that are nearly Maxwellian. For 1/v-absorbers, f'_{ss} is not very sensitive to changes in the spectrum.

TABLE 3.5.3

Calculated Values of K_{exp}

Foil Thickness* (mils)	$\frac{ERI'}{RI'}$	Thermal Flux Perturbation Factor, f'_{ss}	K_{exp} $\left[\frac{ERI'}{(RI')f'_{ss}}\right]$
12.4	0.125	0.750	0.166
7.7	0.150	0.817	0.183
6.66	0.158	0.834	0.189
3.8	0.197	0.889	0.221
3.33	0.208	0.898	0.231
2.3	0.242	0.923	0.262
2.22	0.245	0.926	0.264
1.66	0.275	0.941	0.292
1.11	0.325	0.958	0.339
0.833	0.364	0.967	0.376
0.555	0.426	0.978	0.435

*Density of gold; 19.3 gms/cm^3

Figure 3.5.1 compares the results of experiment to the calculations for gold foils. The experimental results reported are those of Bauman (B2) and Jacks (J1) of the Savannah River Laboratory and Brown (B14) and Childers (C7) of M.I.T. Childers used the cadmium boxes and foils described in Section 2.3. Bauman also gives calculated values for K_{exp} which agree with his experimental results. The calculations of Kelber, with the thermal flux perturbation factors calculated by the methods of Section 3.4, fall significantly below the experimental results. It is difficult to decide which results were correct, so that the experimental values of K_{exp} were used to calculate the cadmium ratio in the lattices. In this case, Eq. (3.5.6) becomes:

$$R_{cd} - 1 = \frac{V_{mod}\bar{f}_{ss} \int_0^{E_c} \sigma_{ACT}(E)\,\phi(E)\,dE \Big/ \sigma_o}{f'_{ss}\,\frac{RI'}{\sigma_o}\,\frac{K_{exp}}{\xi\Sigma_s}}\,, \qquad (3.5.8)$$

where the variation of K_{exp} with foil thickness is understood, and $\bar{f}_{ss}$ is the flux perturbation factor for the foil in the lattice spectrum. It should be noted that the ratio of the flux perturbation factors, $\bar{f}_{ss}/f'_{ss}$, enters into the calculation.

The denominator of Eq. (3.5.8) does not vary from lattice to lattice if the measurements are made with the same foils. The variation with lattice spacing is given by the numerator of Eq. (3.5.8):

$$R_{cd} - 1 \propto V_{mod}\bar{f}_{ss} \int_0^{E_c} \sigma_{ACT}(E)\,\phi(E)\,dE\,. \qquad (3.5.9)$$

It is essential that the measured values of K_{exp} be valid for the lattice in question. If the flux does not vary as 1/E in the region above the gold resonance, the experimental values of K_{exp} would not be meaningful since they were measured in a known 1/E-flux.

It is difficult, if not impossible, to measure the resonance flux in a lattice cell, and it was, therefore, decided to make use of an available computer program coded by Kier (K3) which allows the calculation of the resonance flux as a function of space and energy. The calculations were performed by Kier for an "equivalent" slab problem, since the code has not yet been modified to treat cylinders. An equivalent slab of fuel

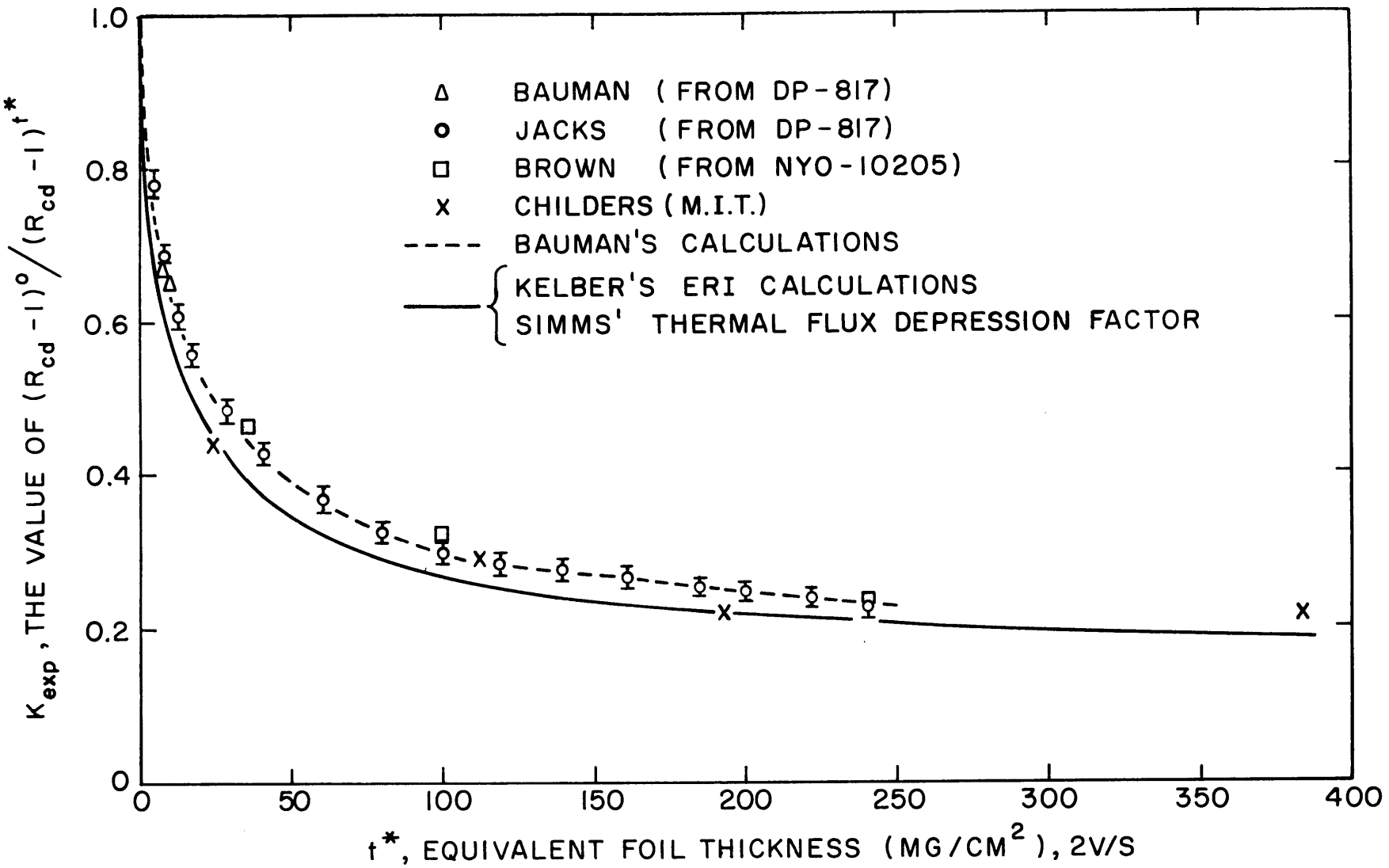

FIG. 3.5.1 COMPARISON OF EXPERIMENTAL AND CALCULATED VALUES OF K_{exp}.

was defined as having the same mean chord length as the rod (the thickness of the slab equals the radius of the rod); the moderator thickness of the slab lattice was taken to be that which gave the same moderator-to-fuel volume ratio as the rod lattice. The lattice of 1/4-inch diameter, 1.03% U^{235}, uranium rods arranged on a 1.25-inch triangular spacing was treated in the calculation. Only the lowest lying resonance of U^{238} was considered. The results are given in Fig. 3.5.2. They indicate that the approximation of a 1/E-spectrum is valid at the cell edge, if the problem solved is truly equivalent.

Kelber has indicated some results of calculations where a low-lying U^{235} resonance caused interference with the gold resonance. However, the effect on the ERI for gold was small and it was within the experimental errors quoted with values of K_{exp}.

3.6 THE CELL CYLINDRICALIZATION PROBLEM

One of the early approximations in the theory of lattices of cylindrical fuel rods arranged in square or triangular arrays was to replace the actual unit cell by an "equivalent" cylindrical cell with the same area. The "equivalent" problem is thus a one-dimensional calculation in which the flux varies with the radial position and is independent of the azimuthal angle. This method was used by Wigner and Seitz (W2) in the theory of the solid state.

Chernick (C6), in connection with early work on water-moderated lattices, pointed out that the procedure might lead to difficulties when the lattices are closely packed. Since then, the problem has received varying amounts of attention. Thie (T1) has examined theoretically the effect of the approximation. The B.N.L. experimental work on H_2O-moderated lattices of slightly enriched uranium rods has been analyzed by Honeck (H9) who notes the extent of the error associated with the approximation. Brown (B14) has suspected that the cell cylindricalization approximation was the cause of the discrepancy that he observed in a closely-packed lattice of slightly enriched uranium rods in D_2O.

This section is devoted to an analysis of the problem and the demonstration that in closely-packed lattices of slightly enriched uranium rods in D_2O, the approximation that the cell may be cylindricalized can introduce serious uncertainties into the theory. The comparison with the

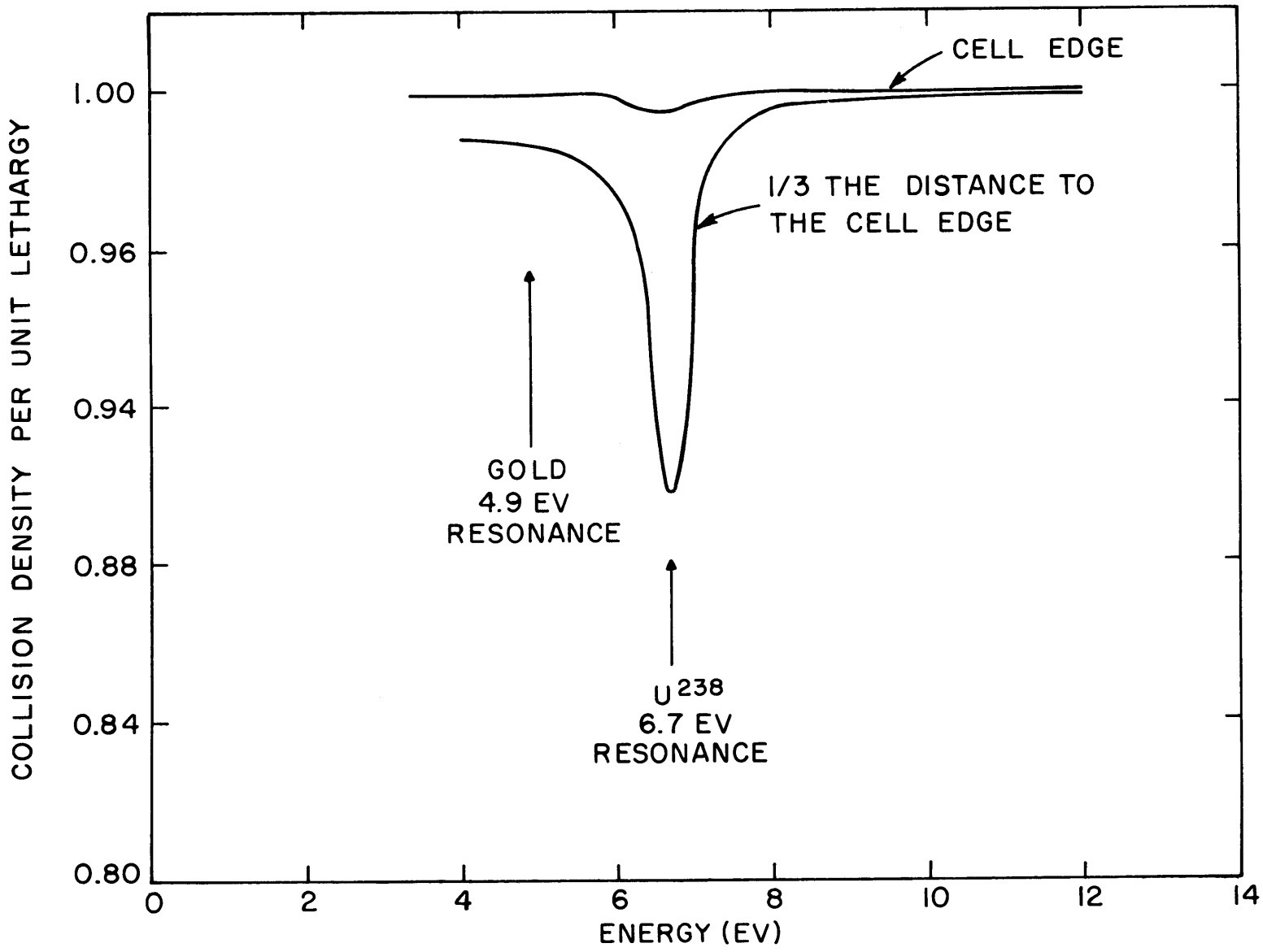

FIG.3.5.2 CALCULATED RESONANCE FLUX IN THE REGION OF THE GOLD RESONANCE.

experiments will be discussed in Chapter IV.

We consider first how cell cylindricalization can introduce errors into the analysis. In an infinite lattice, the condition that there is no net leakage is expressed mathematically by assuming that the cell boundary acts as a perfect reflector of neutrons. Neutrons are reflected from the actual cell boundary, the hexagon, in the case of the triangular array, as shown in Fig. 3.6.1, with the angle of reflection equal to the angle of incidence. In the usual analytical treatment of the one-dimensional cell, similar reflection is assumed to occur at the "equivalent" circular boundary. If a fuel rod is placed in the center of the cell, then there are paths for which the neutron will never enter the rod, regardless of the number of times that it is scattered at the circular boundary of the cell. This possibility is shown in Fig. 3.6.2: if the neutron passes through the point P at an angle ϕ between ϕ_c and $180° - \phi_c$, where ϕ_c is a critical angle defined by:

$$\phi_c = \arcsin (R_o/r) , \tag{3.6.1}$$

and where R_o is the radius of the rod and r is the radial position of the point P, then the neutron will never enter the fuel rod. This situation does not arise in the actual cell because of the corners. Newmarch (N7) was the first to point out this effect of cylindricalization, and concluded that the moderator flux would be overestimated by this approximation.

It is evident that the circular cell approximation can introduce a significant error whenever the rod is close to the outer boundary, in terms of mean free paths. If the cell boundary is far from the rod, neutrons will be scattered before they undergo many reflections from the boundary. Consequently, the boundary condition of reflection is not very important so far as the over-all flux distribution is concerned. A mean free path in heavy water is approximately an inch, and it is likely that the poor agreement between theory and experiment observed by Brown (B14) in the lattice arranged on the 1.25-inch triangular spacing resulted from the failure of the Wigner-Seitz approximation. The experiments to be described in Chapter IV demonstrate the range of validity of the Wigner-Seitz approximation in heavy water.

Next, a method is required to minimize the effect of the circular boundary of the cell while still retaining the simplicity of the one-

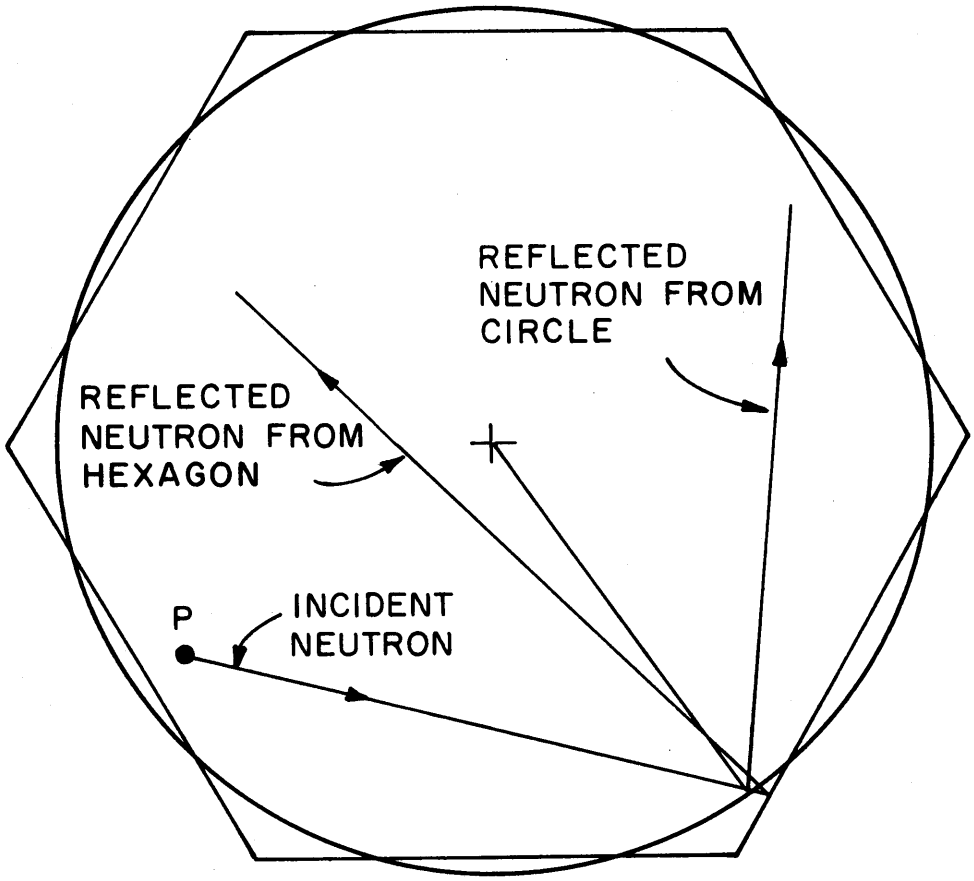

FIG. 3.6.1 REFLECTION OF NEUTRONS FROM THE HEXAGONAL AND EQUIVALENT CELL BOUNDARIES.

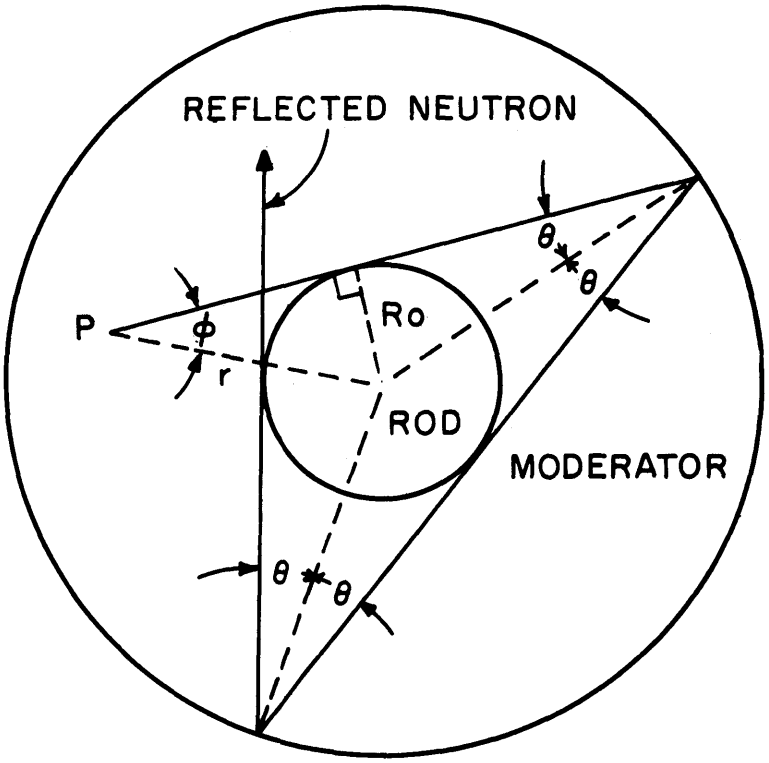

FIG.3.6.2 RESTRICTIVE PATHS FOR NEUTRONS IN THE EQUIVALENT CIRCULAR CELL (NOTE: WHEN ϕ IS BETWEEN ϕ_C AND $180° - \phi_C$, WHERE ϕ_C EQUALS ARCSIN (Ro/r), THEN NEUTRONS FROM POINT P WILL NEVER INTERSECT THE INNER CIRCLE, THE FUEL ROD).

dimensional calculation. To understand the situation, consider a square cell with the inscribed circle, as shown in Fig. 3.6.3. Although the inscribed circle is usually not the "equivalent" circle, it allows a simple analysis of the actual reflection law at the boundary. Figure 3.6.4 is an enlarged section of the situation at the boundary. The problem is to determine the variation of the angle of actual reflection, ϕ, with the azimuthal angle, ψ, for a fixed angle of incidence, θ, with the circular boundary. Consider a neutron originating at point P and headed in a direction so that it intersects the circular boundary at an angle of incidence, θ. The reflection at Q on the circle is, by definition, at equal angles, so that the reflected neutron leaves the boundary at angle θ. Had the neutron continued along the direction PQ, it would have intersected the actual boundary (the square) at point R. The angle the neutron makes with the radius vector AQ is not θ but a different angle, ϕ. For the inscribed circle, $\phi = 2\psi - \theta$ (the circumscribed circle gives $\phi = 2\psi + \theta$) until a corner is reached. As ψ is varied, keeping the angle of incidence equal to θ, the distribution of the angle ϕ is therefore isotropic in the region between corners.

It would be extremely difficult to include the true reflection law at the boundary, especially since there is a complication at the four corners for the square and six corners for the hexagon. However, the isotropic condition, which has been shown to represent a situation close to the actual one, can be created artificially at the boundary in the THERMØS code, or in other ways with the spherical harmonic or S_n methods (H12). Honeck (H11, H13) discusses the details of the analysis and has developed the method used to treat the problem.

In the THERMØS code, the isotropic reflection is substituted for the equal-angle reflection by placing a fictitious region at the outer boundary of the cell. The properties of the region are defined so that the neutrons "forget" the angle at which they were incident on this region; they are then returned to the cell in a very nearly isotropic distribution in angle for any given angle of incidence. The fictitious region is defined so as to have the following properties:

(1) No energy transfer is permitted in it (only diagonal elements of the energy transfer matrix are non-zero),

(2) It is two mean free paths thick,

(3) It is geometrically thin, 0.01 cm,

(4) No absorption is permitted in it.

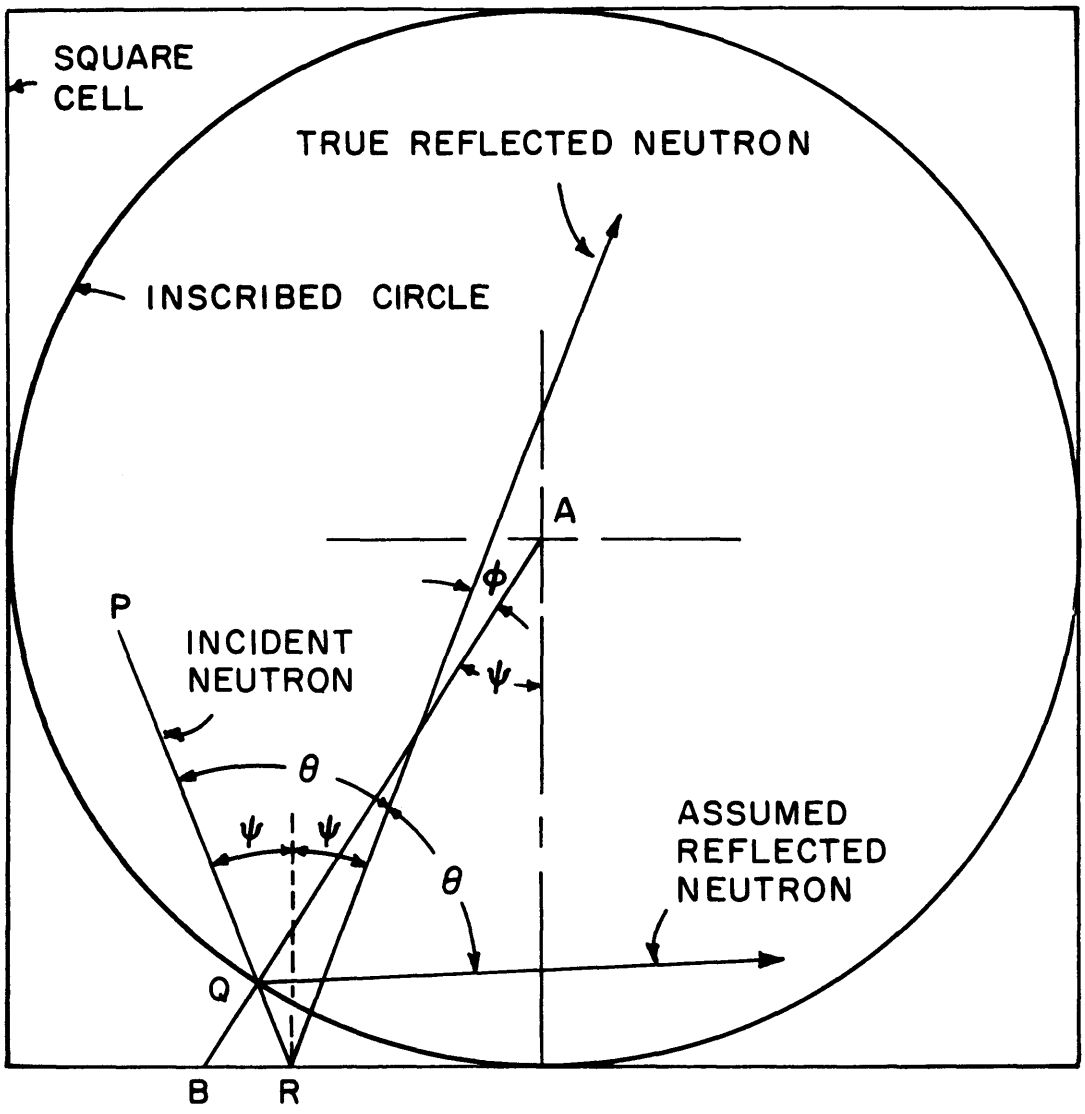

FIG. 3.6.3 REFLECTION OF NEUTRONS FROM THE SQUARE AND THE INSCRIBED CIRCLE BOUNDARIES.

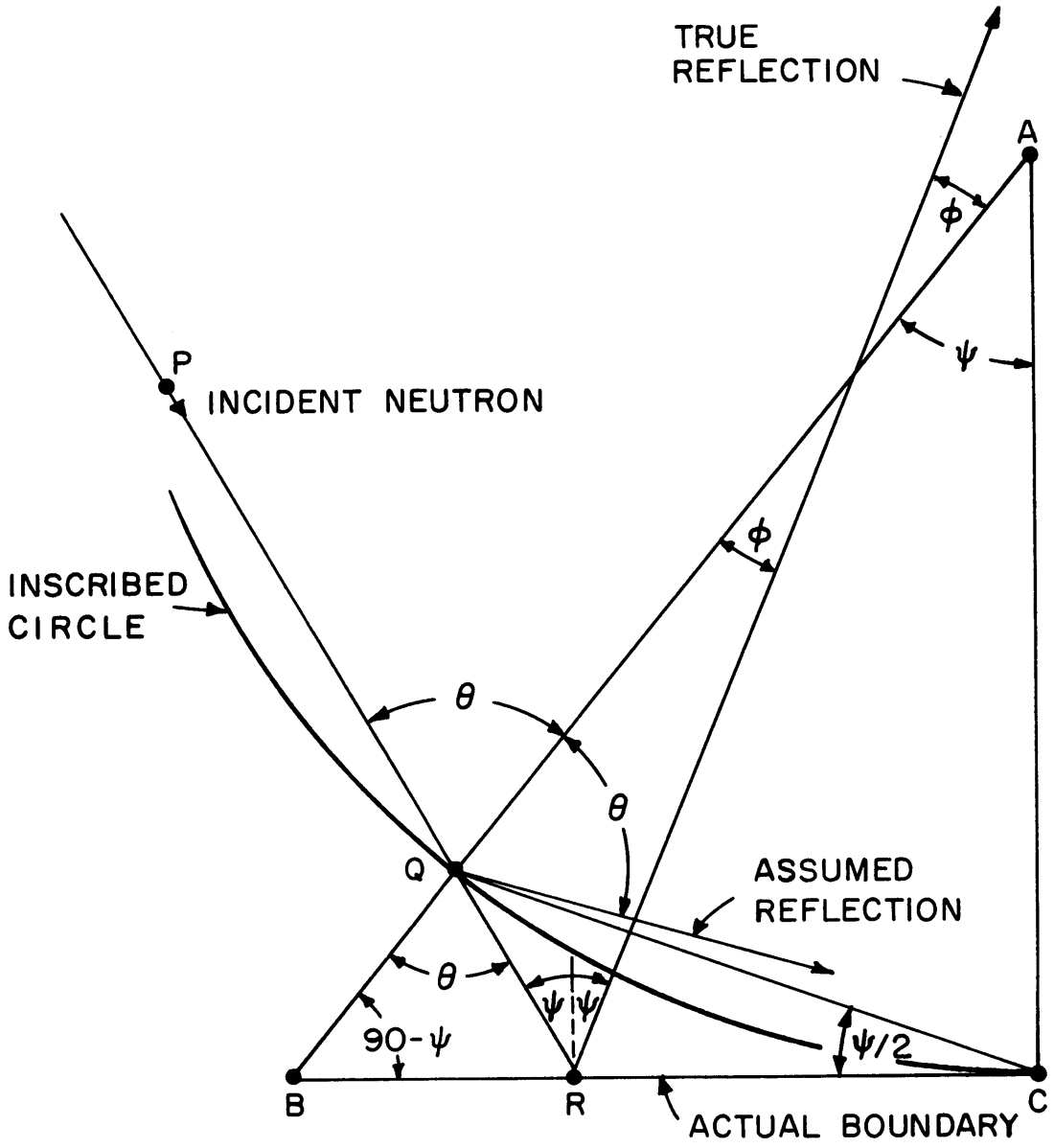

FIG. 3.6.4 THE REFLECTION LAW FOR NEUTRONS AT THE BOUNDARY OF THE ACTUAL CELL.

This modified one-dimensional (1D) calculation needs a little more computer time than the usual one-dimensional calculation, because of the extra region that has been added.

Table 3.6.1 lists some of the nuclear parameters calculated with the two one-dimensional methods, the usual THERMØS and the modified THERMØS methods. The energy exchange kernel, in all cases, was the Honeck-Nelkin model with the diagonal elements adjusted to give the calculated values of $\Sigma_{tr}(E)$.

TABLE 3.6.1

Comparison of Nuclear Parameters for the Lattices with the 1.25-Inch and 2.5-Inch Triangular Spacings Calculated by the Usual and Modified THERMØS Methods. The Honeck-Nelkin kernel with the diagonal elements adjusted was used.

Quantity	Cutoff Energy (ev)	1.25-Inch Spacing		2.5-Inch Spacing	
		Usual 1D	Modified 1D	Usual 1D	Modified 1D
$\zeta_{1/v}$ (a)	0.4	1.260	1.178	1.228	1.211
ζ_{Lu-176} (a)	0.4	1.194	1.120	1.165	1.150
ζ_{Eu-151} (a)	0.14	1.304	1.215	1.265	1.250
f	0.78	0.9773	0.9782	0.9612	0.9616
η	0.78	1.504	1.506	1.510	1.510
$\bar{\sigma}^F_{Pu} / \bar{\sigma}^F_U$ (b)	0.78	1.65	1.66	1.40	1.41

(a) ζ is the over-all disadvantage factor.

(b) This ratio is the ratio of fissions in plutonium-239 to fissions in uranium-235, assuming that the plutonium has no effect on the spectra.

To test the validity of the results of the modified one-dimensional calculation, a two-dimensional (2D) calculation was made for the lattice of 1/4-inch diameter, 1.03% U^{235}, uranium rods on a 1.25-inch triangular spacing. The hexagonal cell was divided into the twelve subsections that contain all the azimuthal variation, without mirror images; each subsection, one of which is shown in Fig. 3.6.5, was divided further into generalized

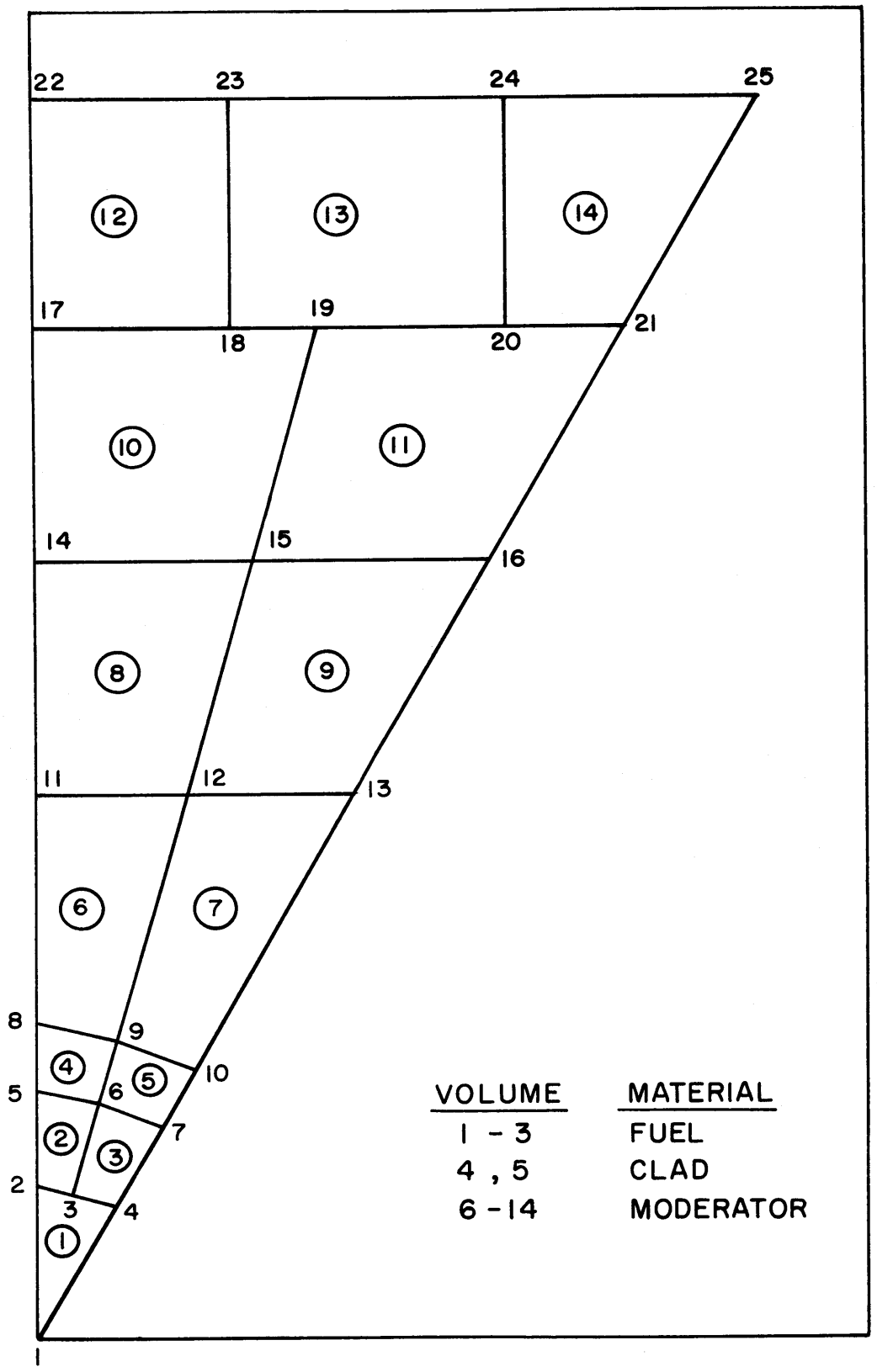

FIG.3.6.5 THE TWO DIMENSIONAL CELL FOR THE THERMOS CALCULATION.

five-sided figures. For example, the five-sided figure Volume (13) is bounded by vertices 18, 23, 24, 20 and 19. Boundary lines 1-22, 22-25, and 25-1 were treated as reflecting boundaries.

The 2D THERMØS calculation was made by using the same energy exchange kernel as was used for the one-dimensional calculations. A comparison of the three results for a 1/v-activator is shown in Fig. 3.6.6. The modified one-dimensional calculation is seen to be very nearly equivalent to the two-dimensional calculation, and requires only one-fifth the computer time needed for the two-dimensional version. It is likely that the modified one-dimensional calculation is sufficiently close to the two-dimensional calculation that it would be difficult to determine by comparison with experiment which is more accurate. However, the usual one-dimensional THERMØS calculation gives results approximately 8% lower in the fuel rod than the modified one-dimensional calculation, and this difference can be observed experimentally.

For the lattice on the 2.5-inch spacing, Fig. 3.6.7 shows that the modified and usual one-dimensional calculations are nearly indistinguishable. Since the cell is larger, the effect of the boundary is smaller than in the lattice with the 1.25-inch spacing. A two-dimensional calculation for the lattice with the 2.5-inch spacing was not made because of the agreement of the results obtained with the two one-dimensional calculations.

3.7 THE CALCULATION OF DISADVANTAGE FACTORS BY THE METHOD OF SUCCESSIVE GENERATIONS

There is considerable interest in the use of methods more accurate than diffusion theory and less costly than THERMØS to calculate reactor parameters. One class of useful methods, often referred to as the "integral transport method" has been reviewed by Fukai (F2). Most of the integral transport methods are basically similar, and one of the more accurate of them, the method of successive generations, has been developed by Stuart and Woodruff (S3).

In the thermal energy range, the quantities of interest are the thermal utilization, f, and η. The method of successive generations allows a reasonably exact calculation to be made for the fuel disadvantage factor. To complete the calculation of the thermal utilization, diffusion theory can be used in the moderator, with the boundary condition at the rod-moderator

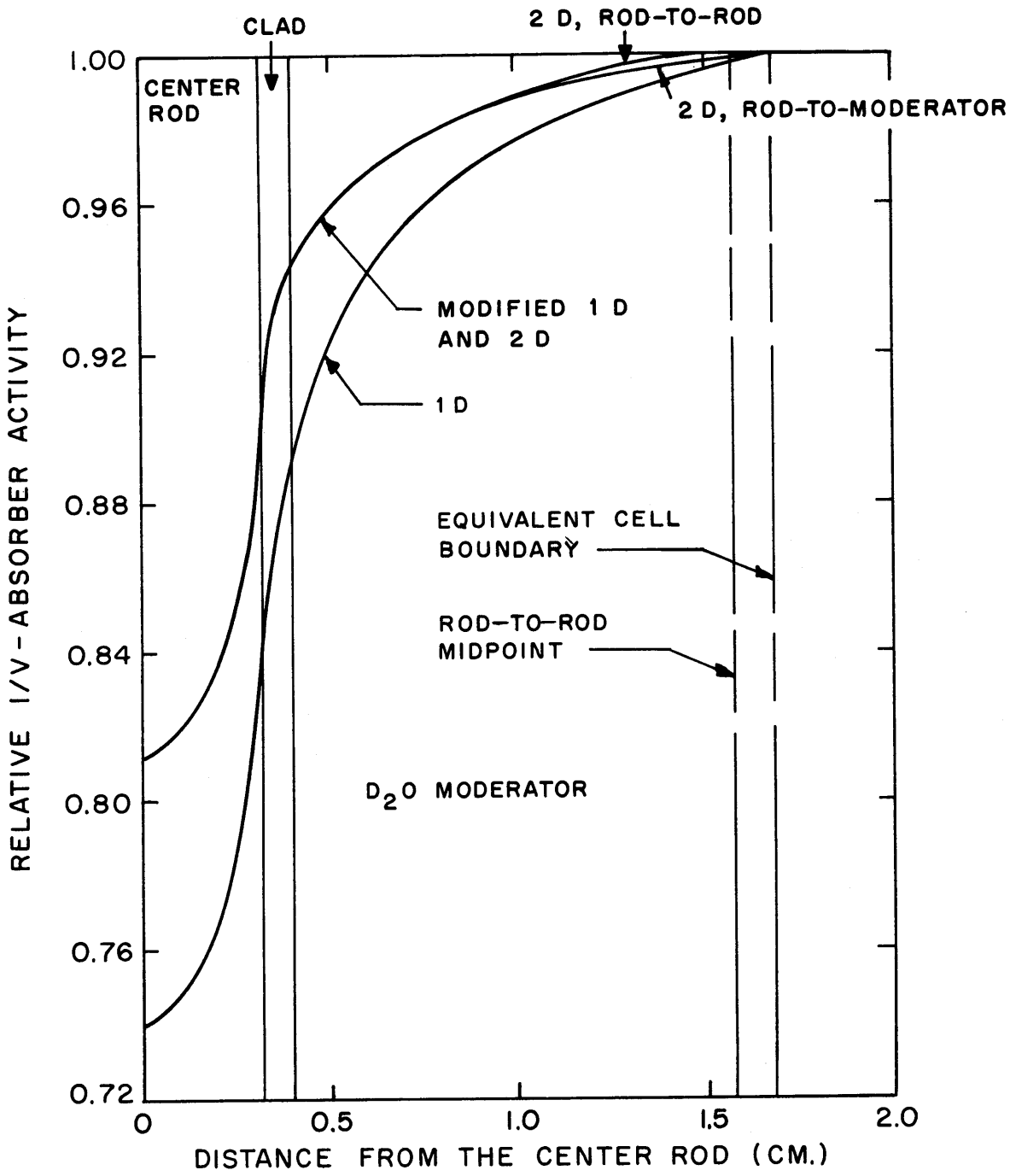

FIG.3.6.6 COMPARISON OF THE ONE AND TWO DIMENSIONAL THERMOS CALCULATIONS FOR THE LATTICE OF 1/4-INCH DIAMETER, 1.03% ENRICHED, URANIUM RODS ON A 1.25-INCH TRIANGULAR SPACING.

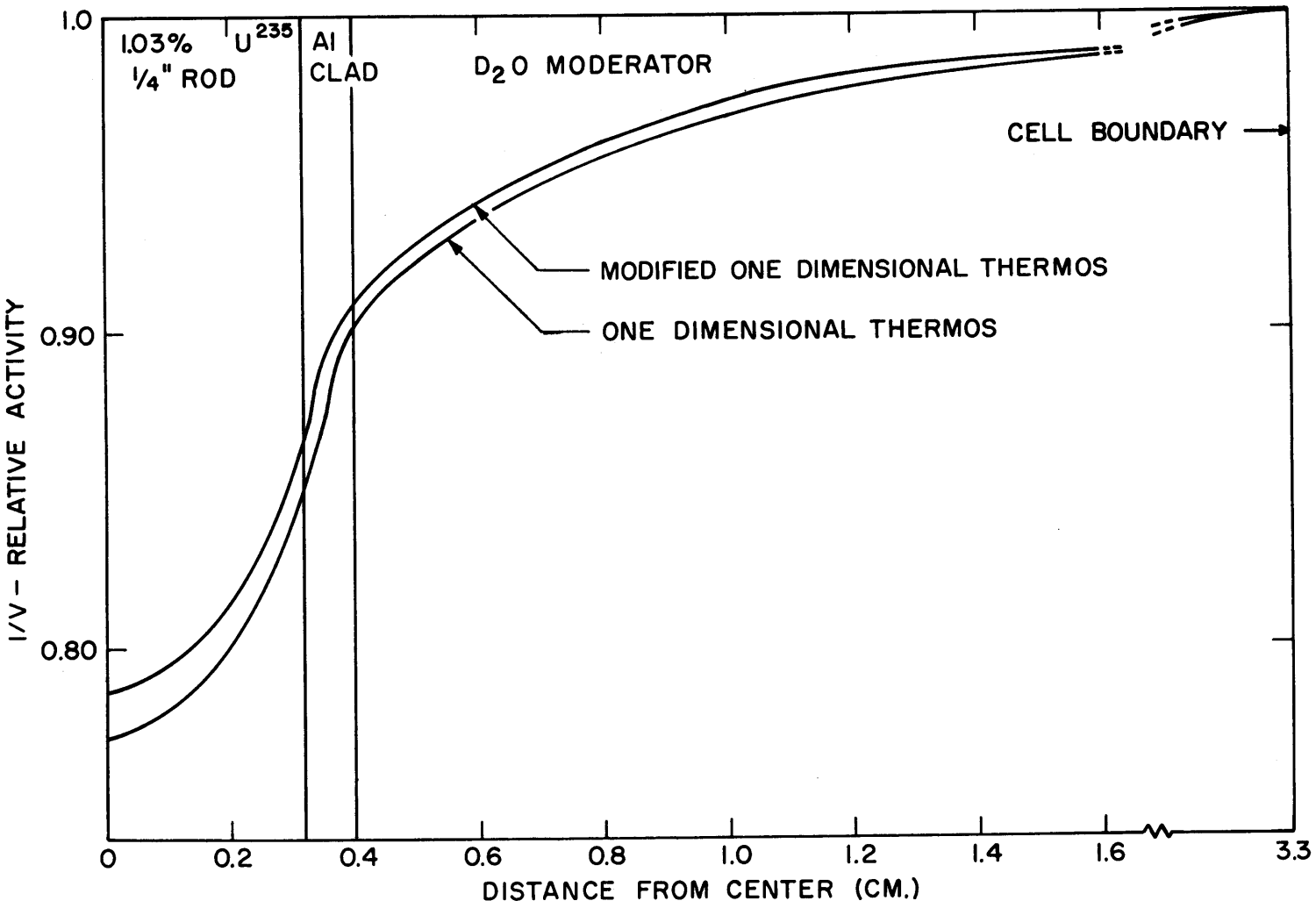

FIG. 3.6.7 COMPARISON OF THE ONE-DIMENSIONAL CALCULATIONS FOR THE LATTICE OF 1.03% ENRICHED URANIUM, 1/4-INCH DIAMETER RODS ARRANGED ON A 2.5-INCH TRIANGULAR SPACING.

interface determined by the integral transport calculation in the rod. One example of such a solution is given in Appendix A in connection with the problem of the flux perturbation due to a foil of finite thickness. It is difficult to find the origin of the use of this method of linking the fuel and moderator calculations, but it seems to have been in use before Amouyal et al. (A4) published their results. Such methods are also referred to as blackness, or thin region, theory (W1).

Honeck (H9) and Brown (B14) have demonstrated that the method of Amouyal, Benoist and Horowitz (ABH) can give results which agree well with experiment. However, they used hardened cross sections calculated with the THERMØS code. It seems desirable to have a simpler method which does not depend on the use of the more accurate, but expensive, THERMØS method.

The portion of the calculation that is most sensitive to the analysis is the fuel disadvantage factor, F, since diffusion theory would be expected to give reasonable results in the weakly absorbing moderator. A few assumptions will allow a general tabulation of some useful quantities of interest. It is assumed that the greater interest lies in the details of the neutron economy of the fuel rod rather than in the diffusion theory result in the moderator. Consequently, the subsequent discussion involves the fuel only.

The directional flux incident on the rod is assumed to be linearly anisotropic. The fuel is considered to be of large enough mass that no energy transfer can occur. Scattering and absorption are allowed. If β is the "blackness" of the rod, then the disadvantage factor, F, of the fuel is:

$$F = \Sigma_a R(2-\beta)/\beta , \tag{3.7.1}$$

where R is the radius of the rod and Σ_a is the macroscopic absorption cross section of the fuel. The calculation of β was broken up into three regions for three ranges of ΣR, and has been coded by McGoff (M4) and modified for use with the QUICK code (see Appendix C).

Region 1 $0 \leq \Sigma R \leq 0.1$,

$$\beta = \frac{2\Sigma_a R P_o}{1 - \frac{\Sigma_s}{\Sigma}(1-P_o)} ; \tag{3.7.2}$$

$$P_o = 1 - \frac{4}{3}\Sigma R + \frac{1}{2}(\Sigma R)^2 \log\frac{2}{\Sigma R} + \frac{1}{2}(\Sigma R)^2\left(\frac{5}{4} - 0.5772\right), \quad (3.7.3)$$

is the first collision probability for a flat, isotropic source.

Region 2 $0.1 < \Sigma R \leq 5.0$,

β is given by a least-square fit to the results of Stuart and Woodruff.

Region 3 $\Sigma R > 5.0$,

$$\beta = \frac{2\Sigma_a R P_o}{1 - \frac{\Sigma_s}{\Sigma}(1-P_o)}, \quad (3.7.4)$$

$$P_o = \frac{1}{2\Sigma R} - \frac{3}{32(\Sigma R)^3}. \quad (3.7.5)$$

The incident neutron spectrum on the rod was assumed to be a Maxwellian spectrum at the moderator temperature. This assumption appears reasonable for heavy water in the lattices of general interest. THERMØS calculations indicated that the scalar flux was close to a Maxwellian spectrum everywhere except in the rod.

Calculations with QUICK gave the disadvantage factor for the fuel rod as a function of energy. The measurable quantity is not the flux disadvantage factor but rather averages of the disadvantage factor with the activation cross section of the detector foils:

$$\overline{F} = \frac{\int_0^{E_c} \sigma_{ACT}(E)\, M(E)\, dE}{\int_0^{E_c} \frac{1}{F(E)}\, \sigma_{ACT}(E)\, M(E)\, dE}, \quad (3.7.6)$$

where M(E) represents the Maxwellian spectrum. These averages were computed by using the EDIT subroutine of the THERMØS code, to insure that comparisons between the two methods would be meaningful. Equation (3.7.6) gives the ratio of the activation of infinitely thin foil at the surface of the rod to the average activation of the foil in the rod below a cutoff energy, E_c.

Figures 3.7.1 to 3.7.3 give the results of calculations using Eq. (3.7.6) for gold, lutetium and europium foils. The foils were assumed

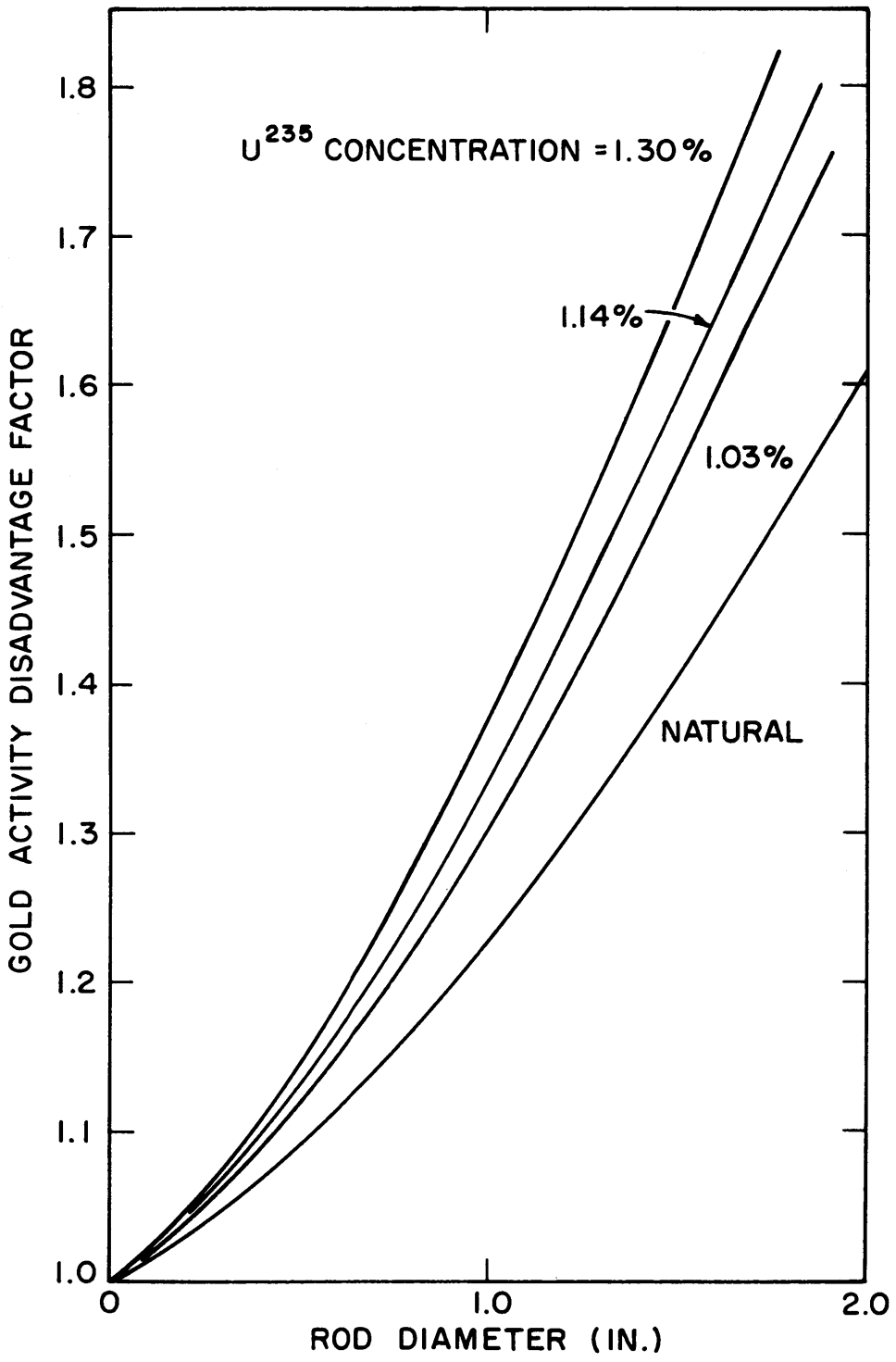

FIG. 3.7.1 RATIO OF THE ACTIVITY OF GOLD FOILS AT THE SURFACE OF A URANIUM METAL ROD TO THE AVERAGE ACTIVITY INSIDE THE ROD BELOW 0.4 EV, CALCULATED BY THE METHOD OF SUCCESSIVE GENERATIONS FOR AN INCIDENT MAXWELLIAN SPECTRUM.

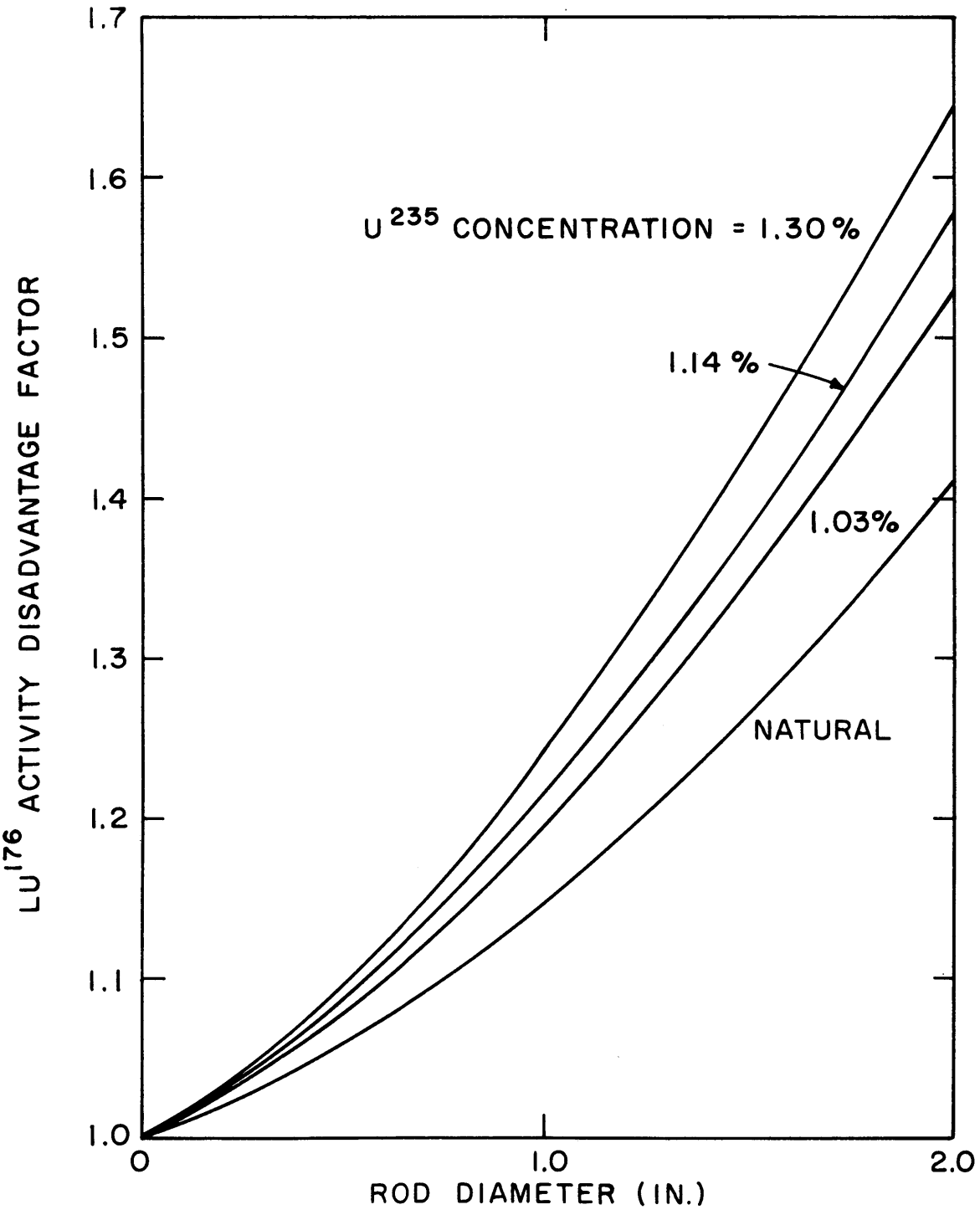

FIG. 3.7.2 RATIO OF THE ACTIVITY OF LUTETIUM FOILS AT THE SURFACE OF A URANIUM METAL ROD TO THE AVERAGE ACTIVITY INSIDE THE ROD BELOW 0.4EV, CALCULATED BY THE METHOD OF SUCCESSIVE GENERATIONS FOR AN INCIDENT MAXWELLIAN SPECTRUM.

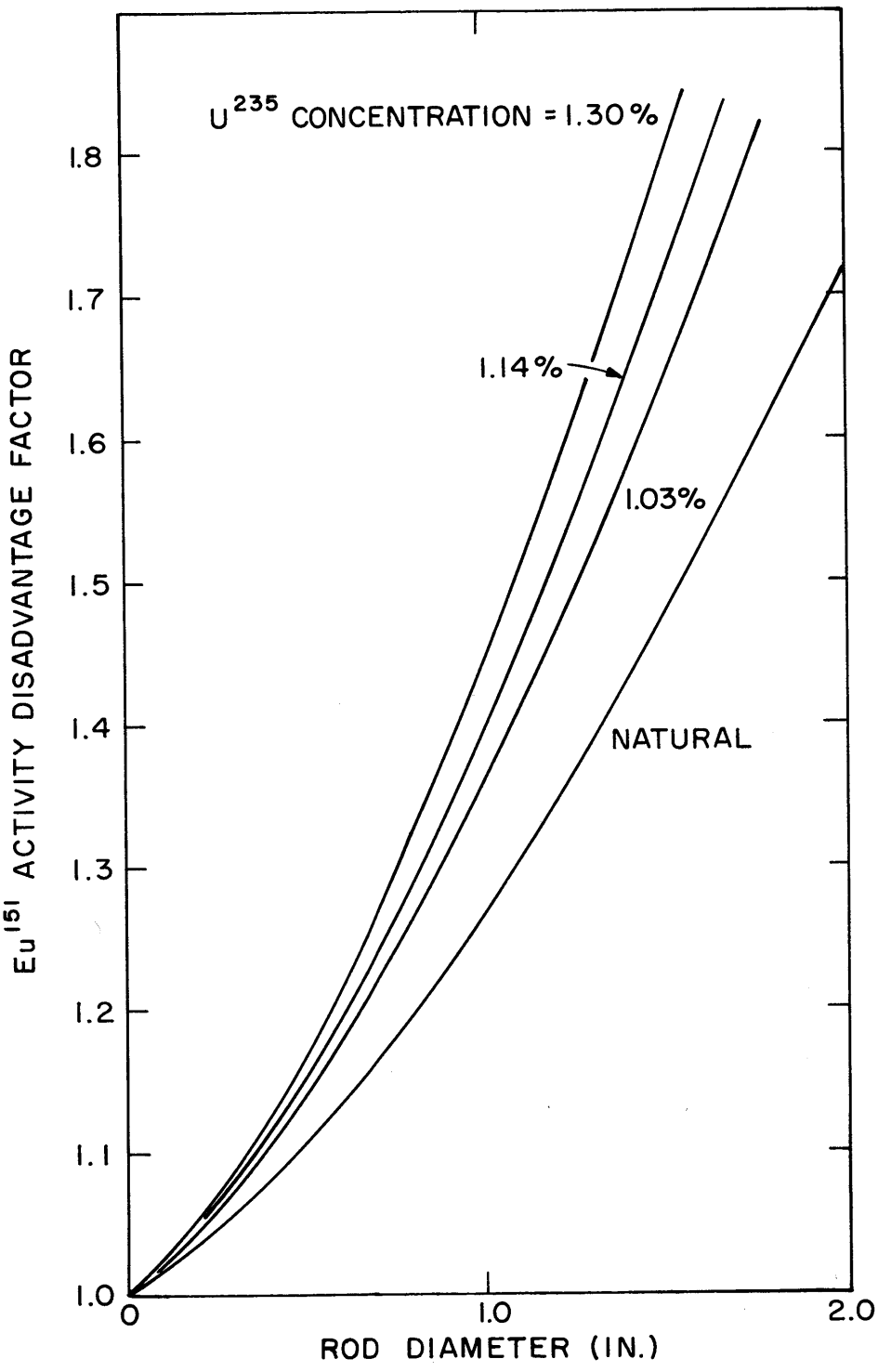

FIG. 3.7.3 RATIO OF THE ACTIVITY OF EUROPIUM FOILS AT THE SURFACE OF A URANIUM METAL ROD TO THE AVERAGE ACTIVITY INSIDE THE ROD BELOW 0.14 EV, CALCULATED BY THE METHOD OF SUCCESSIVE GENERATIONS FOR AN INCIDENT MAXWELLIAN SPECTRUM.

to be infinitely thin. The calculations were made for rod diameters up to 1.3%, for the concentrations of the rods investigated at M.I.T. and in the B.N.L. H_2O-moderated lattice experiments. Because the activation cross sections of the detector foils differ as a function of energy, the averages calculated from Eq. (3.7.6) are different. This result is not possible in single velocity approximations, such as in the ABH method as it is usually applied.

It would be quite costly to check every point on Figs. 3.7.1 to 3.7.3 with experiments or more accurate calculations, but use can be made of those that are already available. THERMØS has been found to predict the flux shape in the natural uranium lattices investigated by Brown (B14). It can therefore be assumed that THERMØS is capable of predicting a disadvantage factor that agrees with experiment. Table 3.7.1 gives the comparison of the calculated results from Eq. (3.7.6) and THERMØS for a 1/v-activator such as gold foils that are effectively infinitely thin. The largest disagreement is for the 1-inch diameter, natural uranium rods; the difference is about 4%. However, the entire set of curves given in Figs. 3.7.1 to 3.7.3 was generated in half the computer time required for a single THERMØS calculation. Once the results of Eq. (3.7.6) are obtained, further calculations, such as those to calculate the over-all disadvantage factor, no longer require the use of a computer.

The value of η for the 2-inch diameter, 1.03% U^{235}, uranium rod was only 0.4% lower than the Maxwellian average value, indicating that the hardening does not affect the value of η very much. The possibilities for use of the method of successive generations have by no means been exhausted and further work in this area is indicated. For example, a good treatment of oxide-fueled rods has not yet been developed.

TABLE 3.7.1

Fuel Disadvantage Factors for 1/v-Activators Below 0.4 ev

Rod Diameter (in.)	U-235 Concentration (%)	Successive Generations Calculation	THERMØS Calculation	THERMØS PROBLEM Description
0.25	1.03	1.051	1.061	D_2O Moderator, 1.25" spacing
0.25	1.14	1.056	1.077	D_2O Moderator, 1.25" spacing
0.25	1.03	1.051	1.077	D_2O Moderator, 2.5" spacing
0.25	1.14	1.056	1.090	D_2O Moderator, 2.5" spacing
1.01	Natural	1.226	1.248	D_2O Moderator, 4.5" spacing
1.01	Natural	1.226	1.253	D_2O Moderator, 5.0" spacing
1.01	Natural	1.226	1.257	D_2O Moderator, 5.75" spacing
1.10	Natural	1.260	1.200	B.N.L. graphite reactor lattice

CHAPTER IV
EXPERIMENTAL RESULTS AND COMPARISON WITH ANALYTICAL METHODS

4.1 THE EXPERIMENTAL RESULTS

A series of intracellular activation measurements has been completed in lattices of 1.03% U^{235}, 1/4-inch diameter, uranium metal rods in heavy water. The experiments were designed to investigate various aspects of the problems discussed in Chapter III. Most of the experiments were made with the gold foils described in Section 2.3, although foils of depleted uranium, lutetium, europium and copper were also used. Table 4.1.1 is a listing of the measurements completed and to be discussed in this chapter.

In the three-rod cluster arrangement used in the experiments, only the area defined by the three rods was available for experimentation, which precluded extending the foil holders any further than the boundary of the cluster. Figure 4.1.1 shows the directions in which experimental flux traverses were made. For example, the rod-to-moderator traverse is in the direction from the center rod to the midpoint between the other two rods of the cluster. The rod-to-moderator traverse would be expected to yield higher activities in the neighborhood of the equivalent cell boundary, since the thermal flux level on the rod-to-rod traverse is decreased by its proximity to the adjacent rod.

The experimental results are tabulated for all the experiments in Tables 4.1.2 to 4.1.5. The convention adopted in designating runs was to use "A" for gold foils, "L" for lutetium alloy foils, "E" for europium powder foils, "DU" for depleted uranium foils and "CU" for copper foils. The numbering also indicates the chronological order in which the experiments were performed.

TABLE 4.4.1

Summary of Intracellular Activity Distribution Measurements

Run	Detector Foil	Triangular Lattice Spacing (in.)	Diameter of Tank (ft.)	Counting Procedure D≡Differential I≡Integral	Standard Deviation[a] for Sub-cadmium Activity(%)	Standard Deviation[a] for Epi-cadmium Activity(%)	Cadmium Ratio at the Cell Edge	Standard Deviation[a] for the Cadmium Ratio (%)
A4	2.5 mil thick Au	2.50	4	D	0.6	0.5	9.00	0.7
A4	2.5 mil thick Au	2.50	4	I	0.4	1.0	9.06	1.0
A5	4.3 mil thick Au	2.50	4	D	0.2	0.4	11.2	0.4
A5	4.3 mil thick Au	2.50	4	I	0.2	0.4	11.2	0.5
A6	2.5 mil thick Au	2.50	4	D	0.3	0.4	9.57	0.5
A6	2.5 mil thick Au	2.50	4	I	0.5	0.6	9.50	0.7
A7	4.3 mil thick Au	2.50	4	D	0.3	0.3	11.6	0.4
A7	4.3 mil thick Au	2.50	4	I	0.3	0.4	11.4	0.4
A8	Dilute Au	2.50	4	D	1.9	1.6	3.5	2.0
A9	10 mil thick Au	2.50	4	D	0.2	0.4	13.9	0.4
A9	10 mil thick Au	2.50	4	I	0.2	0.5	13.9	0.4
A10	10 mil thick Au	2.50	4	D	0.2	0.4	14.0	0.5
A11	4.3 mil thick Au	1.25	3	D	0.4	0.4	3.78	0.5
A12	10 mil thick Au	1.25	3	D	0.4	0.5	4.51	0.5
A13	10 mil thick Au	1.25	3	D	0.4	0.5	4.56	0.5
A14	2.5 mil thick Au	1.25	3	D	0.8	0.5	3.33	0.7
A15	2.5 mil thick Au	1.25	3	D	0.6	0.5	3.31	0.6
A16	4.3 mil thick Au	1.25	3	D	0.5	0.5	3.81	0.6
A17	10 mil thick Au	2.50	3	D	0.3	0.7	13.7	0.8

(a) Standard deviation for counting only.

TABLE 4.4.1

Summary of Intracellular Activity Distribution Measurements (concluded)

Run	Detector Foil	Triangular Lattice Spacing (in.)	Diameter of Tank (ft.)	Counting Procedure D ≡ Differential I ≡ Integral	Standard Deviation[(a)] for Sub-cadmium Activity (%)	Standard Deviation[(a)] for Epi-cadmium Activity (%)	Cadmium Ratio at the Cell Edge	Standard Deviation[(a)] for the Cadmium Ratio (%)
DU2	Dpl. Uran.	2.50	4	D	0.9	0.4	2.08	0.6
DU3	Dpl. Uran.	1.25	3	D	2.0	0.4	1.322	0.6
DU4	Dpl. Uran.	1.25	3	D	3.0	0.6	1.290	0.8
L2	Lu-Al Alloy	2.50	4	I	1.0	–	–	–
L3	Lu-Al Alloy	2.50	4	I	0.7	–	–	–
L4	Lu-Al Alloy	1.25	3	I	2.2	–	–	–
L5	Lu-Al Alloy	1.25	3	I	4.0	–	–	–
E2	Eu Powder	2.50	4	I	1.0	–	–	–
E3	Eu Powder	2.50	4	I	1.6	–	–	–
CU1	5 mil thick Cu	1.25	3	I	1.0	2.0	9.50	2.3

(a) Standard deviation for counting only.

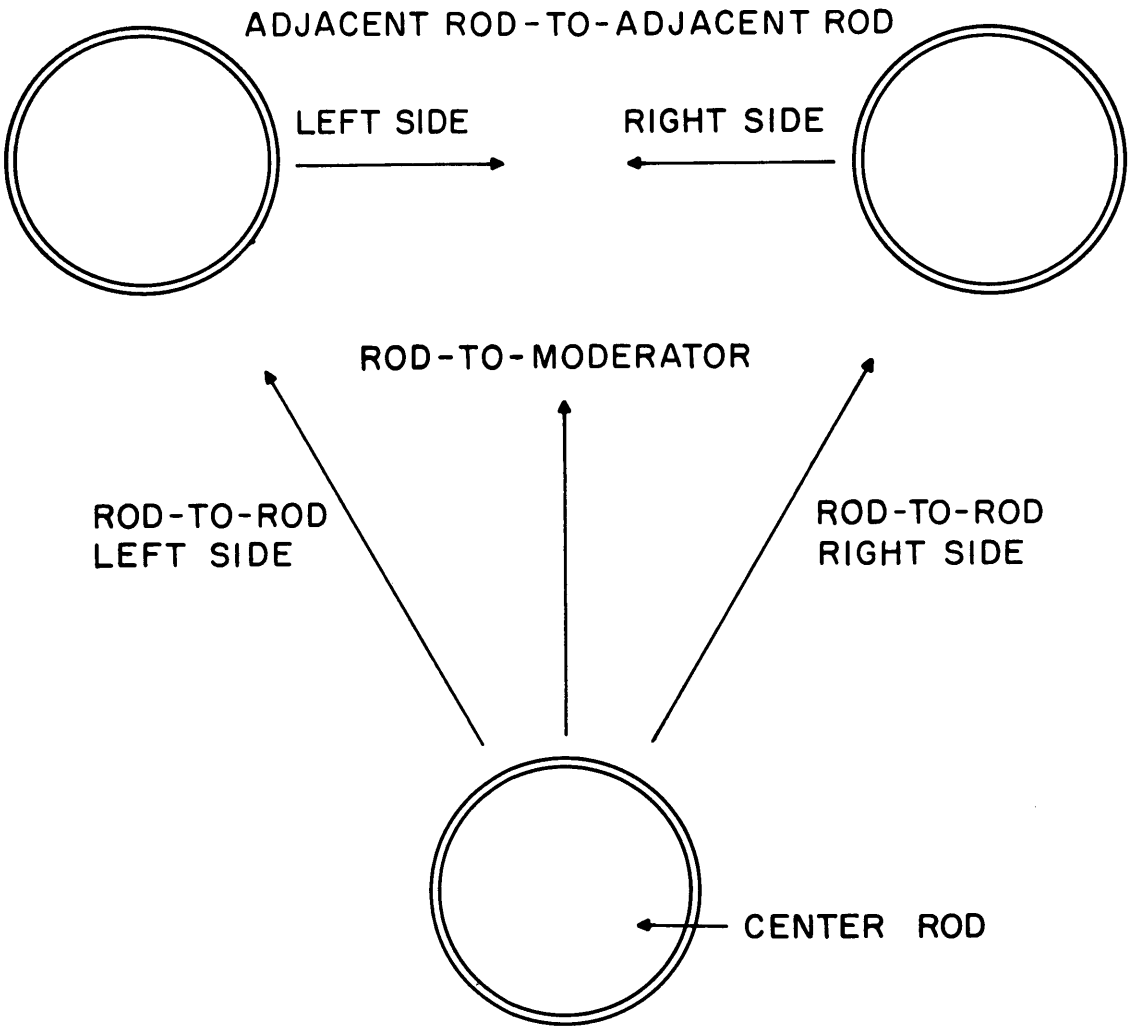

FIG. 4.1.1 DIRECTIONS OF INTRACELLULAR ACTIVITY TRAVERSES IN THE MODERATOR.

TABLE 4.1.2

SUBCADMIUM ACTIVITY DISTRIBUTIONS FOR THE EXPERIMENTS IN THE LATTICE WITH THE 2.5-INCH TRIANGULAR SPACING

RADIAL POSITION (CM)	SYMBOL USED TO PLOT POINT	RUN A8 DILUTE GOLD (STRADDLE)	RUN A4 2.5 MIL THICK GOLD (STRADDLE)[a]	RUN A4 2.5 MIL THICK GOLD (INTEGRAL)[b]	RUN A6 2.5 MIL THICK GOLD (STRADDLE)	RUN A6 2.5 MIL THICK GOLD (INTEGRAL)	RUN A5 4.3 MIL THICK GOLD (STRADDLE)	RUN A5 4.3 MIL THICK GOLD (INTEGRAL)	RUN A7 4.3 MIL THICK GOLD (STRADDLE)	RUN A7 4.3 MIL THICK GOLD (INTEGRAL)	RUN A9 10 MIL THICK GOLD (STRADDLE)	RUN A9 10 MIL THICK GOLD (INTEGRAL)	RUN A10 10 MIL THICK GOLD (STRADDLE)	RUN A17[c] 10 MIL THICK GOLD (STRADDLE)	RUN DU2 5 MIL THICK DEPLETED URANIUM (STRADDLE)	RUN L2 LU-AL ALLOY (INTEGRAL)	RUN L3 LU-AL ALLOY (INTEGRAL)	RUN E2 EUROPIUM POWDER (INTEGRAL)	RUN E3 EUROPIUM POWDER (INTEGRAL)
0.0	×	0.879	0.787	0.795	0.784	0.776	0.802	0.809	0.766	0.767	0.762	0.761	0.753	0.777	0.890	0.838	0.886	0.812	0.805
	○	0.912	0.809	0.798	0.803	0.803	0.787	0.791	0.764	0.761	0.758	0.755	0.760	0.772	0.924				
0.158	×	0.896	0.821	0.819	0.830	0.825	0.812	0.816	0.785	0.778	0.798	0.798	0.798	0.799	0.913	0.874	0.879	0.951	1.054
	○	0.795	0.822	0.815	0.822	0.826	0.812	0.818	0.789	0.789	0.801	0.802	0.796	0.790	0.974				
0.187	×	0.856	0.824	0.821	0.813	0.818	0.826	0.828	0.778	0.775	0.830	0.826	0.833	0.820	0.921	0.896	0.905	0.597	0.693
	○	0.875	0.845	0.840	0.824	0.823	0.824	0.827	0.809	0.811	0.818	0.817	0.828	0.810	0.973				
0.237	×	0.843	0.828	0.838	0.847	0.843	0.844	0.850	0.824	0.825	0.835	0.837	0.847	0.828	0.947	0.899	0.905	0.633	0.770
	○	0.885	0.848	0.856	0.826	0.818	0.831	0.832	0.838	0.835	0.833	0.833	0.844	0.832	0.981				
0.400	×	1.032	0.876	0.877	0.912	0.906	0.913	0.916	0.867	0.886	0.905	0.905	0.877	0.897		0.922	0.929	0.777	0.775
	+	0.962	0.877	0.882	0.890	0.896	0.896	0.897	0.883	0.898	0.911	0.911	0.873	0.886		0.978	0.836		0.894
0.563	×	0.956	0.935	0.927	0.918	0.913	0.939	0.938	0.931	0.932	0.939	0.940	0.923	0.938	0.972	0.967	0.956	0.656	0.727
	○	0.974	0.916	0.924	0.940	0.949	0.938	0.937	0.929	0.927	0.926	0.931	0.909	0.942	0.985	0.971	0.944	0.839	0.935
	+	0.984	0.916	0.917	0.942	0.946	0.945	0.945	0.932	0.930	0.929	0.930	0.932	0.927	0.960				
1.085	×	0.978	0.969	0.965	0.980	0.960	0.971	0.972	0.976	0.975	0.981	0.977	0.962	0.978	1.032	0.982	0.977	0.824	0.904
	○	1.058	0.987	0.979	0.971	0.976	0.966	0.970	0.979	0.982	0.953	0.954	0.965	0.967	0.968	0.966	0.995	0.725	1.105
	+	1.028	0.962	0.961	0.985	0.979	0.972	1.007	0.963	0.961	0.977	0.975	0.977	0.981	0.950				
1.607	×	1.026	1.021	1.020	0.980	0.971	0.986	0.992	1.000	0.997	0.981	0.979	0.987	1.009	1.017	1.003	0.999	0.829	0.902
	○	1.069	1.001	0.996	0.993	0.987	0.999	1.006	0.985	0.985	0.983	0.980	0.979	0.997	0.989	0.969	1.030	1.081	1.221
	+	1.029	0.988	0.988	0.996	0.987	1.004	1.008	0.991	0.988	0.972	0.972	0.990	0.993	1.026				
2.130	×	1.023	1.002	0.998	0.984	0.976	0.995	0.999	0.995	0.990	0.995	0.994	0.990	1.005	0.995	1.009	1.030	0.882	0.995
	○	1.054	1.012	1.010	0.989	1.001	1.008	0.988	0.996	0.993	0.993	0.994	0.995	0.989	0.855	0.998	0.971	1.227	0.981
	+	0.939	1.004	1.007	0.985	0.985	0.991	0.999	0.999	1.001	0.998	1.001	0.993	1.001	1.025				
2.652	×	1.033	0.992	0.987	0.992	1.001	1.012	1.012	0.997	0.998	0.992	0.991	1.006	1.001	1.039	0.999	0.994	1.177	1.332
	○	0.887	0.994	0.996	0.993	0.990	1.002	0.999	1.016	1.017	0.989	0.993	0.992	0.991	0.994	0.992	1.000	0.909	1.006
	+	0.927	1.000	1.006	1.003	1.010	0.995	0.999	0.993	0.995	0.995	0.994	0.994	0.993	0.965				
3.175	×	1.061	0.994	0.999	1.022	1.015	0.995	0.995	0.991	0.988	1.003	1.001	1.008	1.001	1.032	1.001	1.002	0.901	0.993
	○	1.082	0.995	1.005	0.999	0.999	1.007	0.992	1.006	1.002	1.016	1.018	1.003	1.005	1.000	0.999	0.997	0.801	1.013
	+	0.990	0.998	0.993	1.001	1.002	0.998	1.001	0.986	0.988	0.995	0.993	0.996	0.989	1.070				
4.046	×	0.990	1.006	1.004	0.988	0.993	0.989	0.991	0.986	0.987	0.997	0.995	0.993	0.990	0.970	0.992	0.982	0.918	1.002
	○	1.095	1.000	1.024	1.006	1.001	1.019	1.022	0.996	0.995	0.996	0.999	1.000	0.993	0.997	1.012	0.986	0.901	1.020
	+	0.919	1.000	1.001	0.999	1.003	1.007	1.005	0.990	0.992	1.007	1.005	1.000	0.997	0.984				
4.916	×	1.014	0.992	0.989	0.986	0.984	0.997	1.002	0.981	0.980	1.000	1.001	0.995	0.996	1.021	0.999	0.971	0.877	0.980
	○	1.029	1.011	1.007	1.019	1.018	1.003	1.012	1.008	1.014	1.014	1.016	1.000	1.015	1.018	1.005	1.011	0.894	1.023
	+	1.016	0.973	0.979	0.986	0.979	1.000	1.001	0.981	0.982	0.990	0.990	0.981	1.005	0.944				
5.786	×	0.962	0.941	0.948	0.944	0.932	0.952	0.957	0.934	0.935	0.965	0.960	0.974	0.969	0.952	0.946	0.955	0.844	0.943
	+	0.912	0.927	0.930	0.927	0.920	0.943	0.943	0.936	0.938	0.936	0.936	0.940	0.940	0.991				
5.499	○	1.020	0.979	0.980	1.012	1.011	0.991	0.993	1.007	1.020	1.017	1.019	0.990		1.040	1.022	0.995	0.879	1.006

(a) "Straddle" indicates the differential counting method.
(b) "Integral" indicates the integral counting method.
(c) The tank size was 3 feet; all other experiments were made in the 4-foot tank.

TABLE 4.1.3

EPICADMIUM ACTIVITY DISTRIBUTIONS FOR THE EXPERIMENTS IN THE LATTICE WITH THE 2.5-INCH TRIANGULAR SPACING

RADIAL POSITION (CM)	SYMBOL USED TO PLOT POINT	RUN A8 DILUTE GOLD (STRADDLE)	RUN A4 2.5 MIL THICK GOLD (STRADDLE)[a]	RUN A4 2.5 MIL THICK GOLD (INTEGRAL)[b]	RUN A6 2.5 MIL THICK GOLD (STRADDLE)	RUN A6 2.5 MIL THICK GOLD (INTEGRAL)	RUN A5 4.3 MIL THICK GOLD (STRADDLE)	RUN A5 4.3 MIL THICK GOLD (INTEGRAL)	RUN A7 4.3 MIL THICK GOLD (STRADDLE)	RUN A7 4.3 MIL THICK GOLD (INTEGRAL)	RUN A9 10 MIL THICK GOLD (STRADDLE)	RUN A9 10 MIL THICK GOLD (INTEGRAL)	RUN A10 10 MIL THICK GOLD (STRADDLE)	RUN A17[c] 10 MIL THICK GOLD (STRADDLE)	RUN DU2 5 MIL THICK DEPLETED URANIUM (STRADDLE)
0.0	×	0.376	0.103	0.103	0.0930	0.0941	0.0777	0.0773	0.0758	0.0766	0.0587	0.0587	0.0584	0.0672	0.508
	○	0.372	0.0999	0.102	0.0960	0.0963	0.0793	0.0790	0.0782	0.0789	0.0598	0.0598	0.0593	0.0689	0.509
0.158	×	0.378	0.107	0.108	0.106	0.107	0.0832	0.0819	0.0797	0.0810	0.0664	0.0660	0.0611	0.0716	0.527
	○	0.362	0.107	0.107	0.106	0.106	0.0865	0.0865	0.0812	0.0820	0.0676	0.0680	0.0619	0.0724	0.523
0.187	×	0.393	0.113	0.111	0.107	0.107	0.0880	0.0876	0.0821	0.0837	0.0656	0.0654	0.0622	0.0651	0.523
	○	0.398	0.110	0.111	0.106	0.106	0.0834	0.0825	0.0823	0.0827	0.0651	0.0656	0.0631	0.0681	0.542
0.237	×	0.437	0.115	0.114	0.109	0.110	0.0884	0.0873	0.0866	0.0885	0.0682	0.0685	0.0635	0.0708	0.550
	○	0.378	0.115	0.112	0.109	0.109	0.0878	0.0881	0.0861	0.0873	0.0693	0.0690	0.0637	0.0711	0.553
0.642	×	0.414	0.123	0.123	0.115	0.114	0.0981	0.0981	0.0934	0.0942	0.0748	0.0748	0.0765	0.0759	0.892
	○	0.364	0.122	0.123	0.114	0.114	0.0959	0.0958	0.0930	0.0942	0.0763	0.0761	0.0744	0.0767	0.887
	+	0.406	0.123	0.123	0.114	0.114	0.0974	0.0974	0.0920	0.0925	0.0758	0.0759	0.0758	0.0759	0.854
1.486	×	0.404	0.124	0.123	0.115	0.116	0.0986	0.0980	0.0953	0.0961	0.0769	0.0771	0.0767	0.0786	0.917
	○	0.409	0.125	0.126	0.115	0.116	0.0971	0.0957	0.0956	0.0964	0.0785	0.0784	0.0772	0.0785	0.901
	+	0.374	0.124	0.124	0.116	0.118	0.0972	0.0976	0.0940	0.0946	0.0766	0.0768	0.0782	0.0772	0.940
2.330	×	0.409	0.128	0.126	0.115	0.117	0.100	0.100	0.0918	0.0939	0.0782	0.0787	0.0761	0.0784	0.913
	○	0.376	0.126	0.124	0.117	0.118	0.0989	0.101	0.0937	0.0944	0.0772	0.0773	0.0786	0.0784	0.953
	+	0.415	0.125	0.122	0.117	0.116	0.0992	0.0985	0.0936	0.0946	0.0768	0.0766	0.0776	0.0797	0.911
3.175	×	0.424	0.127	0.124	0.117	0.119	0.0976	0.0988	0.0961	0.0967	0.0777	0.0776	0.0784	0.0794	0.934
	○	0.412	0.124	0.128	0.116	0.117	0.0975	0.0960	0.0938	0.0949	0.0784	0.0789	0.0773	0.0791	0.945
	+	0.381	0.124	0.121	0.116	0.118	0.0986	0.0970	0.0964	0.0967	0.0780	0.0779	0.0745	0.0782	0.949
4.019	×	0.411	0.126	0.127	0.117	0.118	0.100	0.100	0.0949	0.0956	0.0767	0.0770	0.0770	0.0801	0.915
	○	0.372	0.127	0.126	0.119	0.119	0.100	0.0988	0.0950	0.0957	0.0779	0.0785	0.0772	0.0784	0.920
	+	0.404	0.129	0.135	0.117	0.116	0.0976	0.0978	0.0973	0.0978	0.0785	0.0789	0.0776	0.0788	0.925
4.864	×	0.375	0.130	0.131	0.117	0.117	0.0983	0.0978	0.0951	0.0965	0.0782	0.0780	0.0782	0.0791	0.948
	○	0.416	0.126	0.125	0.118	0.119	0.102	0.100	0.0951	0.0960	0.0779	0.0786	0.0782	0.0802	0.914
	+	0.458	0.126	0.127	0.119	0.119	0.0968	0.0964	0.0943	0.0956	0.0784	0.0785	0.0758	0.0775	0.918
5.707	×	0.391	0.126	0.126	0.116	0.117	0.0974	0.0954	0.0957	0.0971	0.0776	0.0773	0.0756	0.0793	0.894
	+	0.403	0.124	0.120	0.114	0.114	0.0982	0.0952	0.0931	0.0942	0.0766	0.0774	0.0749	0.0751	0.862
5.499	○	0.362	0.128	0.126	0.116	0.118	0.0966	0.0939	0.0930	0.0944	0.0782	0.0776	0.0767	0.0790	0.930

(a) "Straddle" indicates the differential counting method.
(b) "Integral" indicates the integral counting method.
(c) The tank size was 3 feet; all other experiments were made in the 4-foot tank.

TABLE 4.1.4

SUBCADMIUM ACTIVITY DISTRIBUTIONS FOR THE EXPERIMENTS IN THE LATTICE WITH THE 1.25-INCH TRIANGULAR SPACING

RADIAL POSITION (CM)	SYMBOL USED TO PLOT POINT	RUN A14 2.5 MIL THICK GOLD	RUN A15 2.5 MIL THICK GOLD	RUN A16 4.3 MIL THICK GOLD	RUN A11 4.3 MIL THICK GOLD	RUN A12 10.2 MIL THICK GOLD	RUN A13 10.2 MIL THICK GOLD	RUN DU3 5 MIL THICK DEPLETED URANIUM	RUN DU4 5 MIL THICK DEPLETED URANIUM	RUN CU1 5 MIL THICK COPPER	RUN L4 LUTETIUM ALLOY	RUN L5 LUTETIUM ALLOY
0.0	×	0.814	0.810	0.803	0.817	0.782	0.806	0.796	0.794	0.845	0.971	0.909
	○	0.820	0.794	0.801	0.790	0.777	0.794	0.804	0.815	0.837	0.953	0.928
0.158	×	0.835	0.836	0.829	0.804	0.813	0.814	0.817	0.859	0.878	0.919	0.906
	○	0.831	0.821	0.829	0.803	0.791	0.794	0.789	0.856	0.844	0.923	0.918
0.187	×	0.839	0.829	0.812	0.825	0.830	0.831	0.782	0.869	0.848	0.882	0.992
	○	0.832	0.829	0.810	0.800	0.812	0.818	0.792	0.851	0.857	0.914	0.942
0.237	×	0.825	0.834	0.850	0.852	0.820	0.859	0.896	0.828	0.868	0.900	0.914
	○	0.815	0.833	0.848	0.845	0.852	0.819	0.838	0.819	0.887	0.931	0.965
0.400	×	0.893	0.905	0.887	0.901	0.870	0.902	–	–	0.952	0.937	0.939
	+	0.903	0.905	0.903	0.880	0.887	0.911	–	–	–	0.949	0.965
0.563	×	0.946	0.947	0.953	0.934	0.927	0.945	0.938	1.044	0.942	0.949	0.926
	○	0.959	0.936	0.970	0.945	0.934	0.952	0.958	1.049	0.940	0.926	0.978
	+	0.947	0.928	0.959	0.952	0.948	0.942	0.911	0.946	0.960		
0.972	×	0.968	0.983	0.976	0.992	0.992	0.994	0.967	0.963	1.006	0.969	1.028
	○	0.957	0.975	0.986	0.958	0.984	0.991	0.946	1.081	0.999	0.982	0.988
	+	0.976	0.962	0.993	0.978	0.992	0.987	0.970	0.894	0.995		
1.381	×	0.991	0.980	1.000	0.996	0.992	0.998	1.002	1.010	1.006	1.005	0.959
	○	0.959	0.999	0.996	0.982	0.992	0.983	1.018	0.959	0.997	1.027	1.023
	+	0.990	1.007	1.000	0.991	1.003	1.019	0.982	0.992	0.988		
1.793	×	1.012	1.004	1.001	1.010	0.993	0.993	1.022	1.000	1.009	1.000	1.070
	○	1.027	0.998	0.997	1.019	0.990	0.987	0.990	1.064	1.001	0.959	0.953
	+	1.008	0.996	0.993	0.986	1.016	1.006	0.978	0.960	0.987		
2.202	×	1.003	0.974	0.977	0.985	0.986	1.004	0.902	0.736	1.003	0.974	1.012
	○	0.999	0.975	0.991	1.005	1.026	0.985	1.003	0.913	1.011	0.992	0.993
	+	0.974	0.991	0.990	0.979	1.009	1.021	0.874	0.855	1.006		
2.611	×	0.939	0.930	0.950	0.953	0.965	0.966	0.876	0.954	0.956	0.923	1.009
	○	0.991	0.999	0.998	1.006	0.994	0.992	1.028	0.892	0.996	1.017	1.008
	+	0.968	0.951	0.970	0.972	0.962	0.979	0.928	0.869	0.969		
3.175	○	0.980	0.990	0.980	0.994	1.018	1.020	–	–	–	1.008	0.969
0.563[a]	△	0.948	0.974	0.942	0.958	0.954	0.959			0.950		
	□	0.973	0.967	0.961	0.957	0.975	0.971			0.968		
0.972[a]	△	1.004	0.996	0.994	0.982	0.994	1.000			1.025		
	□	0.991	0.985	1.003	0.997	1.000	1.009			1.012		
1.381[a]	△	1.001	0.997	1.012	1.012	1.012	0.983			1.019		
	□	0.967	0.981	0.993	0.999	1.015	1.000			1.007		

(a) Distance from center of adjacent rods.

TABLE 4.1.5

EPICADMIUM ACTIVITY DISTRIBUTIONS FOR THE EXPERIMENTS IN THE LATTICE WITH THE 1.25-INCH TRIANGULAR SPACING

RADIAL POSITION (CM)	SYMBOL USED TO PLOT POINT	RUN A14 2.5 MIL THICK GOLD	RUN A15 2.5 MIL THICK GOLD	RUN A16 4.3 MIL THICK GOLD	RUN A11 4.3 MIL THICK GOLD	RUN A12 10.2 MIL THICK GOLD	RUN A13 10.2 MIL THICK GOLD	RUN DU3 5 MIL THICK DEPLETED URANIUM	RUN DU4 5 MIL THICK DEPLETED URANIUM	RUN CU1 5 MIL THICK COPPER
0.0	×	0.348	0.392	0.308	0.334	0.217	0.262	0.583	0.672	0.107
	○	0.369	0.364	0.319	0.307	0.259	0.246	0.583	0.708	0.101
0.158	×	0.368	0.405	0.314	0.337	0.257	0.270	0.651	0.712	0.103
	○	0.379	0.378	0.321	0.323	0.256	0.263	0.614	0.722	0.105
0.187	×	0.379	0.406	0.323	0.343	0.258	0.274	0.653	0.737	0.107
	○	0.384	0.390	0.331	0.324	0.246	0.265	0.642	0.763	0.105
0.237	×	0.389	0.418	0.340	0.346	0.267	0.279	0.856	0.903	0.103
	○	0.405	0.402	0.334	0.334	0.265	0.272	0.814	1.048	0.106
0.500	×	0.423	0.428	0.348	0.360	0.284	0.286	2.66	2.988	0.118
	+	0.401	0.430	0.348	0.358	0.281	0.281	2.61	3.012	
0.601	×	0.421	0.433	0.346	0.357	0.280	0.285	2.82	3.160	0.116
	+	0.424	0.426	0.350	0.361	0.284	0.283	2.82	3.100	0.119
1.257	×	0.427	0.435	0.351	0.356	0.284	0.287	3.06	3.398	0.121
	○	0.428	0.430	0.357	0.362	0.283	0.286	3.09	3.449	0.117
	+	0.425	0.434	0.357	0.364	0.285	0.290	3.07	3.426	0.116
1.912	×	0.435	0.433	0.355	0.358	0.284	0.287	3.11	3.535	0.117
	○	0.433	0.430	0.350	0.360	0.287	0.288	3.12	3.457	0.119
	+	0.426	0.425	0.357	0.357	0.285	0.293	3.11	3.411	0.115
2.567	×	0.423	0.437	0.353	0.357	0.281	0.289	2.86	3.146	0.117
	○	0.430	0.430	0.357	0.360	0.284	0.290	3.20	3.404	0.116
	+	0.424	0.428	0.353	0.354		0.286	2.88	3.193	0.119
3.175	○	0.426	0.432	0.357	0.364	0.284	0.286	3.14	3.442	
0.826[a]	△	0.425	0.431	0.357	0.362	0.287	0.286	2.94		
	□	0.425	0.431	0.359	0.359	0.286	0.286	2.95		

(a) Distance from center of adjacent rods.

4.2 RESULTS FOR THE GOLD FOILS

4.2.1 Experimental Results

Gold foils of different thickness were irradiated in lattices with 1.25- and 2.5-inch triangular spacing, respectively. The experimental results are shown in Figs. 4.2.1 to 4.2.17. The same symbols are used in all of these figures, and the designations of the different traverses are defined in the legend given in Table 4.2.1. Unless otherwise mentioned, the differential counting technique was used.

TABLE 4.2.1

Legend for the Graphs of Intracellular Activation Distributions.

Symbol	In Moderator
×	Center rod-to-left adjacent rod
+	Center rod-to-right adjacent rod
○	Center rod-to-moderator
△	Left adjacent rod-to-right adjacent rod, up to the center-line
□	Right adjacent rod-to-left adjacent rod, up to the center-line
Symbol	**In Fuel**
×	Bottom foil holder in the lattice with the 2.5-inch spacing
○	Top foil holder in the lattice with the 2.5-inch spacing
×	Bottom of 60 mil button in the lattice with the 1.25-inch spacing
○	Top of 60 mil button in the lattice with the 1.25-inch spacing

4.2.2 Counting Techniques for Gold

In the early stages of experimentation, it was decided to investigate whether any differences would occur if both the integral and differential techniques were used to count the gold foils used in an experiment. The results of the experiments in which the two counting techniques were used are tabulated in Tables 4.1.2 and 4.1.4 and plotted for Runs A4, A5 and A9 in Figs. 4.2.2, 4.2.3, 4.2.5, 4.2.6, 4.2.8 and 4.2.9. The values of the cadmium ratio at the edge of the cell, obtained with the two counting techniques, are listed in Table 4.1.1; for no case is the difference greater than 1%, which is within the uncertainty due to the counting statistics. Since there

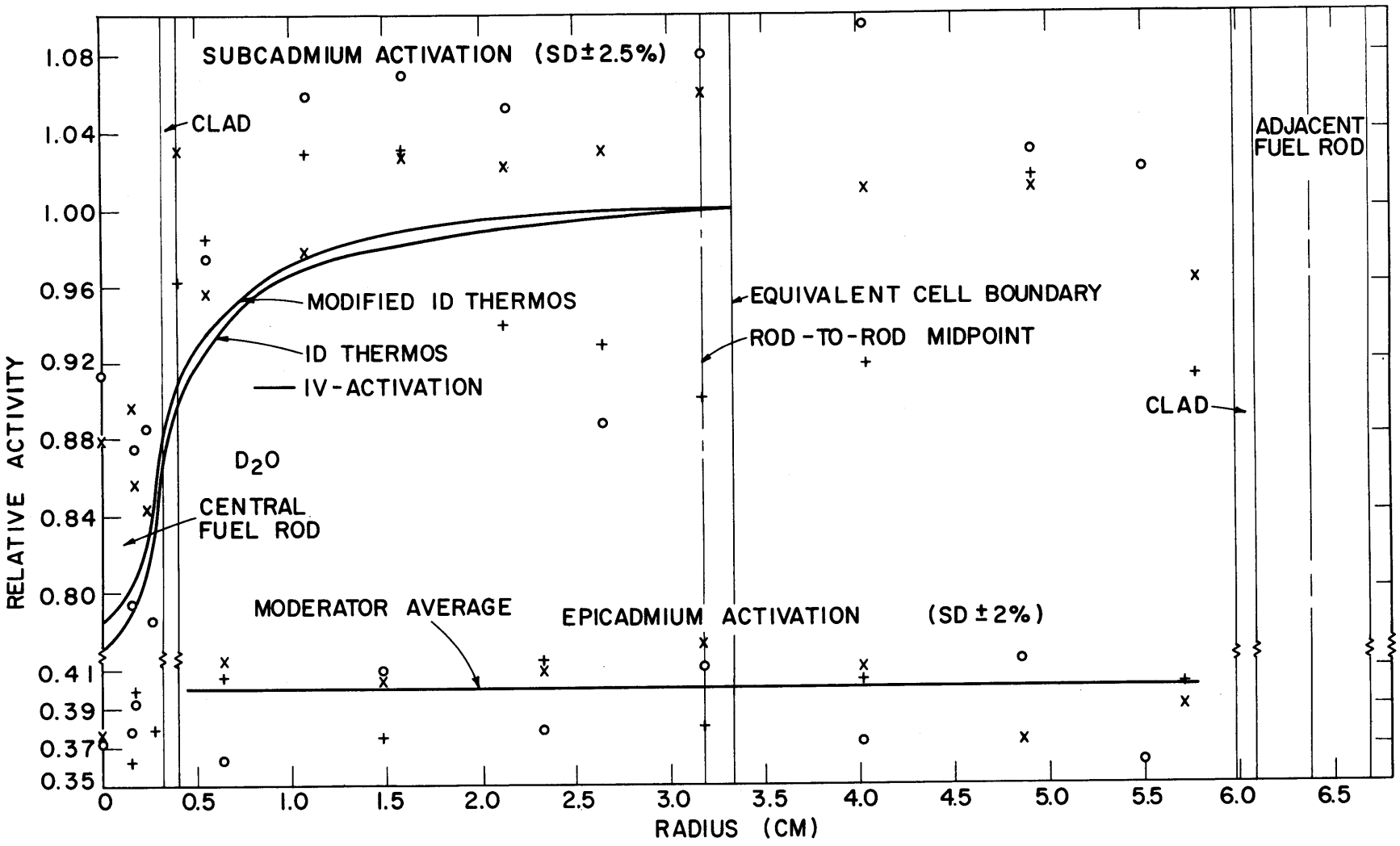

FIG. 4.2.1 GOLD ACTIVITY DISTRIBUTION FOR RUN A 8; DILUTE GOLD FOILS IN A LATTICE OF 1/4-INCH DIAMETER, 1.03% U-235, URANIUM RODS ON A 2.5-INCH TRIANGULAR SPACING.

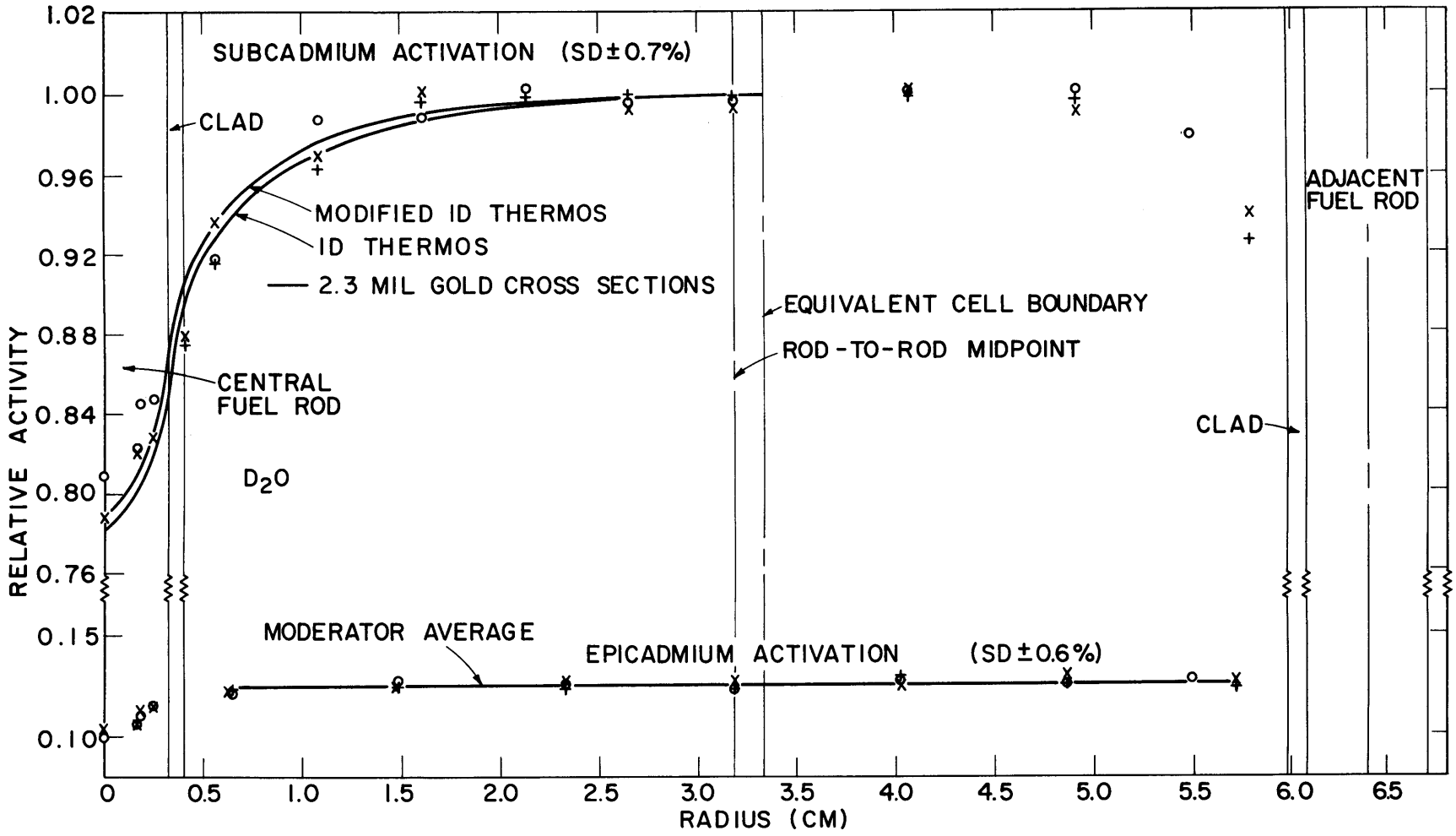

FIG. 4.2.2 GOLD ACTIVITY DISTRIBUTION FOR RUN A4; 2.5 MIL THICK GOLD FOILS IN A LATTICE OF 1/4-INCH DIAMETER, 1.03% U-235, URANIUM RODS ON A 2.5-INCH TRIANGULAR SPACING.

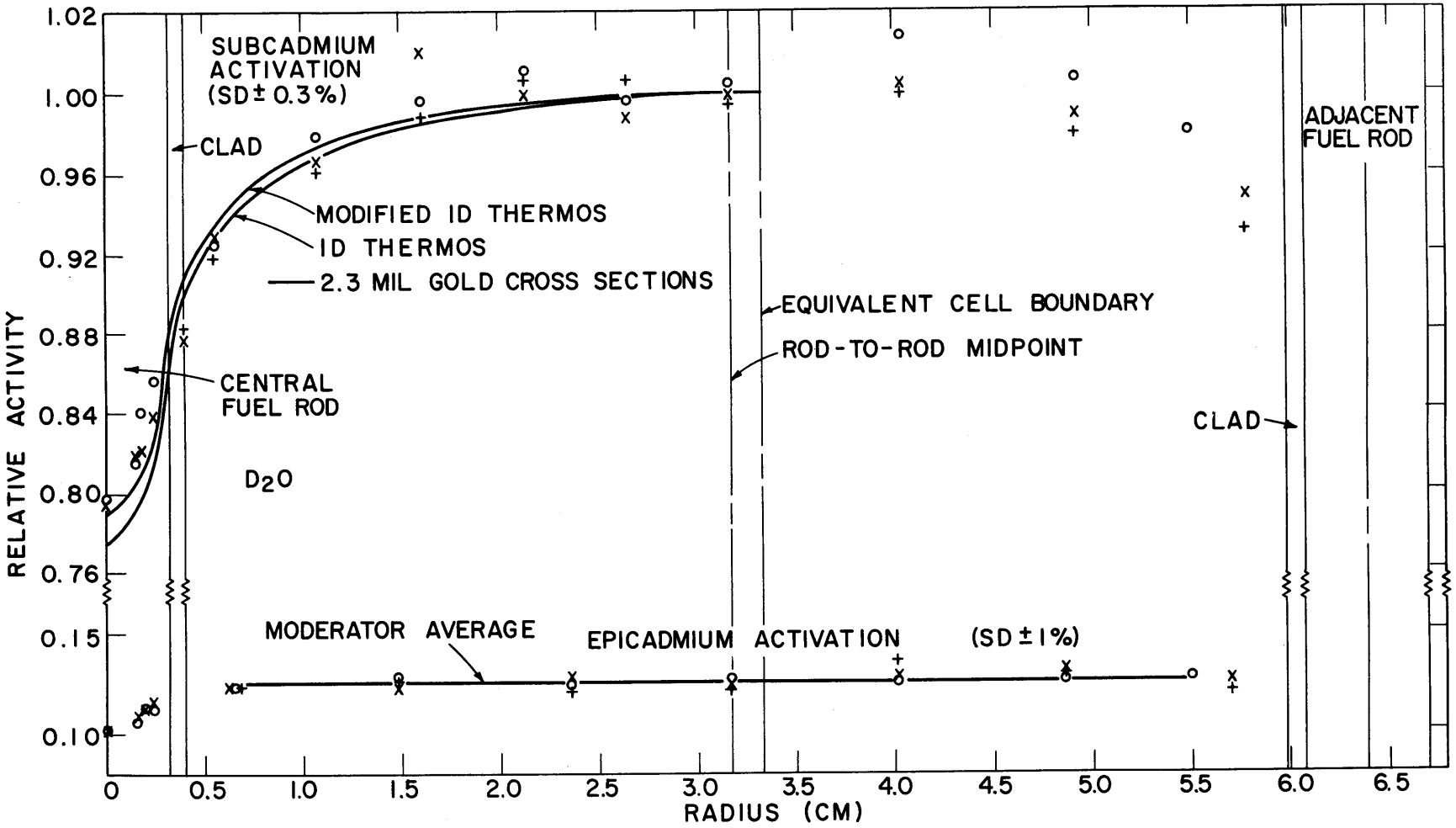

FIG. 4.2.3 GOLD ACTIVITY DISTRIBUTION FOR RUN A4; 2.5 MIL THICK GOLD FOILS IN A LATTICE OF 1/4-INCH DIAMETER, 1.03% U-235, URANIUM RODS ON A 2.5-INCH TRIANGULAR SPACING COUNTED BY THE INTEGRAL METHOD.

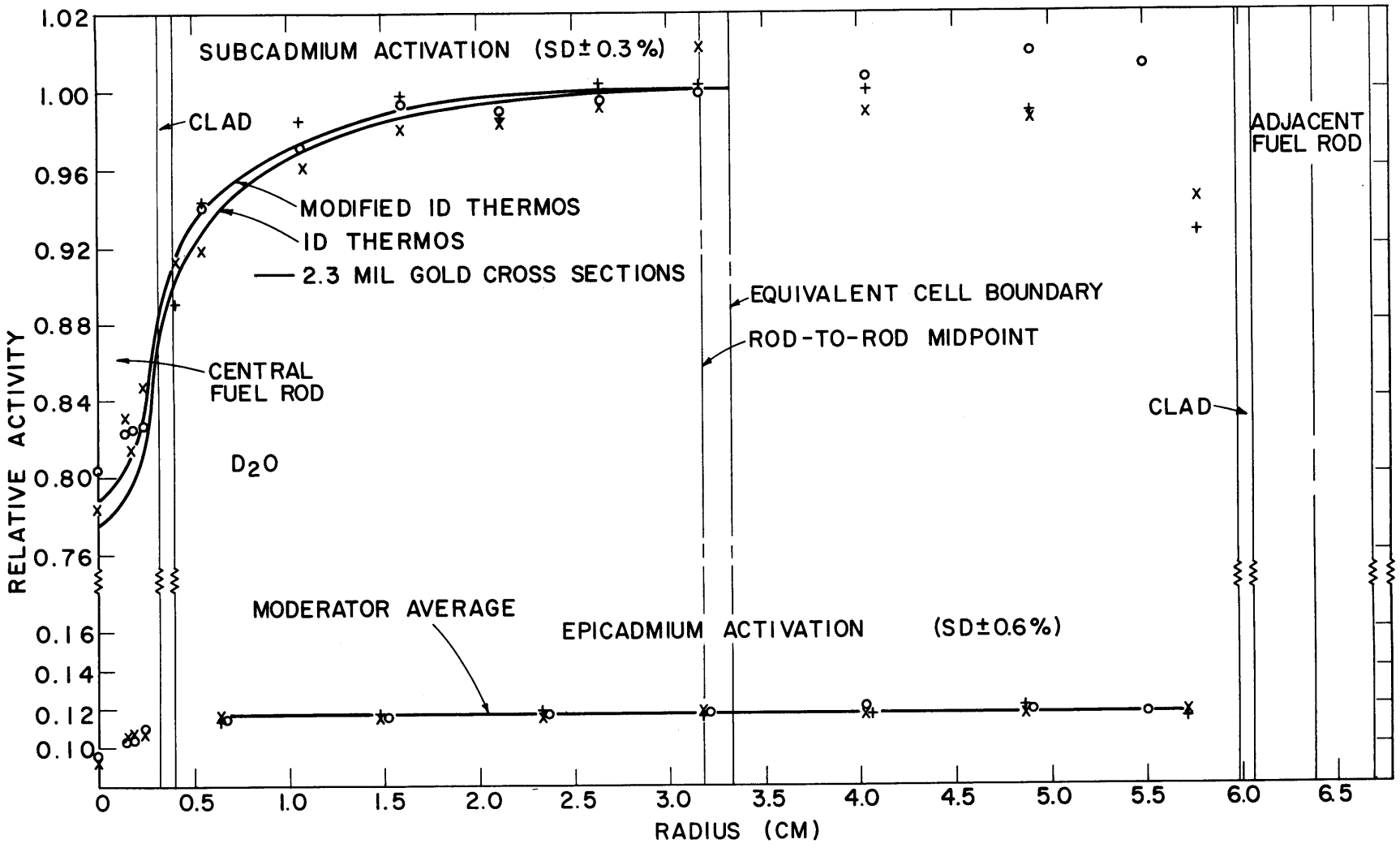

FIG. 4.2.4 GOLD ACTIVITY DISTRIBUTION FOR RUN A6; 2.5 MIL THICK GOLD FOILS IN A LATTICE OF 1/4-INCH DIAMETER, 1.03% U-235, URANIUM RODS ON A 2.5-INCH TRIANGULAR SPACING.

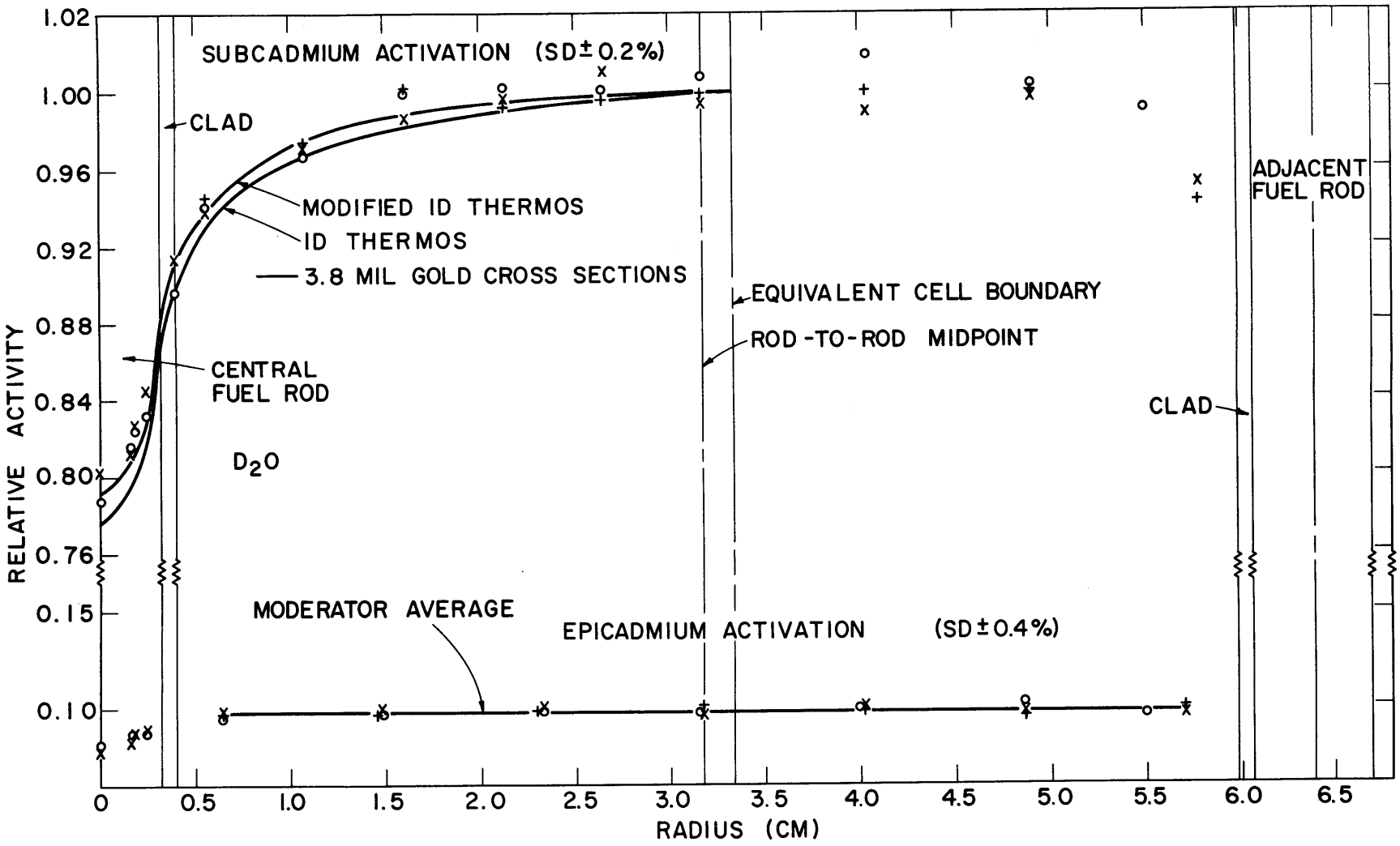

FIG. 4.2.5 GOLD ACTIVITY DISTRIBUTION FOR RUN A5; 4.3 MIL THICK GOLD FOILS IN A LATTICE OF 1/4-INCH DIAMETER, 1.03% U-235, URANIUM RODS ON A 2.5-INCH TRIANGULAR SPACING.

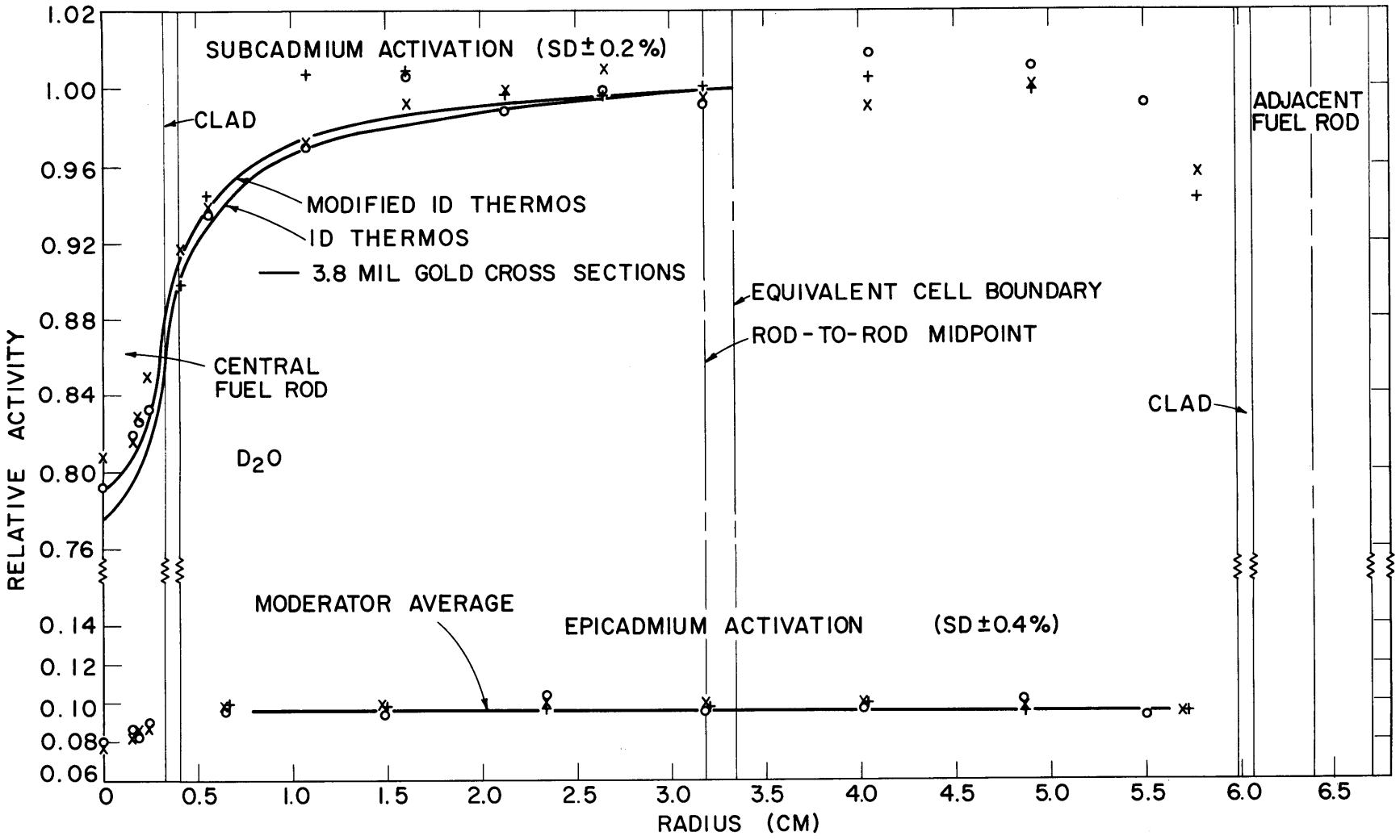

FIG. 4.2.6 GOLD ACTIVITY DISTRIBUTION FOR RUN A5; 4.3 MIL THICK GOLD FOILS IN A LATTICE OF 1/4-INCH DIAMETER, 1.03% U-235, URANIUM RODS ON A 2.5-INCH TRIANGULAR SPACING COUNTED BY THE INTEGRAL METHOD.

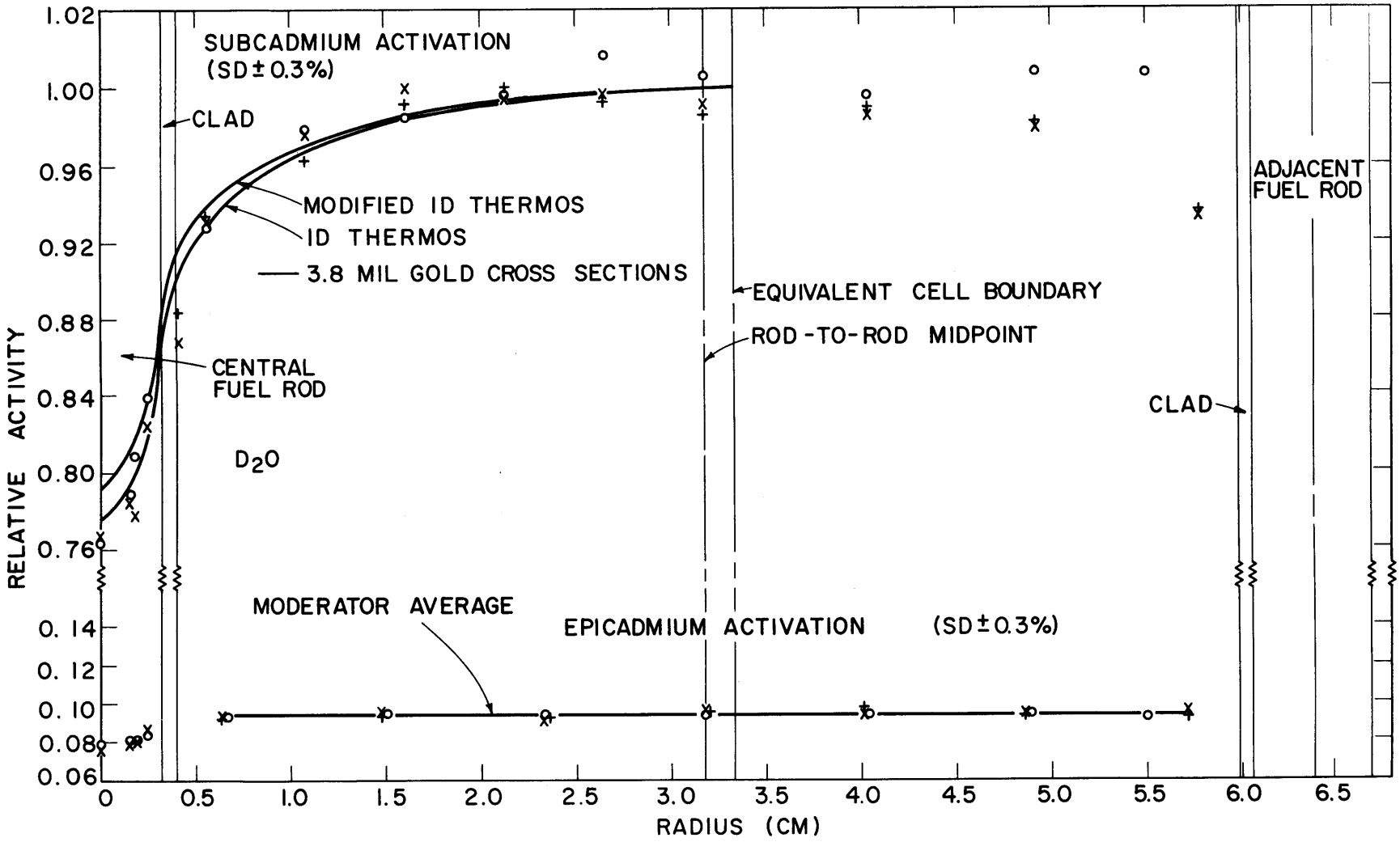

FIG. 4.2.7 GOLD ACTIVITY DISTRIBUTION FOR RUN A7; 4.3 MIL THICK GOLD FOILS IN A LATTICE OF 1/4-INCH DIAMETER, 1.03% U-235, URANIUM RODS ON A 2.5-INCH TRIANGULAR SPACING.

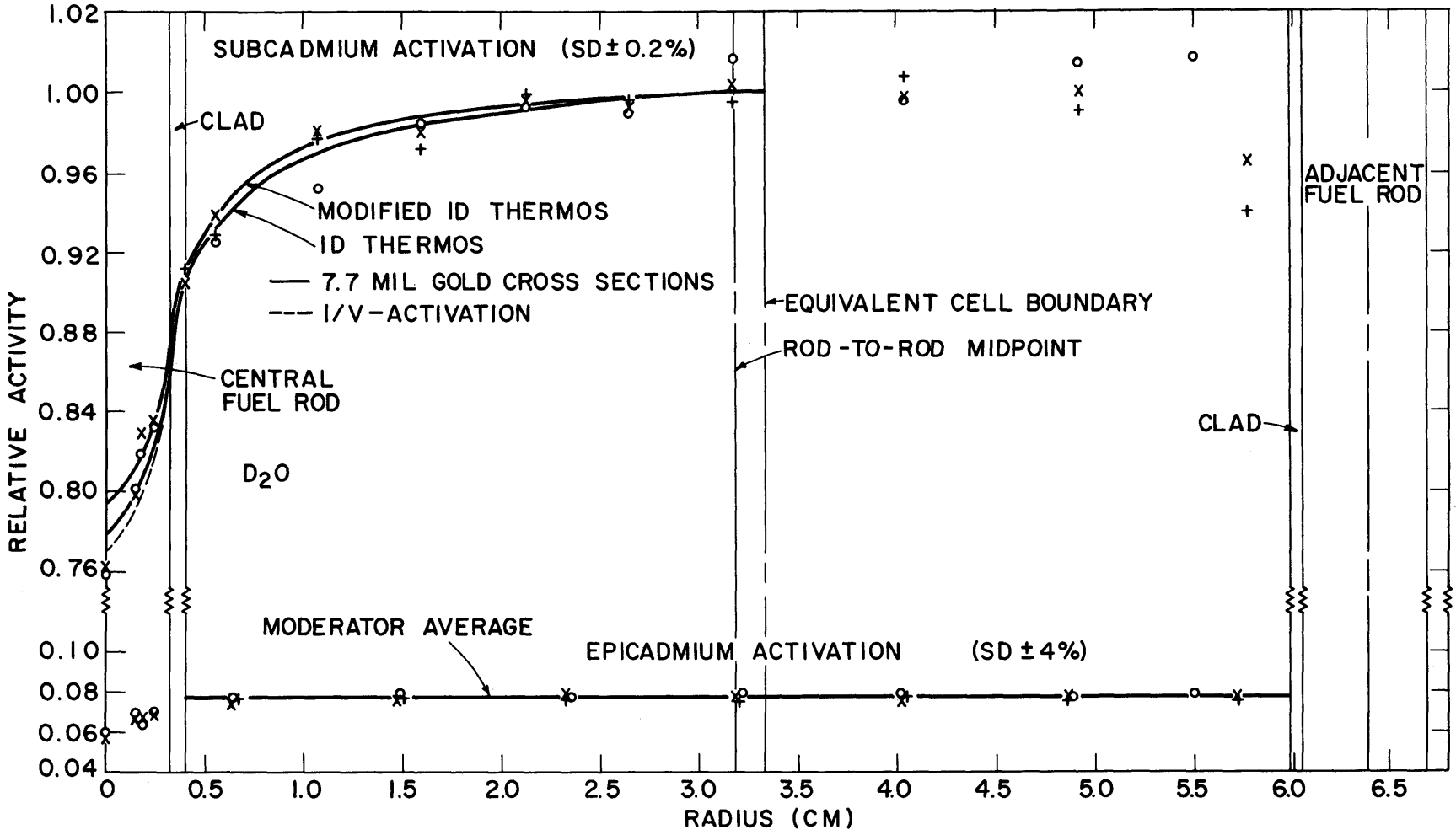

FIG. 4.2.8 GOLD ACTIVITY DISTRIBUTION FOR RUN A9; 10 MIL THICK GOLD FOILS IN A LATTICE OF 1/4-INCH DIAMETER, 1.03% U-235, URANIUM RODS ON A 2.5-INCH TRIANGULAR SPACING.

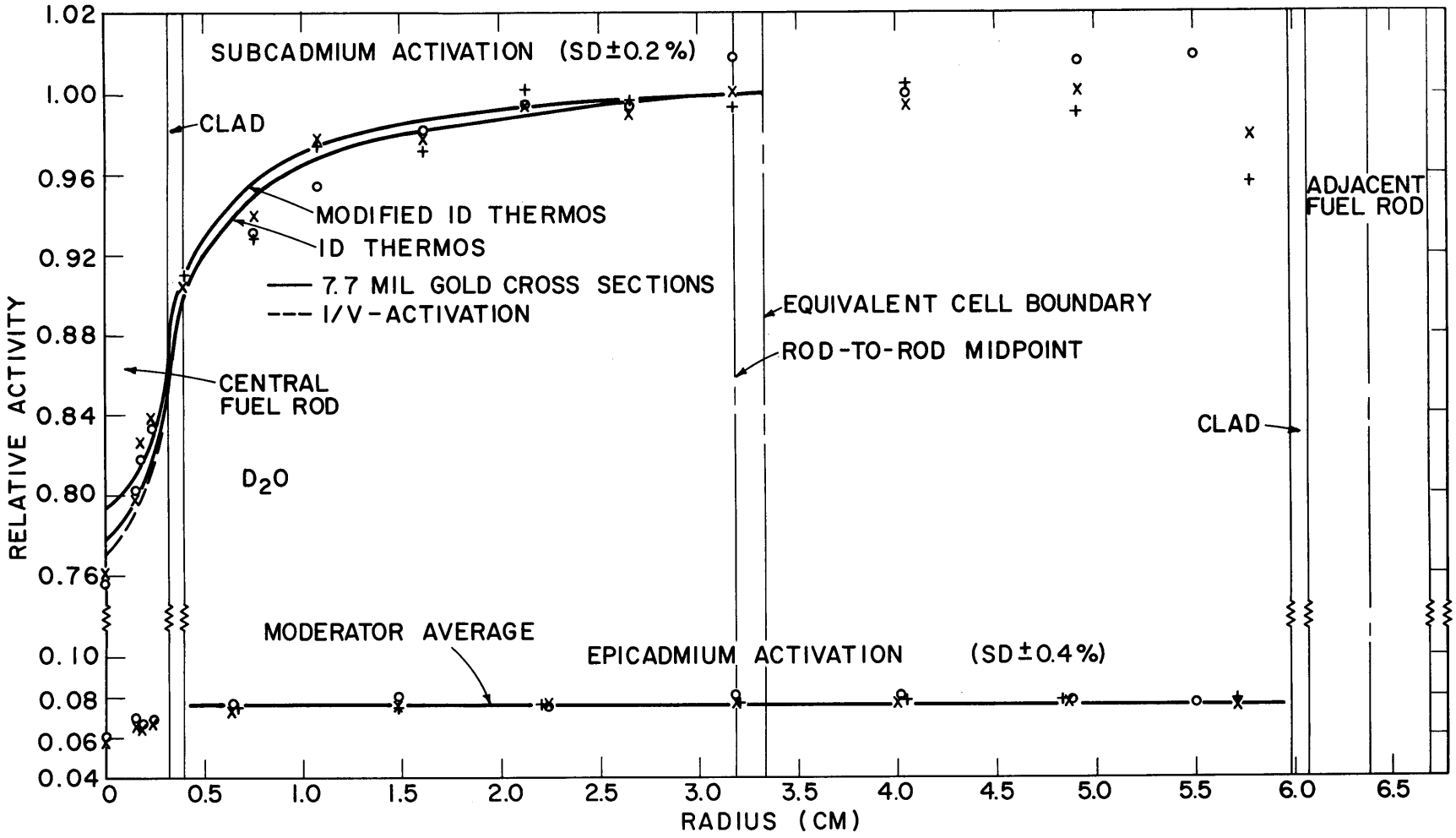

FIG. 4.2.9 GOLD ACTIVITY DISTRIBUTION FOR RUN A 9; 10 MIL THICK GOLD FOILS IN A LATTICE OF 1/4-INCH DIAMETER, 1.03% U-235, URANIUM RODS ON A 2.5-INCH TRIANGULAR SPACING COUNTED BY THE INTEGRAL METHOD.

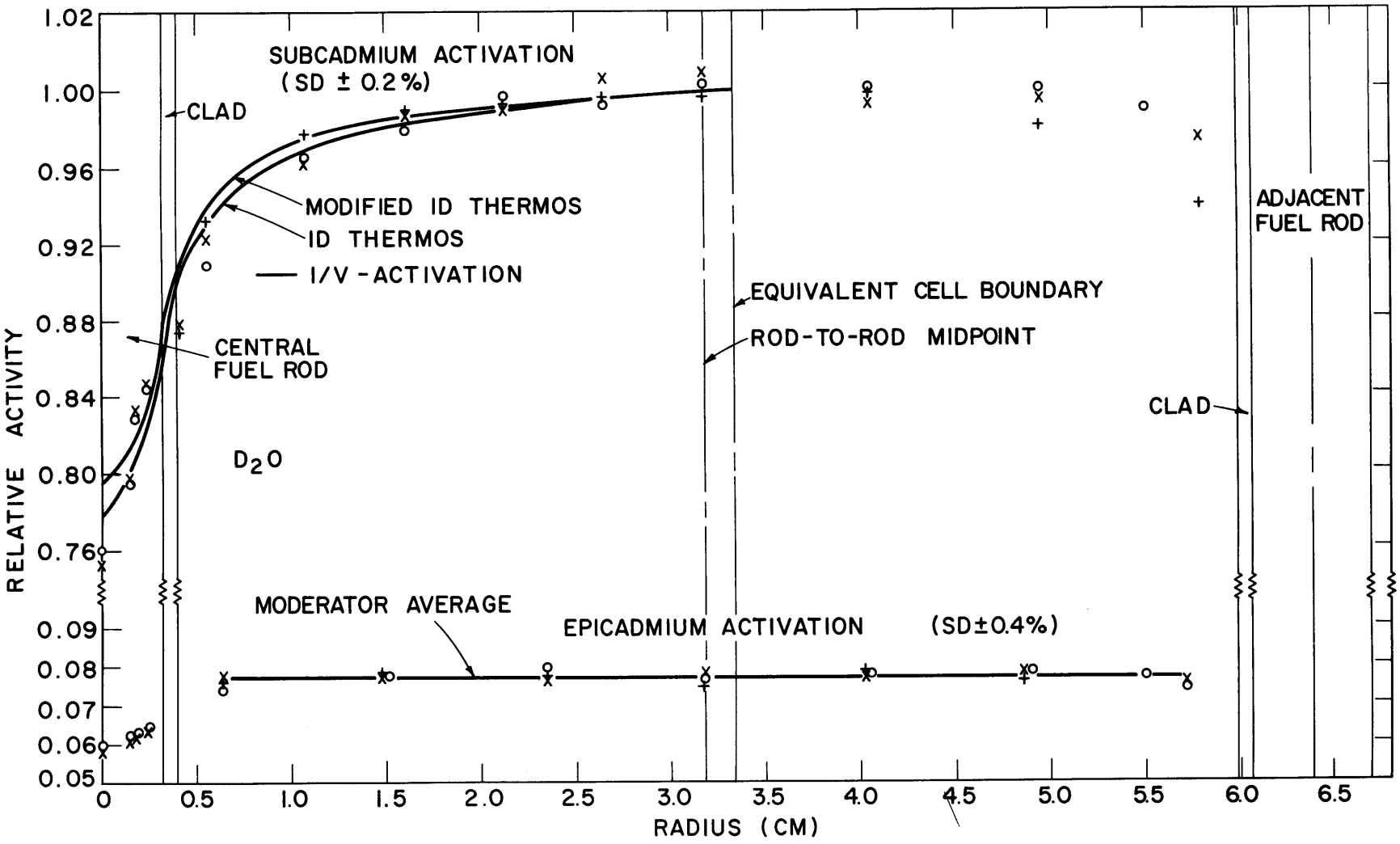

FIG. 4.2.10 GOLD ACTIVITY DISTRIBUTION FOR RUN A10; 10 MIL THICK GOLD FOILS IN A LATTICE OF 1/4-INCH DIAMETER, 1.03% U-235, URANIUM RODS ON A 2.5-INCH TRIANGULAR SPACING.

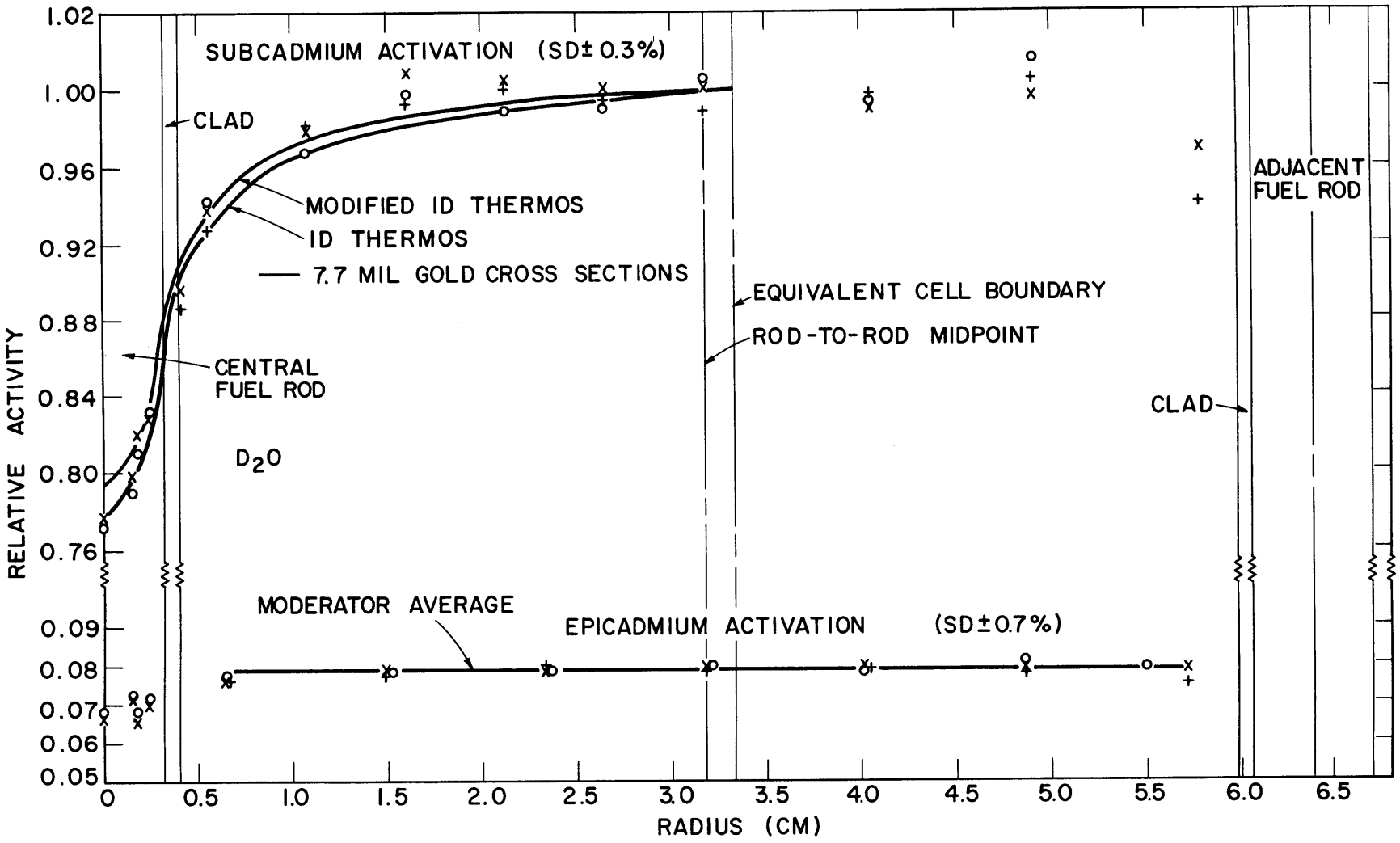

FIG. 4.2.11 GOLD ACTIVITY DISTRIBUTION FOR RUN A17; 10 MIL THICK GOLD FOILS IN A LATTICE OF 1/4-INCH DIAMETER, 1.03% U-235, URANIUM RODS ON A 2.5-INCH TRIANGULAR SPACING.

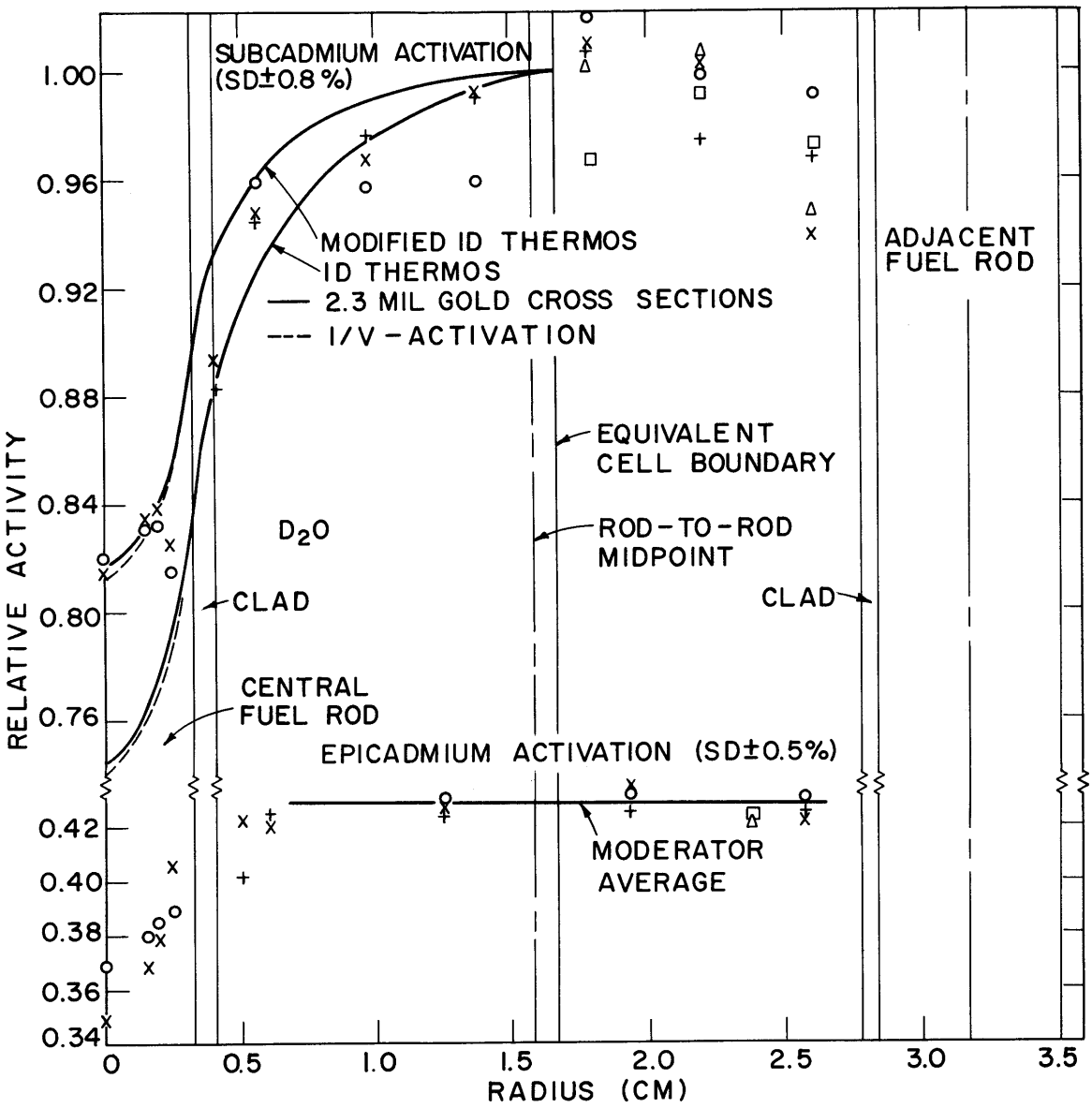

FIG. 4.2.12 GOLD ACTIVITY DISTRIBUTION FOR RUN A14; 2.5 MIL THICK GOLD FOILS IN A LATTICE OF 1/4-INCH DIAMETER, 1.03% U-235, URANIUM RODS ON A 1.25-INCH TRIANGULAR SPACING.

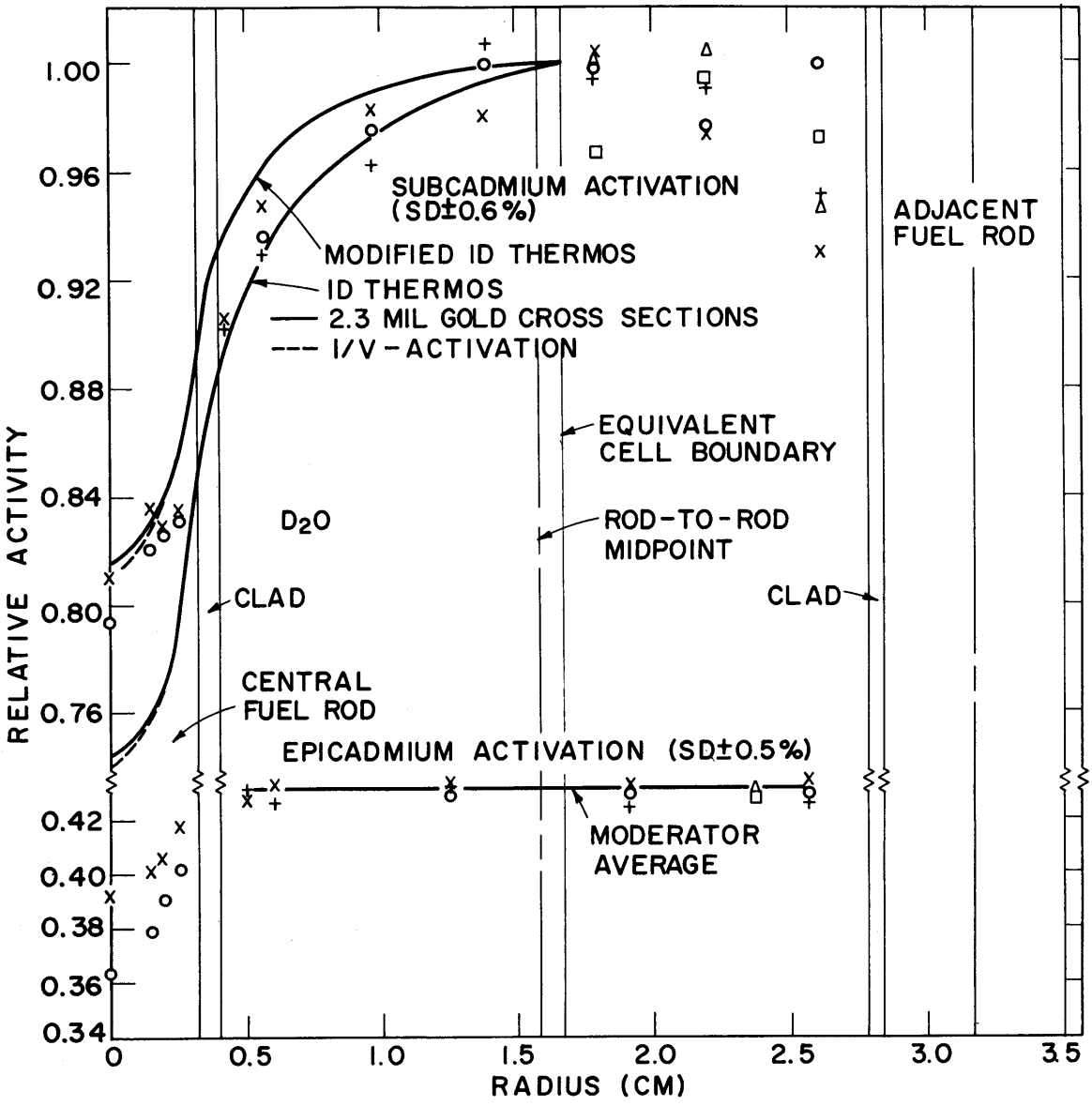

FIG. 4.2.13 GOLD ACTIVITY DISTRIBUTION FOR RUN A15; 2.5 MIL THICK GOLD FOILS IN A LATTICE OF 1/4-INCH DIAMETER, 1.03% U-235, URANIUM RODS ON A 1.25-INCH TRIANGULAR SPACING.

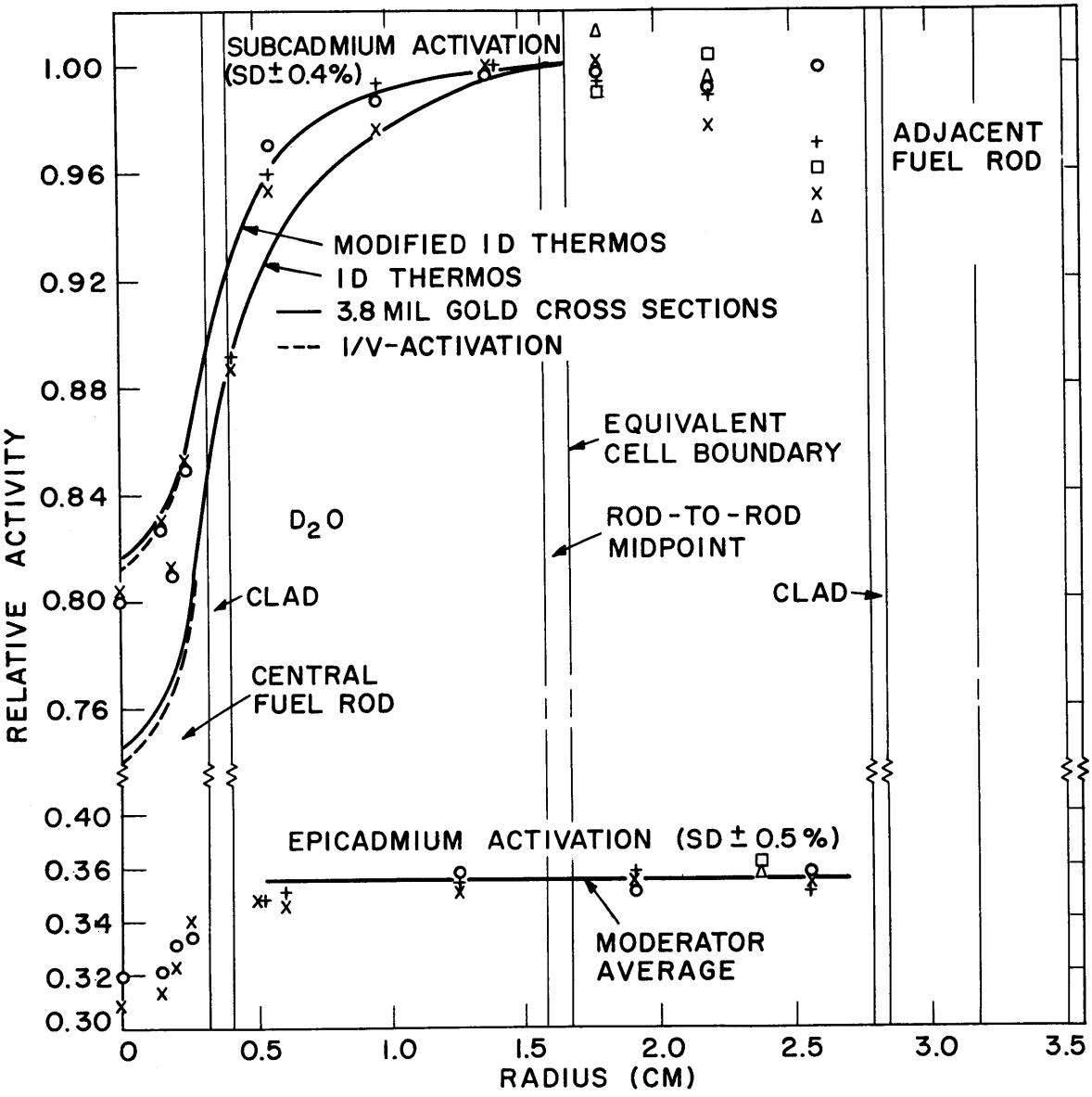

FIG. 4.2.14 GOLD ACTIVITY DISTRIBUTION FOR RUN A16; 4.3 MIL THICK GOLD FOILS IN A LATTICE OF 1/4-INCH DIAMETER, 1.03% U-235, URANIUM RODS ON A 1.25-INCH TRIANGULAR SPACING.

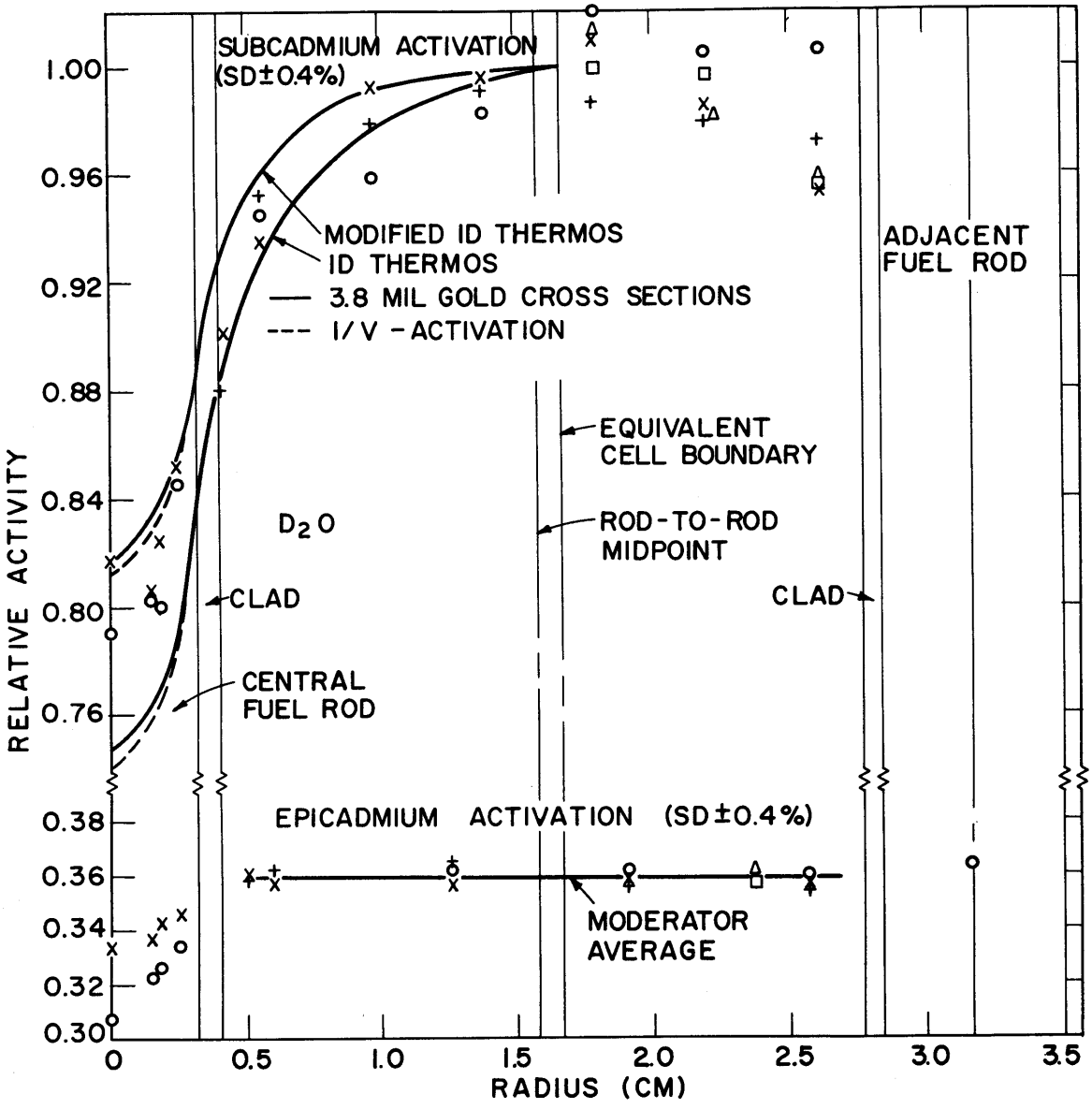

FIG. 4.2.15 GOLD ACTIVITY DISTRIBUTION FOR RUN A11; 4.3 MIL THICK GOLD FOILS IN A LATTICE OF 1/4-INCH DIAMETER, 1.03% U-235, URANIUM RODS ON A 1.25-INCH TRIANGULAR SPACING.

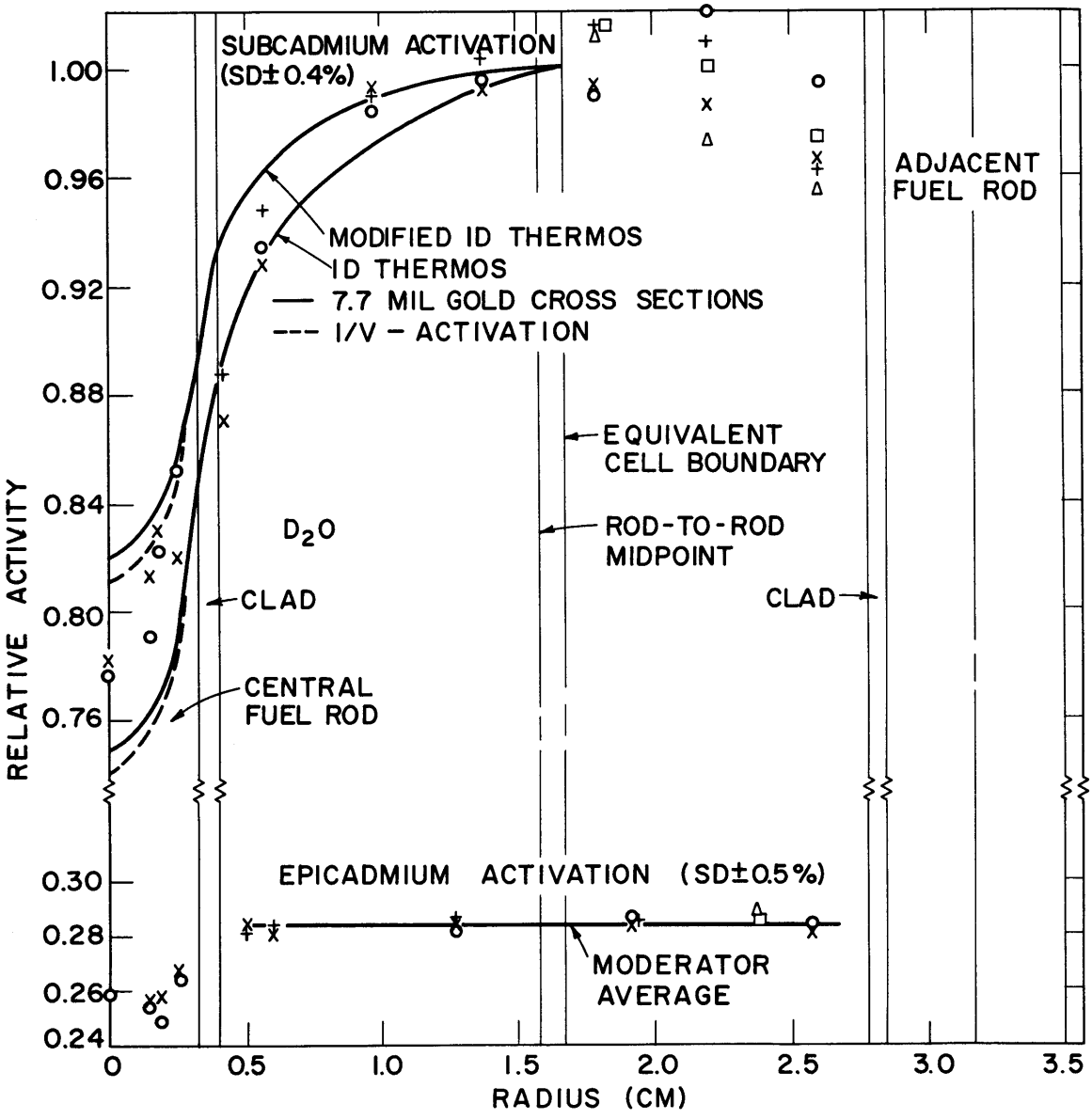

FIG. 4.2.16 GOLD ACTIVITY DISTRIBUTION FOR RUN A12; 10 MIL THICK GOLD FOILS IN A LATTICE OF 1/4-INCH DIAMETER, 1.03% U-235, URANIUM RODS ON A 1.25-INCH TRIANGULAR SPACING.

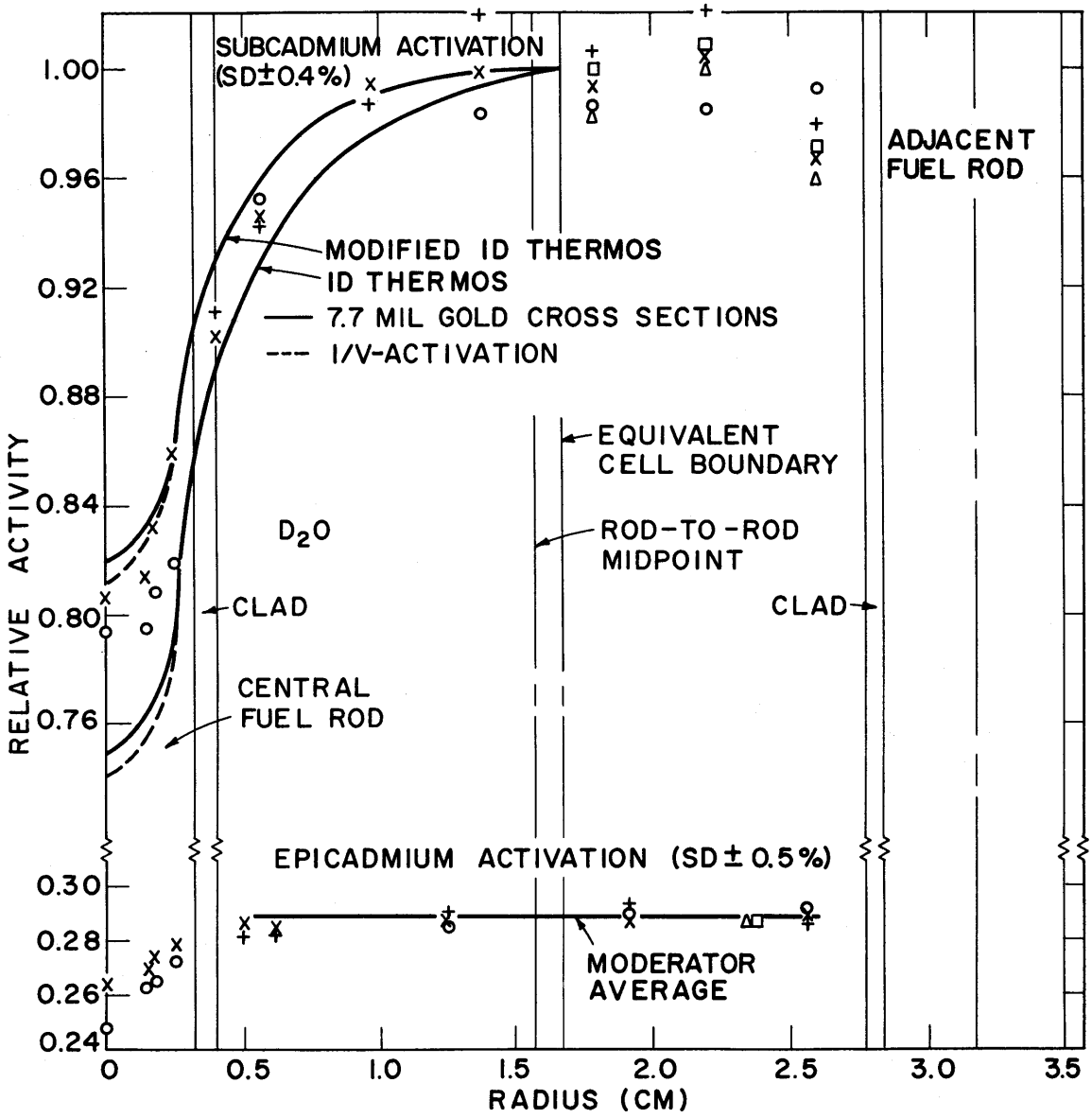

FIG. 4.2.17 GOLD ACTIVITY DISTRIBUTION FOR RUN A13; 10 MIL THICK GOLD FOILS IN A LATTICE OF 1/4-INCH DIAMETER, 1.03% U-235, URANIUM RODS ON A 1.25-INCH TRIANGULAR SPACING.

was apparently no significant difference between the results obtained with the two counting methods, subsequent counting was done with the differential technique.

The statistical uncertainty given on Figs. 4.2.1 to 4.2.17 is the uncertainty due to counting.* In general, several passes were made through the automatic sample changer to spread any counter drift over all the foils in the experiment. The counting uncertainty for the experiment was computed by the ACTIVE code from the experimental data for the saturated activity determined in each pass. The procedure is discussed further in Appendix D.

4.2.3 Azimuthal Symmetry

The use of the three-rod cluster permitted a study to determine if the lattice was azimuthally symmetric about the center rod, with respect to the measurement of the intracellular flux traverses. If the lattice is azimuthally symmetric, the center rod-to-left adjacent rod traverse should agree with the center rod-to-right adjacent rod traverse. The usual procedure in making intracellular flux measurements has been to omit one of the two traverses, under the assumption that the lattice was azimuthally symmetric.

The results plotted in Figs. 4.2.1 to 4.2.17 indicate that as the foil thickness (and weight) increases, the scatter of the data decreases. A plausible explanation for this trend may be that as the foil weight increases, the weight can be determined more accurately, and the activity of the foil is less affected by possible damage during handling. To investigate the lattice symmetry, consider the activities of the foils on the two rod-to-rod traverses that are most distant from the center rod, and consequently the foils farthest from each other. The activity of these foils should show the greatest differences if the lattice is not symmetric. Table 4.2.2 gives the results for the ratio of the activities of the foils on opposite sides of the foil holder. For the lattice with the 2.5-inch triangular spacing, the foils on the left side gave activities about 2% higher than the right side; the opposite trend is indicated for the lattice with the 1.25-inch triangular spacing. The lattices were loaded separately and the opposite trend is therefore not significant.

Two alternative conclusions can be drawn. One is that the lattices

*A discussion of the total experimental uncertainty together with the averaged experimental results is given in Appendix I.

TABLE 4.2.2

Comparison of the Thermal Activities of Gold Foils Along the Rod-to-Rod Traverse

Run	Foil Thickness (mils)	Lattice Spacing (inches)	Ratio,[(a)] Most Distant Foil	Ratio,[(a)] Next Most Distant Foil	Standard Deviation (%)
A8	dilute	2.5	1.054	0.998	1.9
A4	2.5	2.5	1.015	1.019	0.6
A6	2.5	2.5	1.018	1.000	0.3
A5	4.3	2.5	1.009	0.997	0.2
A7	4.3	2.5	0.997	1.000	0.3
A9	10.2	2.5	1.030	1.010	0.2
A10	10.2	2.5	1.036	1.014	0.2
A17	10.2	2.5	1.030	0.991	0.3
A14	2.5	1.25	0.970	1.029	0.8
A15	2.5	1.25	0.977	0.982	0.6
A16	4.3	1.25	0.979	0.986	0.5
A11	4.3	1.25	0.980	1.006	0.4
A12	10.2	1.25	1.003	0.977	0.4
A13	10.2	1.25	0.986	0.983	0.4

(a) The activity of the foil on the left side divided by the activity of the foil on the right side.

been asymmetric in an amount corresponding to the measured difference of two per cent. It seems more plausible, however, that the comparison given in Table 4.2.2 indicates an inability to make measurements of the thermal activations that are reproducible to better than one or two per cent. Unfortunately, there appear to be no other experiments on intracellular flux traverses in which this problem has been investigated. It is recommended that future intracellular measurements be made with two symmetric traverses included.

4.2.4 A Comparison of the Experimental and Predicted Values of the Cadmium Ratio

One of the problems involved in a comparison of theory and experiment for the intracellular traverses is to normalize the theory to the measurements in such a way that they can be compared reasonably. Brown (B14) has discussed the method that he used to normalize the theoretical activation curve to experiment. He normalized by equating the average theoretical and experimental activities in a small region near the edge of the cell, or by a similar process in the neighborhood of the center of the cell. The activation curve is much flatter in the moderator near the edge of the cell, so that he concluded that this was probably the better place at which to normalize. Experimentally, the rod-to-rod and rod-to-moderator traverses are nearly indistinguishable in the vicinity of the edge of the cell, so that this procedure is apparently justified. Because of the extra rod-to-rod traverse used in the present experiments, more experimental points are available near the boundary of the cell. With the exception of Run A8 involving the dilute gold foils, the points at the cell edge were within approximately 2% of each other, as indicated in Tables 4.1.2 and 4.1.4. A shift in the theoretical curve along the relative activity scale could change the over-all curve by only 2%, if the shift is restricted to the experimental points farthest away from the average.

However, when a second experiment is made, the normalization may be somewhat arbitrary, because of the possibility that the shape of the thermal activations are the same while the cadmium ratios are different. For the duplicate experiments made here, however, the cadmium ratios were within the statistical uncertainty, and this possibility did not actually occur.

At first, it was believed that an alternative method of normalization could be used. If the cadmium ratio could be predicted, it would be possible to normalize the theoretical results to the experimental epicadmium activity, which is constant in the moderator. Thus, it would not be necessary to decide whether to normalize the thermal activation at the cell edge or at the cell center. The average epicadmium activity in the moderator for all the experimental points in a typical run (A11) is within 2% of the experimental point farthest from the average. Unfortunately, the additional experimental quantities needed to predict the cadmium ratio are not available to better than 5%, as discussed in Section 3.5, so that any such normalization would be valid only to about 5%.

It seems more desirable, as an additional test of the analytical methods, to predict the cadmium ratio in the lattice and see how it compares with the experimental value, and to normalize the experiment at the cell edge, as before. To predict the cadmium ratio, the values of the quantities in Eq. (3.5.8) must be known. For gold, there is some question about the proper values of the effective resonance integrals, ERI', as discussed in Section 3.5. The values chosen for K_{exp} are listed in Table 4.2.3 along with the other parameters used to calculate the cadmium ratio. Table 4.2.3 also compares the calculated and experimental values of the cadmium ratio which have been measured to date by the M.I.T. Lattice Project. The lattices with (triangular) spacings of 4.5, 5.0 and 5.75 inches, respectively, contained natural uranium rods, 1.0 inch in diameter; the remaining data are the results of the measurements in the lattices of slightly enriched uranium.

The predicted values for $(R_{cd}-1)$ are understood to include a 3% uncertainty in the resonance integral and a 3% uncertainty in K_{exp} [the ratio of $(R_{cd}-1)$ for the infinitely thin gold foil to $(R_{cd}-1)$ for the finite gold foil in a 1/E-flux]. The experimental values of $(R_{cd}-1)$ have an uncertainty of about 2%, owing to the uncertainty in the axial flux measurements. The predicted values for the natural uranium lattices compare well with experiment. The results for the closely packed lattices of slightly enriched uranium indicate that the predictions have not been as successful. It is possible that the values of the resonance integral, RI', and $\xi\Sigma_s$ are not correct. The value of RI' chosen, 1605 barns, was calculated from the resonance parameters listed in Table 3.5.1, which is within

TABLE 4.2.3

Comparison of Predicted Values of the Cadmium Ratio at the Cell Edge for Gold Foils with the Experimental Values

Lattice Spacing (in.)	Foil Thickness (mils)	Equivalent Foil Thickness (mils)	Volume of Moderator, V_{mod} (cm^3/cm)	$\frac{\phi_{th}\bar{\sigma}_{ACT}}{\sigma_o}$ (a)	K_{exp} (b)	$\frac{ERI'}{\sigma_o}$ (c)	$R_{cd}-1$ Predicted (d)	$R_{cd}-1$ Experimental	Difference (%) (e)
4.50	2.0	1.97	107.3	0.915	0.317 ± 1%	4.80	3.49	3.57 ± 2%	−2.2
5.00	2.0	1.97	133.1	0.940	0.317 ± 1%	4.80	4.46	4.50 ± 2%	−0.9
5.75	2.0	1.97	178.9	0.952	0.317 ± 1%	4.80	6.05	5.96 ± 2%	+1.5
1.25	2.5	2.3	8.21	7.377	0.29 ± 3%	4.35	2.36	2.32 ± 3%	+1.7
2.50	2.5	2.3	34.4	7.466	0.29 ± 3%	4.35	10.0	8.28 ± 4%	+20.
1.25	4.3	3.8	8.21	7.125	0.24 ± 3%	3.46	2.87	2.79 ± 2.5%	+2.8
2.50	4.3	3.8	34.4	7.196	0.24 ± 3%	3.46	12.1	10.4 ± 3.0%	+16.
1.25	10.2	7.7	8.21	6.592	0.22 ± 3%	2.93	3.14	3.48 ± 2.5%	−9.8
2.50	10.2	7.7	34.4	6.630	0.22 ± 3%	2.93	13.2	13.0 ± 2.5%	+1.5

(a) Defined in Eq. (3.5.8)

(b) K_{exp} is the experimental ratio of the cadmium ratio, R_{cd}, minus one for the infinitely thin foil to that for the finite thickness foil.

(c) ERI'/σ_o is the total effective resonance integral divided by the 2200 m/sec value of σ_{ACT}.

(d) Calculated from Eq. (3.5.8); $\xi\Sigma_s = 0.17\ cm^{-1}$.

(e) Predicted value minus experimental value divided by experimental value in per cent.

3% of the experimental value quoted by Jirlow and Hohansson (J2). The value of $\xi\Sigma_s$, 0.17 cm^{-1}, was chosen to fit the results for the natural uranium lattices. In any case, $\xi\Sigma_s$ is a constant for heavy water and is independent of the lattice spacing.

Table 4.2.4 shows the variation of the gold cadmium ratio with lattice spacing, with the properties of the foil and heavy water treated as independent parameters. If the variation predicted by Eq. (3.5.9) is correct, the value of $(R_{cd}-1)_{exp}/V_{mod}\bar{\sigma}^*_{ACT}\phi_{th}$ should be independent of the lattice spacing. The results indicate that there is again good agreement for the natural uranium lattices, but the results for the lattices with slightly enriched uranium could not be improved by simply adjusting the foil or heavy water properties.

TABLE 4.2.4

Variation with Lattice Spacing of the Gold Cadmium Ratio at the Cell Edge

Lattice Spacing (in.)	Foil Thickness (mils)	$V_{mod}\bar{\sigma}^*_{ACT}\phi_{th}$ (Relative)[a]	$(R_{cd}-1)_{exp}$	$\frac{(R_{cd}-1)_{exp}}{V_{mod}\bar{\sigma}^*_{ACT}\phi_{th}}$
4.50	2.0	0.979	3.57 ± 2%	3.65
5.00	2.0	1.25	4.50 ± 2%	3.60
5.75	2.0	1.69	5.96 ± 2%	3.52
1.25	2.5	0.605	2.32 ± 3%	3.83
2.50	2.5	2.56	8.28 ± 4%	3.22
1.25	4.3	0.584	2.79 ± 2.5%	4.77
2.50	4.3	2.47	10.4 ± 3%	4.20
1.25	10.2	0.541	3.48 ± 2.5%	6.43
2.50	10.2	2.28	13.0 ± 2.5%	5.70

(a) Defined in Eq. (3.5.8).

The volume ratios for the lattices are given in Table 4.2.5. The volume ratio of moderator-to-fuel, V_{mod}/V_{fuel}, in the enriched uranium lattice with the 2.5-inch triangular spacing was 108, almost three times as large as in any of the other lattices studied. It is not evident at this

TABLE 4.2.5

Volume Fractions of Lattices Studied

Rod Diameter (in.)	U-235 Concentration of the Fuel Rod	Triangular Spacing (in.)	Volume of Moderator (cm^3/cm)	Volume Fraction of the Fuel	Volume Fraction of the Moderator	$\frac{V_{mod}}{V_{fuel}}$
1.010	Natural	4.50	107.6	0.0456	0.951	20.9
1.010	Natural	5.00	134.1	0.0370	0.961	26.0
1.010	Natural	5.75	179.2	0.0280	0.970	34.8
0.250	1.03%	1.25	8.21	0.0363	0.942	25.9
0.250	1.03%	2.50	34.4	0.0091	0.983	108.0

TABLE 4.2.6

Measurements of the Cadmium Ratio at the Cell Edge in the Lattice of 1/4-Inch Diameter, 1.03% U-235 Uranium Rods on a 1.25-Inch Triangular Spacing

t, Foil Thickness (mils)	Cadmium Ratio (intracellular measurement)	Cadmium Ratio (independent measurement)
2.5	3.32 ± 2%	3.45 ± 1%
4.3	3.79 ± 2%	3.76 ± 1%
10.2	4.48 ± 2%	4.61 ± 1%

time whether the disagreement observed is with the theoretical treatment for this lattice, or the more closely packed lattice with the 1.25-inch spacing. What Table 4.2.4 indicates is that no simple adjustment of the foil or heavy water properties can bring all the results into agreement.

It is possible that the experimental cadmium ratios measured in the intracellular activation measurements are incorrect. Separate, independent checks of the gold-cadmium ratio were made by using the same foils and cadmium boxes described in Chapter II. In connection with the axial buckling experiments, Harrington (H3) measured the cadmium ratio with 10.2 mil thick gold foils in the lattice with the 1.25-inch spacing; he found R_{cd} equal to 4.5 ± 2%. The value of the cadmium ratio measured in the

intracellular experiments was 4.48 ± 2%. Other separate measurements of the cadmium ratio made at symmetrical positions in the lattice at the same height are listed in Table 4.2.6. The results indicate that the cadmium ratios measured in the course of an intracellular activation measurement are acceptable.

4.2.5 Comparison of THERMØS Calculations with Experiment

Figures 4.2.1 to 4.2.17 include the calculated results for the intracellular activation distributions. The energy exchange kernel used in all cases was the Honeck-Nelkin kernel with the diagonal elements of the matrix adjusted to give the calculated values of $\Sigma_{tr}(E)$. The activation cross sections used are the effective values for gold foils discussed in Section 3.4 and in Appendix C. The gold foils of different thickness are distinguished from one another by their effective cross sections. Where possible, the activation distribution for a 1/v-activator is also included; a 1/v-cross section corresponds to infinitely thin gold foils. The modified one-dimensional calculation gives very nearly the same results as the two-dimensional calculation, as shown in Fig. 3.6.6. It is not clear that a statistical comparison between theory and experiment would be any more meaningful than conclusions reached by inspection of the results; the latter method was therefore used.

The use of the dilute gold foils has been found to be unsatisfactory; the irradiation time required was 100 hours, compared to the 5 to 8 hours required for the thicker foils. The experimental scatter, shown in Fig. 4.2.1, is too great to justify their continued use in this type of experiment. It is possible that the gold content varies from foil to foil, and perhaps an intercalibration by means of a foil wheel technique would have been preferable to weighing. Such a calibration would have required an unusually long irradiation time in the exponential tank, and it appeared more advantageous to use larger foils instead.

The results of the entire set of experiments with gold foils indicate that the corrections applied in the present work for the flux perturbation due to the use of finite foils are adequate. The results obtained by using the 10.2 mil thick gold foils are consistently lower than those obtained with the 2.5 and 4.3 mil thick gold foils. The 10.2 mil thick gold foils were originally used with the idea of perturbing the flux as much as possible,

and it is surprising that the results agree as well as they do.

The experiments with the 2.5 and 4.3 mil thick gold foils give results that agree best with the modified one-dimensional THERMØS calculations. A difference of about 2% in the activation of the foils at the center of the fuel rod is the average discrepancy between theory and experiment for these foil sizes.

The comparison of the results for the two lattice spacings indicates that the largest single discrepancy between theory and experiment was due to the assumption that the cell could be cylindricalized. The modified one-dimensional calculation predicted the activation shape in both lattices. The usual one-dimensional calculation gives substantially the same result in the lattice with the 2.5-inch triangular spacing as the modified one-dimensional calculation. However, the one-dimensional calculation agrees neither with experiment nor with the modified one-dimensional calculation for the lattice with the 1.25-inch triangular spacing.

In the lattice with the 1.25-inch triangular spacing, an additional traverse was made, the adjacent rod-to-adjacent rod traverse, as shown in Fig. 4.1.1. The experimental points are reflected in the graphs along the one-dimensional scale by maintaining their distance from the center of the adjacent rod. The reflections give the same shape as the rod-to-rod traverses from the center rod.

The epicadmium activations of the gold foils were spatially constant in the moderator, as far as could be determined. The activation shape in the rod was almost the same as that of the subcadmium activation. It is believed that this is a result of shielding of the 4.9 ev resonance of gold by the 6.7 ev resonance of U-238; no attempt to calculate the epicadmium activation shape in the rod has been made.

4.3 THE USE OF OTHER DETECTOR FOILS

Experiments have also been made with detectors of depleted uranium, lutetium, europium and copper. The results of the experiments are shown in Figs. 4.3.1 to 4.3.9. The experiment with copper foils was a joint effort with D'Ardenne (D1); the results are shown in Fig. 4.3.1. Copper was treated as a 1/v-activator, since the foils used were not self-shielded; the average flux perturbation was estimated, by the methods developed in Appendix A, to be less than 2%. The activity levels for the cadmium-covered

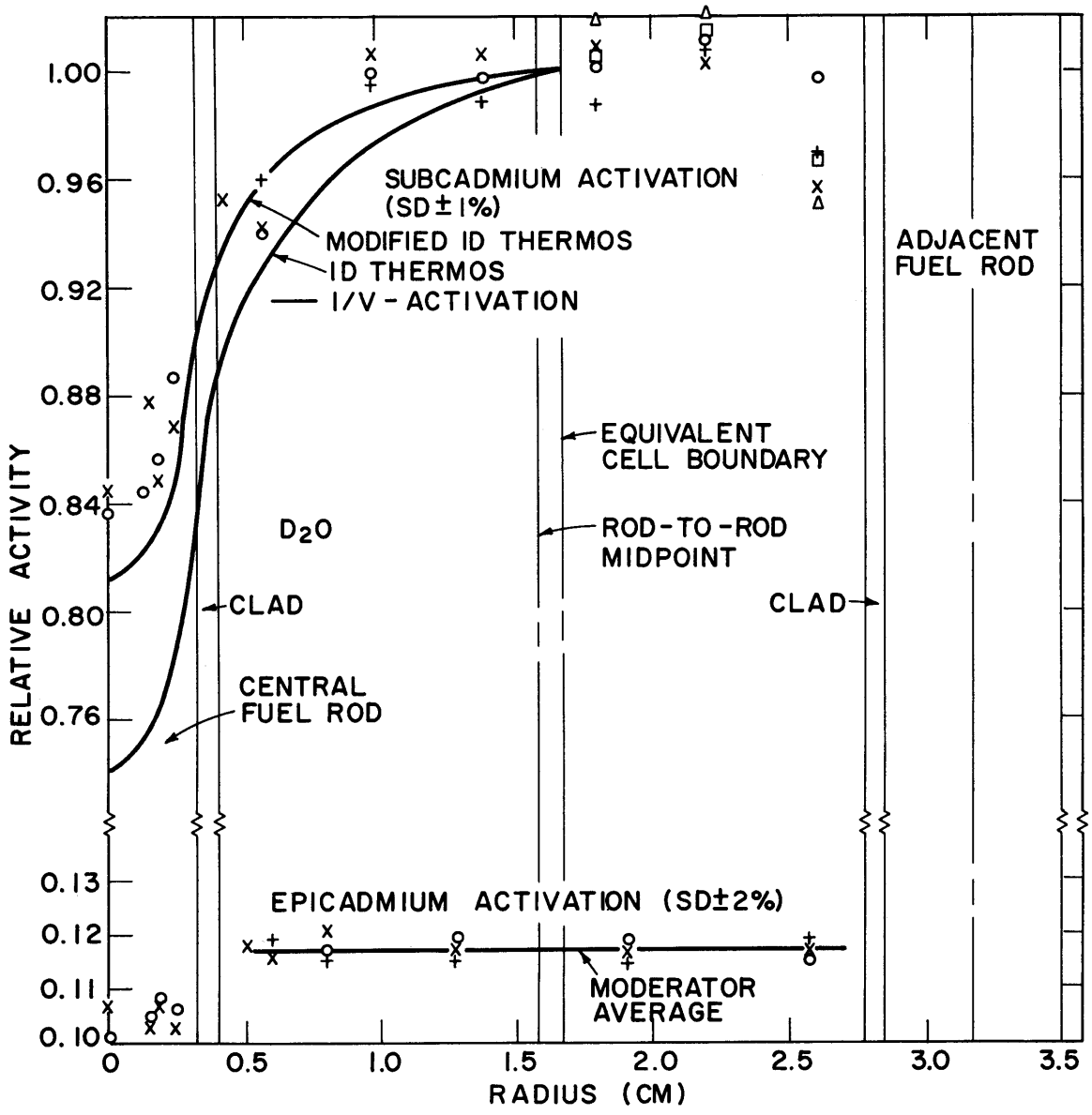

FIG. 4.3.1 COPPER ACTIVATION DISTRIBUTION FOR RUN CU1; 5 MIL THICK COPPER FOILS IN A LATTICE OF 1/4-INCH DIAMETER, 1.03% U-235, URANIUM RODS ON A 1.25-INCH TRIANGULAR SPACING.

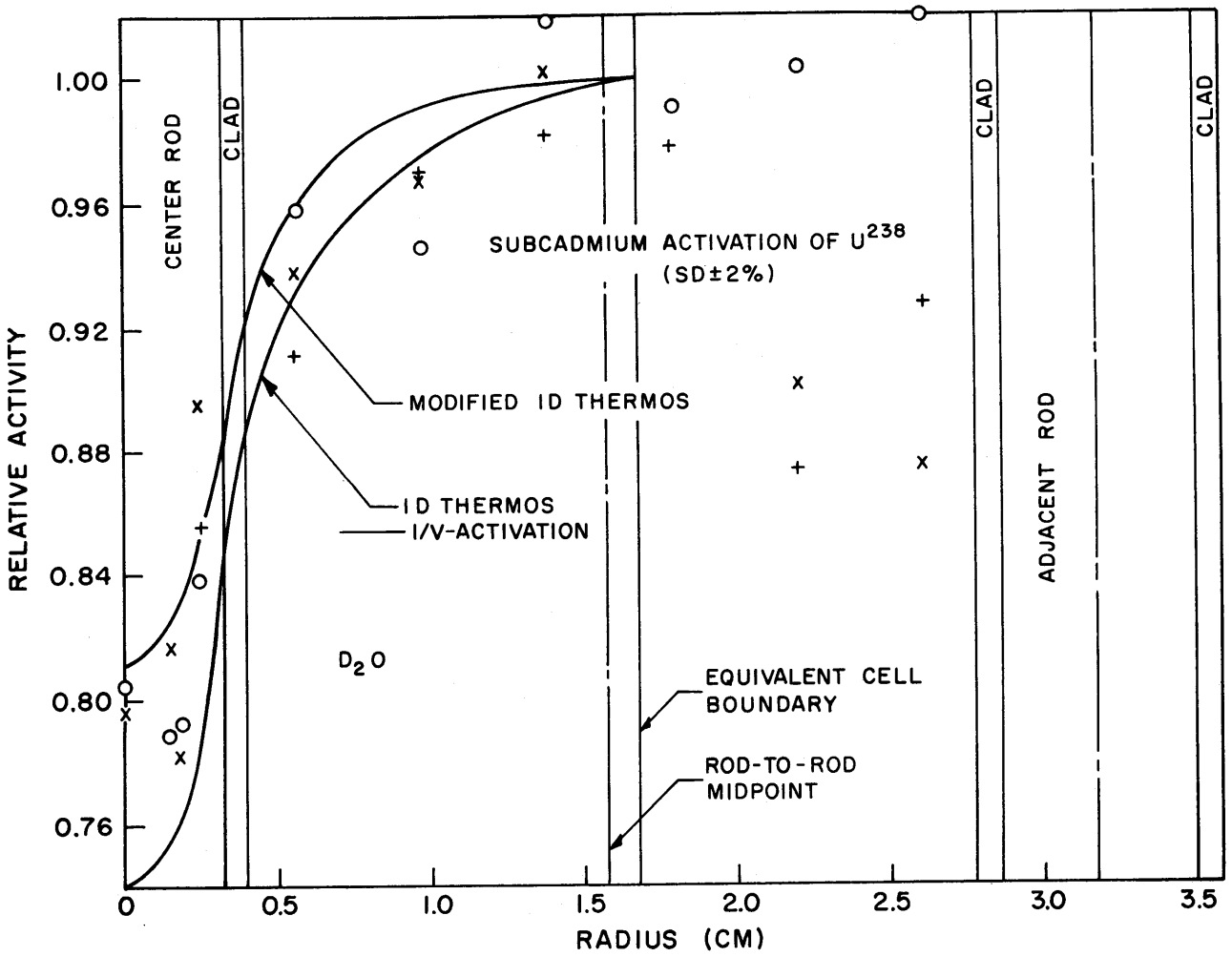

FIG. 4.3.2 SUBCADMIUM DEPLETED URANIUM ACTIVATION FOR RUN DU3; DEPLETED URANIUM FOILS IN A LATTICE OF 1/4 - INCH DIAMETER, 1.03%U-235, URANIUM RODS ON A 1.25 - INCH TRIANGULAR SPACING.

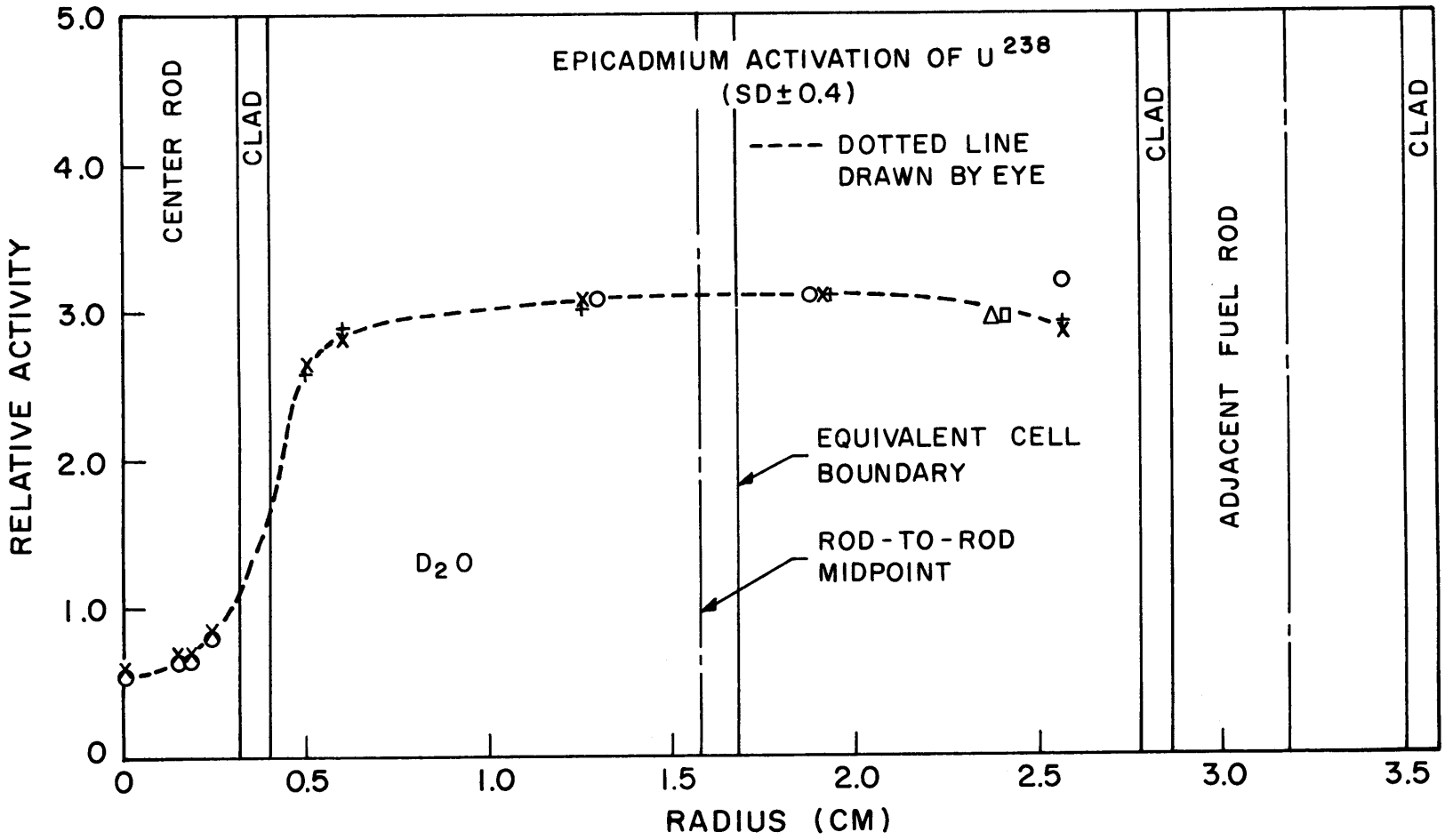

FIG. 4.3.3 EPICADMIUM DEPLETED URANIUM ACTIVATION FOR RUN DU3; DEPLETED URANIUM FOILS IN A LATTICE OF 1/4-INCH DIAMETER, 1.03%U-235, URANIUM RODS ON A 1.25-INCH TRIANGULAR SPACING.

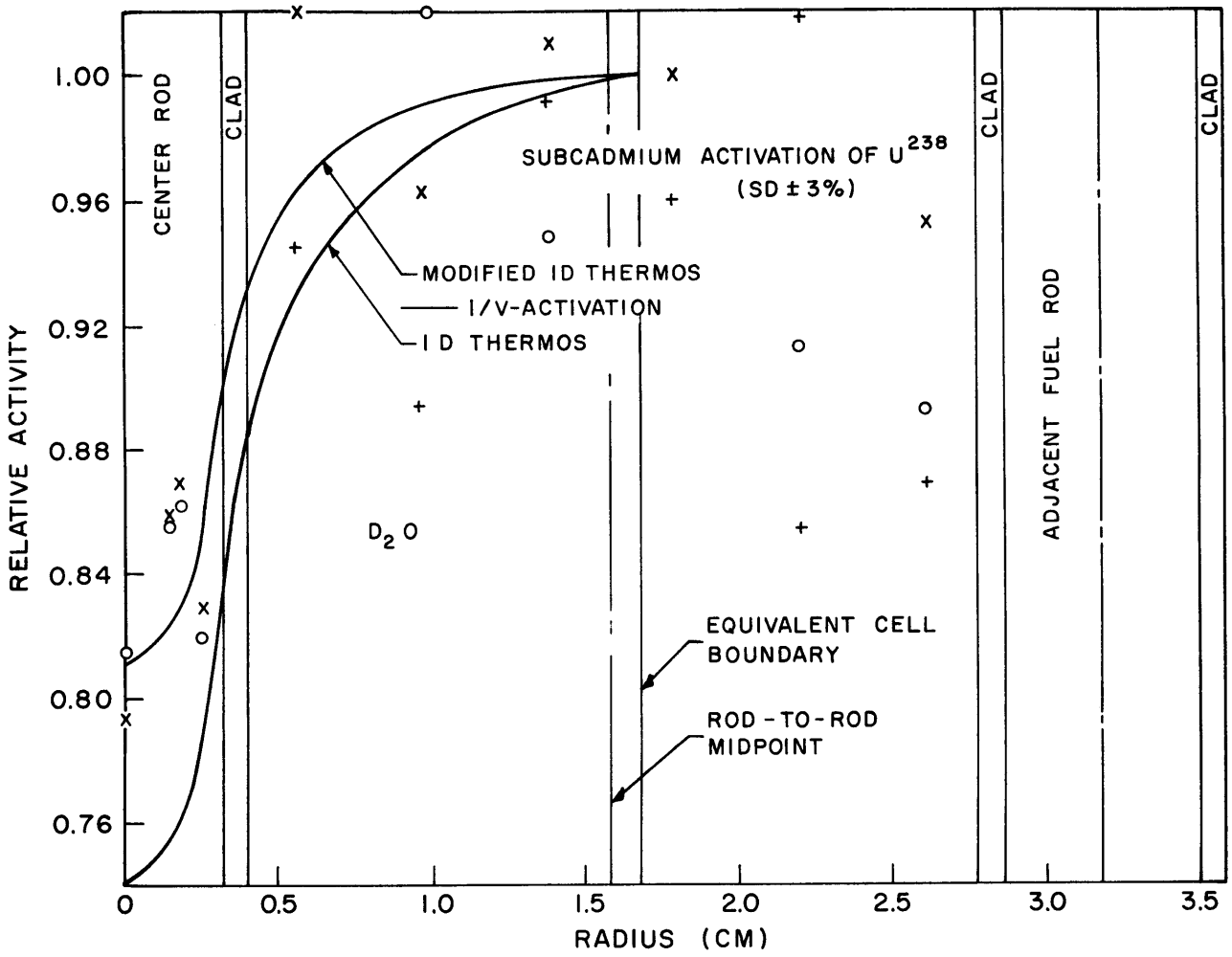

FIG. 4.3.4 SUBCADMIUM DEPLETED URANIUM ACTIVATION FOR RUN DU4; DEPLETED URANIUM FOILS IN A LATTICE OF 1/4-INCH DIAMETER, 1.03% U-235, URANIUM RODS ON A 1.25-INCH TRIANGULAR SPACING.

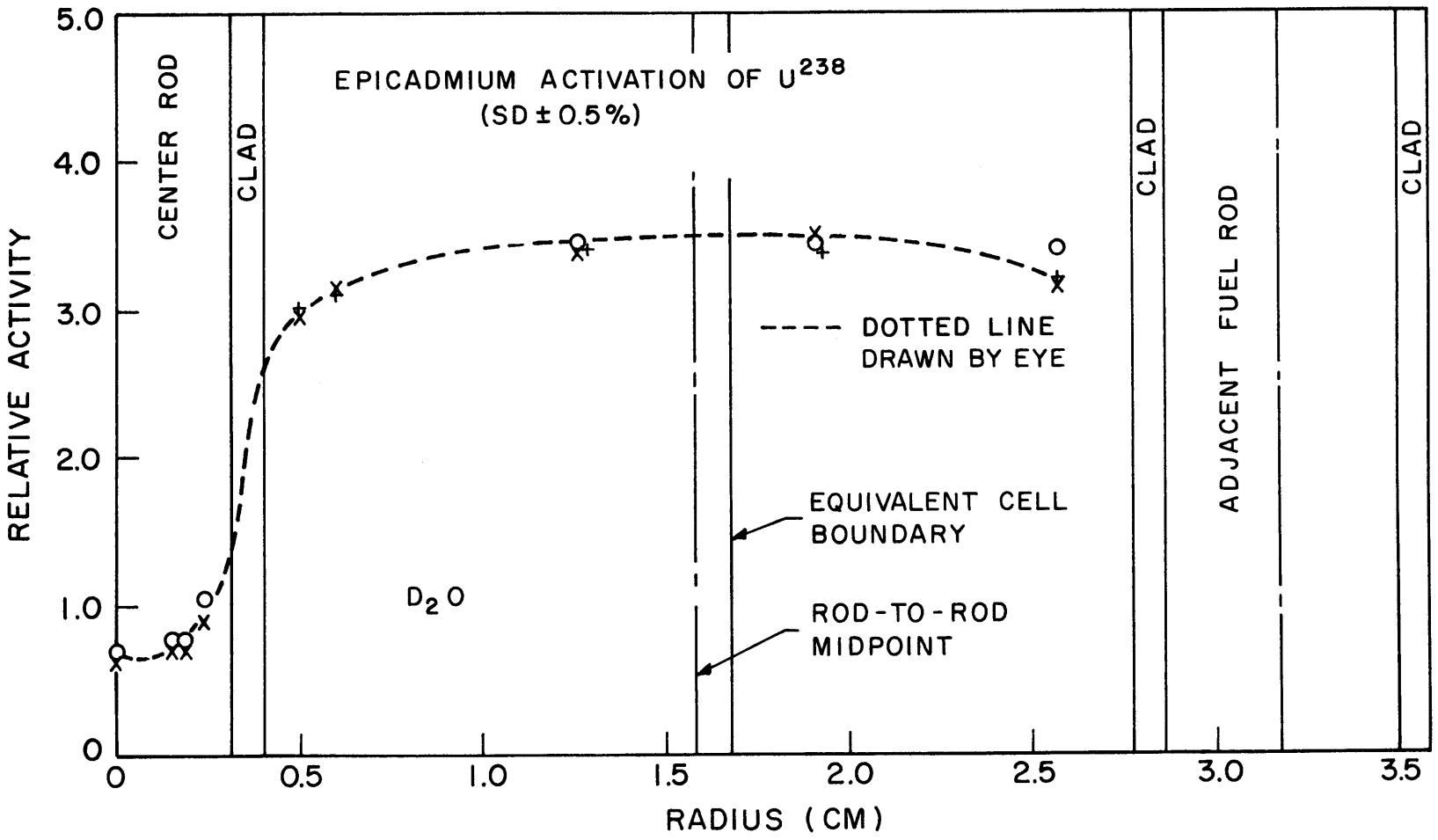

FIG. 4.3.5 EPICADMIUM DEPLETED URANIUM ACTIVATION FOR RUN DU4; DEPLETED URANIUM FOILS IN A LATTICE OF 1/4-INCH DIAMETER, 1.03% U-235, URANIUM RODS ON A 1.25-INCH TRIANGULAR SPACING.

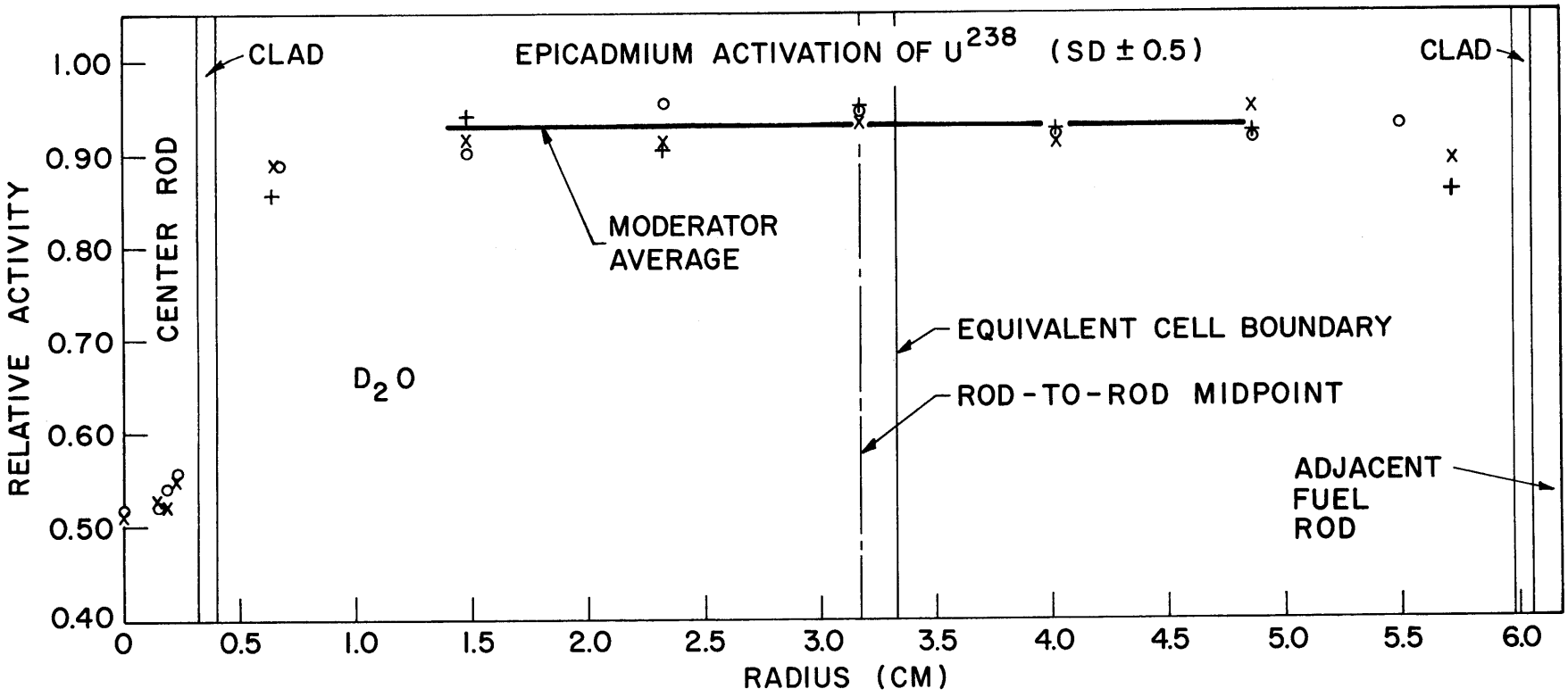

FIG. 4.3.6 EPICADMIUM ACTIVATION DISTRIBUTION FOR RUN DU2; DEPELETED URANIUM FOILS IN A LATTICE OF 1/4-INCH DIAMETER, 1.03% U-235, URANIUM RODS ON A 2.5-INCH TRIANGULAR SPACING.

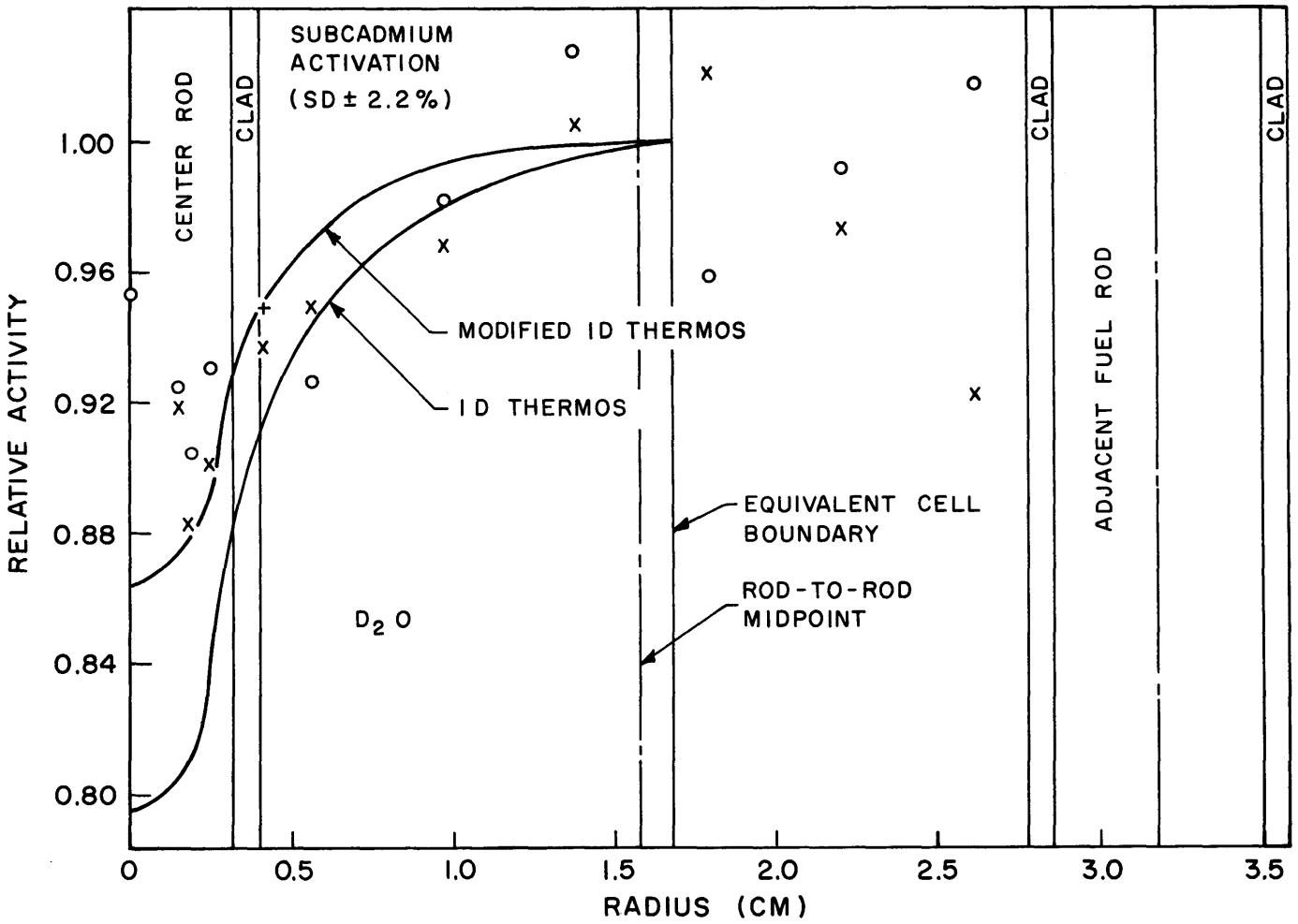

FIG. 4.3.7 LUTETIUM ACTIVATION DISTRIBUTION FOR RUN L4; LUTETIUM ALLOY FOILS IN A LATTICE OF 1/4-INCH DIAMETER, 1.03%U-235, URANIUM RODS ON A 1.25-INCH TRIANGULAR SPACING.

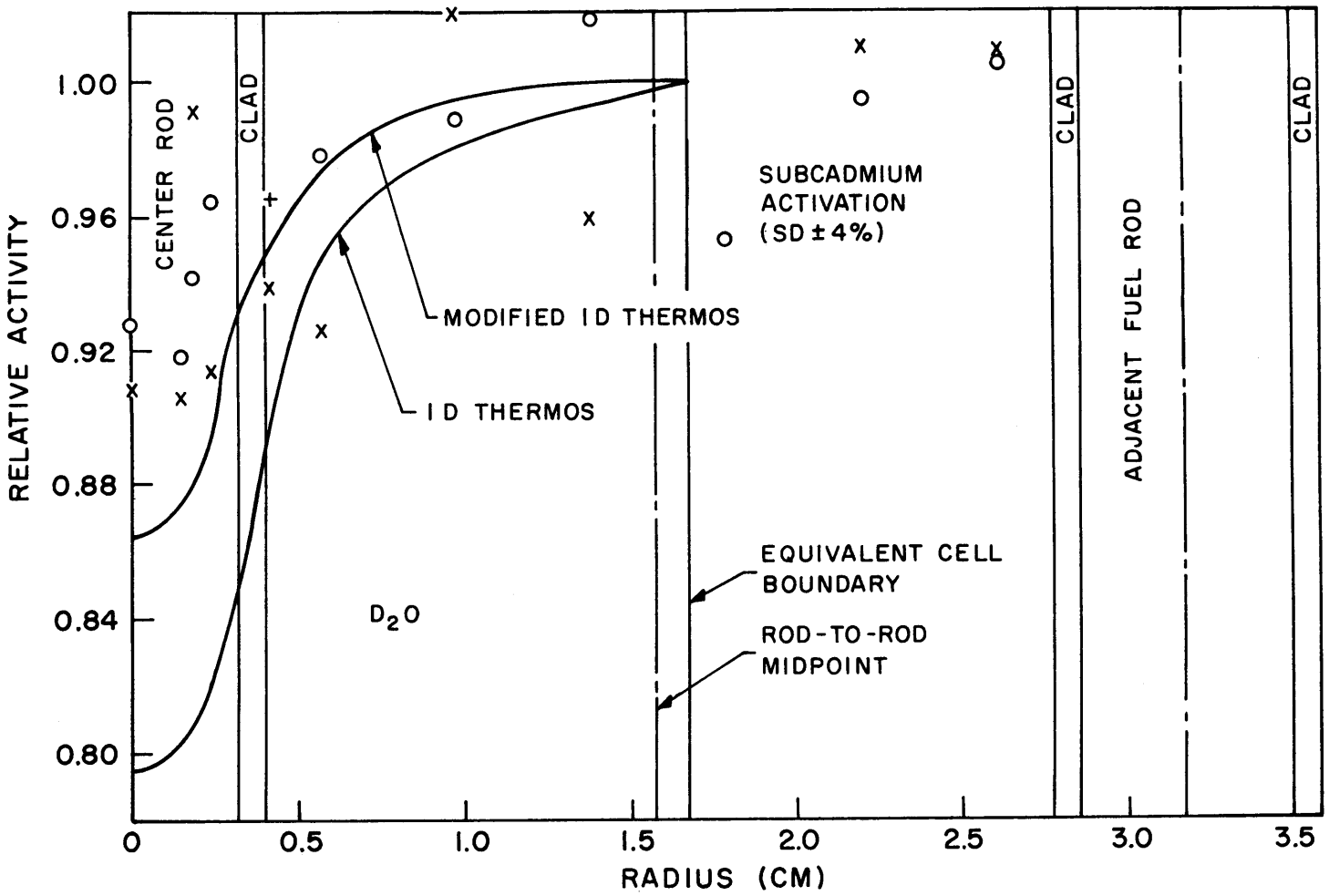

FIG. 4.3.8 LUTETIUM ACTIVATION DISTRIBUTION FOR RUN L5; LUTETIUM ALLOY FOILS IN A LATTICE OF 1/4-INCH DIAMETER, 1.03% U-235, URANIUM RODS ON A 1.25-INCH TRIANGULAR SPACING.

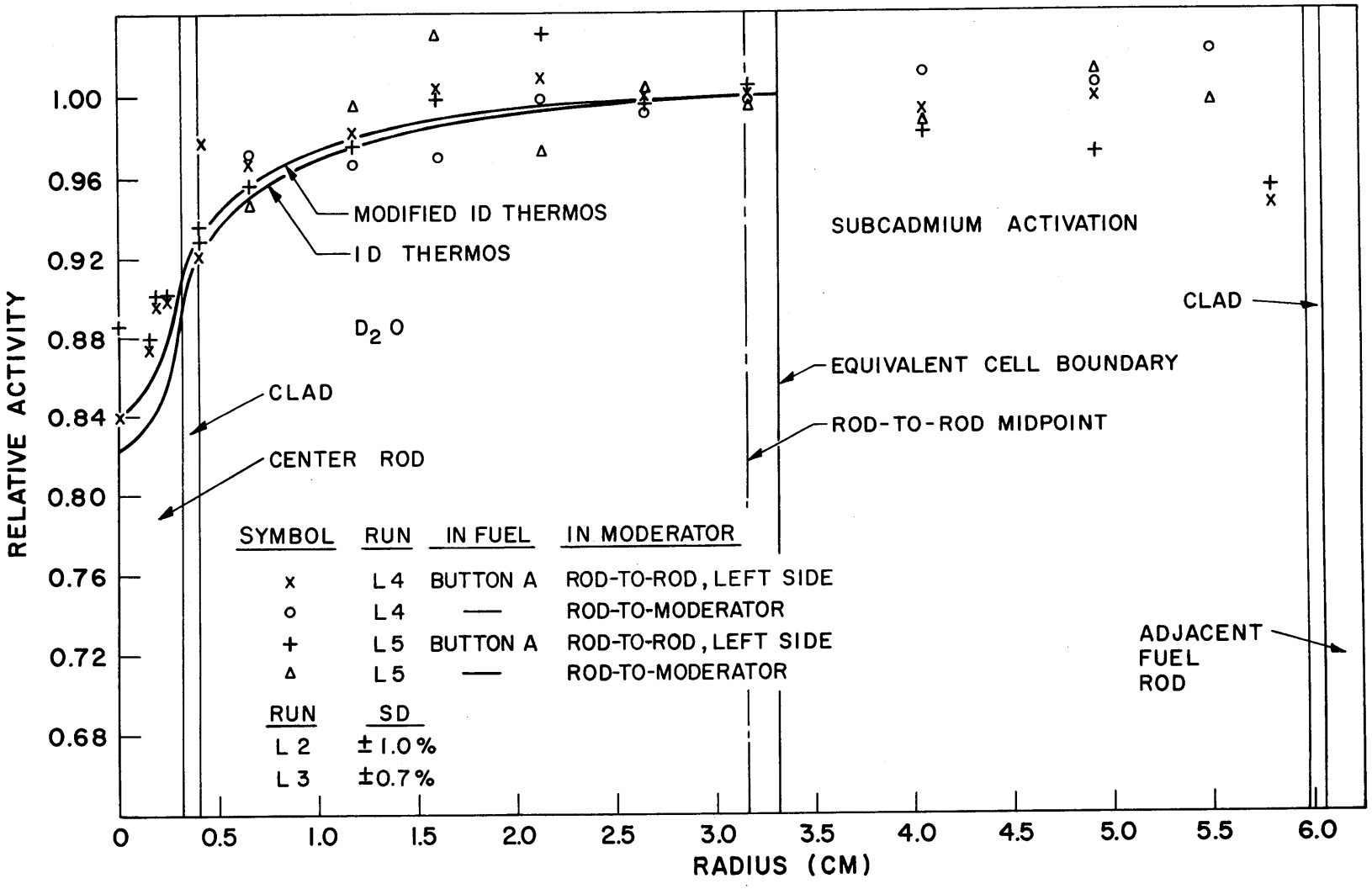

FIG. 4.3.9 SUBCADMIUM LUTETIUM ACTIVATION DISTRIBUTION FOR RUNS L2 AND L3; LUTETIUM ALLOY FOILS IN A LATTICE OF 1/4-INCH DIAMETER, 1.03% U-235, URANIUM RODS ON A 2.5-INCH TRIANGULAR SPACING.

foils were only twice the background level. The subcadmium activation was 3% higher than the THERMØS calculation at the center of the fuel rod.

The depleted uranium foils were irradiated in the lattice to investigate the epicadmium activation distribution. Figures 4.3.2 to 4.3.6 show the results obtained for the Np^{239} activity. The subcadmium activation distributions in the lattice with the 1.25-inch triangular spacing show a substantial scatter; the subcadmium activation was only 35% of the total activation. The subcadmium activation shapes are probably determined best when the cadmium ratio is greater than 3, as they were for the experiments with the gold foils. The epicadmium activation distributions indicate that the moderator flux was depleted somewhat in uranium-238 resonance neutrons in the vicinity of the rod. The gold experiments, on the other hand, gave flat epicadmium distributions in the moderator, even near the fuel rod. The large dip in the activation of the depleted uranium foils within the rod is due to the shielding effect of the uranium of the rod. A second experimental run in the lattice with the 2.5-inch triangular spacing was not completed because of experimental difficulties.

The results obtained by using europium powder foils are listed in Table 4.1.2; they were not plotted because the scatter was too large. No epicadmium activity was detectable. The scatter probably was a result of the low counting rates (as low as twice the background in Run E2) and the nature of the foils themselves. The foils were fabricated from Eu_2O_3 powder by Brown (B14). It was noticed in these experiments that the background level of the irradiated foil was 10% higher than background 100 hours after irradiation, probably because of activation of some contaminant in the foil.

The experimental results for the lutetium alloy foils are shown in Figs. 4.3.7 to 4.3.9; the comparison with the THERMØS calculations are also included. The lutetium foils were effectively infinitely thin. The results in the lattice with the 2.5-inch triangular spacing have less scatter than those in the lattice with the 1.25-inch triangular spacing. No epicadmium activity was detectable. The most likely cause of the scatter was the low counting rates. Longer irradiations (more than 30 hours) might have yielded better results, as in the experiments in the lattice with the 2.5-inch triangular spacing.

The motivation involved in irradiating foils such as lutetium and europium which have non-1/v-cross sections was to obtain data more sensitive to the "hardening" of the energy spectrum than the results obtained using gold. However, the alloy or powder foils have been largely unsatisfactory for the intracellular traverses in lattices requiring small foils, although the alloy seems to give the better results. Brown (B14) has been more successful with the larger powder foils that he used in lattices of 1-inch diameter, natural uranium rods.

CHAPTER V
CONCLUSIONS AND RECOMMENDATIONS FOR FUTURE WORK

A series of intracellular activation distribution measurements made by Brown (B14), in lattices of 1-inch diameter, natural uranium rods moderated by heavy water, were in agreement (about 2%) with one-dimensional THERMØS calculations. But when measurements were made in a lattice of 1/4-inch diameter, 1.03% U^{235}, uranium rods on a 1.25-inch triangular spacing, the predicted activation distribution near the center of the fuel rod fell 8% below the experimental distribution. Brown suspected that the most likely cause for this discrepancy was the failure of the approximation in the calculation that the hexagonal cell could be replaced by an equivalent circular cell, the cell cylindricalization, or Wigner-Seitz, approximation. From the results discussed in this report, it has been established that this approximation was, indeed, the cause of the discrepancy.

It was first shown that a change in the scattering model, or the use of simple prescriptions to account for the effects of anisotropic scattering, had a relatively insignificant effect on the calculated intracellular activation distributions for D_2O-moderated lattices. The Honeck-Nelkin model for D_2O, with a simple adjustment of the diagonal elements (for anisotropic scattering) seems adequate for future calculations in D_2O-moderated lattices. A similar study for lattices of natural uranium rods in graphite, discussed in Appendix E, indicates that the details of the scattering model are more important in that type of lattice than in heavy water lattices. The magnitudes of the effects of flux perturbation by foils and leakage from the tank were shown to be too small to account for the observed discrepancy. The one-dimensional THERMØS calculation agreed with the experimental intracellular activation distribution in the (wider) lattice with the 2.5-inch triangular spacing (1/4-inch diameter, 1.03% U^{235}, uranium rods), which indicates that the cell cylindricalization approximation in the tighter lattice with the 1.25-inch triangular spacing could be the source of the observed discrepancy. Finally, a two-dimensional calculation,for which the cell cylindricalization approximation is not made, agreed with experiment in

the lattice with the 1.25-inch triangular spacing. It may be concluded, therefore, that the approximation that the cell can be cylindricalized can lead to the serious discrepancies between theory and experiment for closely-packed lattices moderated by heavy water.

The two-dimensional THERMØS calculation requires about five times as much computer time as the one-dimensional calculation. Honeck (H13), in the course of studies of H_2O-moderated lattices, suggested a method for modifying the one-dimensional calculation so that it would reproduce the result of the two-dimensional calculation for the intracellular activation distribution, but without the corresponding increase in computer time. The method, which involves replacement of the equal-angle reflection condition at the cell boundary by an isotropic reflection condition, was applied to D_2O-moderated lattices; the results indicate that the modified one-dimensional calculation predicted the intracellular activation distributions as well as the two-dimensional calculation did. The limits of applicability of the modified one-dimensional calculation should be investigated in future work.

The results of the experiments with gold foils of different thickness indicate that the analytical methods developed in this work to treat the flux perturbation problem are adequate; gold foils, as thick as 10 mils, were used in some of the experiments. In the experiments, the gold foils, 2 and 4 mils thick, gave the best balance of irradiation time, count rate, accuracy of foil weight and correction required for flux perturbation so that their future use is recommended.

The analytical results indicated that leakage would not be a serious problem for the smaller (3-foot diameter) exponential tank used at M.I.T. It is possible that future work in small exponential assemblies, such as those studied by Peak (P5), may require significant leakage corrections. However, the discrepancy between theory and experiment that Peak observed for the intracellular activation distributions in the miniature lattice was probably due to the failure of the cell cylindricalization approximation.

A method of normalization of theory and experiment was suggested that was based on the prediction of the cadmium ratio of the foils used in the intracellular activation distribution measurements. However, it was found that uncertainties in the effective resonance integrals of the foils

are too large, so that the method will require additional work before it could replace the usual methods of normalization of the subcadmium activation distribution at either the center or the edge of the cell.

The epicadmium intracellular activation distribution has received little attention in the past. Measurements with depleted uranium foils have been made to provide some additional data in this area. The results with gold foils indicated that the flux at the gold resonance (4.9 ev) is spatially flat in the moderator. The distribution of activities of depleted uranium foils indicated that the resonance flux at the U^{238} resonance energies was depressed in the vicinity of the fuel rod. Future work to determine the fine structure of the resonance flux, such as the work at Chalk River (T7), should prove useful.

The use of wire detectors has been considered as a means of obtaining greater detail in the rod, and the use of wire probes would permit comparison with the results obtained with foils. It seems reasonable to require, as a basis of comparison that the foil and the wire have the same weight and mean chord length. On this basis, a wire, about 1/4 inch long and 1/128 inch in diameter, would be required if the comparison is to be with a foil, 1/16 inch in diameter and 4.3 mils thick. The experimental difficulties involved in using such thin wires would be considerable, but such experiments seem to be worthwhile and should be considered further.

One of the difficulties involved in using detector foils having non-1/v-activation cross sections in the thermal energy range is that the available nuclides having this property do not occur in a convenient metallic form, such as gold. It appears worthwhile to improve the methods of fabrication of powder foils to make possible the use of a wider class of foil material that would otherwise be difficult or expensive to use.

APPENDIX A
THE THERMAL NEUTRON FLUX PERTURBATION PROBLEM

The flux perturbation factor is the ratio of the neutron activation of a foil of finite size (for which the flux is perturbed) to that of the same foil if there were no flux perturbation. In practice, it is not possible to achieve the latter condition, and it has become common procedure to use the so-called infinitely thin foil, i.e., a foil thin enough that it does not significantly perturb the flux. The activity ratio, corrected for the weights of the foils, is the flux perturbation factor. This appendix is intended to provide a more general discussion than that of Section 3.4, where the problem was introduced.

For a foil in a large cavity, the neutron flux perturbation factor is equal to the escape probability, $\overline{P}$, as derived in Section 3.4. When the foil is in a diffusing medium, the flux perturbation is larger, since the incident neutron flux is perturbed. Much of the recent analytical and experimental work has involved the case of a foil in a diffusing medium, because of its importance in practical situations.

Bothe (B10) seems to have been the first to treat the flux perturbation problem in a diffusing medium. His first method was to use integral transport theory in the foil to obtain the self-shielding effect and diffusion theory in the moderator to obtain the depression of the total flux at the foil surface as compared with the flux at infinity. The combination of these two effects is the flux perturbation effect. Although the result is presumably well-known, it seems desirable to indicate how it was derived and to note the approximations used.

The integral transport theory calculation of the disadvantage factor has been reviewed by Fukai (F2). The disadvantage factor, F, is the ratio of the flux at the surface of the foil to the average flux in the foil. Theys (T2) has derived the disadvantage factor for an incident isotropic directional flux as:

$$F = \xi_a \frac{2 - \Gamma_a}{\Gamma_a}, \tag{A.1}$$

where $\xi_a = \Sigma_a t^*$ and Γ_a (sometimes called the blackness, β, of the absorbing body) is the probability that a neutron entering the foil isotropically will be absorbed. From the reciprocity theorem (T2), $\Gamma_a = 2\xi_a \overline{P}$, where $\overline{P}$ is the escape probability for neutrons from a flat, isotropic source in the foil. Then, Eq. (A.1) becomes:

$$F = \frac{1 - \xi_a \overline{P}}{\overline{P}} . \tag{A.2}$$

In most experiments, the foil is much smaller than any dimension of the experimental assembly, and it seems reasonable to assume that the foil is better approximated as a sphere than as an infinite slab in comparison to the external medium. To make the problem amenable to solution, it is assumed that the foil may be replaced by a sphere having the same volume-to-surface area as the foil: in this case, the radius of the sphere, R, is equal to $\frac{3}{2}$ t*.

The solution of the diffusion equation which satisfies the boundary condition that the flux at infinity be finite, with a constant source density everywhere, is:

$$\frac{\phi(r)}{\phi_\infty} = 1 - \frac{Ae^{-\kappa r}}{r} , \tag{A.3}$$

where A is an arbitrary constant and κ is the inverse of the diffusion length. Since the boundary condition at the surface of the foil is known from the integral transport calculation, A can be determined. The result for the flux at the surface of the foil is:

$$\frac{\phi(R)}{\phi_\infty} = \frac{1}{1 + \frac{\xi_a}{2F} \frac{R}{D} \left(\frac{1}{\kappa R + 1}\right)} . \tag{A.4}$$

The total flux perturbation factor, f_{ss}, is the ratio ϕ/ϕ_∞:

$$f_{ss} = \frac{\overline{\phi}}{\phi_\infty} = \frac{1}{F} \frac{1}{1 + \frac{\xi_a}{2F} \frac{R}{D} \left(\frac{1}{\kappa R + 1}\right)} . \tag{A.5}$$

On substituting for R in terms of t* and using Eq. (A.2) for F, ϕ/ϕ_∞ becomes:

$$f_{ss} = \frac{\bar{\phi}}{\phi_\infty} = \frac{\bar{P}}{1 + \xi_a \bar{P}\left(\frac{3t^*}{D}\frac{2}{3\kappa t^* + 2} - 1\right)} \,. \tag{A.6}$$

To put Eq. (A.6) in more familiar terms, replace D by $\lambda_{tr}/3$ and κ by $1/L$:

$$f_{ss} = \frac{\bar{\phi}}{\phi_\infty} = \frac{\bar{P}}{1 + \xi_a \bar{P}\left(\frac{t^*}{\lambda_{tr}}\frac{2L}{3t^* + 2L} - 1\right)} \,. \tag{A.7}$$

Hanna (H1) writes Eq. (A.7) as:

$$f_{ss} = \frac{\bar{\phi}}{\phi_\infty} = \frac{\bar{P}(1+\epsilon)}{1 + g\xi_a \bar{P}} \,. \tag{A.8}$$

He defines $(1+\epsilon)$ as the correction for the edge effect. A simple correction for the edge effect is included in the calculation of f_{ss} [Eq. (A.7)] by evaluating $\bar{P}$ for a slab of effective thickness, t*, which has the same mean chord length as the actual foil.

Comparison of the denominators of Eqs. (A.7) and (A.8) gives:

$$g = \frac{t^*}{\lambda_{tr}}\frac{2L}{2L + 3t^*} - 1 \,. \tag{A.9}$$

For heavy water, λ_{tr} is approximately 2.5 cm and L is approximately 100 cm; the foil thickness is of the order of mils, and $g = -1$. Then Eq. (A.7) reduces to:

$$f_{ss} = \frac{\bar{\phi}}{\phi_\infty} = \frac{\bar{P}}{1 - \xi_a \bar{P}} = \frac{1}{\bar{F}} \,. \tag{A.10}$$

The result would have been obtained, had the external flux depression been neglected; there appears, therefore, to be an inconsistency, since the flux perturbation factor should have reduced to $\bar{P}$, not $1/F$. The assumption that the incident flux could be calculated by diffusion theory apparently caused the inconsistency. Wachspress (W1) discusses a similar situation in his work on thin region theory.

Bothe also derived another expression for g for when $t^* \ll \lambda_{tr}$, and obtained the result:

$$g = 0.68\ t^*/\lambda_{tr} \,, \tag{A.11}$$

in terms of the variables defined here. For 10 mil thick gold foils in heavy water, the effect of the diffusing medium on the flux perturbation factor is only 0.3% of the effect in a vacuum. Hence, the escape probability, $\overline{P}$, should be a good approximation for $\overline{\phi}/\phi_\infty$ for D_2O. Others (R2) have tried to modify Eq. (A.8) by calculating g with varying degrees of rigor. Dalton (D2), rather than approach the problem from the more conventional methods, has computed directly numerical solutions of the Boltzmann equation.

To compare the analytical methods with experiment, it is necessary to take into account the energy dependence of the cross sections. The experiment is usually made in a flux that is close to a Maxwellian spectrum, M(E), at the moderator temperature. Dalton simply uses the flux-averaged cross sections in his single velocity method. The simplicity of the spatial dependence implicit in the escape probability approximation allows a more rigorous approach to the energy dependence. The activation of the foil of finite thickness is:

$$\text{Activation of the finite foil} = \int_0^{E_c} \overline{P}\sigma_{ACT}(E)\, M(E)\, dE\,, \qquad (A.12)$$

where E_c is the energy of the cadmium cutoff. The activation of the infinitely thin foil ($\overline{P} = 1$) is:

$$\text{Activation of the infinitely thin foil} = \int_0^{E_c} \sigma_{ACT}(E)\, M(E)\, dE\,. \qquad (A.13)$$

The flux perturbation factor for the finite foil is the ratio of Eqs. (A.12) and (A.13):

$$\text{Flux Perturbation Factor, } \overline{f}_{ss} = \frac{\int_0^{E_c} \overline{P}\sigma_{ACT}(E)\, M(E)\, dE}{\int_0^{E_c} \sigma_{ACT}(E)\, M(E)\, dE}\,. \qquad (A.14)$$

Calculations for $\overline{f}_{ss}$ based on Eq. (A.14) for gold, cobalt and copper foils have been made with the QUICK code described in Appendix C. The results of these calculations are shown in Fig. A.1. The values of f_{ss}

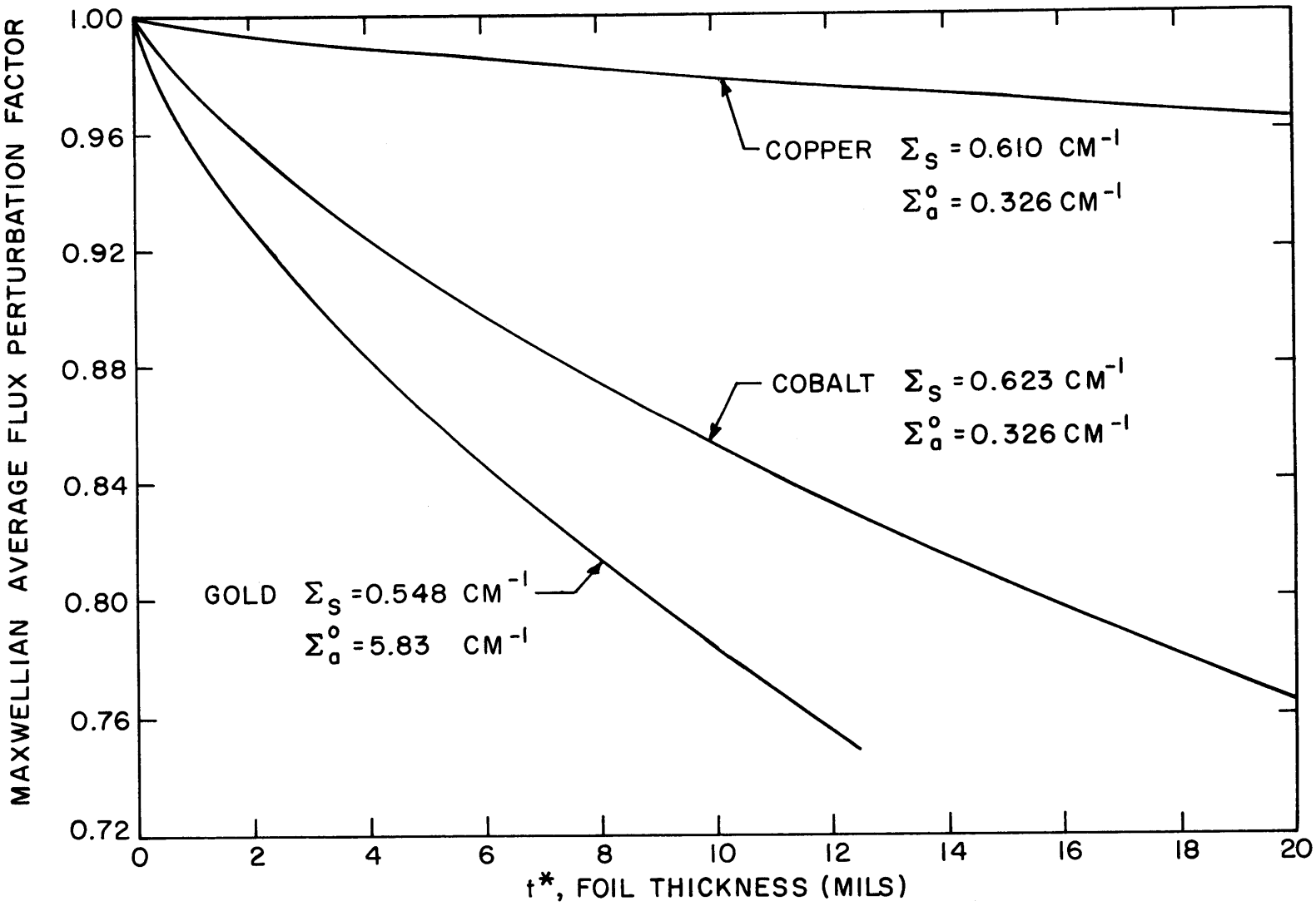

FIG. A.1 MAXWELLIAN AVERAGE FLUX PERTURBATION FACTOR FOR DETECTOR FOILS.

calculated from Eq. (A.14) for gold foils are compared in Table A.1 to the values of f_{ss} calculated, using cross sections, at a neutron speed of 2200 m/sec. The results of this comparison indicate that the values of f_{ss} calculated with 2200 m/sec cross sections are consistent with the energy average, $\bar{f}_{ss}$.

TABLE A.1

Comparison of Values of the Flux Perturbation Factor Calculated by Using 2200 m/sec Cross Sections and by Assuming an Incident Maxwellian Spectrum

Foil Thickness, t* (mils)	Value of f_{ss} Using 2200 m/sec Cross Sections	Value of f_{ss} Calculated from Eq. (A.14)
2.3	0.927	0.923
3.8	0.894	0.889
7.7	0.823	0.817
20.6	0.665	0.661

The experimental data available for H_2O provide a stringent test of these calculations because λ_{tr} for H_2O is less than λ_{tr} for D_2O, and, therefore, the flux perturbation should be greater in H_2O than in D_2O. Zobel (Z2) has made experiments with gold foils of various thickness in an H_2O medium. Figure A.2 shows the comparison of the experimental results of Zobel, with the calculated values of Dalton, and with the values calculated from Eq. (A.14). The results of Dalton's calculations with flux-averaged cross sections agree with the experiment within the quoted experimental uncertainty. The escape probability method of Eq. (A.14) gives results that are 6% higher than experiment for a 10 mil thick gold foil. It is possible that Dalton's result would be sensitive to the cross sections used. However, Dalton's method has no provision for any spectrum variation. In any event, the escape probability method should give better results for D_2O than H_2O with no greater error than that which occurred in the comparison with Zobel's experiment.

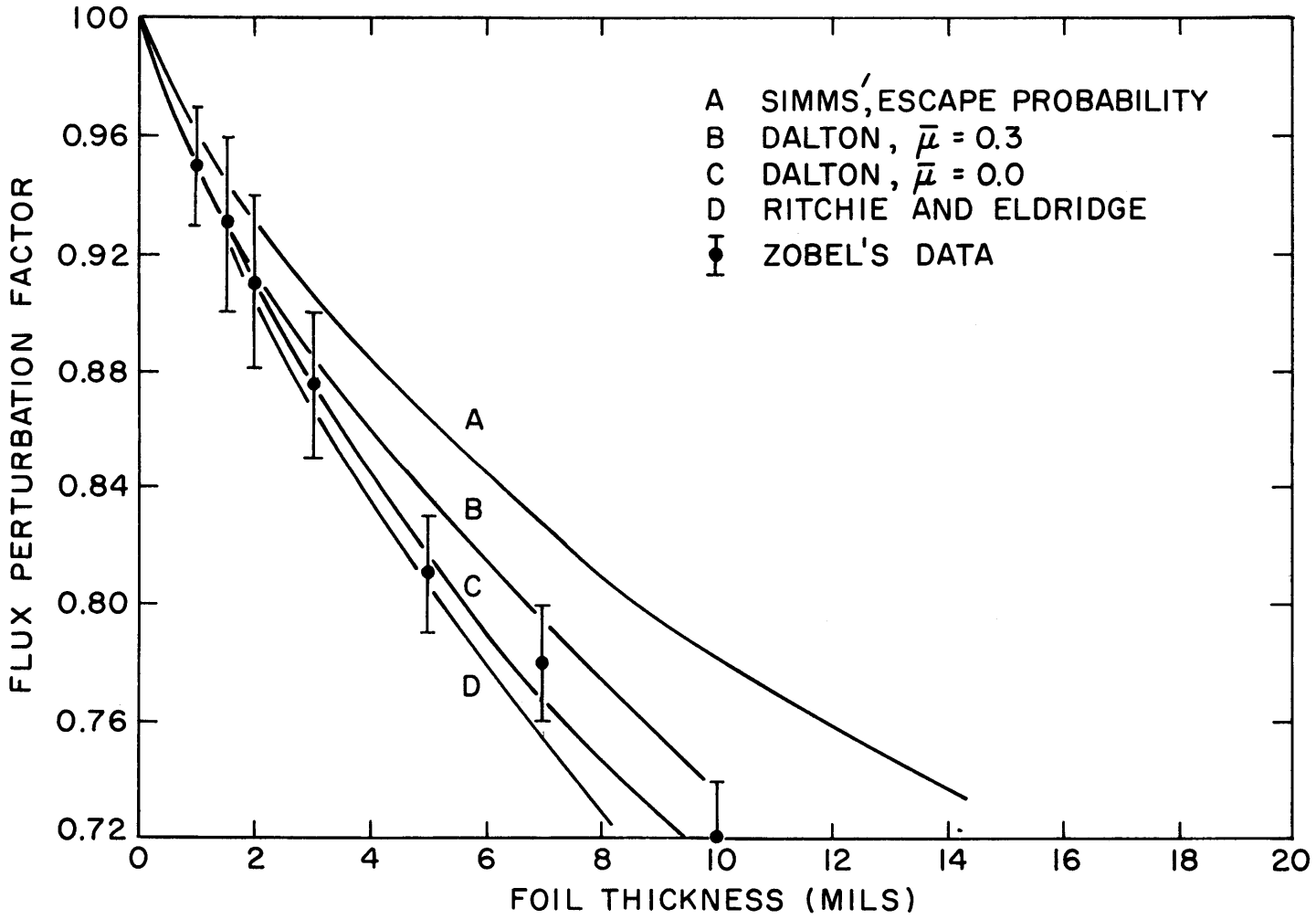

FIG. A.2 COMPARISON OF THEORY AND EXPERIMENT FOR THE FLUX PERTURBATION OF GOLD FOILS IN H_2O. THE EXPERIMENTAL DATA ARE THOSE OF ZOBEL (TRANS. AM. NUCL. SOC. 5, 1, JUNE, 1962).

APPENDIX B
EFFECTS OF FOIL INTERACTION AND MYLAR TAPE

Four experiments were made to investigate the possible effects, on the foil activations in the moderator, of the presence of the mylar tape and of the interaction between adjacent foils. The experiments were made in the test position of the three-rod cluster in the lattice with the 1.25-inch triangular spacing during measurements of intracellular flux traverses. The three-rod cluster is shown in Fig. 2.5.1 and the location of the test position in Fig. 2.5.3.

The foil holders in the moderator were similar to those used throughout the experiments in the lattice with the 1.25-inch triangular spacing. The design of the foil holder is shown in Fig. B.1. The holders were fabricated from aluminum, 12 mils thick, and foils from the file of 4.3 mil thick gold foils were used. The rod-to-moderator traverse section was eliminated because no foils were to be irradiated in this direction. The lattice was assumed to be azimuthally symmetric; the validity of this assumption has been discussed in Chapter IV. In the case of symmetry, if there are no perturbations on either side of the holder, the activities of the foils located in symmetrical positions should be the same. It is assumed that when a perturbation is introduced on one side of the holder, the effect is negligible on the other side.

The first experiment was designed to investigate the effect of the mylar tape used throughout the experimental program. A special holder, with foil holes on the left side and 6 mil deep holes on the right side was fabricated from 12 mil thick aluminum. A single strip of 2 mil mylar tape was placed over the foils on the right side of the holder. Eight strips of mylar tape were placed on the left side, four each on top and bottom. The left side, therefore, had eight times as much mylar covering the foils than did the right side. The object of the experiment was to see if this large quantity of mylar would perturb the flux.

The results of the first experiment are given in Table B.1. The maximum difference occurred at a radial position of 2.61 cm, with the

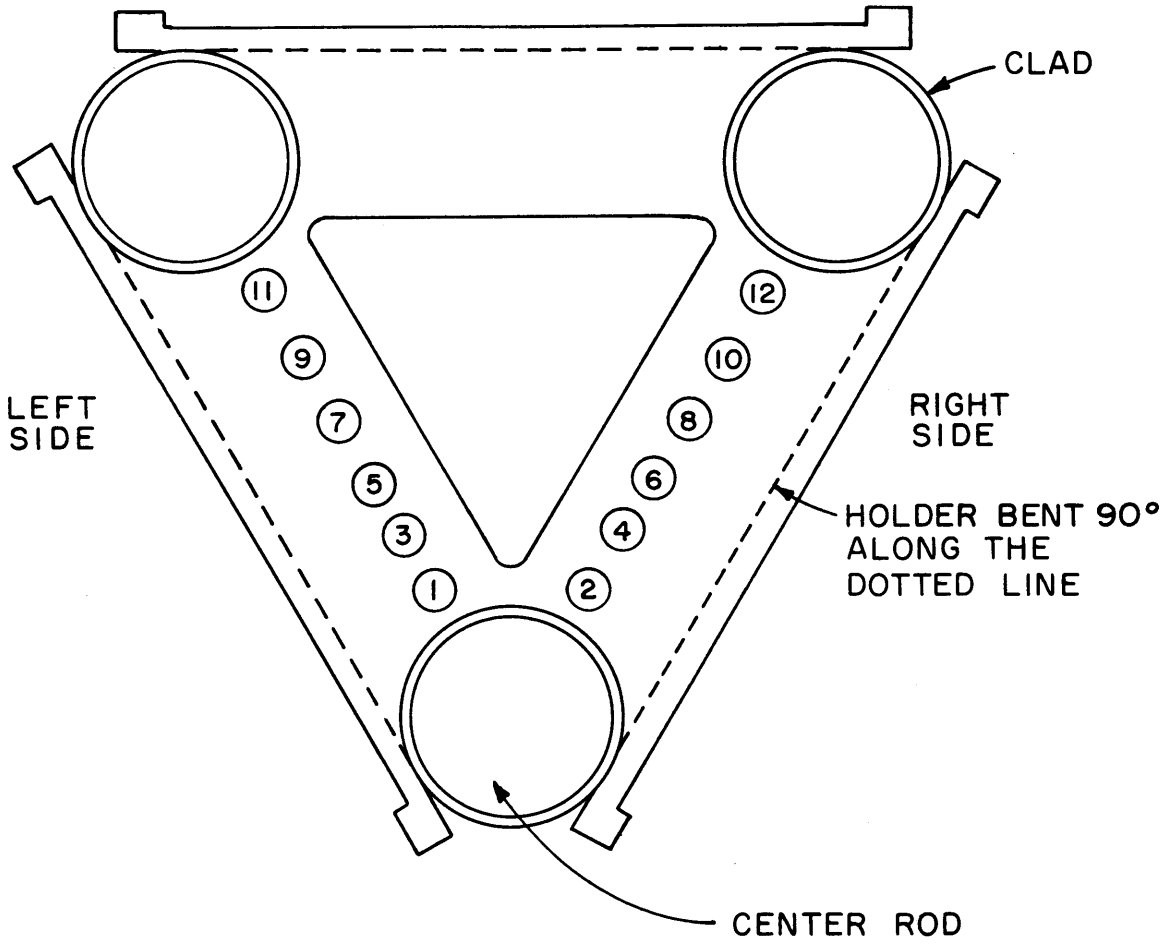

FIG. B.1 TOP VIEW OF THE FOIL HOLDER FOR THE PERTURBATION EXPERIMENTS IN THE MODERATOR.

TABLE B.1

Ratios of Foil Activities for 4.3 mil Thick Gold Foils In the Test Position of the Three-Rod Cluster

Radial Position (cm)	Ratio of Foil Activity for: (a)	Exp. 1 SD, ± 0.3%	Exp. 2 SD, ± 0.6%	Exp. 3 SD, ± 0.4%	Exp. 4 SD, ± 0.4%	Run A11 SD, ± 0.5%	Run A16 SD, ± 0.6%
0.563	#1/#2	0.992	0.998	0.999	0.997	0.986	0.995
0.972	#3/#4	1.010	1.004	0.994	0.994	1.010	0.987
1.381	#5/#6	0.998	0.995	1.006	0.981	1.003	0.998
1.793	#7/#8	1.005	–	–	–	1.017	1.006
2.202	#9/#10	1.008	0.995	0.998	1.015	1.004	0.990
2.611	#11/#12	1.013	1.011	1.000	0.989	0.985	0.985

(a) Numbers refer to Fig. B.1.

foil in position 11 (see Fig. B.1) having an activity 1.013 ± 0.3% higher than the foil in position 12. This ratio is approximately what would be expected from a typical experiment involving no perturbation. For comparison, gold intracellular experiments, Runs A11 and A16, are included in Table B.1. Since these experiments were performed in the same lattice using 4.3 mil thick foils, they are examples in which no perturbation was introduced intentionally. It may be concluded, therefore, that the mylar had a negligible effect on the activation of the foils.

Experiments 2, 3 and 4 were designed to investigate the interaction between adjacent foils spaced about 1/6 inch apart. In experiment 2, foil position 7 was occupied by a cadmium foil, 1/16 inch in diameter and 20 mils thick. Position 7 was not occupied in experiment 3. In experiment 4, position 8 was empty and position 7 had the same cadmium foil. This rotation was made to eliminate some of the possible variables. Experiments 2 and 3 compared a cadmium foil to an empty position on the same side of the holder, while experiments 2 and 4 compared them on opposite sides. The results are listed in Table B.1. The ratios of foil activities adjacent to position 7 show that in no case was the perturbation detectable above the normally expected deviations as exemplified by the results of Runs A11 and A16.

The fact that the presence of the cadmium foil cannot be detected indicates that the foils do not interact, since a cadmium foil should have a greater effect than a gold foil in a thermal flux (75% of the captures in the gold were at energies below the cadmium cutoff). Although the foils were quite close together, they were laid flat on the holder. In this position, the solid angle subtending one foil by another was much smaller than that if they had been placed vertically, facing each other. Unlike H_2O-moderated lattices, D_2O-moderated lattices are less affected by local perturbations, because thermal neutrons can travel farther in D_2O than in H_2O (the scattering cross section of H_2O is much greater than the scattering cross section in D_2O). This expectation was verified by the experiments in which a cadmium foil, 20 mils thick, had no noticeable effect on a neighboring gold foil 1/6 of an inch away.

APPENDIX C
THE QUICK CODE

The QUICK code was programmed to calculate disadvantage factors and escape probabilities as functions of energy. The punched card output from the program can be used as cross section input to the THERMØS code. The program was written so that it could be expanded for use with arrangements other than slabs by the interchange of subroutines in the binary running deck. At present, the code has capabilities for slabs and cylinders.

McGoff (M4) has coded a subprogram, CYLDIP, which calculates the disadvantage factor for cylinders by means of a method based on the results of Stuart and Woodruff (S3). In the analysis, it is assumed that the incident directional flux is linearly anisotropic, consistent with diffusion theory. The subprogram was modified for use with the QUICK code. CYLDIP is restricted to the calculation of the disadvantage factor.

Subroutine DPRESS was programmed to calculate disadvantage factors and escape probabilities for slabs. The approximations used are discussed in Section 3.4 and Appendix A. For an isotropic incident directional flux, the disadvantage factor, F, is related to the escape probability, $\overline{P}$:

$$\frac{1}{F} = \frac{\overline{P}}{1 - \Sigma_a t \overline{P}} , \tag{C.1}$$

$$\overline{P} = \frac{P_o}{1 - \frac{\Sigma_s}{\Sigma}(1-P_o)} , \tag{C.2}$$

$$P_o = \frac{1 - 2E_3(\Sigma t)}{2\Sigma t} , \tag{C.3}$$

where $E_3(\Sigma t)$ is the exponential integral tabulated by Case, deHoffmann and Placzek (C5) for optical thickness, Σt. The exponential integrals were calculated by Subroutine EI, originally coded by Honeck for use in

the THERMØS code. The subroutine was found to give the same results as those tabulated by Case, deHoffmann and Placzek.

For convenience, the output of the QUICK code is such that the activation cross section has been multiplied by the escape probability. The result is an effective cross section for the nuclide in question for the foil size used:

$$\sigma^{*}_{ACT}(E) = \overline{P}\sigma_{ACT}(E) . \tag{C.4}$$

An estimate of the flux perturbation factor, $\overline{f}_{ss}$, for the foil in a Maxwellian spectrum is included as part of the output:

$$\overline{f}_{ss} = \frac{\int_0^{E_{MAX}} \sigma^{*}_{ACT}(E)\, M(E)\, dE}{\int_0^{E_{MAX}} \sigma_{ACT}(E)\, M(E)\, dE} , \tag{C.5}$$

where E_{MAX} is the upper energy limit. A similar calculation is performed with the inverse of the disadvantage factor:

$$\sigma^{*}_{ACT}(E) = \frac{1}{\overline{F}}\, \sigma_{ACT}(E) , \tag{C.6}$$

$$\left(\frac{\overline{1}}{F}\right) = \frac{\int_0^{E_{MAX}} \sigma^{*}_{ACT}(E)\, M(E)\, dE}{\int_0^{E_{MAX}} \sigma_{ACT}(E)\, M(E)\, dE} . \tag{C.7}$$

The running deck of QUICK consists of the main program, QUICK, and DPRESS and EI for slab calculations or CYLDIP for calculations involving cylinders. The FORTRAN listings of the program are given along with the input instructions; a test problem is included. Results of calculations for metallic gold foils (slabs) are included in Tables C.1 to C.10.

TABLE C.1

Effective Activation Cross Sections for 0.5 mil Thick Gold Foils

Group	Energy (ev)	Activation Cross Section σ_{ACT}/σ^{o} (a)	Effective Activation Cross Sections $\sigma_{ACT}/F\sigma^{o}$ (b)	$\overline{P}\sigma_{ACT}/\sigma^{o}$ (c)
1	0.00025	10.0000	9.3018	8.7026
2	0.00101	5.0000	4.7770	4.6139
3	0.00228	3.3333	3.2205	3.1455
4	0.00405	2.5000	2.4308	2.3878
5	0.00632	2.0000	1.9528	1.9250
6	0.00911	1.6667	1.6322	1.6127
7	0.01240	1.4286	1.4022	1.3878
8	0.01619	1.2500	1.2291	1.2180
9	0.02049	1.1111	1.0941	1.0853
10	0.02530	1.0000	0.9858	0.9787
11	0.03061	0.9091	0.8971	0.8912
12	0.03643	0.8333	0.8231	0.8181
13	0.04276	0.7692	0.7603	0.7561
14	0.04959	0.7143	0.7065	0.7028
15	0.05692	0.6667	0.6597	0.6565
16	0.06517	0.6231	0.6169	0.6141
17	0.07485	0.5814	0.5760	0.5735
18	0.08612	0.5420	0.5372	0.5351
19	0.09919	0.5051	0.5008	0.4990
20	0.11398	0.4711	0.4674	0.4658
21	0.13123	0.4391	0.4358	0.4344
22	0.15248	0.4073	0.4045	0.4033
23	0.17901	0.3759	0.3735	0.3724
24	0.21241	0.3451	0.3430	0.3421
25	0.25464	0.3152	0.3134	0.3127
26	0.30816	0.2865	0.2850	0.2844
27	0.37598	0.2594	0.2581	0.2576
28	0.46183	0.2341	0.2330	0.2326
29	0.57023	0.2106	0.2098	0.2094
30	0.70666	0.1892	0.1885	0.1882

(a) σ^{o} is the activation cross section at 2200 m/sec.

(b) F is the disadvantage factor for an incident, isotropic flux.

(c) $\overline{P}$ is the escape probability from a flat, isotropic source of neutrons in the foil.

TABLE C.2

Effective Activation Cross Sections for 1.0 mil Thick Gold Foils

Group	Energy (ev)	Activation Cross Section σ_{ACT}/σ^{o} (a)	Effective Activation Cross Sections $\sigma_{ACT}/F\sigma^{o}$ (b)	$\overline{P}\sigma_{ACT}/\sigma^{o}$ (c)
1	0.00025	10.0000	8.9324	7.8891
2	0.00101	5.0000	4.6509	4.3513
3	0.00228	3.3333	3.1537	3.0130
4	0.00405	2.5000	2.3885	2.3069
5	0.00632	2.0000	1.9233	1.8700
6	0.00911	1.6667	1.6102	1.5727
7	0.01240	1.4286	1.3851	1.3573
8	0.01619	1.2500	1.2154	1.1939
9	0.02049	1.1111	1.0828	1.0657
10	0.02530	1.0000	0.9764	0.9625
11	0.03061	0.9091	0.8891	0.8775
12	0.03643	0.8333	0.8161	0.8064
13	0.04276	0.7692	0.7542	0.7459
14	0.04959	0.7143	0.7011	0.6939
15	0.05692	0.6667	0.6550	0.6487
16	0.06517	0.6231	0.6127	0.6071
17	0.07485	0.5814	0.5722	0.5674
18	0.08612	0.5420	0.5339	0.5297
19	0.09919	0.5051	0.4978	0.4942
20	0.11398	0.4711	0.4648	0.4616
21	0.13123	0.4391	0.4334	0.4307
22	0.15248	0.4073	0.4024	0.4000
23	0.17901	0.3759	0.3717	0.3696
24	0.21241	0.3451	0.3414	0.3397
25	0.25464	0.3152	0.3121	0.3106
26	0.30816	0.2865	0.2839	0.2827
27	0.37598	0.2594	0.2572	0.2562
28	0.46183	0.2341	0.2322	0.2314
29	0.57023	0.2106	0.2091	0.2085
30	0.70666	0.1892	0.1880	0.1874

(a) σ^{o} is the activation cross section at 2200 m/sec.

(b) F is the disadvantage factor for an incident, isotropic flux.

(c) $\overline{P}$ is the escape probability from a flat, isotropic source of neutrons in the foil.

TABLE C.3

Effective Activation Cross Sections for 2.3 mil Thick Gold Foils

Group	Energy (ev)	Activation Cross Section σ_{ACT}/σ^{o} (a)	Effective Activation Cross Sections $\sigma_{ACT}/F\sigma^{o}$ (b)	$\overline{P}\sigma_{ACT}/\sigma^{o}$ (c)
1	0.00025	10.0000	8.2249	6.4161
2	0.00101	5.0000	4.4172	3.8363
3	0.00228	3.3333	3.0291	2.7442
4	0.00405	2.5000	2.3088	2.1395
5	0.00632	2.0000	1.8670	1.7547
6	0.00911	1.6667	1.5679	1.4880
7	0.01240	1.4286	1.3520	1.2921
8	0.01619	1.2500	1.1886	1.1421
9	0.02049	1.1111	1.0606	1.0234
10	0.02530	1.0000	0.9576	0.9272
11	0.03061	0.9091	0.8730	0.8476
12	0.03643	0.8333	0.8021	0.7807
13	0.04276	0.7692	0.7420	0.7236
14	0.04959	0.7143	0.6902	0.6743
15	0.05692	0.6667	0.6453	0.6313
16	0.06517	0.6231	0.6040	0.5917
17	0.07485	0.5814	0.5644	0.5537
18	0.08612	0.5420	0.5270	0.5176
19	0.09919	0.5051	0.4917	0.4836
20	0.11398	0.4711	0.4593	0.4522
21	0.13123	0.4391	0.4286	0.4224
22	0.15248	0.4073	0.3981	0.3928
23	0.17901	0.3759	0.3679	0.3633
24	0.21241	0.3451	0.3382	0.3343
25	0.25464	0.3152	0.3093	0.3060
26	0.30816	0.2865	0.2815	0.2788
27	0.37598	0.2594	0.2552	0.2530
28	0.46183	0.2341	0.2305	0.2287
29	0.57023	0.2106	0.2077	0.2062
30	0.70666	0.1892	0.1868	0.1856

(a) σ^{o} is the activation cross section at 2200 m/sec.

(b) F is the disadvantage factor for an incident, isotropic flux.

(c) $\overline{P}$ is the escape probability from a flat, isotropic source of neutrons in the foil.

TABLE C.4

Effective Activation Cross Sections for 2.5 mil Thick Gold Foils

Group	Energy (ev)	Activation Cross Section σ_{ACT}/σ^{o} (a)	Effective Activation Cross Sections $\sigma_{ACT}/F\sigma^{o}$ (b)	$\overline{P}\sigma_{ACT}/\sigma^{o}$ (c)
1	0.00025	10.0000	8.1376	6.2538
2	0.00101	5.0000	4.3896	3.7761
3	0.00228	3.3333	3.0146	2.7120
4	0.00405	2.5000	2.2995	2.1191
5	0.00632	2.0000	1.8604	1.7405
6	0.00911	1.6667	1.5630	1.4775
7	0.01240	1.4286	1.3481	1.2840
8	0.01619	1.2500	1.1854	1.1356
9	0.02049	1.1111	1.0580	1.0181
10	0.02530	1.0000	0.9554	0.9228
11	0.03061	0.9091	0.8711	0.8438
12	0.03643	0.8333	0.8005	0.7774
13	0.04276	0.7692	0.7405	0.7207
14	0.04959	0.7143	0.6889	0.6718
15	0.05692	0.6667	0.6441	0.6291
16	0.06517	0.6231	0.6029	0.5898
17	0.07485	0.5814	0.5635	0.5520
18	0.08612	0.5420	0.5261	0.5161
19	0.09919	0.5051	0.4910	0.4822
20	0.11398	0.4711	0.4586	0.4510
21	0.13123	0.4391	0.4280	0.4213
22	0.15248	0.4073	0.3976	0.3918
23	0.17901	0.3759	0.3675	0.3625
24	0.21241	0.3451	0.3378	0.3336
25	0.25464	0.3152	0.3089	0.3055
26	0.30816	0.2865	0.2812	0.2783
27	0.37598	0.2594	0.2549	0.2526
28	0.46183	0.2341	0.2303	0.2284
29	0.57023	0.2106	0.2075	0.2060
30	0.70666	0.1892	0.1866	0.1854

(a) σ^{o} is the activation cross section at 2200 m/sec.

(b) F is the disadvantage factor for an incident, isotropic flux.

(c) $\overline{P}$ is the escape probability from a flat, isotropic source of neutrons in the foil.

TABLE C.5

Effective Activation Cross Sections for 3.8 mil Thick Gold Foils

Group	Energy (ev)	Activation Cross Section σ_{ACT}/σ^{o} (a)	Effective Activation Cross Sections $\sigma_{ACT}/F\sigma^{o}$ (b)	$\overline{P}\sigma_{ACT}/\sigma^{o}$ (c)
1	0.00025	10.0000	7.5692	5.3170
2	0.00101	5.0000	4.2166	3.4116
3	0.00228	3.3333	2.9245	2.5132
4	0.00405	2.5000	2.2421	1.9921
5	0.00632	2.0000	1.8198	1.6516
6	0.00911	1.6667	1.5323	1.4113
7	0.01240	1.4286	1.3239	1.2326
8	0.01619	1.2500	1.1658	1.0944
9	0.02049	1.1111	1.0416	0.9843
10	0.02530	1.0000	0.9415	0.8944
11	0.03061	0.9091	0.8591	0.8197
12	0.03643	0.8333	0.7901	0.7566
13	0.04276	0.7692	0.7313	0.7026
14	0.04959	0.7143	0.6808	0.6558
15	0.05692	0.6667	0.6368	0.6149
16	0.06517	0.6231	0.5964	0.5771
17	0.07485	0.5814	0.5576	0.5407
18	0.08612	0.5420	0.5209	0.5061
19	0.09919	0.5051	0.4863	0.4734
20	0.11398	0.4711	0.4544	0.4432
21	0.13123	0.4391	0.4243	0.4144
22	0.15248	0.4073	0.3943	0.3858
23	0.17901	0.3759	0.3645	0.3573
24	0.21241	0.3451	0.3353	0.3291
25	0.25464	0.3152	0.3068	0.3016
26	0.30816	0.2865	0.2794	0.2751
27	0.37598	0.2594	0.2534	0.2498
28	0.46183	0.2341	0.2290	0.2261
29	0.57023	0.2106	0.2064	0.2041
30	0.70666	0.1892	0.1857	0.1838

(a) σ^{o} is the activation cross section at 2200 m/sec.

(b) F is the disadvantage factor for an incident, isotropic flux.

(c) $\overline{P}$ is the escape probability from a flat, isotropic source of neutrons in the foil.

TABLE C.6

Effective Activation Cross Sections for 4.3 mil Thick Gold Foils

Group	Energy (ev)	Activation Cross Section σ_{ACT}/σ^{o} (a)	Effective Activation Cross Sections $\sigma_{ACT}/F\sigma^{o}$ (b)	$\overline{P}\sigma_{ACT}/\sigma^{o}$ (c)
1	0.00025	10.0000	7.3506	5.0076
2	0.00101	5.0000	4.1522	3.2842
3	0.00228	3.3333	2.8916	2.4421
4	0.00405	2.5000	2.2213	1.9461
5	0.00632	2.0000	1.8051	1.6191
6	0.00911	1.6667	1.5213	1.3870
7	0.01240	1.4286	1.3152	1.2136
8	0.01619	1.2500	1.1587	1.0791
9	0.02049	1.1111	1.0357	0.9717
10	0.02530	1.0000	0.9365	0.8838
11	0.03061	0.9091	0.8548	0.8107
12	0.03643	0.8333	0.7863	0.7488
13	0.04276	0.7692	0.7280	0.6957
14	0.04959	0.7143	0.6778	0.6498
15	0.05692	0.6667	0.6341	0.6095
16	0.06517	0.6231	0.5940	0.5723
17	0.07485	0.5814	0.5555	0.5365
18	0.08612	0.5420	0.5189	0.5024
19	0.09919	0.5051	0.4846	0.4701
20	0.11398	0.4711	0.4529	0.4402
21	0.13123	0.4391	0.4229	0.4118
22	0.15248	0.4073	0.3931	0.3835
23	0.17901	0.3759	0.3635	0.3553
24	0.21241	0.3451	0.3343	0.3274
25	0.25464	0.3152	0.3060	0.3001
26	0.30816	0.2865	0.2787	0.2738
27	0.37598	0.2594	0.2528	0.2488
28	0.46183	0.2341	0.2285	0.2252
29	0.57023	0.2106	0.2060	0.2033
30	0.70666	0.1892	0.1854	0.1832

(a) σ^{o} is the activation cross section at 2200 m/sec.

(b) F is the disadvantage factor for an incident, isotropic flux.

(c) $\overline{P}$ is the escape probability from a flat, isotropic source of neutrons in the foil.

TABLE C.7

Effective Activation Cross Sections for 7.7 mil Thick Gold Foils

Group	Energy (ev)	Activation Cross Section σ_{ACT}/σ^{o} (a)	Effective Activation Cross Sections $\sigma_{ACT}/F\sigma^{o}$ (b)	$\overline{P}\sigma_{ACT}/\sigma^{o}$ (c)
1	0.00025	10.0000	6.0536	3.5838
2	0.00101	5.0000	3.7708	2.6382
3	0.00228	3.3333	2.7027	2.0668
4	0.00405	2.5000	2.1042	1.6976
5	0.00632	2.0000	1.7235	1.4408
6	0.00911	1.6667	1.4601	1.2520
7	0.01240	1.4286	1.2672	1.1074
8	0.01619	1.2500	1.1197	0.9931
9	0.02049	1.1111	1.0032	0.9004
10	0.02530	1.0000	0.9089	0.8237
11	0.03061	0.9091	0.8310	0.7592
12	0.03643	0.8333	0.7655	0.7041
13	0.04276	0.7692	0.7096	0.6566
14	0.04959	0.7143	0.6614	0.6151
15	0.05692	0.6667	0.6194	0.5786
16	0.06517	0.6231	0.5807	0.5447
17	0.07485	0.5814	0.5436	0.5119
18	0.08612	0.5420	0.5083	0.4805
19	0.09919	0.5051	0.4750	0.4506
20	0.11398	0.4711	0.4443	0.4229
21	0.13123	0.4391	0.4152	0.3965
22	0.15248	0.4073	0.3863	0.3700
23	0.17901	0.3759	0.3575	0.3435
24	0.21241	0.3451	0.3291	0.3172
25	0.25464	0.3152	0.3014	0.2914
26	0.30816	0.2865	0.2748	0.2665
27	0.37598	0.2594	0.2495	0.2426
28	0.46183	0.2341	0.2257	0.2200
29	0.57023	0.2106	0.2036	0.1990
30	0.70666	0.1892	0.1834	0.1796

(a) σ^{o} is the activation cross section at 2200 m/sec.

(b) F is the disadvantage factor for an incident, isotropic flux.

(c) $\overline{P}$ is the escape probability from a flat, isotropic source of neutrons in the foil.

TABLE C.8

Effective Activation Cross Sections for 10.2 mil Thick Gold Foils

Group	Energy (ev)	Activation Cross Section σ_{ACT}/σ^{o} (a)	Effective Activation Cross Sections $\sigma_{ACT}/F\sigma^{o}$ (b)	$\overline{P}\sigma_{ACT}/\sigma^{o}$ (c)
1	0.00025	10.0000	5.2440	2.9268
2	0.00101	5.0000	3.5125	2.2953
3	0.00228	3.3333	2.5777	1.8556
4	0.00405	2.5000	2.0287	1.5530
5	0.00632	2.0000	1.6717	1.3348
6	0.00911	1.6667	1.4219	1.1706
7	0.01240	1.4286	1.2374	1.0426
8	0.01619	1.2500	1.0956	0.9401
9	0.02049	1.1111	0.9832	0.8562
10	0.02530	1.0000	0.8920	0.7861
11	0.03061	0.9091	0.8164	0.7268
12	0.03643	0.8333	0.7527	0.6759
13	0.04276	0.7692	0.6983	0.6317
14	0.04959	0.7143	0.6514	0.5930
15	0.05692	0.6667	0.6104	0.5589
16	0.06517	0.6231	0.5726	0.5270
17	0.07485	0.5814	0.5363	0.4961
18	0.08612	0.5420	0.5017	0.4664
19	0.09919	0.5051	0.4691	0.4381
20	0.11398	0.4711	0.4391	0.4118
21	0.13123	0.4391	0.4105	0.3865
22	0.15248	0.4073	0.3820	0.3612
23	0.17901	0.3759	0.3538	0.3358
24	0.21241	0.3451	0.3259	0.3106
25	0.25464	0.3152	0.2986	0.2857
26	0.30816	0.2865	0.2724	0.2616
27	0.37598	0.2594	0.2474	0.2385
28	0.46183	0.2341	0.2239	0.2166
29	0.57023	0.2106	0.2022	0.1962
30	0.70666	0.1892	0.1821	0.1773

(a) σ^{o} is the activation cross section at 2200 m/sec.

(b) F is the disadvantage factor for an incident, isotropic flux.

(c) $\overline{P}$ is the escape probability from a flat, isotropic source of neutrons in the foil.

TABLE C.9

Effective Activation Cross Sections for 12.4 mil Thick Gold Foils

Group	Energy (ev)	Activation Cross Section σ_{ACT}/σ^{o} (a)	Effective Activation Cross Sections $\sigma_{ACT}/F\sigma^{o}$ (b)	$\overline{P}\sigma_{ACT}/\sigma^{o}$ (c)
1	0.00025	10.0000	4.6306	2.4990
2	0.00101	5.0000	3.2941	2.0501
3	0.00228	3.3333	2.4714	1.6983
4	0.00405	2.5000	1.9650	1.4428
5	0.00632	2.0000	1.6286	1.2528
6	0.00911	1.6667	1.3903	1.1068
7	0.01240	1.4286	1.2130	0.9914
8	0.01619	1.2500	1.0760	0.8980
9	0.02049	1.1111	0.9670	0.8208
10	0.02530	1.0000	0.8783	0.7560
11	0.03061	0.9091	0.8046	0.7007
12	0.03643	0.8333	0.7424	0.6531
13	0.04276	0.7692	0.6893	0.6116
14	0.04959	0.7143	0.6433	0.5751
15	0.05692	0.6667	0.6031	0.5428
16	0.06517	0.6231	0.5660	0.5126
17	0.07485	0.5814	0.5304	0.4832
18	0.08612	0.5420	0.4965	0.4549
19	0.09919	0.5051	0.4644	0.4278
20	0.11398	0.4711	0.4348	0.4026
21	0.13123	0.4391	0.4067	0.3783
22	0.15248	0.4073	0.3787	0.3540
23	0.17901	0.3759	0.3508	0.3295
24	0.21241	0.3451	0.3232	0.3051
25	0.25464	0.3152	0.2963	0.2810
26	0.30816	0.2865	0.2704	0.2576
27	0.37598	0.2594	0.2457	0.2351
28	0.46183	0.2341	0.2225	0.2137
29	0.57023	0.2106	0.2009	0.1938
30	0.70666	0.1892	0.1811	0.1753

(a) σ^{o} is the activation cross section at 2200 m/sec.

(b) F is the disadvantage factor for an incident, isotropic flux.

(c) $\overline{P}$ is the escape probability from a flat, isotropic source of neutrons in the foil.

TABLE C.10

Effective Activation Cross Sections for 20.6 mil Thick Gold Foils

Group	Energy (ev)	Activation Cross Section σ_{ACT}/σ^{o} (a)	Effective Activation Cross Sections $\sigma_{ACT}/F\sigma^{o}$ (b)	$\overline{P}\sigma_{ACT}/\sigma^{o}$ (c)
1	0.00025	10.0000	3.1165	1.5981
2	0.00101	5.0000	2.6075	1.4527
3	0.00228	3.3333	2.1163	1.2863
4	0.00405	2.5000	1.7513	1.1417
5	0.00632	2.0000	1.4852	1.0223
6	0.00911	1.6667	1.2865	0.9241
7	0.01240	1.4286	1.1336	0.8425
8	0.01619	1.2500	1.0129	0.7739
9	0.02049	1.1111	0.9153	0.7156
10	0.02530	1.0000	0.8349	0.6655
11	0.03061	0.9091	0.7675	0.6220
12	0.03643	0.8333	0.7102	0.5838
13	0.04276	0.7692	0.6610	0.5501
14	0.04959	0.7143	0.6181	0.5201
15	0.05692	0.6667	0.5806	0.4933
16	0.06517	0.6231	0.5458	0.4679
17	0.07485	0.5814	0.5122	0.4431
18	0.08612	0.5420	0.4802	0.4189
19	0.09919	0.5051	0.4498	0.3956
20	0.11398	0.4711	0.4218	0.3737
21	0.13123	0.4391	0.3950	0.3525
22	0.15248	0.4073	0.3682	0.3311
23	0.17901	0.3759	0.3416	0.3094
24	0.21241	0.3451	0.3152	0.2875
25	0.25464	0.3152	0.2893	0.2659
26	0.30816	0.2865	0.2644	0.2446
27	0.37598	0.2594	0.2405	0.2241
28	0.46183	0.2341	0.2181	0.2045
29	0.57023	0.2106	0.1972	0.1860
30	0.70666	0.1892	0.1779	0.1688

(a) σ^{o} is the activation cross section at 2200 m/sec.

(b) F is the disadvantage factor for an incident, isotropic flux.

(c) $\overline{P}$ is the escape probability from a flat, isotropic source of neutrons in the foil.

Input Instructions for QUICK

Card Type	Format	List
1	(12A6)	72 characters to be used for the problem identification.
2	(I5)	IX; the number of velocity groups; if IX is zero, the problem terminates; a maximum of 30 groups is permitted.
3	(7E10.5)	V(I), I=1, IX; the velocity mesh.
4	(7E10.5)	DV(I), I=1, IX; the velocity intervals.
5	(3I5)	NACT; if NACT=0, the activation cross section varies as 1/v. NABS; if NABS=0, the absorption cross section varies as 1/v. NSCAT; if NSCAT=0, the scattering cross section is constant.
6	(7E10.5)	If NACT was zero, a single number, the cross section at v_o; if not, the activation cross section, 7 per card until IX is reached.
7	(7E10.5)	If NABS=0, a single number, the absorption cross section at v_o; if not, the absorption cross sections, 7 per card, until IX is reached.
8	(7E10.5)	If NSCAT=0, a single number, the scattering cross section; if not, the scattering cross section at each velocity point, 7 per card, until IX is reached.
9	(I5,E10.5)	NTIMES; the number of different thickness to be calculated. DENSY; the density of the material.
10	(7E10.5)	TH(I), I=1, NTIMES; the thickness to be calculated; a maximum of 10 is permitted.

GO TO CARD TYPE 1. TWO BLANK CARDS WILL TERMINATE THE RUN.

MAIN PROGRAM QUICK

QUICK CALLS DPRESS OR CYLDIP

```
*     LIST 8
*     LABEL
CQUICK   PROGRAM CALCULATES SELF-SHIELDING FACTORS
      DIMENSION SIGACT(30),SIGA(30),SIGS(30),TH(10),F0(30,10),F1(30,10),
     1HOL(30),XSECA(30,10),XSECB(30,10),DV(30),PHI(30)
      DIMENSION V(30)
 10   FORMAT(14I5)
 12   FORMAT(12A6)
 16   FORMAT(1H1,12X,12A6)
 18   FORMAT(1H0,12X,52HINVERSE DISADVANTAGE FACTORS FOR ISOTROPIC INCID
     1ENCE  )
 19   FORMAT(1H0,12X,50HSELF-SHIELDING FACTORS BASED ON ESCAPE PROBABILI
     1TY  )
 20   FORMAT(7E10.5)
 25   FORMAT(1H0,12X,5HGROUP,2X,6HENERGY,10(4H TH=F6.4))
 33   FORMAT(I5,E10.5)
 40   FORMAT(12X,I4,2X,F8.5,10F10.5)
 60   FORMAT(18HP0 CASE THICKNESS=F6.4,5X,7HGROUPS=I3)
 70   FORMAT(7F10.4)
 80   FORMAT(18HEP CASE THICKNESS=F6.4,5X,7HGROUPS=I3)
 90   FORMAT(1H ,12X,12HGROUP ENERGY,10X,5H XSEC,12X,3HDP0,11X,4HPBAR)
 91   FORMAT(1H0,12X,10HTHICKNESS=F8.5)
 92   FORMAT(1H0,50X,23HEFFECTIVE CROSS SECTION)
 95   FORMAT(12X,I4,F9.5,3F15.4)
 1    CONTINUE
      READ 12,(HOL(I),I=1,12)
      READ 10,IX
      IF(IX)199,199,69
 69   CONTINUE
      READ 20,(V(I),I=1,IX)
      READ 20,(DV(I),I=1,IX)
      ASUM=0.0
      DO 510 I=1,IX
      B=V(I)*V(I)
      PHI(I)=B*EXPF(-B)
      PHI(I)=PHI(I)*V(I)*DV(I)
 510  ASUM=ASUM + PHI(I)
      READ 10,NACT,NABS,NSCAT
C     NACT=0,XSEC IS 1/V
C     NABS=0,XSEC IS 1/V
C     NSCAT=0,SXSEC IS CONSTANT
      IF(NACT)100,102,100
 100  READ 20,(SIGACT(I),I=1,IX)
      GO TO 106
 102  READ 20,A
      DO 104 I=1,IX
 104  SIGACT(I)=A/V(I)
 106  CONTINUE
      PQ=0.0
      DO 520 I=1,IX
 520  PQ=PQ+PHI(I)*SIGACT(I)
      PQ=PQ/ASUM
      IF(NABS)108,110,108
 108  READ 20,(SIGA(I),I=1,IX)
      GO TO 114
 110  READ 20,B
      DO 112 I=1,IX
 112  SIGA(I)=B/V(I)
 114  CONTINUE
      IF(NSCAT)116,118,116
 116  READ 20,(SIGS(I),I=1,IX)
      GO TO 122
 118  READ 20,C
      DO 120 I=1,IX
 120  SIGS(I)=C
 122  CONTINUE
      READ 33,NTIMES,DENSY
      READ 20,(TH(I),I=1,NTIMES)
      DO 1000 J=1,NTIMES
      DO 900 I=1,IX
      XA=SIGA(I)*TH(J)*DENSY
      XS=SIGS(I)*TH(J)*DENSY
      CALL DIP(XA,XS,FDP0,PBAR)
      F0(I,J)=FDP0
      F1(I,J)=PBAR
 900  CONTINUE
 1000 CONTINUE
      PRINT 16,(HOL(I),I=1,12)
      PRINT 18
      PRINT 25,(TH(I),I=1,NTIMES)
      DO 130 I=1,IX
      B=V(I)*V(I)*0.0253
 130  PRINT 40,I,B,(F0(I,J),J=1,NTIMES)
      PRINT 16,(HOL(I),I=1,12)
      PRINT 19
      PRINT 25,(TH(I),I=1,NTIMES)
      DO 140 I=1,IX
      B=V(I)*V(I)*0.0253
 140  PRINT 40,I,B,(F1(I,J),J=1,NTIMES)
      DO 300 J=1,NTIMES
      DO 300 I=1,IX
      XSECA(I,J)=SIGACT(I)*F0(I,J)
 300  XSECB(I,J)=SIGACT(I)*F1(I,J)
      PUNCH12,(HOL(I),I=1,12)
      DO 310 J=1,NTIMES
      PUNCH 60,TH(J),IX
 310  PUNCH 70,(XSECA(I,J),I=1,IX)
      DO 320 J=1,NTIMES
      PUNCH 80,TH(J),IX
      PUNCH 70,(XSECB(I,J),I=1,IX)
 320  CONTINUE
      DO 330 J=1,NTIMES
      PRINT 16,(HOL(I),I=1,12)
      PRINT 91,TH(J)
      PRINT 92
      PRINT 90
      BSUM=0.0
      CSUM=0.0
      DO 319 I=1,IX
      BSUM=BSUM+PHI(I)*XSECA(I,J)
      CSUM=CSUM+PHI(I)*XSECB(I,J)
      B=V(I)*V(I)*0.0253
 319  PRINT 95,I,B,SIGACT(I)  ,XSECA(I,J),XSECB(I,J)
      BSUM=BSUM/ASUM
      CSUM=CSUM/ASUM
      PRINT 98,PQ,BSUM,CSUM
 98   FORMAT(/12X,13HMAX. AVER =  ,3F15.4)
      AX=BSUM/PQ
      BX=CSUM/PQ
      PRINT 99,AX,BX
 99   FORMAT(/12X,21HFLUX DPRESS FACTOR = ,7X,2F15.4)
 330  CONTINUE
      GO TO 1
 199  CONTINUE
      CALL EXIT
      END
```

SUBROUTINE CYLDIP

```
*     LIST8
*     LABEL
CCYLDIP
      SUBROUTINE DIP(XA,XS,FISO,FP1)
      DIMENSION  C(4,16)
      IF (N) 20,10,20
 10   N=1
      C(1,1)=-1.9239
      C(1,2)=4.1524
      C(1,3)=-.75139
      C(1,4)=-1.5
      C(1,5)=2.0198
      C(1,6)=-2.0469
      C(1,7)=.0087506
      C(1,8)=.018832
      C(1,9)=1.1056
      C(1,10)=-1.9788
      C(1,11)=.95011
      C(1,12)=-.082311
      C(1,13)=2.6419
      C(1,14)=-7.7384
      C(1,15)=6.3019
      C(1,16)=-1.1875
      C(4,1)=.64427
      C(4,2)=-5.4605
      C(4,3)=15.119
      C(4,4)=-13.063
      C(4,5)=-20.54
      C(4,6)=211.4
      C(4,7)=-602.67
      C(4,8)=521.33
      C(4,9)=23.771
      C(4,10)=-195.49
      C(4,11)=528.16
      C(4,12)=-450.34
      C(4,13)=-5.5277
      C(4,14)=44.63
      C(4,15)=-122.24
      C(4,16)=105.97
      C(2,1)=.11009
      C(2,2)=-1.69
      C(2,3)=4.1539
      C(2,4)=-2.6879
      C(2,5)=2.0945
      C(2,6)=-4.4897
      C(2,7)=8.7384
      C(2,8)=-8.3451
      C(2,9)=1.165
      C(2,10)=3.8918
      C(2,11)=-21.129
      C(2,12)=20.942
      C(2,13)=1.2353
      C(2,14)=-8.0142
      C(2,15)=18.164
      C(2,16)=-14.435
      C(3,1)=-.14535
      C(3,2)=.41075
      C(3,3)=-.32558
      C(3,4)=.058606
      C(3,5)=1.3831
      C(3,6)=.25993
      C(3,7)=-2.8592
      C(3,8)=1.2193
      C(3,9)=1.2044
      C(3,10)=-1.0316
      C(3,11)=-1.4214
      C(3,12)=1.2406
      C(3,13)=-.056999
      C(3,14)=-.39361
      C(3,15)=.70542
      C(3,16)=-.24843
 20   X=XA+XS
      IF(X)21,21,22
 21   FP1=1.0
      GO TO 200
 22   CONTINUE
      SR=XS/X
      IF (X-.1) 30,30,40
 30   TEMP=1.-1.3333333*X+0.5*X*X*(LOGF(2./X)+.672784)
      P0=2.*X*TEMP
      P1=1.-TEMP
      GO TO 60
 40   IF (X-5.) 70,70,50
 50   P0=1.-.1875/(X*X)
      P1=1.-.437*X**(-.408)
 60   BETA=(1.-SR)*P0/(1.-SR*P1)
      GO TO 130
 70   IF (X-2.) 90,90,80
 80   IF (SR-0.6) 85,85,50
 85   M=4
      GO TO 120
 90   IF (X-.5) 110,110,100
 100  IF (SR-0.6) 105,105,107
 105  M=2
      GO TO 120
 107  M=3
      GO TO 120
 110  M=1
 120  X2=X*X
      X3=X2*X
      X4=X3*X
      SR2=SR*SR
      SR3=SR2*SR
      BETA=(C(M,1)+C(M,2)*SR+C(M,3)*SR2+C(M,4)*SR3)*X4+
     1(C(M,5)+C(M,6)*SR+C(M,7)*SR2+C(M,8)*SR3)*X+
     2(C(M,9)+C(M,10)*SR+C(M,11)*SR2+C(M,12)*SR3)*X2+
     3(C(M,13)+C(M,14)*SR+C(M,15)*SR2+C(M,16)*SR3)*X3
      BETA=1.-1./(1.+BETA)
 130  IF (BETA) 140,140,150
 140  BETA=1.E-10
 150  FP1=XA*(2.-BETA)/BETA
      FP1=1.0/FP1
 200  CONTINUE
      FISO=1.0
      RETURN
      END
```

SUBROUTINE DPRESS

DPRESS CALLS EI

```
*     LIST8
*     LABEL
CDPRESS         OCTOBER 24,1962
      SUBROUTINE DIP(XA,XS,FDP0,FP1)
      DIMENSION ENX(10)
      NX=4
      XT=XA+XS
      IF(XT)10,10,20
  10  FDP0=1.0
      FP1=1.0
      GO TO 1000
  20  CONTINUE
      CALL EI(XT,NX,ENX)
      PE=(1.0-2.0*ENX(3))/(2.0*XT)
      PC=1.0-PE
      G=1.0+(XA/XT)*(PC/(1.0-PC)-XT)
      FDP0=1.0/G
      PBAR=PE/(1.0-(XS/XT)*(1.0-PE))
C     PBAR=PROB. THAT A NEUTRON WILL ESCAPE FOR A FLAT - ISOTROPIC BIRTH
      FP1=PBAR
 1000 CONTINUE
      RETURN
      END
```

SUBROUTINE EI

```
*     LIST8
*     LABEL
CEI
C     SUBROUTINE  -EI-
 1    SUBROUTINE EI(X,NX,ENX)
      DIMENSIONENX(10)
 5    IF(NX)6,6,10
 6    NX=1
 10   IF(X)30,30,50
 30   ENX(1)=1.0E+30
      IF(NX-1)150,150,35
 35   DO40I=2,NX
      A=FLOATF(I)
 40   ENX(I)=1./(A-1.)
      GOTO150
 50   IF(X-75.)80,60,60
 60   DO70I=1,10
 70   ENX(I)=0.
      GOTO150
 80   A=EXPF(-X)
      IF(X-1.0)90,120,120
 90   B=LOGF(X)
      IF(X-0.001)100,100,110
 100  ENX(1)=X-B-0.577215665
      GOTO130
 110  ENX(1)=-.577215665-B+X*(1.+X*(-.25+X*(.055555555+X*(-.010416666+X*
     1(.16666666E-2+X*(-.23148147E-3+X*(.28344669E-4+X*(-.31001981E-5+X*
     2.30619240E-6)))))))
      GOTO130
 120  B=.2372905+X*(4.53079235+X*(5.1266902+X))
      C=2.4766331+X*(8.6660126+X*(6.1265272+X))
      ENX(1)=((A/X)*B)/C
 130  IF(NX-1)150,150,135
 135  DO140I=2,NX
      B=FLOATF(I)-1.
 140  ENX(I)=(A-X*ENX(I-1))/B
 150  CONTINUE
      RETURN
      END
```

TEST RUN FOR QUICK

```
*     DATA
          SELF-SHIELDING FOR METALLIC GOLD SLABS   PBAR CASE
   30
.10000E+00.20000E+00.30000E+00.40000E+00.50000E+00.60000E+00.70000E+00
.80000E+00.90000E+00.1000E+001.1000E+001.2000E+001.3000E+001.4000E+00
1.5000E+001.6050E+001.7200E+001.8450E+001.9800E+002.1225E+002.2775E+00
2.4550E+002.6600E+002.8975E+003.1725E+003.4900E+003.8550E+004.2725E+00
4.7475E+005.2850E+00
.10000E+00.10000E+00.10000E+00.10000E+00.10000E+00.10000E+00.10000E+00
.10000E+00.10000E+00.10000E+00.10000E+00.10000E+00.10000E+00.10000E+00
.10000E+00.11000E+00.12000E+00.13000E+00.14000E+00.14500E+00.16500E+00
.19000E+00.22000E+00.25500E+00.29500E+00.34000E+00.39000E+00.44500E+00
.50500E+00.57000E+00
    0    0    0
1.0
98.8
9.3
    2 0.059
0.0194    0.0259
          END DATA FOR GOLD CASE
    0
```

APPENDIX D
THE ACTIVE CODE

The ACTIVE code was designed to process the automatic counter data for activity decaying with a single half-life. The code consists of three subroutines so designed that the code can handle constant of time counting or constant total number of counts by the interchange of one subroutine. At present, only the latter has been coded.

Since the measurements allow the repeated use of foils, the program was designed to read in the entire foil "library" and select the weights (or calibrations) of the foils used in the experiment, eliminating the need for punching the weight information more than once. The code punches the library at the end of each run for future use.

The running deck consists of four subprograms, ACTIVE, PRNTO, CALC and MICRO. ACTIVE is the main program, performing the handling of the foil weight library. PRNTO prints out the foil weight library, when desired. Subroutine CALC applies the counting corrections to the data from the automatic sample changer; it also normalizes the data by dividing the count rate by the foil weight or calibration. MICRO, if desired, will apply an over-all time correction to all the foils, and a J_o and axial correction to individual foils. The output of MICRO has been found particularly useful for the data reduction for the intracellular flux traverses.

The output activities from CALC are corrected for decay from time zero, decay during counting, background, deadtime and foil weight. When several passes through the automatic sample changer are made, the average count rate is used. The average is calculated by weighting the individual results with the number of preset counts for the pass. An estimate of the standard deviation, σ, of this average is made by taking the square root of the sums of the squares of the deviations of each pass from the average weighted by the number of counts in the pass and divided by the number of passes:

$$\text{Average CR} = \sum_i c_i CR_i , \tag{D.1}$$

and

$$\sigma^2 = \sum_i \frac{c_i}{N} (CR_i - \text{Average CR})^2 , \tag{D.2}$$

where

$$c_i = \frac{\text{counts in the } i^{th} \text{ pass}}{\text{total counts}} . \tag{D.3}$$

The average σ/CR for all foils should be approximately equal to the reciprocal of the square root of the total preset counts. This was found to be the case in nearly all the runs in which the foil activities were at least ten times the background rate. Table D.1 gives a comparison between the average deviation calculated from the deviations of individual passes from the $\sqrt{1/C_{TOTAL}}$.

TABLE D.1

Deviations for the Counting of Gold Foils

Run No.	Technique[a]	Type[b]	No. of Foils	No. of Passes	Uncertainty[c] σ (%)	$\frac{1}{\sqrt{C_{TOTAL}}}$ (%)
A4	I	B	37	6	0.24	0.28
A4	I	C	29	2	1.5	1.0
A5	D	C	29	3	0.58	0.40
A5	D	B	37	4	0.42	0.17
A5	I	B	37	3	0.17	0.20
A5	I	C	29	3	0.29	0.40
A6	D	C	29	5	0.54	0.44
A6	D	B	37	5	0.34	0.22
A6	I	B	37	3	0.35	0.40
A6	I	C	29	6	0.54	0.57
A7	D	C	29	5	0.31	0.31
A7	D	B	37	6	0.21	0.20
A7	I	B	37	4	0.15	0.17
A7	I	C	29	3	0.34	0.40
A8	D	C	29	4	1.48	1.58
A8	D	B	37	3	1.01	1.29
A9	D	C	29	6	0.35	0.40
A9	D	B	37	6	0.17	0.14
A9	I	B	37	6	0.15	0.14
A9	I	C	29	6	0.48	0.40
A10	D	B	29	4	0.66	0.50
A10	D	B	37	5	0.34	0.15
A11	D	C	24	6	0.37	0.40
A11	D	B	35	4	0.38	0.25
A12	D	C	23	5	0.36	0.44
A12	D	B	35	5	0.64	0.31
A13	D	C	26	5	0.43	0.44
A13	D	B	35	4	0.21	0.25
A14	D	C	26	4	0.41	0.50
A14	D	B	35	4	0.56	0.50
A15	D	C	26	5	0.43	0.44
A15	D	B	35	3	0.27	0.40

(a) "I" indicates the integral counting method; "D" indicates the differential method.
(b) "B" indicates bare foils; "C" indicates cadmium-covered foils.
(c) σ is based on Eq. (D.2).

Input Instructions for ACTIVE

Card Type	Format	List
1	(2I5)	NORUNS; number of runs with this nuclide. If NORUNS is equal to zero, the program calls EXIT. Repeat card Types 4 to 11, NORUNS times. NOHITS; if NOHITS is equal to zero, MICRO will not be called.
2	(I5,E12.5,55H)	LMAX; total number of foils in the foil weight library, if any. DKAY; decay constant for this nuclide.
3	(6E12.5)	Skip this card if LMAX was equal to zero. WT(L), L=1, LMAX; the weight of the L^{th} foil (use three decimal places maximum for printout purposes).
4	(72H___)	A zero in column one for printer control and any legal characters up to column 72. Columns 2-72 will be recorded with the output.
5	(2I5)	LNEW; total number of new foils added to library or replaced in the foil library. The maximum number of foils may not exceed 1000 without changing the program. NPRIN; if zero PRNTO will not be called. If LNEW=0, skip to card Type 7.
6	(4(I5,E10.5))	L,WT(L); L is the number of the foil added or replaced and WT(L) is its weight. L may exceed LMAX, but must be less than 1000 and greater than zero. Repeat LNEW times. Skip this card if LNEW=0.
7	(2I5,6E10.5)	NMAX; number of foils per pass (≤ 1000). NPASS; total number of passes (≤ 6).

Card Type	Format	List
		ROT; rotation time of the sample changer; that is, the time interval between the time the counter stops counting and time it begins with the next foil. BG, BG1; the background is allowed to vary linearly. The rate is BG + BG1 * TIME. SEPT, SLOPE; the deadtime, τ, is assumed to vary linearly with the count rate: τ = SEPT + SLOPE * CTRATE.
8	(6E10.5)	COUNTS(J), J=1, NPASS; total number of counts for the J^{th} pass.
9	(6E10.5)	DELAY(J), J=1, NPASS–1; time delay between the last foil and the recycled first foil. If DELAY(J) is zero, then it is assumed to be equal to ROT * (NMAX + 1).
10	(14I5)	ND(I), I=1, NMAX; the number corresponding to the I^{th} foil in the pass. If the 12^{th} foil in the foil library is counted in the 30^{th} position, ND(30) would be 12.
11	(7E10.5)	CT(I,J), I=1, NMAX; counting time for the I^{th} foil of the J^{th} pass. The first foil, I=1, must start a new card for each pass. Repeat J times.
IF NOHITS (CARD TYPE 1) WAS ZERO, SKIP CARDS 12 AND 13.		
12	(I5,E10.5)	NCARDS; number of cards to be read by micro after this one. TMCFR; time correction factor.
13	(2E10.5,10I5)	HTFR; height correction. JOCFR; J_o-correction. NW; number of foils to which HTFR, JOCFR and TMCFR are to be applied. WD(I), I=1, NW; counting position of the foils to which corrections are to be applied. A

zero skips a line in the output.

GO TO CARD TYPE 4 NORUNS times.

GO TO CARD TYPE 1 for different foil library.

MAIN PROGRAM ACTIVE

```
*      LIST8
*      LABEL
CACTIVE    PROGRAM  BY RICHARD SIMMS       MAY 15,1963
       DIMENSION WT(1000),ND(100),CT(100,6),SATCT(100,6),RELTM(100,6)
       DIMENSION DELAY(6),COUNTS(6),DIF(6),AVCT(100),MD(20)
       DIMENSION HOLR(11),ADENT(12)
       COMMON WT,ND,CT,SATCT,RELTM,DELAY,COUNTS,DIF,AVCT,MD,HOLR,ADENT
       COMMON DKAY,LMAX,NMAX,NPASS
 1     READ 10,NORUNS,NOHITS
C      NORUNS=NO. OF RUNS OF A SINGLE ISOTOPE
C      A BLANK CARD TERMINATES RUN
       IF(NORUNS)100,100,102
 100   CALL EXIT
 102   CONTINUE
       DO2J=1,1000
   2   WT(J)=0.0
C      PROGRAM NOW READS IN FOIL LIBRARY
       READ 12,LMAX,DKAY,(HOLR(I),I=1,11)
C      DKAY=DECAY CONSTANT, LMAX=NUMBER OF FOILS IN THE FOIL LIBRARY
       IF(LMAX)110,110,104
 104   IF(LMAX-1000)108,108,106
 106   PRINT 14
       CALL EXIT
 108   CONTINUE
       READ 16,(WT(L),L=1,LMAX)
 110   CONTINUE
       MAX=LMAX
 201   READ 18,(ADENT(I),I=1,12)
       PRINT 20,(ADENT(I),I=1,12)
C      NEW FOILS ADDED OR REPLACED
       READ 10,LNEW,NPRIN
C      IF NPRIN IS ZERO, THE PRINT OUT OF THE LIBRARY WILL BE OMITTED
       NAM=LNEW
       IF(LMAX+LNEW)120,120,121
 120   PRINT 22
       CALL EXIT
 121   IF(LNEW)150,150,122
 122   IF(LNEW-1000)124,124,123
 123   PRINT 24
       CALL EXIT
 124   CONTINUE
       PRINT 26
 140   READ 28,MA,A,MB,B,MC,C,MD,D
       PRINT 30,MA,A,MB,B,MC,C,MD,D
       IF(MD)125,125,130
 125   IF(MC)126,126,132
 126   IF(MB)136,136,134
 130   WT(MD)=D
       IF(MD-MAX)132,132,131
 131   MAX=MD
 132   WT(MC)=C
       IF(MC-MAX)134,134,133
 133   MAX=MC
 134   WT(MB)=B
       IF(MB-MAX)136,136,135
 135   MAX=MB
 136   WT(MA)=A
       IF(MA-MAX)138,138,137
 137   MAX=MA
 138   CONTINUE
       NAM=NAM-4
       IF(NAM)142,142,140
 142   CONTINUE
C      MAX=MAX NO. OF FOILS TO DATE
 150   CONTINUE
       IF(MAX-1000)4,4,3
   3   PRINT 32
       CALL EXIT
   4   CONTINUE
       LMAX=MAX
       IF(NPRIN)210,210,206
 206   CALL PRNTO(WT,MAX)
C      PRNTO PRINTS OUT LIBRARY
 210   CONTINUE
       CALL CALC
       IF(NOHITS)220,220,215
 215   CALL MICRO
 220   CONTINUE
       NORUNS=NORUNS-1
       IF(NORUNS)200,200,201
 200   PUNCH 12,MAX,DKAY,(HOLR(I),I=1,11)
       PUNCH 16,(WT(I),I=1,MAX)
       GO TO 1
  10   FORMAT(6I5)
  12   FORMAT(I5,E12.5,11A5)
  14   FORMAT(27H1LIBRARY EXCEEDS 1000 FOILS)
  16   FORMAT(6E12.5)
  18   FORMAT(1X,11A6,1A5)
  20   FORMAT(1H1,10X,21HANALYSIS OF FOIL DATA,10X,11A6,1A5)
  22   FORMAT(15HONO FOILS GIVEN)
  24   FORMAT(24HOFOILS ADDED EXCEED 1000)
  26   FORMAT(11X,20HFOIL WEIGHTS CHANGED/11X,4(4X,1HI,12X,2HWT))
  28   FORMAT(4(I5,1PE14.5))
  30   FORMAT(11X,4(I5,1PE14.5))
  32   FORMAT(24HOTOTAL FOILS EXCEED 1000)
       END
```

SUBROUTINE CALC

```
*     LIST8
*     LABEL
CCALC     PROGRAM BY RICHARD SIMMS  MAY 18,1963   FOR PRESET COUNTS
      SUBROUTINE CALC
      DIMENSION WT(1000),ND(100),CT(100,6),SATCT(100,6),RELTM(100,6)
      DIMENSION DELAY(6),COUNTS(6),DIF(6),AVCT(100),MD(20)
      DIMENSION HOLR(11),ADENT(12)
      COMMON WT,ND,CT,SATCT,RELTM,DELAY,COUNTS,DIF,AVCT,MD,HOLR,ADENT
      COMMON DKAY,LMAX,NMAX,NPASS
      READ 10, NMAX,NPASS,ROT,BG,BG1,SEPT,SLOPE
      READ 62,(COUNTS(I),I=1,NPASS)
      READ 62,(DELAY(I),I=1,NPASS)
      READ 12,(ND(I),I=1,NMAX)
      DO 100 J=1,NPASS
  100 READ 14,(CT(I,J),I=1,NMAX)
C     ND IS THE NUMBER OF THE FOIL COUNTED IN THE I-TH POSITION
C     WT= FOIL WEIGHT
C     CT=COUNTING TIME
C     ROT = ROTATION TIME OF AUTOMATIC SAMPLE CHANGER
C     RELTM=RELATIVE TIME
C     SATCT = COUNTS PER UNIT TIME PER UNIT WEIGHT AT TIME ZERO
C     BACKGROUND=BG+BG1*TIME    CPM
C     DEADTIME= SEPT+SLOPE*COUNTRATE
C     DELAY= DELAY TIME BETWEEN CYCLES
C     COUNTS= TOTAL NUMBER OF COUNTS FOR THE J-TH PASS
      PRINT 20,(ADENT(I),I=1,12)
      PRINT 19,(J,J=1,6)
      DO 21 I=1,NMAX
   21 PRINT 17,I,ND(I),(CT(I,J),J=1,NPASS)
      RS=0.0
      J=1
 1000 DO 110 I=1,NMAX
     `RELTM(I,J)=RS
      A=COUNTS(J)/CT(I,J)
      DTIME=SEPT+SLOPE*A
      BGR=BG+BG1*RELTM(I,J)
      REALK=COUNTS(J)/(1.0-DTIME*A)-BGR*CT(I,J)
      IF(DKAY)502,501,502
  501 A=1.0
      B=CT(I,J)
      CA=1.0
      GO TO 503
  502 CONTINUE
      A=EXPF(DKAY*RELTM(I,J))
      B=1.0-EXPF(-DKAY*CT(I,J))
      CA=DKAY
  503 CONTINUE
      M=ND(I)
      SATCT(I,J)=  CA*REALK*A/(B*WT(M))
  110 RS=RELTM(I,J)+CT(I,J)+ROT
      IF(J-NPASS)112,114,114
  112 RS=RS+FLOATF(NMAX)*ROT
      IF(DELAY(J))204,204,200
  200 CONTINUE
      RS=RELTM(NMAX,J)+CT(NMAX,J)+DELAY(J)
  204 CONTINUE
      J=J+1
      GO TO 1000
  114 CONTINUE
      IF(NPASS-3)300,300,301
  300 M=NPASS
      GOTO302
   301 M=3
   302 CONTINUE
      PRINT 20,(ADENT(I),I=1,12)
      PRINT 60,BG,BG1,SEPT,SLOPE,DKAY
      PRINT 402,(COUNTS(J),J=1,M)
      PRINT 40
      DO 120 I=1,NMAX
      L=ND(I)
  120 PRINT42,I,ND(I),WT(L),(RELTM(I,J),SATCT(I,J),J=1,M)
      IF(NPASS-3)306,306,304
  304 CONTINUE
      PRINT 20,(ADENT(I),I=1,12)
      PRINT 60,BG,BG1,SEPT,SLOPE,DKAY
      PRINT 402,(COUNTS(J),J=4,NPASS)
      PRINT 40
      DO 122 I=1,NMAX
      L=ND(I)
  122 PRINT42,I,ND(I),WT(L),(RELTM(I,J),SATCT(I,J),J=4,NPASS)
  306 CONTINUE
      DEVE=0.0
      B=0.0
      DO 307 J=1,NPASS
      B=B+COUNTS(J)
  307 CONTINUE
      PRINT 20,(ADENT(I),I=1,12)
      PRINT 80,(J,J=1,6)
      DO92I=1,NMAX
      A=0.0
      DO90J=1,NPASS
   90 A=A+SATCT(I,J)*COUNTS(J)
      A=A/B
      AVCT(I)=A
      DO 91 J=1,NPASS
   91 DIF(J)=SATCT(I,J)/A-1.0
      SUMSQ=0.0
      DO 411 K=1,NPASS
  411 SUMSQ=SUMSQ+DIF(K)*DIF(K)*COUNTS(K)
      SUMSQ=SUMSQ/(B*FLOATF(NPASS))
      SUMSQ=SQRTF(SUMSQ)
      DEVE=DEVE+SUMSQ
   92 PRINT 81,I,ND(I),A,SUMSQ,(DIF(J),J=1,NPASS)
      DEVE=100.0*DEVE/FLOATF(NMAX)
      PTDEV=100.0/SQRTF(B)
      PRINT 85,DEVE,PTDEV
   10 FORMAT(2I5,6E10.5)
   12 FORMAT(14I5)
   14 FORMAT(7E10.5)
   17 FORMAT(2I5,6F14.3)
   19 FORMAT(10H0  I ND(I),6(7X,5HCT(I,I1,1H)))
   20 FORMAT(1H1,10X,21HANALYSIS OF FOIL DATA,10X,11A6,1A5)
   40 FORMAT(5H0   I,5H    L,9X,5HWT(L),3(10X,4HTIME,8X,6HCTRATE))
   42 FORMAT(2I5,0PF14.5,3(0PF14.2,1PE14.5))
   60 FORMAT(18H0BACKGROUND RATE = 1PE12.5,3H + 1PE12.5, 5H*TIME/
     111H DEAD TIME=1PE12.5,3H + 1PE12.5,7H*CTRATE/
     217H DECAY CONSTANT = 1PE12.5)
   62 FORMAT(7E10.5)
   80 FORMAT(10X,10H    I  NO.,7X,14HAVERAGE CTRATE,5X,9HSUMSQ**.5,5X,6(
     13X,4HDIF(I2,1H)))
   81 FORMAT(10X,2I5,5X,1PE14.5,7X,0PF9.5,5X,0P6F10.5)
  402 FORMAT(24X,3(5X,9HCOUNTS = 1PE14.5))
   85 FORMAT(1H0,26X,38HTHE GRAND AVERAGE OF THE DEVIATIONS IS F9.5,
     19H PERCENT./27X,46HTHE INVERSE OF THE SQRT OF THE TOTAL COUNTS IS
     2F9.5,9H PERCENT.)
      RETURN
      END
```

SUBROUTINE PRNTO

```
*     LIST8
*     LABEL
CPRNTO
C    PROGRAM PRINTS OUT AN ARRAY
      SUBROUTINE PRNTO(FW,NMAX)
      DIMENSIONFW(1000),WORD(4),IWD(4)
      J=1
  200 IF(NMAX-J*200)204,204,202
  202 J=J+1
      GO TO 200
  204 NPAGE=J
      MX=NMAX-200*(NPAGE-1)
      J=1
  206 IF(MX-J*50)210,210,208
  208 J=J+1
      GO TO 206
  210 NCOLM=J
      NW=MX-50*(NCOLM-1)
C     NPAGE=NUMBER OF PAGES
C     NCOLM=NUMBER OF COLUMNS ON LAST PAGE
C     NW=NUMBER OF WORDS IN THE LAST COLUMN
      MX=0
  212 IF(NPAGE-1)230,230,214
  214 NPAGE=NPAGE-1
      PRINT 614
      PRINT 616
      DO 218 M=1,50
      DO 216 J=1,4
      JX=50*(J-1)+MX+M
      WORD(J)=FW(JX)
  216 IWD(J)=JX
      PRINT 618,(IWD(J),WORD(J),J=1,4)
  218 CONTINUE
      MX=MX+200
      GO TO 212
  230 PRINT 614
      PRINT 616
      DO 240 M=1,NW
      NC=NCOLM
      DO 238 J=1,NC
      JX=50*(J-1)+MX+M
      WORD(J)=FW(JX)
  238 IWD(J)=JX
      PRINT 618,(IWD(J),WORD(J),J=1,NC)
  240 CONTINUE
      NC=NCOLM-1
      IF(NC)321,321,319
  319 CONTINUE
      NW=NW+1
      IF(NW-50)10,10,20
   10 CONTINUE
      DO 242 M=NW,50
      DO 241 J=1,NC
      JX=50*(J-1)+MX+M
      WORD(J)=FW(JX)
  241 IWD(J)=JX
      PRINT 618,(IWD(J),WORD(J),J=1,NC)
  242 CONTINUE
  321 CONTINUE
   20 CONTINUE
  618 FORMAT(20X,4(I4,F10.3,10X))
  614 FORMAT(1H1,30X,12HFOIL WEIGHTS)
  616 FORMAT(1HO,19X,4(4H NO.,4X,6HWEIGHT,10X) )
      RETURN
      END
```

SUBROUTINE MICRO

```
*     LIST8
*     LABEL
CMICRO            PROGRAM  BY  R. SIMMS    5/18/63
      SUBROUTINE MICRO
      DIMENSION WT(1000),ND(100),CT(100,6),SATCT(100,6),RELTM(100,6)
      DIMENSION DELAY(6),COUNTS(6),DIF(6),AVCT(100),MD(20)
      DIMENSION HOLR(11),ADENT(12)
      COMMON WT,ND,CT,SATCT,RELTM,DELAY,COUNTS,DIF,AVCT,MD,HOLR,ADENT
      COMMON DKAY,LMAX,NMAX,NPASS
      READ 10,NCARDS,TMCFR
C     NCARDS IS THE NUMBER OF CARDS OF CORRECTIONS TO BE READ IN
C     TMCFR IS THE TIME CORRECTION FACTOR
      PRINT 12,(ADENT(I),I=1,12)
      PRINT 14,TMCFR
      PRINT 16
      DO 200 I=1,NCARDS
      READ 18,HTFR,BJOFR,NW,(MD(J),J=1,NW)
C     HTFR IS THE HEIGHT CORRECTION FACTOR
C     BJOFR IS THE J-ZERO CORRECTION FACTOR
C     NW IS THE NUMBER OF FOILS HAVING THIS SET OF CORRECTIONS
C     MD(J) IS THE COUNTING POSITION TO WHICH THE CORRECTIONS APPLY
C     MD(J) IS THE COUNTING POSITION TO WHICH THE CORRECTIONS APPLY
C     A ZERO COUNTING POSITION SKIPS A LINE
      A=HTFR*BJOFR*TMCFR
      DO 140 J=1,NW
      L=MD(J)
      IF(L)105,105,110
  105 PRINT 20
      GO TO 140
  110 CONTINUE
      CTRATE = A*AVCT(L)
      PRINT 22,ND(L),AVCT(L),HTFR,BJOFR,CTRATE
  140 CONTINUE
  200 CONTINUE
      RETURN
   10 FORMAT(I5,E10.5)
   12 FORMAT(1H1,10X,21HANALYSIS OF FOIL DATA,10X,11A6,1A5)
   14 FORMAT(1HO,10X,30HTHE TIME CORRECTION FACTOR IS  F10.5)
   16 FORMAT(1HO,10X,8HFOIL NO.,5X18HAVERAGE COUNT RATE,5X,9HHT FACTOR,
     15X,10HJ-0 FACTOR,5X,13HCORR. CT RATE)
   20 FORMAT(1H )
   18 FORMAT(2E10.5,10I5)
   22 FORMAT(14X,I5,9X,1PE12.5,7X,0PF9.5,5X,0PF10.5,6X,1PE12.5)
      END
```

TEST RUN FOR THE ACTIVE CODE

```
*      DATA
     1     1
    60 0.17830E-03           10 MIL GOLD FOIL LIBRARY
 0.94000E 01 0.94060E 01 0.94060E 01 0.94080E 01 0.94130E 01 0.94150E 01
 0.94160E 01 0.94190E 01 0.94200E 01 0.94200E 01 0.94220E 01 0.94230E 01
 0.94240E 01 0.94250E 01 0.94250E 01 0.94280E 01 0.94280E 01 0.94280E 01
 0.94300E 01 0.94320E 01 0.94330E 01 0.94350E 01 0.94350E 01 0.94350E 01
 0.94360E 01 0.94360E 01 0.94370E 01 0.94410E 01 0.94430E 01 0.94440E 01
 0.94450E 01 0.94450E 01 0.94450E 01 0.94470E 01 0.94490E 01 0.94490E 01
 0.94500E 01 0.94500E 01 0.94500E 01 0.94510E 01 0.94510E 01 0.94510E 01
 0.94530E 01 0.94530E 01 0.94540E 01 0.94540E 01 0.94550E 01 0.94550E 01
 0.94560E 01 0.94590E 01 0.94590E 01 0.94600E 01 0.94600E 01 0.94600E 01
 0.94600E 01 0.94600E 01 0.94600E 01 0.94600E 01 0.94650E 01 0.94650E 01
0RUN A12  CD COVD 10 MIL GOLD 1.25-IN PITCH  3-FT TANK  5/7/63
     0     1
    23     5 0.25      40.0
10000.0    10000.0    10000.0    10000.0    10000.0    10000.0
0.0
    40    41    42    43    44    45    46    47    48    49     1     2     3     4
     5     6     7     8     9    10    11    13    14
7.69        7.36        7.38        7.13        7.30        7.32        7.61
7.24        6.71        6.83        5.95        6.03        6.01        6.10
6.00        6.00        6.02        6.03        6.05        6.04        6.01
6.02        6.03
7.92        7.60        7.46        7.34        7.50        7.76        7.87
7.46        6.92        6.97        6.41        6.25        6.10        6.17
6.26        6.16        6.28        6.19        6.22        6.23        6.23
6.28        6.15
8.29        7.72        7.72        7.51        7.75        7.87        8.33
7.56        7.06        7.28        6.45        6.33        6.34        6.47
6.43        6.32        6.48        6.57        6.38        6.35        6.39
6.47        6.53
8.44        8.08        8.04        7.76        8.07        8.02        8.47
7.83        7.42        7.53        6.66        6.54        6.65        6.79
6.62        6.60        6.57        6.64        6.68        6.63        6.65
6.66        6.68
8.70        8.31        8.32        8.00        8.26        8.55        8.76
8.17        7.72        7.62        6.86        6.76        6.94        6.94
6.81        6.76        6.82        6.85        6.85        6.87        6.88
6.72        6.85
     8 0.8542
0.485       1.0              9     1     2     3     4     0     5     6     7     8
0.485       1.0001           4     0     9    10     0
0.453       1.0002           4    11     0    19     0
0.453       1.0010           4    12    15    20     0
0.453       1.0024           4    13    16    21     0
0.453       1.0043           4    14    17     0     0
0.453       1.0066           2    18     0
0.453       1.0060           2    22    23
     0
```

APPENDIX E
GRAPHITE-MODERATED LATTICES

From the results of Chapter III, it appeared that the details of the energy exhange kernel were not important in the intracellular flux calculations. The Nelkin kernel gave very nearly the same result as the Brown-St. John kernel for the heavy water-moderated lattices studied. The availability of Parks' kernel for graphite prompted a study of some graphite-moderated lattices for which experimental data were already available. The calculations were performed by Kyong (K8) who used the THERMØS code.

Parks' kernel for graphite takes into account the effects of the crystalline binding in graphite. The details of this scattering model are discussed by Parks (P3, P4). The kernel was generated for use with THERMØS by Suich (S4) who used the SUMMIT code (B3). The diagonal elements of the energy exchange kernel have been adjusted so that the integrated kernel will give the observed scattering cross section given in BNL-325 (H15). The diagonal adjustment does not destroy the detailed balance requirement implicit in the energy exchange kernel, since the off-diagonal elements of the kernel are unaffected.

Comparisons between the results obtained with Parks' kernel and with the free gas kernel are shown in Figs. E.1, E.2 and E.3; the free gas models used correspond to mass-12 and mass-27. The results indicate that Parks' kernel cannot be duplicated by simply increasing the mass in the free gas model. The quantity, $P(E_i \rightarrow E_f)$, is the probability per unit energy interval of transfer from initial energy, E_i, to a final energy, E_f. When the target nuclei are stationary, $P(E_i \rightarrow E_f)$ is a constant between E_i and αE_i. The target nuclei should appear stationary at high neutron energy. Figure E.3 shows that even at an initial neutron energy of 14.8 kT_M, the motion of the moderator contributes to the scattering process. In the low energy range (0.04 kT_M)shown in Fig. E.1, the lattice vibrations cause the "steps" on the curve. Neutrons of energy 0.04 kT_M are capable of being upscattered to energies corresponding to the lattice vibrational energies.

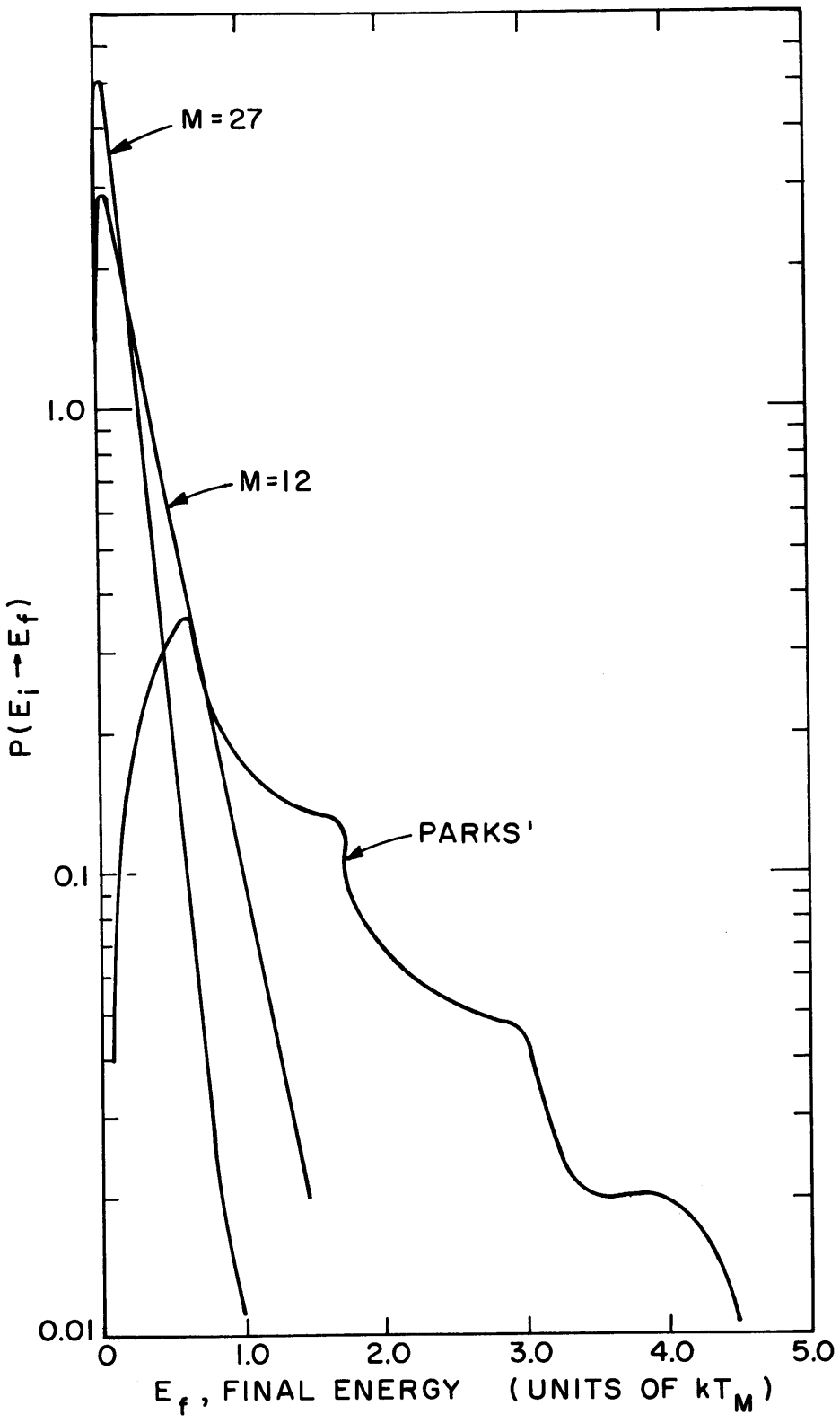

FIG. E.1 COMPARISON OF PARKS' KERNEL WITH THE FREE GAS KERNELS FOR AN INITIAL ENERGY OF 0.04 kT_M.

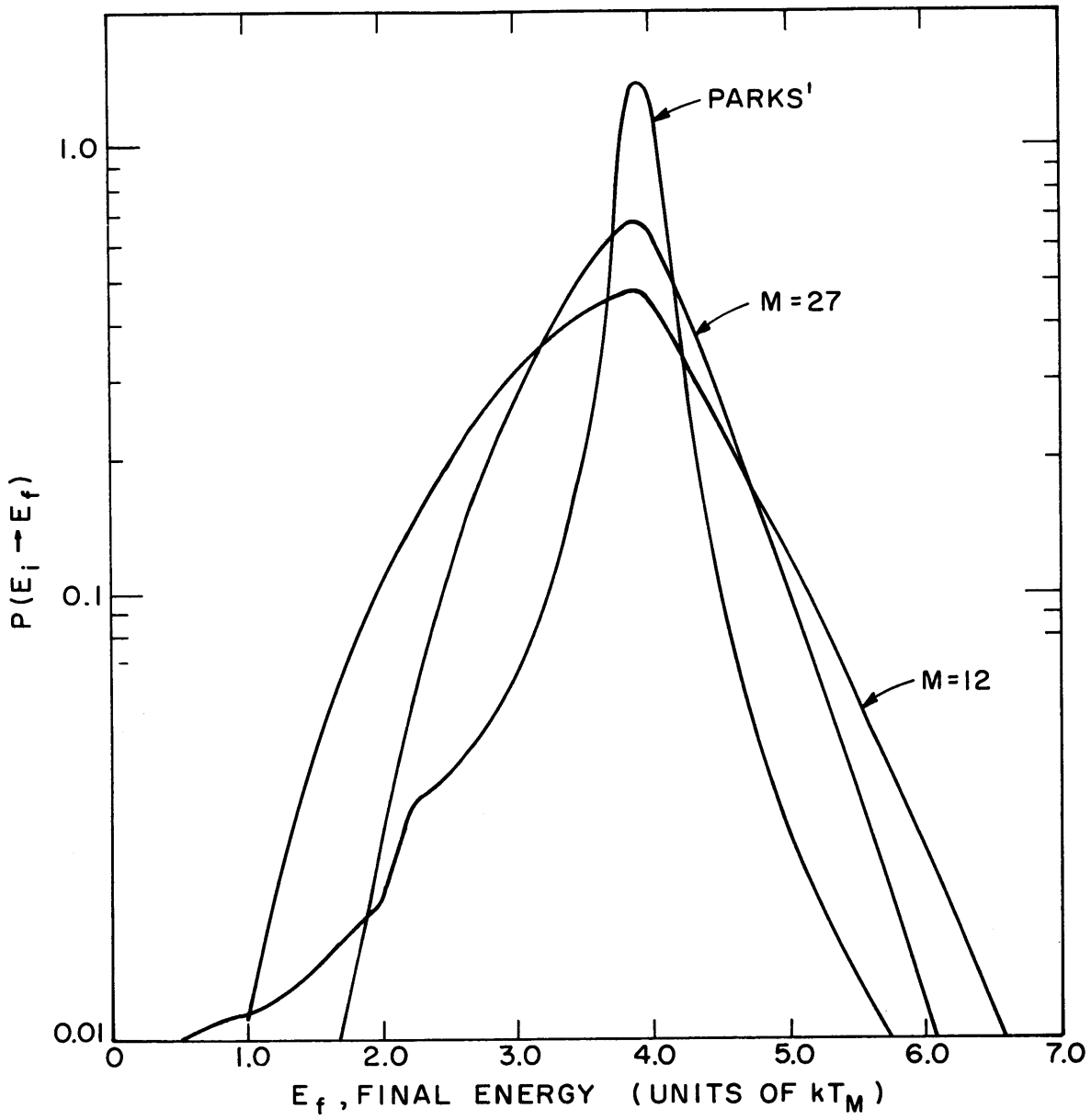

FIG. E.2 COMPARISON OF PARKS' KERNEL WITH THE FREE GAS KERNELS FOR AN INITIAL ENERGY OF 3.9 kT_M.

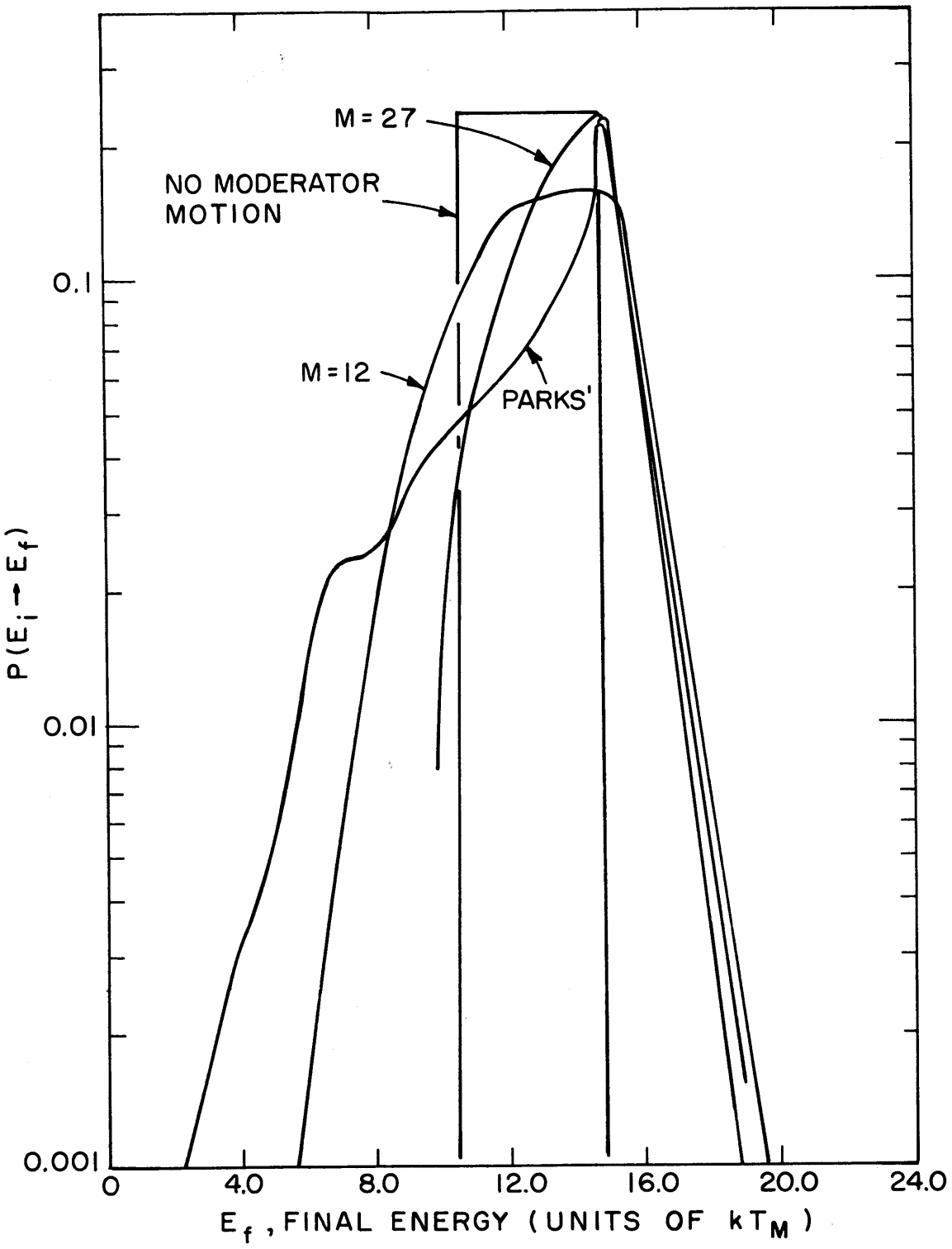

FIG. E.3 COMPARISON OF PARKS' KERNEL WITH THE FREE GAS KERNELS FOR AN INITIAL ENERGY OF 14.8 kT_M.

A set of THERMØS calculations was made for the lattice cell corresponding to the original BNL Brookhaven reactor lattice cell. The BNL cell consisted of a 1.1-inch diameter, natural uranium rod clad in an aluminum jacket, in an air channel 36 cm^2 in area. Six aluminum fins were attached to each rod. The rod sat, horizontally, on the fins, slightly off-center. The calculation was made by assuming that the rod could be placed in the center of the cell; the free gas kernel (mass-12) and Parks' kernel were used. The results of the calculations and the intracellular Dy^{164} activation measurements of Price for the BNL cell (P10) are shown in Fig. E.4. Parks' kernel gives results that are in better agreement with experiment and which are significantly different from those calculated with the mass-12 kernel. However, neither of the calculations predicted the activations in the air gap. The Dy^{164} foils were placed on the aluminum fin, which might have had an effect on the shape of the activation curve. It seems more likely that the calculation in the air channel is somewhat in error.

Figures E.5, E.6 and E.7 show the calculated neutron spectra for Parks' and the mass-12 kernels at the cell center, air-graphite interface and the cell edte of the BNL lattice cell. The spectra are normalized to one neutron absorbed in the cell. Again, a difference is evident between the two models, with Parks' kernel predicting the harder spectra.

To investigate the effects of the air gap, a set of GLEEP experiments (L1) was analyzed with THERMØS, and with the two kernels. The lattices consisted of 1-inch diameter, natural rods on a 7-inch square spacing and moderated by graphite. The lattice experiments were run as exponential measurements in the thermal column of the GLEEP reactor. The width of the air channel was varied by inserting graphite sleeves into the air space. Experiments were made for air gaps having diameters of 1.5, 2.0, 2.75 and 3.75 inches. Both bare and cadmium-covered manganese wires were irradiated. The results are shown in Figs. E.8 to E.11. The wires were irradiated along the rod-to-rod traverse, which should give activations slightly smaller than those calculated with THERMØS. However, there still remains about a 5% discrepancy between the experiments and the calculations with Parks' kernel at the edge of the cell. It is thought that either the presence of the air channel or the assumed slowing-down source distribution in the calculations (flat source) is the cause of the observed discrepancies.

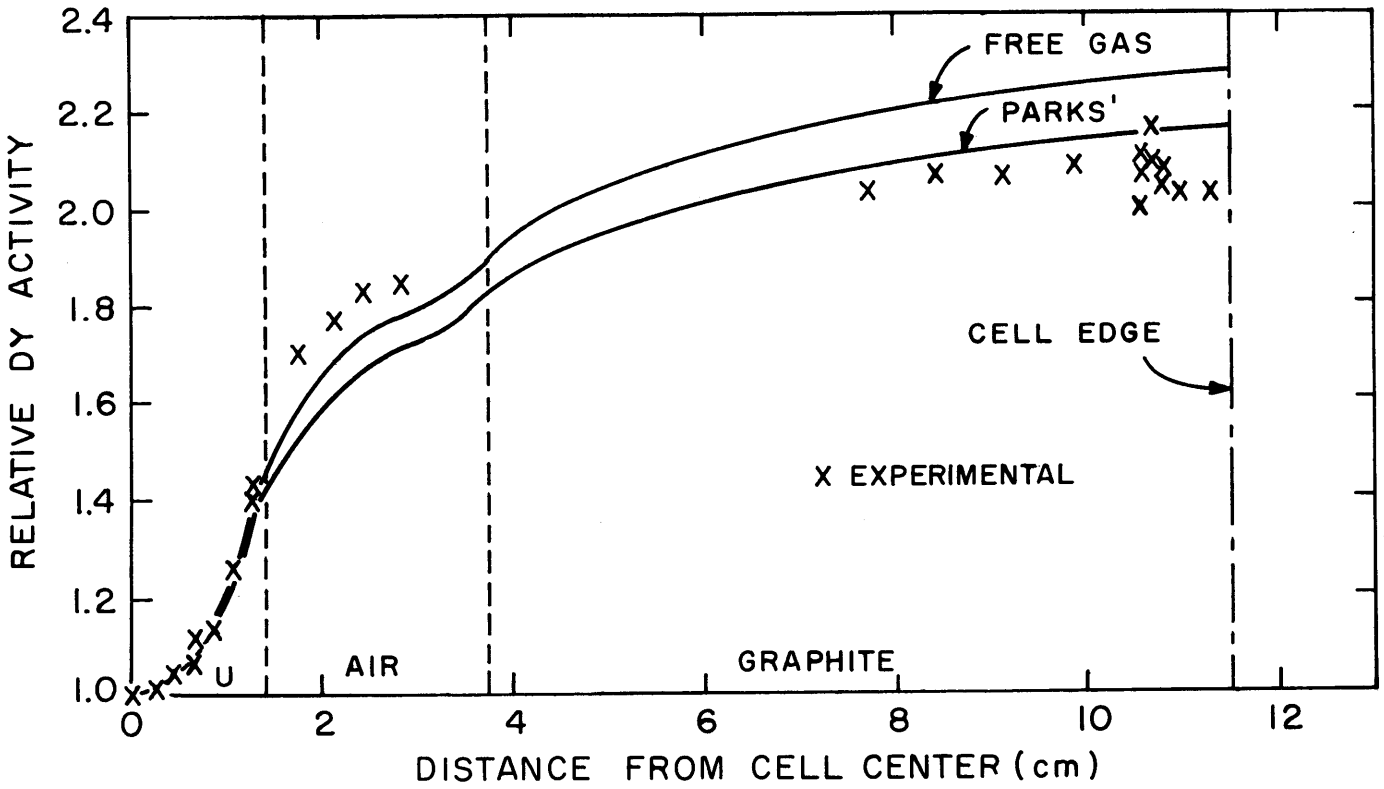

FIG. E.4 INTRACELLULAR DYSPROSIUM FOIL ACTIVATION DISTRIBUTION FOR THE BNL GRAPHITE REACTOR LATTICE.

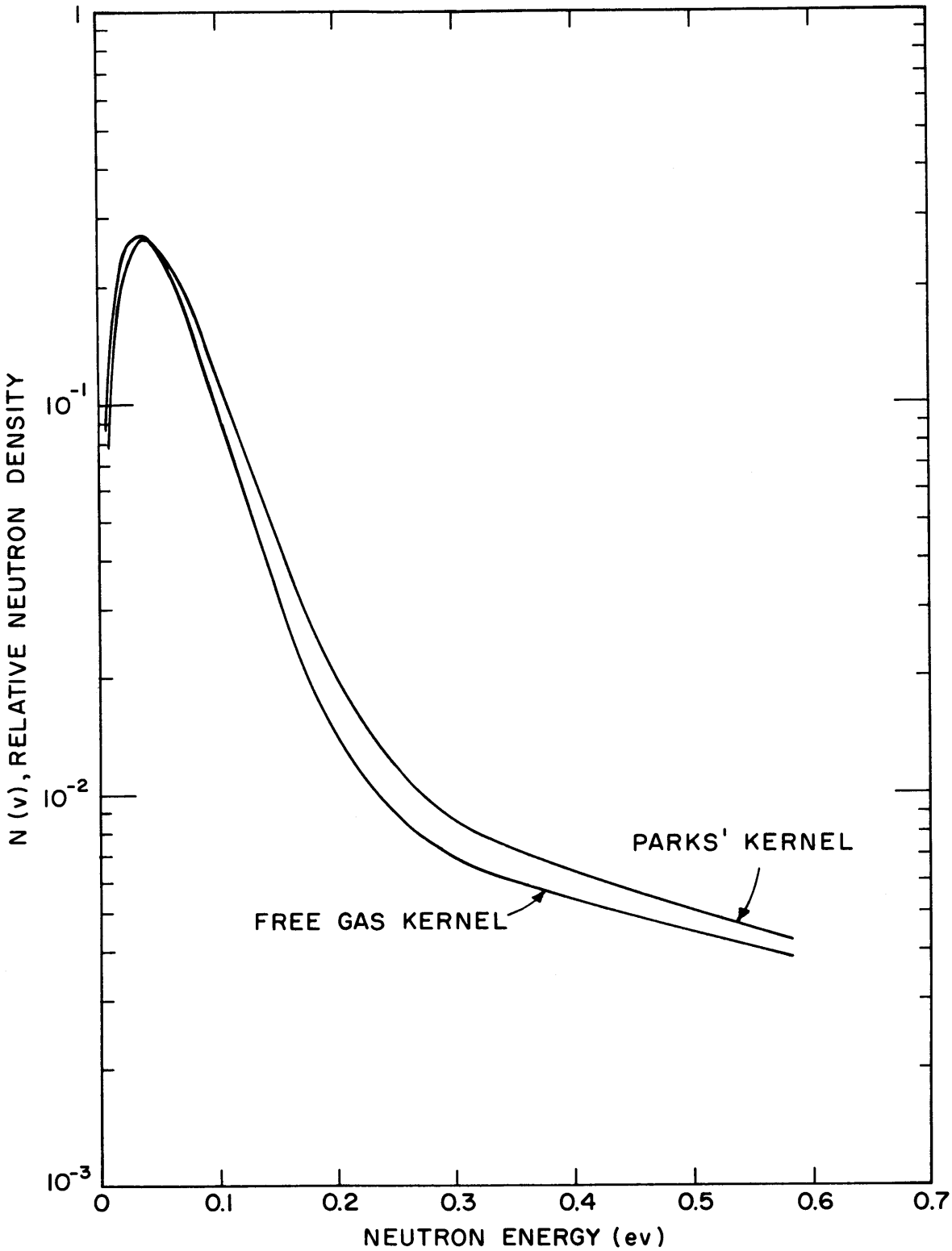

FIG. E.5 CALCULATED NEUTRON SPECTRA AT THE CENTER OF THE CELL FOR THE BNL LATTICE.

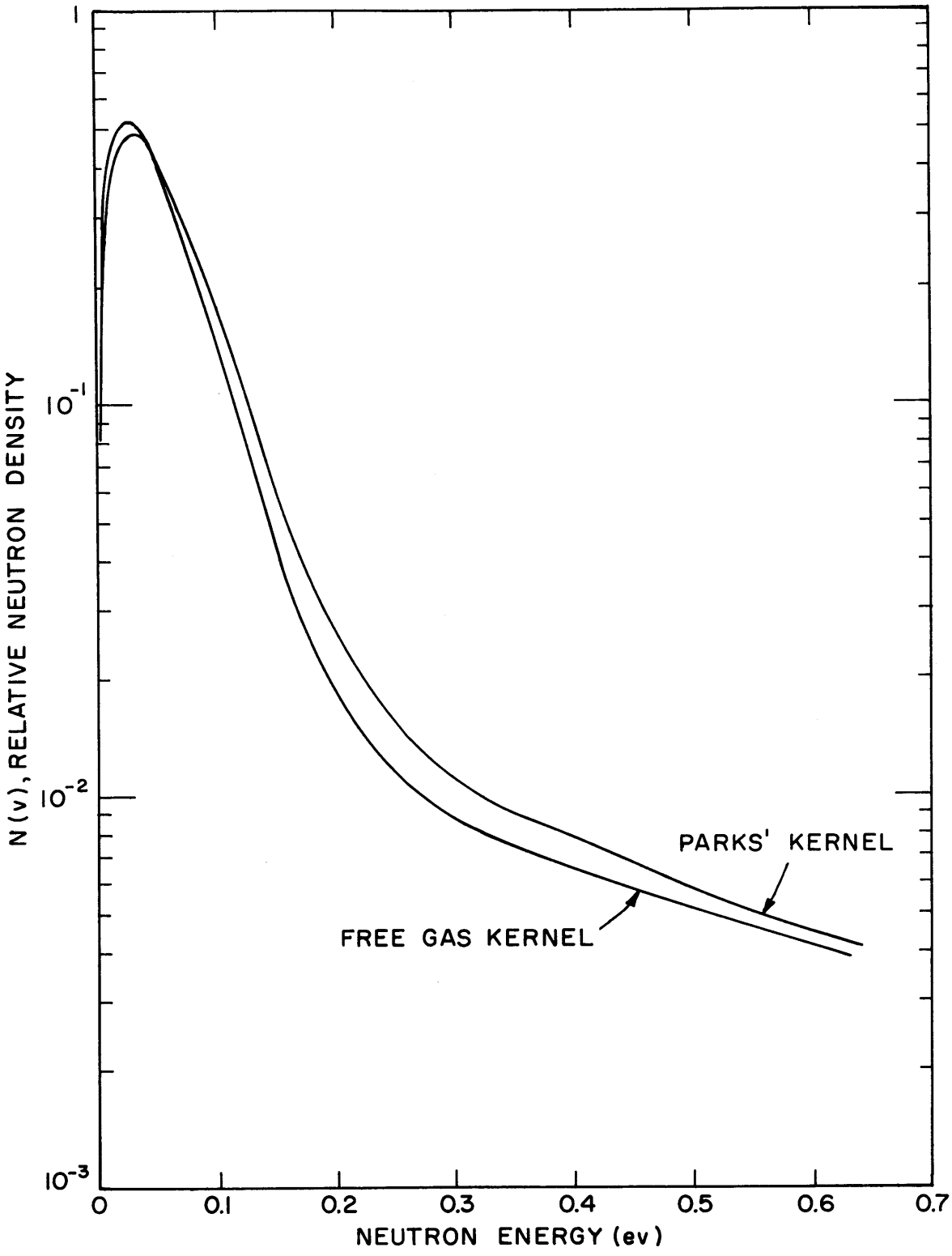

FIG. E.6 CALCULATED NEUTRON SPECTRA AT THE AIR-MODERATOR INTERFACE FOR THE BNL LATTICE.

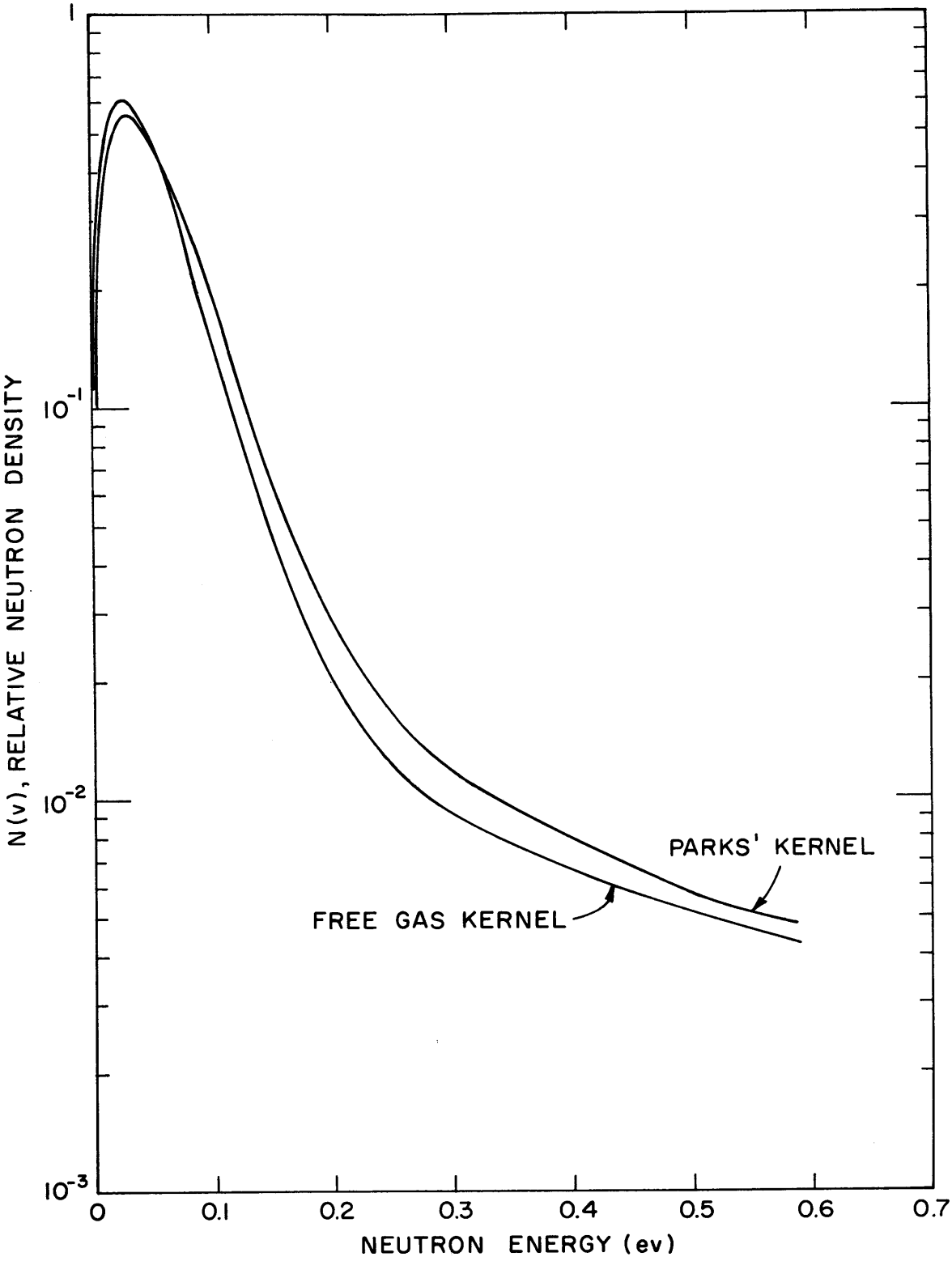

FIG. E.7 CALCULATED NEUTRON SPECTRA AT THE CELL BOUNDARY FOR THE BNL LATTICE.

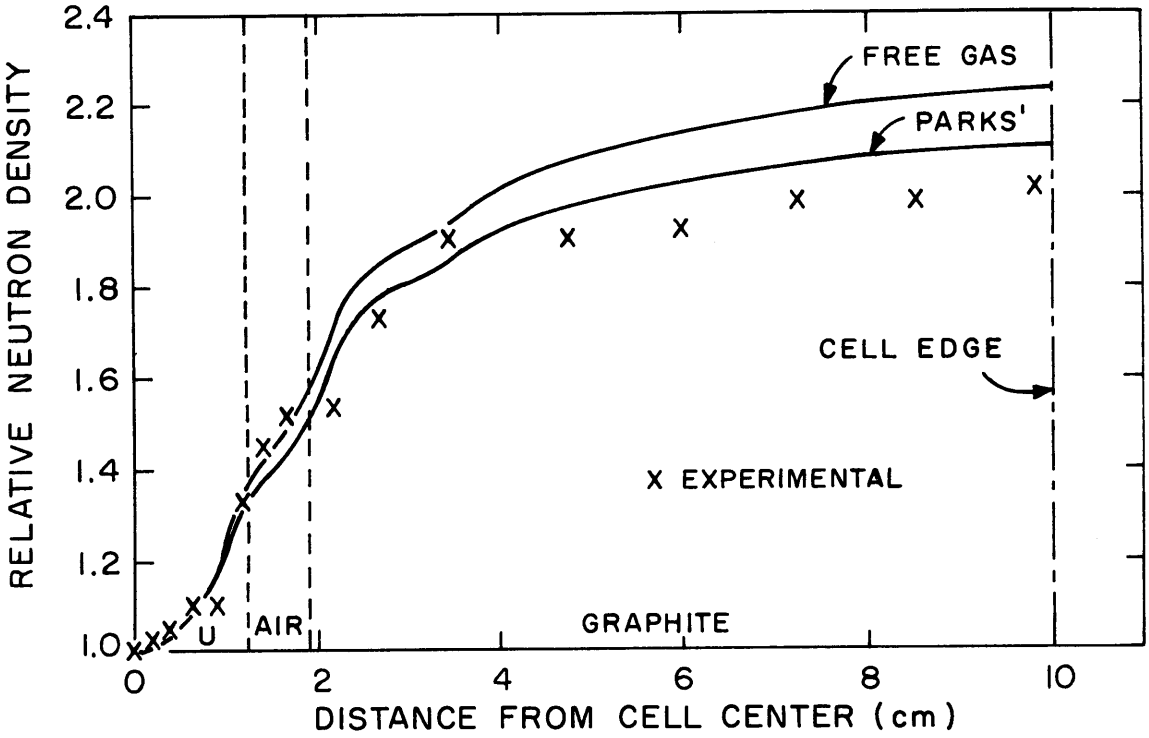

FIG. E.8 INTRACELLULAR MANGANESE WIRE ACTIVATION DISTRIBUTION FOR THE GLEEP LATTICE WITH THE 1.5-INCH CHANNEL DIAMETER.

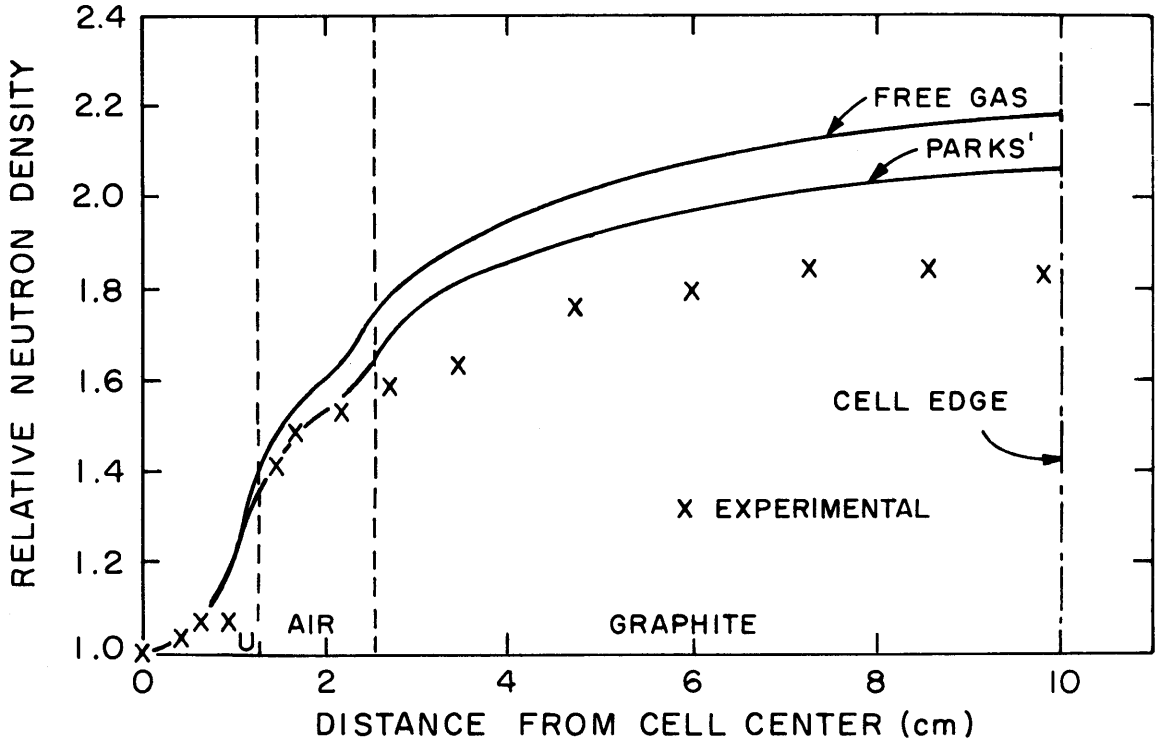

FIG. E.9 INTRACELLULAR MANGANESE WIRE ACTIVATION DISTRIBUTION FOR THE GLEEP LATTICE WITH THE 2.0-INCH CHANNEL DIAMETER.

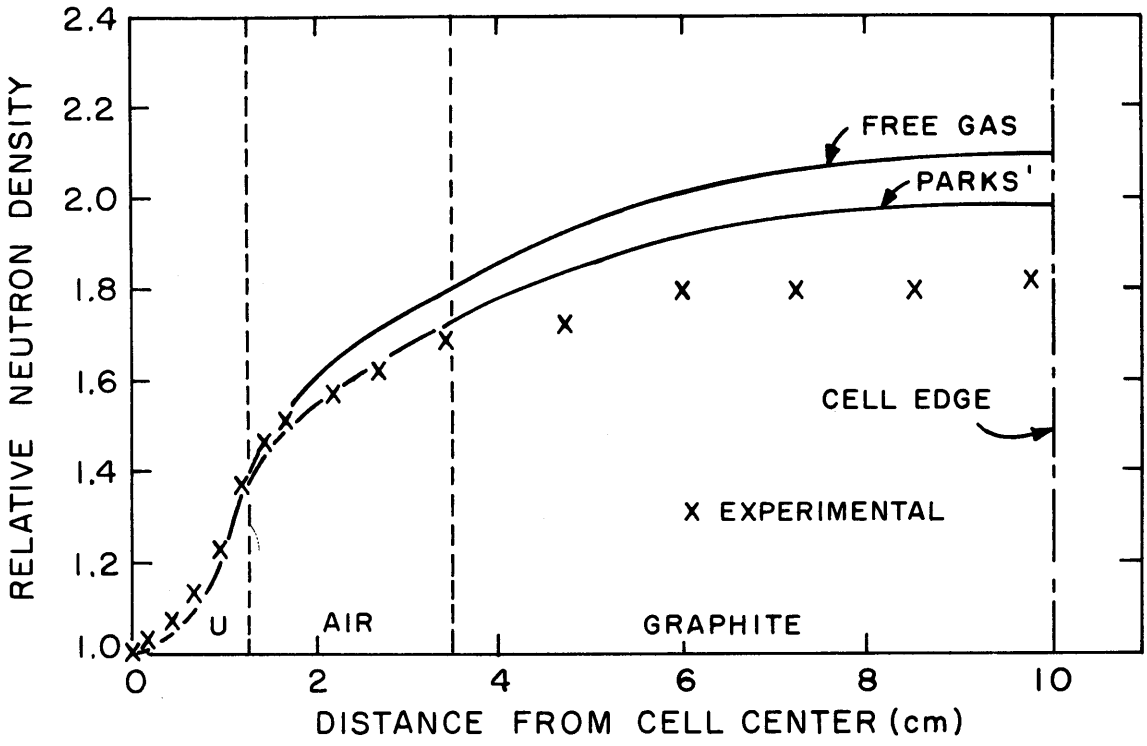

FIG. E.10 INTRACELLULAR MANGANESE WIRE ACTIVATION DISTRIBUTION FOR THE GLEEP LATTICE WITH THE 2.75-INCH CHANNEL DIAMETER.

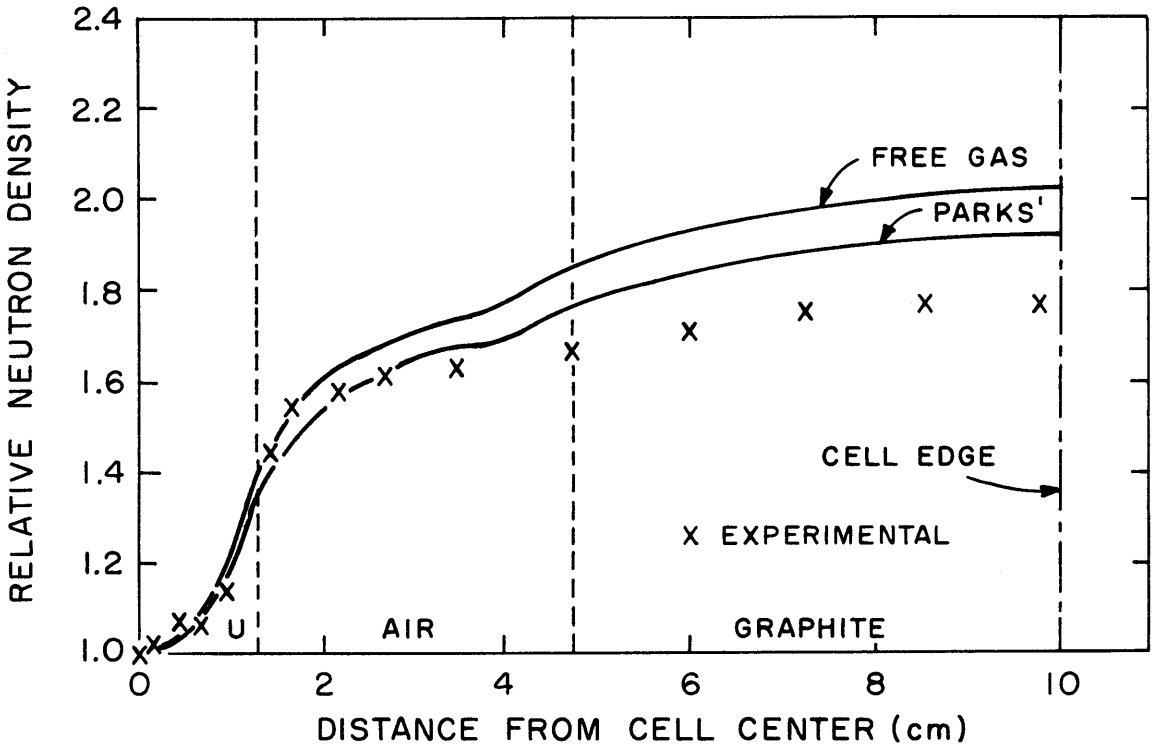

FIG. E.11 INTRACELLULAR MANGANESE WIRE ACTIVATION DISTRIBUTION FOR THE GLEEP LATTICE WITH THE 3.75-INCH CHANNEL DIAMETER.

APPENDIX F
DATA INPUT FOR COMPUTER CALCULATIONS

The physical properties of the lattices studied are listed in Table F.1. The 30-group cross section set used by the THERMØS code and in the other calculations are tabulated in BNL-5826 (H8). The velocity mesh used for the 30-energy group calculations is given in Table F.2. The velocity mesh is the "standard" mesh used by THERMØS.

TABLE F.1
Properties of the Lattices Studied

Property	Natural Uranium Metal Rod Lattices	1.03% U^{235}, Uranium Metal Rod Lattices
Fuel Rod Diameter (in.)	1.010	0.250
Aluminum Clad Thickness (in.)	0.028	0.028
Aluminum Tube O.D. (in.)	1.080	0.318
Heavy Water Purity (%)	99.75	99.75
N_{25} (atoms/cm-barn)	0.0003454	0.0004975
N_{28} (atoms/cm-barn)	0.04759	0.04734
N_D (atoms/cm-barn)	0.06623	0.06623
N_H (atoms/cm-barn)	0.0001507	0.0001507
N_O (atoms/cm-barn)	0.03319	0.03319

TABLE F.2

Thirty Energy Group Mesh Spacing
Used in the Multigroup Calculations.

Group	Velocity[(a)]	Velocity Increments[(a)]	Energy (ev)
1	0.10000	0.10000	0.00025
2	0.20000	0.10000	0.00101
3	0.30000	0.10000	0.00228
4	0.40000	0.10000	0.00405
5	0.50000	0.10000	0.00632
6	0.60000	0.10000	0.00911
7	0.70000	0.10000	0.01240
8	0.80000	0.10000	0.01619
9	0.90000	0.10000	0.02049
10	1.00000	0.10000	0.02530
11	1.10000	0.10000	0.03061
12	1.20000	0.10000	0.03643
13	1.30000	0.10000	0.04276
14	1.40000	0.10000	0.04959
15	1.50000	0.10000	0.05692
16	1.60500	0.11000	0.06517
17	1.72000	0.12000	0.07485
18	1.84500	0.13000	0.08612
19	1.98000	0.14000	0.09919
20	2.12250	0.14500	0.11398
21	2.27750	0.16500	0.13123
22	2.45500	0.19000	0.15248
23	2.66000	0.22000	0.17901
24	2.89750	0.25500	0.21241
25	3.17250	0.29500	0.25464
26	3.49000	0.34000	0.30816
27	3.85500	0.39000	0.37598
28	4.27250	0.44500	0.46183
29	4.74750	0.50500	0.57023
30	5.28500	0.57000	0.70666

(a) In units of v_o (2200 m/sec).

APPENDIX G
NOMENCLATURE

1D	one-dimensional
2D	two-dimensional
*	effective value
$\bar{}$	average value
A_{eff}	Brown-St. John effective mass
A_{epi}	epicadmium activation
A_i	a constant used in Eq. (3.2.1)
A_{th}	subcadmium activation
a	parameter defined in Eq. (3.5.3)
B_m^2	material buckling
C	a constant used in Eq. (3.5.3)
CR	count rate
C_{TOTAL}	total number of counts
D	diffusion coefficient
D_o	diffusion coefficient of fuel
D_1	diffusion coefficient of moderator
d	distance
E	energy
E_f	final energy of scattered neutron
E_i	initial energy of neutron
ERI	effective resonance integral
ERI'	ERI with the 1/v-contribution
F	disadvantage factor
$F(\lambda)$	probability defined by Eq. (3.3.9)
$F(\lambda,a)$	probability defined by Eq. (3.3.10)
f	thermal utilization
f_{ss}	flux perturbation factor
g	a function defined by Eq. (A.8)
$J_o(x)$	Bessel function of the zeroth order of the argument, x
$J_1(x)$	Bessel function of the first order of the argument, x

K_{exp}	Resonance parameter defined by Eq. (3.5.2)
kT_M	moderator temperature
L	diffusion length
$\overline{\ell}$	mean chord length
M(E)	Maxwellian spectrum
mod	moderator
N(E,r)	neutron density at r and E
P_n	spherical harmonic approximation of order n
P_o	escape probability for a neutron originating from a flat, isotropic source in a body, for a pure absorber
$\overline{P}$	escape probability, scattering not necessarily zero
$P(E_i \rightarrow E_f)$	probability of transfer from E_i to E_f
q	slowing-down density
R, R_o	radius
ΔR	incremental radial distance
r	radial position
RI	resonance integral
RI'	RI with the 1/v-contribution
R_{cd}	cadmium ratio
R(r)	reaction rate at r
S	surface area
S_n	Carlson's S_n-approximation
T_M	moderator temperature
t	foil thickness
t*	effective foil thickness
tr	abr. for transport
V	volume
V_{mod}	moderator volume
v	velocity
v_r	relative velocity
α	radial buckling
β	β-ray
β	volume fraction
β	blackness
Γ_a	capture probability

γ	axial buckling
γ	γ-ray
ΔR	incremental radial distance
ζ	over-all disadvantage factor
η	number of fast neutrons per capture in uranium
θ	angle
κ	inverse diffusion length
κ_i	a constant used in Eq. (3.2.1)
λ	number of mean free paths
λ_{tr}	number of transport mean free paths
μ	direction cosine
ξ	average logarithmic decrement
ξ_a	optical thickness
π	3.14159
$\Sigma_{(t,s,a,ACT)}$	macroscopic cross section (total, scattering, absorption or activation)
$\sigma_{(t,s,a,ACT)}$	microscopic cross section (total, scattering, absorption or activation)
σ_{tr}	transport cross sections
σ^o	2200 m/sec value of σ
$\sigma_s(E_i \rightarrow E_f,\mu)$	differential scattering cross section
$\sigma_s(E_i \rightarrow E_f)$	scattering kernel
$\sigma_{s_1}(E_i \rightarrow E_f)$	first Legendre component of the differential scattering cross section
$\sigma_s(v_r)$	scattering cross section for a relative velocity, v_r
σ	standard deviation
τ	deadtime
ϕ	flux
ϕ_c	a critical angle
ψ	azimuthal angle
ω	frequency

APPENDIX H
REFERENCES

A1 Arcipiani, B., D. Ricabarra and G. H. Ricabarra, "A Note on the Measurement of the U^{238} Cadmium Ratio," Nuclear Sci. and Eng., 14, 3, (1962).

A2 Alexander, J. H. and G. W. Hinman, "Anisotropic Scattering in DSN," Trans. Am. Nuclear Soc., 5, 2, 408 (1962).

A3 Amaldi, E., "The Production and Slowing Down of Neutrons," Handbuch der Physik, 38, 2, Springer-Verlag, Berlin (1959).

A4 Amouyal, A., P. Benoist, and J. Horowitz, "A New Method for the Determination of the Thermal Utilization Factor of a Cell," J. Nuclear Energy, 6, 79 (1957).

B1 Bauman, N. P., "The Neutron Diffusion Coefficient in D_2O Between 20°C and 220°C," Trans. Am. Nuclear Soc., 5, 1, 42 (1962).

B2 Bauman, N. P., "Resonance Integrals and Self-Shielding Factors for Detector Foils," DP-817, January, 1963.

B3 Bell, J., "SUMMIT – An IBM 7090 Program for Computation of Crystalline Scattering Kernels," GA-2492 (1962).

B4 Beyster, J. R., W. M. Lopez, R. E. Nather and J. L. Wood, "Measurement of Low Energy Neutron Spectra," Trans. Am. Nuclear Soc., 2, 2 (1959).

B5 Beyster, J. R., W. M. Lopez and R. E. Nather, "Integral Neutron Thermalization," TID-11064 (1959).

B6 Beyster, J. R., J. L. Wood, R. B. Walton and W. M. Lopez, "Measurements of Low Energy Spectra," Trans. Am. Nuclear Soc., 3, 1 (1960).

B7 Beyster, J. R., J. L. Wood and H. C. Honeck, "Spatially Dependent Neutron Spectra," Trans. Am. Nuclear Soc., 3, 2, (1960).

B8 Beyster, J. R., et al., "Measurements of Neutron Spectra in Water, Polyethylene, and Zirconium Hydride," Nuclear Sci. and Eng. 9, 168 (1961).

B9 Bohl, H., and E. Gelbard, "SLOP - 1: A Thermal Multigroup Program for the IBM 704," WAPD-TM-188 (1960).

B10 Bothe, W., "Zur Methodik der Neutronensonden," Zeits f. Physik, 120, 437 (1943).

B11 Brown, H. D., and D. S. St. John, "Neutron Energy Spectrum in D_2O," DP-33 (1954).

B12 Brown, P. S., I. Kaplan, A. E. Profio, and T. J. Thompson, "Measurements of Spatial and Spectral Distributions of Thermal Neutrons in Heavy Water Natural Uranium Lattices," Proceedings of the Brookhaven Conference on Neutron Thermalization, BNL-719 (1962).

B13 Brown, P. S., P. F. Palmedo, T. J. Thompson, A. E. Profio and I. Kaplan, "Measurements of Microscopic and Macroscopic Flux Distributions in Natural Uranium, Heavy Water Lattices," Trans. Am. Nuclear Soc., 5, 1 (1962).

B14 Brown, P. S., T. J. Thompson, I. Kaplan and A. E. Profio, "Measurement of the Spatial and Energy Distribution of Thermal Neutrons in Uranium, Heavy Water Lattices," NYO-10205 (1962).

B15 Buslik, A. J., "The Description of the Thermal Neutron Spatially Dependent Spectrum by Means of Variational Principles," to be published in the Bettis Technical Review.

C1 Calame, G. P., F. D. Federighi, and P. A. Ombrellaro, "A Two-Mode Variational Procedure for Calculating Thermal Diffusion Theory Parameters," Nuclear Sci. and Eng., 10, 31 (1961).

C2 Calame, G. P., and F. D. Federighi, "A Variational Procedure for Determining Spatially Dependent Thermal Spectra," Nuclear Sci. and Eng., 10, 190 (1961).

C3 Carlson, B. G., "Solution of the Transport Equation by S_n Approximations," LA-1891 (1955).

C4 Carlson, B., and G. Bell, "Solution of the Transport Equation by the S_n Method," Proceedings of the Second United Nations International Conference on the Peaceful Uses of Atomic Energy, 15, 535 (1958).

C5 Case, K., F. de Hoffmann, and G. Placezek, "Introduction to the Theory of Neutron Diffusion, Part I," U.S. Government Printing Office, Washington, D.C. (1953).

C6 Chernick, J., "Results of Univac Survey of the Thermal Utilization of BNL Experimental Lattices," BNL-1797 (1954).

C7 Childers, K., personal communication.

C8 Cohen, E. R., "Neutron Thermalization Theory," Proceedings of the First United Nations International Conference on the Peaceful Uses of Atomic Energy, 5, 405 (1956).

C9 Cohen, E. R., and R. Goldstein, "Theory of Resonance Absorption of Neutrons," Nuclear Sci. and Eng., 13, 132 (1962).

C10 Crandall, J. L., "Status of the United States Effort in D_2O Reactor Physics," DP-787 (1962).

C11 Crandall, J. L., "Efficacy of Experimental Physics Studies on Heavy Water Lattices," DP-833 (1963).

D1 D'Ardenne, W., personal communication.

D2 Dalton, G. R., and R. K. Osborn, "Flux Perturbations by Thermal Neutron Detectors," Nuclear Sci. and Eng., 9, 198 (1961).

D3 Dalton, G. R., "The Effects of Anisotropy on Neutron Detector Flux Depression," Trans. Am. Nuclear Soc., 5, 1 (1962).

D4 Dawson, C., "T.E.T. – a Thermal Energy Transport Code," coded at the David Taylor Model Basin, unpublished.

D5 Doerner, R. C. and F. H. Helm, "Flux Perturbations by Detecting Foils," ANL memorandum (1961).

E1 Egelstaff, P., S. Cocking, R. Royston and I. Thorson, "The Thermal Neutron Scattering Law for Light and Heavy Water," IAEA Vienna Conference on Inelastic Scattering, Paper IS/P/10 (1960).

E2 Egelstaff, P., et al., "On the Evaluation of the Thermal Neutron Scattering Law," Nuclear Sci. and Eng., 12.

F1 Francis, N. C., J. C. Stewart, L. S. Bohl, and T. J. Krieger, "Variational Solutions to the Transport Equation," in Progress in Nuclear Energy, Series I, Vol. 3, The Stonebridge Press, Bristol, England (1959).

F2 Fukai, Y., "Comparison of Flux Ratio Calculations in Lattices by Integral Transport Theory," Nuclear Sci. and Eng., 13, 345 (1962).

G1 Glasstone, S. and M. Edlund, The Elements of Nuclear Reactor Theory, D. Van Nostrand Company, Inc., Princeton, New Jersey, (1952).

G2 Goldman, D., and F. Federighi, "A Comparison of Calculated and Experimental Thermal Energy Exchange Cross Sections," Trans. Am. Nuclear Soc., 4, 1 (1961).

G3 Goertzel, G., "The Method of Discrete Ordinates," Nuclear Sci. and Eng., 4, 581 (1958).

G4 Graves, W. E., "Analysis of the Substitution Technique for the Determination of D_2O Lattice Bucklings," DP-832 (1963).

H1 Hanna, G. C., "The Depression of Thermal Neutron Flux and Density by Absorbing Foils," Nuclear Sci. and Eng., 11, 338 (1961).

H2 Hanna, G. C., "The Neutron Flux Perturbation Due to an Absorbing Foil; a Comparison of Theories and Experiments," Nuclear Sci. and Eng., 15, 325 (1963).

H3 Harrington, J., personal communication.

H4 Hellens, R. L. and E. Andersen, "Some Problems in the Interpretation of Exponential Experiments," IAEC Symposium on Exponential and Critical Experiments (1963).

H5 Honeck, H. C., "A Method for Computing Thermal Neutron Distributions in Reactor Lattices as Functions of Space and Energy," Sc.D. Thesis, Massachusetts Institute of Technology, June, 1959.

H6 Honeck, H. C., "The Distribution of Thermal Neutrons in Space and Energy in Reactor Lattices. Part I: Theory," Nuclear Sci. and Eng., 8, 193 (1960).

H7 Honeck, H. C., and I. Kaplan, "The Distribution of Thermal Neutrons in Space and Energy in Reactor Lattices. Part II: Comparison of Theory and Experiment," Nuclear Sci. and Eng., 8, 203 (1960).

H8 Honeck, H. C., "THERMØS, a Thermalization Transport Theory Code for Reactor Lattice Calculations," BNL-3826 (1961).

H9 Honeck, H. C., "The Calculation of the Thermal Utilization and Disadvantage Factor in Uranium Water Lattices," IAEA Conference on Light Water Lattices, June, 1962.

H10 Honeck, H. C., "An Incoherent Scattering Model for Heavy Water," Trans. Am. Nuclear Soc., 5, 1 (1962).

H11 Honeck, H. C., "Some Methods for Improving the Cylindrical Reflecting Boundary Condition in Cell Calculations of the Thermal Neutron Flux," Trans. Am. Nuclear Soc., 5, 2 (1962).

H12 Honeck, H. C., "The Calculation of the Thermal Utilization and Disadvantage Factor in Uranium Water Lattices," submitted for publication in Nuclear Sci. and Eng., in May, 1963 (also called BNL-7047).

H13 Honeck, H. C., "Boundary Conditions for Cylindrical Cell Calculations," to be published.

H14 Honeck, H. C., "A Review of the Methods for Computing Thermal Neutron Spectra," an invited paper presented at ANS June, 1963 Meeting in Salt Lake City, Utah.

H15 Hughes, D. J., and J. A. Harvey, "Neutron Cross Sections," BNL-325.

H16 Hurwitz, H., M. Nelkin, and G. Habetler, "Neutron Thermalization: 1. Heavy Gaseous Moderator," Nuclear Sci. and Eng., 1, 280 (1956).

J1 Jacks, G. M., "A Study of Thermal and Resonance Neutron Flux Detectors," DP-608 (1961).

J2 Jirlow, K., and E. Johansson, "The Resonance Integral of Gold," J. Nuclear Energy Part A: Reactor Science, 11, 101 (1960).

K1 Kaplan, I., A. E. Profio, and T. J. Thompson, "Heavy Water Lattice Project Annual Report," NYO-10208, September, 1962.

K2 Kelber, C. N., "Resonance Integrals for Gold and Indium Foils," Nucleonics, 20, 8 (1962).

K3 Kier, P., personal communication concerning calculations made at the M.I.T. Computation Center.

K4 Kim, H., personal communication.

K5 Kouts, H., et al., "Exponential Experiments with Slightly Enriched Uranium Rods in Ordinary Water," Proceedings of the First United Nations International Conference on the Peaceful Uses of Atomic Energy, paper 600 (1955).

K6 Kouts, H., and R. Sher, "Experimental Studies of Slightly Enriched 0.6-inch Diameter Metallix Uranium, Water Moderated Lattices," in Progress in Nuclear Energy, Series II, Reactors, Vol. 2, Pergamon Press, London (1961).

K7 Krieger, T. J., and M. S. Nelkin, "Slow-Neutron Scattering by Molecules," Phys. Rev., 106, 290 (1957).

K8 Kyong, S. H., personal communication.

K9 Kaplan, I., "Measurements of Reactor Parameters in Subcritical and Critical Assemblies; A Review," NYO-10207 (1962).

L1 Lloyd, J. M., and J. E. C. Mills, "The Fine Structure Thermal Neutron Distribution in Natural Uranium-Graphite Lattices," AERE RP/R 1825.

M1 MacDougall, J. D., "Application of Scattering Law Data to the Calculation of Thermal Neutron Spectra," Proceedings of the Brookhaven Conference on Neutron Thermalization, BNL-719 (1962).

M2 Madell, J. T., T. J. Thompson, A. E. Profio, and I. Kaplan, "Spatial Distribution of the Neutron Flux on the Surface of a Graphite-Lined Cavity," NYO-9657 (1962).

M3 Malaviya, B. K., and A. E. Profio, "Measurements of the Diffusion Parameters of Heavy Water by the Pulsed-Neutron Technique," Trans. Am. Nuclear Soc., 6, 1 (1963).

M4 McGoff, D., personal communication.

N1 Nelkin, M. S., "Neutron Thermalization in Water," Trans. Am. Nuclear Soc., 2, 2 (1959).

N2 Nelkin, M. S., and E. R. Cohen, "Recent Work in Neutron Thermalization," in Progress in Nuclear Energy, Series I, Vol. 3, Pergamon Press, London (1959).

N3 Nelkin, M. S., "The Scattering of Slow Neutrons by Water," Phys. Rev., 119, 791 (1960).

N4 Nelkin, M. S., "Slow Neutron Inelastic Scattering and Neutron Thermalization," GA-1689 (1960). (Also presented at the IAEA Symposium on Inelastic Scattering of Neutrons in Solids and Liquids, Vienna, October (1960).)

N5 Nelkin, M. S., "Neutron Thermalization," in Nuclear Reactor Theory, Proceedings of Symposia in Applied Mathematics, Vol. 11, American Mathematical Society, Providence (1961).

N6 Nelkin, M. S., personal communication.

N7 Newmarch, D., "Errors Due to the Cylindrical Cell Approximation in Lattice Calculations," Atomic Energy Establishment Winfrith Report AEEW-R34 (1960).

O1 Osborn, R. K., "A Discussion of Theoretical Analyses of Probe-Induced Thermal Flux Perturbation," Nuclear Sci. and Eng., 15, 245 (1963).

P1 Palmedo, P. F., I. Kaplan, and T. J. Thompson, "Measurements of the Material Bucklings of Lattices of Natural Uranium Rods in D_2O," NYO-9660 (1962).

P2 Palmedo, P. F. and P. Benoist, "Interaction of Macroscopic Flux and Fine Structure in Heterogeneous Reactors," IAEA Symposium on Exponential and Critical Experiments (1963).

P3 Parks, D. E., "The Calculation of Thermal Neutron Scattering Kernels in Graphite," GA-2438 (1961).

P4 Parks, D. E., "The Effects of Atomic Motions on the Moderation of Neutrons," Nuclear Sci. and Eng., 9, 4, 430 (1961).

P5 Peak, J. C., I. Kaplan, and T. J. Thompson, "Theory and Use of Small Subcritical Assemblies for the Measurement of Reactor Parameter," NYO-10204 (1962).

P6 Pfeiffer, R. A., and W. W. Stone, "TRAM for the Philco 2000," KAPL-M-RPC-1.

P7 Poole, M. J., "Measurement of Neutron Spectra in Moderator and Reactor Lattices. Aqueous Moderators," J. Nuclear Energy, 5, 325 (1957).

P8 Poole, M. J., "Measurement of Neutron Spectra in Reactors," ORNL-2739 (1958).

P9 Poole, M. J., M. S. Nelkin, and R. S. Stone, "The Measurement and Theory of Reactor Spectra," in Progress in Nuclear Energy, Series I, Vol. 2, Pergamon Press, London (1958).

P10 Price, G. A., "Thermal Utilization Measurements," BNL-1992 (1954).

R1 Rhodes, W. A., and D. Vargofcak, "ULCER and QUICKIE, Multigroup Diffusion Theory Programs for Thermalization Studies," Trans. Am. Nuclear Soc., 5, 1 (1962).

R2 Ritchie, R. H., and H. B. Eldridge, "Thermal Neutron Flux Depression by Absorbing Foils," Nuclear Sci. and Eng., 8, 300 (1960).

S1 Selengut, D. S., "Diffusion Coefficients for Heterogeneous Systems," HW-60220 (1959).

S2 Schiff, D., and S. Stein, "Escape Probability and Capture Fractions for Gray Slabs," WAPD-149 (1956).

S3 Stuart, G., and R. Woodruff, "Method of Successive Generations," Nuclear Sci. and Eng., 3, 331 (1958).

S4 Suich, J. E., "Temperature Coefficients in Heterogeneous Reactor Lattices," Ph.D. Thesis, Massachusetts Institute of Technology (1963).

T1 Thie, J., "The Failure of Neutron Transport Approximations in Small Cells in Cylindrical Geometry," Nuclear Sci. and Eng., 9, 286 (1961).

T2 Theys, M. H., "Integral Transport Theory of Thermal Utilization Factor in Infinite Slab Geometry," Nuclear Sci. and Eng., 7, 58 (1960).

T3 Thompson, T. J., I. Kaplan, and A. E. Profio, "Heavy Water Lattice Project Report," NYO-9658 (1961).

T4 Tralli, N., and J. Agresta, "Spherical Harmonics Calculations for a Cylindrical Cell of Finite Height," Nuclear Sci. and Eng., 10, 2 (1961).

T5 Tassan, S., "Cadmium Ratios of U^{235} Fission in Slightly Enriched Uranium, Light Water Moderated Lattices," Nuclear Sci. and Eng., 16, 2 (1963).

T6 Tunnicliffe, P. R., D. J. Skillings, and B. G. Childley, "A Method for the Accurate Determination of Relative Initial Conversion Ratios," Nuclear Sci. and Eng., 15, 3 (1963).

T7 Turner, R. B., et al., "The Slowing-Down Spectrum in a CANDU-Type Reactor," Nuclear Sci. and Eng., 16, 1 (1963).

W1 Wachspress, E. L., "Thin Regions in Diffusion Theory Calculations," Nuclear Sci. and Eng., 3, 2 (1958).

W2 Weinberg, A. M., and E. P. Wigner, The Physical Theory of Neutron Chain Reactors, The University of Chicago Press, Chicago (1958).

W3 Weitzberg, A., I. Kaplan, and T. J. Thompson, "Measurements of Neutron Capture in U^{238} in Lattices of Uranium Rods in Heavy Water," NYO-9659 (1962).

W4 Wigner, E. P., and J. E. Wilkins, "Effect of Temperature of the Moderator on the Velocity Distribution of Neutrons with Numerical Calculations for H as Moderator," AECD-2275 (1944).

W5 Wolberg, J. R., T. J. Thompson, I. Kaplan, "A Study of the Fast Fission Effect in Lattices of Uranium Rods in Heavy Water," NYO-9661 (1962).

Y1 Young, J. C., G. D. Trimble, J. R. Brown, D. H. Houston, Y. D. Naliboff, and J. R. Beyster, "Neutron Spectra in Multiplying and Non-Multiplying Media," Trans. Am. Nuclear Soc., 5, 2 (1962).

Y2 Yvon, J., "La Diffusion Macroscopique des Neutrons, Une Methode d'Approximation," J. Nuclear Energy, 4, 305 (1957).

Z1 Ziering, S., and D. Schiff, "Yvon's Method for Slabs," Nuclear Sci. and Eng., 3, 635 (1958).

Z2 Zobel, W., "Experimental Determination of Flux Depression and Other Corrections for Gold Foils Exposed in Water," Trans. Am. Nuclear Soc., 5, 1 (1962).

Z3 Zweifel, P. F., "Neutron Self-Shielding," Nucleonics, 18, 11 (1960).

APPENDIX I
AVERAGED EXPERIMENTAL RESULTS

After completion of this report, it was suggested by Professor T. J. Thompson that it would be possible to obtain an improved estimate of the experimental uncertainties by averaging the results from several experiments, although the measurements involved the use of foils that differed in thickness. This addendum is a discussion of the results obtained by averaging the gold activation distributions in each of the two lattices studied.

In each lattice, there were four experiments involving the use of foils; these experiments are considered to yield representative results. The experiments were made with the 2.5 and 4.3 mil thick gold foils. The results given in Tables 4.1.2 and 4.1.4 were averaged, assuming that the individual points had equal weights. Since the experiments were performed with foils of similar properties and were counted with about the same accuracy, each experiment should carry about the same weight. The averaged results are given in Tables I.1 and I.2 and are plotted in Figs. I.1 and I.2. The uncertainty "ϵ" given at each position is the standard deviation of the average:

$$\epsilon = \sqrt{\sum_{i=1}^{n} \frac{\left[\overline{A}_{th} - \left(A_{th}\right)_i\right]^2}{n(n-1)}}, \qquad \text{(I.1)}$$

where in all cases there were four measurements (i.e., $n = 4$). The average of the standard deviations for all points in a lattice was about 0.7%. It is of interest to compare the values of ϵ in Tables I.1 and I.2 with the values of the standard deviation for counting statistics only as given for the subcadmium activity in Table 4.4.1 (p. 92). The average value of ϵ is only slightly greater (approximately 0.2%) than the counting statistics. This very small increase is due to other experimental uncertainties, such

TABLE I.1

Subcadmium Activation Distribution Based on the Average of the Experiments with Gold Foils in the Lattice with the 1.25-inch Triangular Spacing

Radial Position (cm)	Symbol Used to Plot Point	Average Activity*	ϵ
0.000	×	0.807	± 0.003
	○	0.802	± 0.006
0.158	×	0.826	± 0.008
	○	0.821	± 0.006
0.187	×	0.826	± 0.005
	○	0.820	± 0.008
0.237	×	0.840	± 0.007
	○	0.835	± 0.007
0.400	×	0.894	± 0.005
	+	0.897	± 0.006
0.563	×	0.945	± 0.004
	○	0.957	± 0.008
	+	0.946	± 0.007
0.972	×	0.980	± 0.005
	○	0.969	± 0.007
	+	0.977	± 0.006
1.381	×	0.992	± 0.004
	○	0.984	± 0.009
	+	0.997	± 0.004
1.793	×	1.007	± 0.003
	○	1.010	± 0.008
	+	0.996	± 0.005
2.202	×	0.985	± 0.007
	○	0.992	± 0.006
	+	0.983	± 0.004
2.611	×	0.943	± 0.005
	○	0.998	± 0.003
	+	0.965	± 0.005

*Average based on Runs A11, A16, A14 and A15.

TABLE I.2

Subcadmium Activation Distribution Based on the Average of the Experiments with Gold Foils in the Lattice with the 2.50-inch Triangular Spacing

Radial Position (cm)	Symbol Used to Plot Point	Average Activity*	ϵ
0.000	×	0.785	± 0.007
	○	0.791	± 0.010
0.158	×	0.816	± 0.006
	○	0.811	± 0.008
0.187	×	0.810	± 0.007
	○	0.825	± 0.007
0.237	×	0.836	± 0.006
	○	0.836	± 0.004
0.400	×	0.892	± 0.010
	+	0.886	± 0.004
0.563	×	0.931	± 0.006
	○	0.931	± 0.005
	+	0.936	± 0.005
1.085	×	0.969	± 0.002
	○	0.976	± 0.005
	+	0.971	± 0.005
1.607	×	0.997	± 0.009
	○	0.995	± 0.004
	+	0.994	± 0.004
2.130	×	0.994	± 0.004
	○	0.999	± 0.006
	+	0.995	± 0.004
2.652	×	0.998	± 0.005
	○	1.001	± 0.007
	+	0.998	± 0.003
3.175	×	1.001	± 0.005
	○	1.002	± 0.003
	+	0.996	± 0.003
4.046	×	0.992	± 0.005
	○	1.005	± 0.005
	+	0.999	± 0.003
4.916	×	0.989	± 0.004
	○	1.010	± 0.003
	+	0.985	± 0.005
5.786	×	0.943	± 0.004
	+	0.933	± 0.004
5.499	○	0.997	± 0.008

*Average based on Runs A4, A5, A6 and A7.

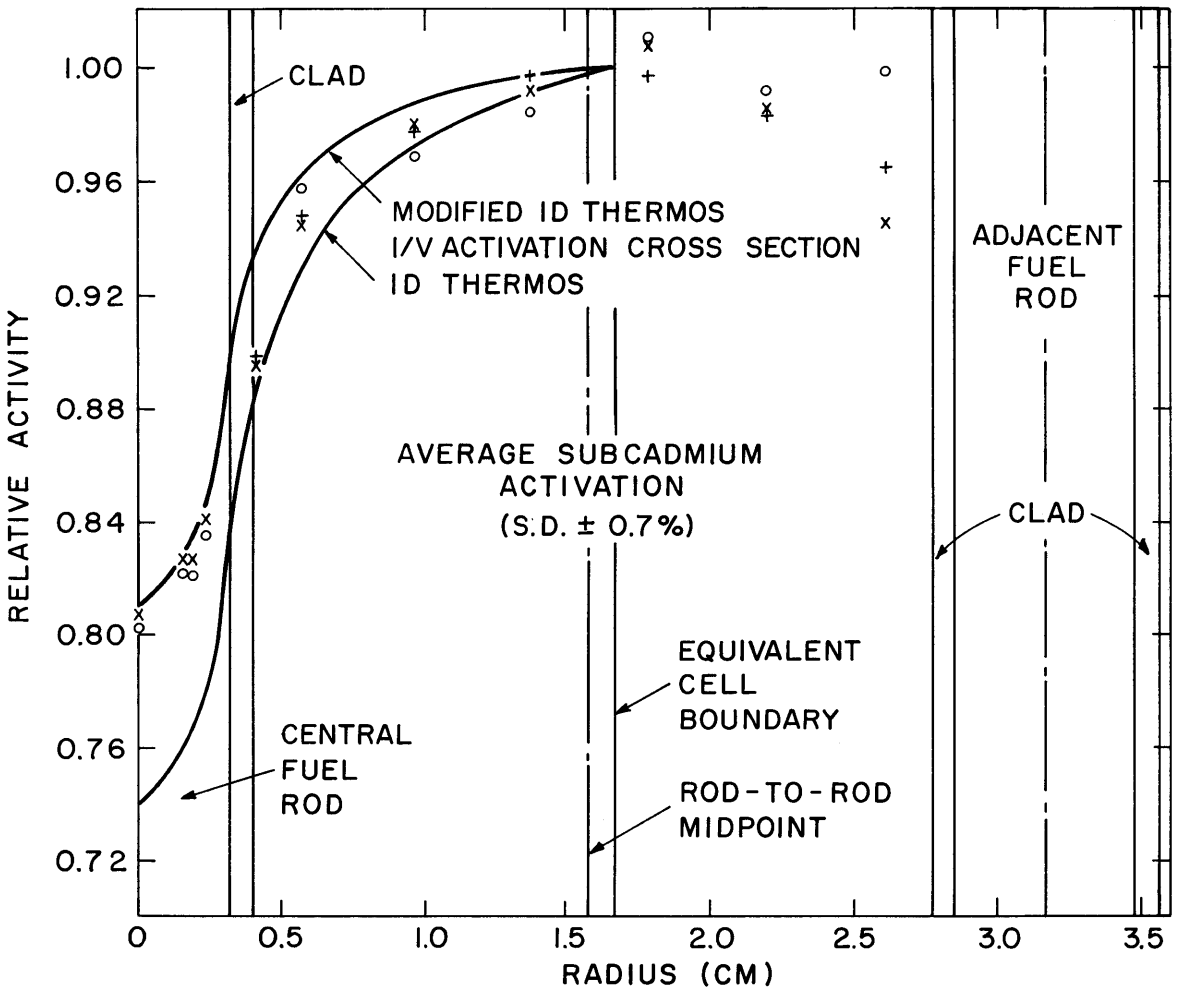

FIG. I.1 SUBCADMIUM ACTIVATION DISTRIBUTION BASED ON THE AVERAGE OF THE EXPERIMENTS WITH GOLD FOILS IN THE LATTICE WITH THE 1.25 - INCH TRIANGULAR SPACING.

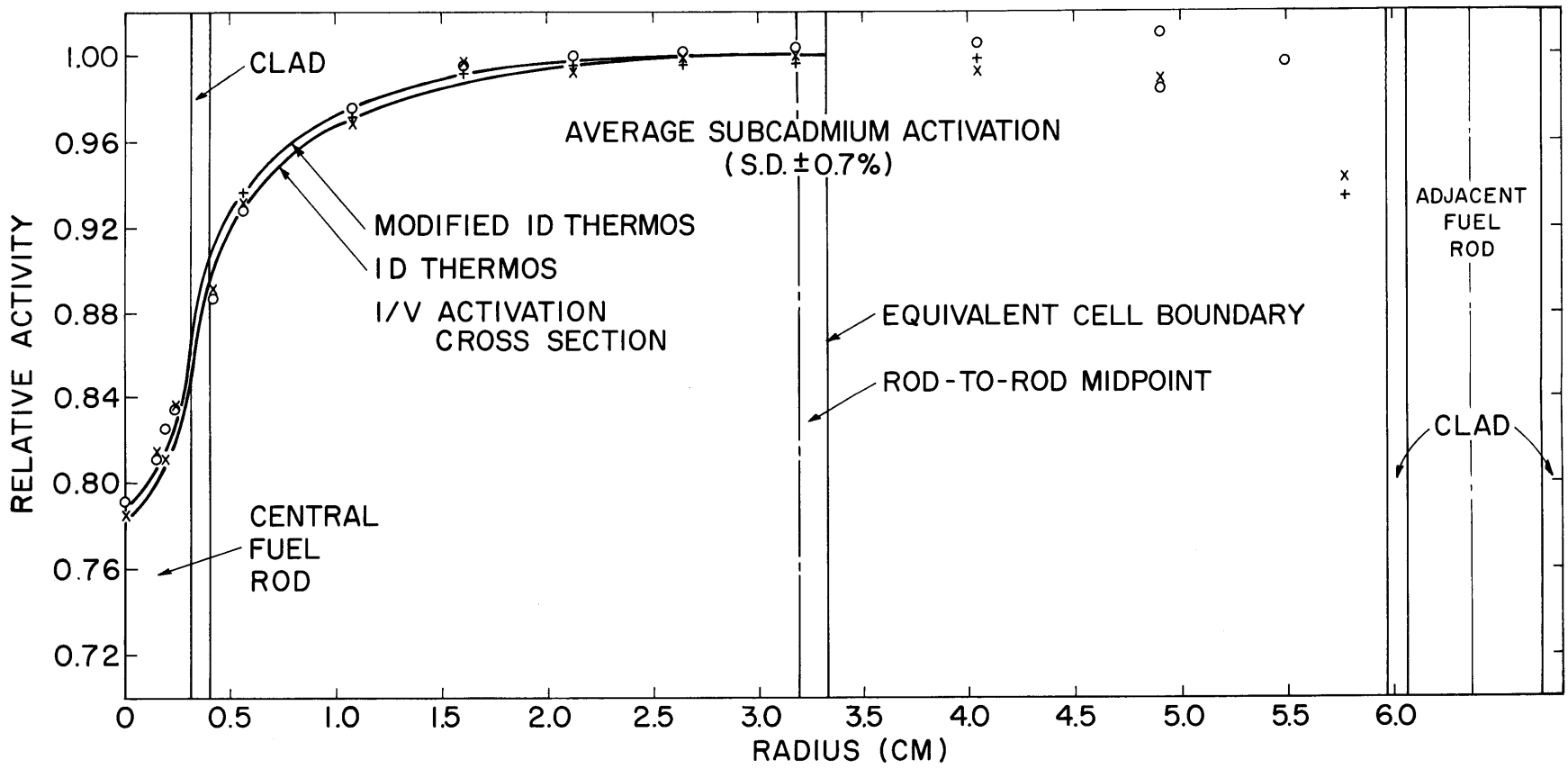

FIG. I.2 SUBCADMIUM ACTIVATION DISTRIBUTION BASED ON THE AVERAGE OF THE EXPERIMENTS WITH GOLD FOILS IN THE LATTICE WITH THE 2.50-INCH TRIANGULAR SPACING.

as the positioning of the foils for both irradiation and counting. There seems to be no other significant trend in the data based on the average results.

A comparison with the results of THERMØS calculations are included in Figs. I.1 and I.2. The conclusions based on the individual experiments also apply to the results based on the averages. Those conclusions are summarized in Chapter V.